# Microfluidic tools for bottom-up synthetic biology

**Dissertation**
zur Erlangung des akademischen Grades

**Doktor der Naturwissenschaften**
**(Dr. rer. nat.)**

von Dipl.-Pharm. Dorothee Krafft

geb. am 01.10.1988 in Ankum

genehmigt durch die Fakultät für Verfahrens- und Systemtechnik der Otto-von-Guericke-Universität Magdeburg

Gutachter/innen:
Professor Kai Sundmacher
Professor Seraphine Wegner
Professor Tsing-Young Dora Tang

Promotionskolloquium am 13.12.2024

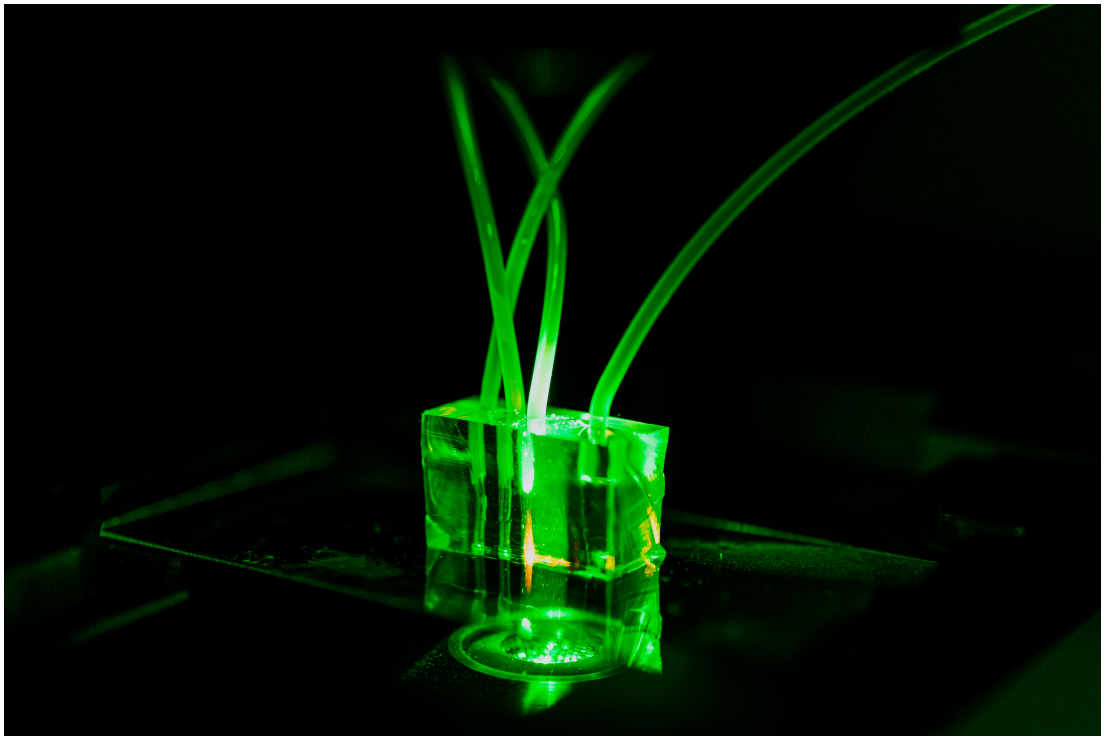

**Figure 1:** Microfluidic chip during double emulsion production.

# Abstract

Bottom-up synthetic biology aims to rebuild biological cells from scratch. This thesis shows how microfluidic technology can be used to produce, observe and manipulate model membranes with a focus on bottom-up synthetic biology applications.

One of the features of life is compartmentalization. Creating cell-like compartments and encapsulating complex solutions is a fundamental task for bottom-up synthetic biology. Commonly used model compartments are lipid vesicles especially giant unilamellar vesicles (GUV). Although there are a lot of established methods to produce GUVs, new methods have to be developed to improve the modular cell building process, mainly the possibility to efficiently encapsulate a broad range of biological parts and modules. In this regard, the second chapter of the thesis shows how microfluidic devices can be used to generate monodisperse compartments with a higher encapsulation efficiency than current standard methods such as electroformation. After the production of double emulsions, various approaches for removal of residual oil are explored to create a phospholipid bilayer membrane.

Next the integration of other complex modules such as energy supply and metabolic reactions with the compartment modules is tested. First an energy module is created from inverted membrane vesicles (IMV). The module is characterized via batch experiments and later encapsulated into water-in-oil droplets inside a microfluidic system. The second combination experiment employs the microfluidic vesicle production method presented before by encapsulating a complex metabolic pathway, the CETCH cycle, inside double emulsions.

Another challenge where microfluidic tools are useful is the observation of processes inside of compartments or across their membrane. New methods are needed as the batch measurements, common in molecular biology, are often not suitable. One example is the vanishingly low volume of the solution inside the vesicle compared to the volume of the outer solution. As a result changes in fluorescence inside the vesicles are diminishable and in addition measurements on a single vesicle level are very difficult to perform or not possible depending on the experimental setup. A microfluidic design for physical immobilization of GUVs and the exchange of the outer solution is presented here. The possibilities and limitations of this device are explored with a membrane transport assay. The influence of lipid composition and detergents on the membrane permeability are measured and a membrane protein, OmpF, is reconstituted in membrane and the changes in permeability are measured.

# Zusammenfassung

Die synthetische bottom-up-Biologie zielt darauf ab, biologische Zellen von Grund auf neu zu konstruieren. Diese Arbeit zeigt, wie die Mikrofluidiktechnologie zur Herstellung, Beobachtung und Manipulation von Modellmembranen verwendet werden kann, wobei der Schwerpunkt auf Anwendungen der synthetischen bottom-up-Biologie liegt.

Eines der Merkmale des Lebens ist die Kompartimentierung. Häufig verwendete Modellkompartimente sind Lipidvesikel, insbesondere riesige unilamellare Vesikel (GUV). Obwohl es eine Reihe etablierter Methoden zur Herstellung von GUVs gibt, müssen neue Methoden entwickelt werden, um den modularen Aufbau von Zellen zu ermöglichen. Insbesondere soll ein breites Spektrum an biologischen Teilen und Modulen während der Produktion mit hoher Effizienz in die Vesikel eingebracht werden. In diesem Zusammenhang zeigt das zweite Kapitel der Arbeit, wie Mikrofluidiktechnologie verwendet werden kann, um monodisperse Kompartimente mit einer höheren Einschlusseffizienz als die derzeitigen Standardmethoden, wie z.B. Elektroformmation, herzustellen. Nach der Produktion von Doppelemulsionen werden verschiedene Ansätze zur Entfernung von Resten organischer Phase getestet, um Phospholipiddoppelmembranen zu erhalten.

Anschließend wird die Integration anderer komplexer Module wie Energieversorgung und Stoffwechselreaktionen mit den Kompartimentmodulen getestet. Zunächst wird ein Energiemodul aus invertierten Membranvesikeln (IMV) entwickelt. Das Modul wird durch Batch-Experimente charakterisiert und später mit Hilfe eines Mikrofluidiksystems in Wasser-in-Öl-Tröpfchen eingeschlossen. Das zweite Kombinationsexperiment nutzt die zuvor entwickelte Methode zur Produktion von Vesikeln mittels Mikrofluidik um einen komplexen Stoffwechselweg, den CETCH Zyklus, in Doppelemulsionen einzuschließen.

Eine weitere Herausforderung, bei der mikrofluidische Systeme verwendet werden, ist die Messung von Prozessen innerhalb von Kompartimenten oder an deren Membran. Dafür werden neue Methoden benötigt, da in der Molekularbiologie übliche Methoden häufig nicht geeignet sind. Zum Beispiel ist das Volumen der Lösung im Inneren des Vesikels im Vergleich zum Volumen der äußeren Lösung verschwindend gering. Infolgedessen sind Fluoreszenzänderungen im Inneren der Vesikel in Batch-Experimenten nur schwer messbar und Messungen eines einzelnen Vesikels sind sehr schwierig oder nicht möglich. Es wird ein mikrofluidisches Design für die Immobilisierung von GUVs und dem Austausch der äußeren Lösung vorgestellt, mit dem solche Messungen ermöglicht werden sollen. Die Möglichkeiten und Grenzen dieses Systems werden anhand eines Membrantransportassays untersucht. Der Einfluss von Lipidzusammensetzung und Detergenzien auf die Membranpermeabilität und auf ein Membranprotein, welches in die Membran eingebracht wird, werden gemessen.

# Publications and Statement on Authorship

**Publications**

Thomas Beneyton, Dorothee Krafft, Claudia Bednarz, Christin Kleineberg, Christian Woelfer, Ivan Ivanov, Tanja Vidaković-Koch, Kai Sundmacher & Jean-Christophe Baret (2018). Out-of-equilibrium microcompartments for the bottom-up integration of metabolic functions. Nature Communications, 9(1), 1-10.

Dorothee Krafft, Sebastián López Castellanos, Rafael B. Lira, Rumiana Dimova, Ivan Ivanov, Kai Sundmacher (2019). Compartments for synthetic cells: osmotically assisted separation of oil from double emulsions in a microfluidic chip. ChemBioChem, 20(20), 2604-2608.

Sunidhi C. Shetty, Naresh Yandrapalli, Kerstin Pinkwart, Dorothee Krafft, Tanja Vidakovic-Koch, Ivan Ivanov, Tom Robinson (2021). Directed signaling cascades in monodisperse artificial eukaryotic cells. ACS nano, 15(10), 15656-15666.

**Conference contributions**

Dorothee Krafft, Christin Kleineberg, Claudia Bednarz, Ivan Ivanov, Tanja Vidaković-Koch, Kai Sundmacher (2016). A cell-free, self-sustaining metabolic platform. In EU-SynBioS Symposium, London, UK. (Presentation)

Dorothee Krafft, Minhui Wang, Lado Otrin, Tanja Vidaković-Koch, Ivan Ivanov, Kai Sundmacher (2017) Functionalized membranes for bottom-up synthetic biology. DECHEMA Symposium Systems Biology meets Synthetic Biology, Frankfurt, Germany. (Presentation)

Dorothee Krafft, Sebastián López Castellanos, Ivan Ivanov, Kai Sundmacher (2017) A Microfluidic Assay for Real Time Membrane Transport Monitoring. International Symposium on New Horizons in Membrane Transport and Communication, Frankfurt, Germany. (Presentation & Poster)

Dorothee Krafft, Sebastián López Castellanos, Ivan Ivanov, Kai Sundmacher (2018) Microfluidic production and oil removal from double emulsions. Symposium on Microfluidics for Synthetic Biology and Health Applications, Bordeaux, France. (Poster)

**Technical and scientific cooperation**

This work would not have been possible without help of other scientists from sharing their methods to use of equipment and joint experiments.

Sebastian Lopez-Castellanos did his master thesis in the Sundmacher group under my supervision. He worked on microfluidic GUV production and oil detachment from double emulsions. Some of the experiments shown in chapter 2 of this thesis were done in collaboration with Sebastian. The results of his work are documented in detail in his thesis: "Lopez-Castellanos, Sebastian. Vesicles-On-A-Chip: A novel microfluidic-based method for the generation of giant unilamellar vesicles. Otto-von-Guericke-Universität Magdeburg, 2018."

The IMV project presented in chapter 3 was the result of a collaboration between the MPI DCTS in Magdeburg and the Baret group at the University of Bordeaux, France. The E. coli membrane isolation and and production of IMVs was done by Claudia Bednarz (MPI DCTS), Christin Kleineberg (MPI DCTS) did additional characterization of the IMV ATP production (not shown in this thesis) and Thomas Beneyton ( Bordeaux Univeristy) did the measurement of IMVs and enzymes encapsulated in microfluidic droplets. The initial proof of work of the IMVs, the selection of the enzymes and the optimization of an reaction environment for the IMVs and the enzymes was done by me.

The experiments shown in chapter 3 encapsulating enzymes from the CETCH cycle were done in close collaboration with Christoph Diehl from the Erb group in Marburg.

The production of the silicon wafers was supported by the MPI for Dynamics and Self-Organization (Göttingen), where I was able to use their clean room and microfabrication facility and got training and assistance on the production process.

Some of the membrane characterization experiments and confocal microscopy images were done at the MPI of Colloids and Interfaces (Potsdam/Golm) with the help of Rafael Lira.

For the initial microfluidic experiments I used microfluidic designs from Julien Petit (MPI for Dynamics and Self-Organization) and Tom Robinson (MPI of Colloids and Interfaces) shared the CAD files of his designs for microfluidic traps and taught me how to operate the trap chips.

# Abbreviations

| | |
|---|---|
| alpha-HL | alpha-Hemolysin |
| ATP | Adenosine triphosphate |
| BSA | Bovine serum albumine |
| CAD | Computer aided design |
| Ca | Capillary number |
| CETCH cycle | crotonyl-CoA/ethylmalonyl-CoA/hydroxybutyryl-CoA cycle |
| CMC | critical micelle concentration |
| D | Diffusion coefficient |
| DMSO | Dimethyl sulfoxide |
| DOPC | 1,2-dioleoyl-sn-glycero-3-phsophocholine |
| DPhPC | 1,2-diphytanoyl-sn-glycero-3-phosphocholine |
| E. coli | Escherichia coli |
| FRAP | fluorescence recovery after photobleaching |
| GUV | Giant unilamellar vesicle |
| HRP | Horseradish peroxidase |
| I | Fluorescent light from microfluidic channel |
| IF | Inner fluid |
| IMV | Inverted membrane vesicle |
| IPTG | Isopropyl $\beta$-D-1-thiogalactopyranoside |
| ITO | Indium tin oxide |
| LUV | Large unilamellar vesicle |
| MF | Middle fluid |
| MOPS | 3-(N-morpholino)propanesulfonic acid |
| NAD | Nicotinamide adenine dinucleotide |
| OA | Oleic acid |
| OF | Outer fluid |
| OG | Octyl glucoside |
| OmpF | Outer membrane porin F |
| o-POE | n-Octylpolyoxyethylene |

| | |
|---|---|
| P | Permeability coefficient |
| PC | Phosphatidylcholine |
| PDMS | Polydimethylsiloxan |
| PEG | Polyethylene glycol |
| POPC | 1-palmitoyl-2-oleoyl-sn-glycero-3-phosphocholine |
| PVA | Poly vinyl alcohole |
| | |
| Re | Reynolds number |
| RT | Room temperature |
| | |
| SD | Standard deviation |
| SDS | Sodium dodecyl sulfate |
| $\sigma$ | Interfacial tension |
| SUV | Small unilamellar vesicle |
| | |
| o/w | Oil-in-water emulsion |
| w/o | Water-in-oil emulsion |
| w/o/w | Water-in-oil-in-water emulsion (double emulsion) |

# Contents

# Chapter 1

# Introduction

This chapter gives a short overview about the three underlying topics of this thesis. The first topic is a short introduction to the field of synthetic biology, its development and the different paths towards a minimal cell. It is followed by a short overview of the biology and biophysics of cell membranes as this thesis focuses on creation, analysis and manipulation of compartments as one of the key features of life and thus an essential module for a synthetic cell. Finally the focus is on microfluidics, a technology which enables progress in synthetic biology for the creation and handling of cell-like compartments. This mixture of topics from biology and chemistry to engineering reflects the interdisciplinary character of the whole thesis. In the end the central questions and hypotheses of this thesis are discussed and a short chapter overview is given.

## 1.1 Synthetic biology

Synthetic biology aims to design and engineer biological parts, novel devices and systems - as well as to redesign existing natural biological systems (Kitney & Freemont (2012)). It is an interdisciplinary field with biologists, chemists and engineers working together.
The field covers a broad spectrum of topics from application focused creation of controllable and reproducible tiny factories to more fundamental questions about cellular functions and potentially new insights to what life is.

**What is life?** This is a question asked since the beginning of philosophical thinking. The physicist Erwin Schroedinger saw the ability of a system to maintain or decrease its internal entropy as a defining feature of life (Schrödinger (1946)) (Weiss (2018)).
Biologists and philosophers tried to define life and, as a result, lists with fundamental features of life have been published. The biochemist Daniel E. Koshland listed in his essay "The Seven Pillars of Life" the seven fundamental features of life: Program

(an organized plan, DNA), Improvisation (Adaptation to the environment), Compartmentalization (confinement to a limited volume surrounded by a membrane), Energy (movement and metabolism), Regeneration (compensation for losses), Adaptability (fast response to stimuli) and Seclusion (selective chemical reactions) (Koshland (2002)).
There are other definitions with slightly different criteria.
Some biological phenomena only fit a part of the criteria, most notably viruses. Additionally a non-biological machine constructed by humans could fulfil all the criteria too (Weiss (2018)). These examples show that there is a grey zone and one aspect of synthetic biology is to explore it.

### 1.1.1 Engineering principles

Synthetic biology is, more than most other biological fields, strongly influenced and to a certain extent founded by engineers and computer scientists who aimed to transfer engineering principles to biological systems. They were inspired by electronic circuits and computers, which work with standardized parts with a seemingly infinite number of possible combinations to fulfil the required task.
A modular design allows for independent and rapid development of features which can later be combined (Garcia & Trinh (2019)). Ideally these modules should be standardized and reproducible to easily combine them with other modules.
Parts and modules used as building blocks have to be defined and categorised (Weiss (2018)). Second, building blocks have to be described. In silico models and simulations can help with the prediction of behaviour at various conditions (Weiss (2018)).
The next step is standardization of the modules allowing their combination in as many variations as possible. This requirement can only be met if the research groups pioneering the development of different parts and modules are working closely together.
Creating these modules or building blocks is approached in two different ways that also represent two general approaches in synthetic biology, the 'top-down' and the 'bottom-up' approach. The top-down approach uses genes as parts or building blocks to program existing cells (Smolke (2009)). The iGEM competition and the BioBricks foundation introduced standards for those biological parts that are essentially DNA sequences.
In the bottom-up approach the possible parts are broader, from small organic molecules to large polymers or other components like nanoparticles. They are assembled into functional modules. The bottom-up community did not largely standardize parts or modules yet.

### 1.1.2 Top-down and bottom-up approach

One branch of the diverse field of synthetic biology is the quest to create a minimal cell. This quest has been approached from the two directions mentioned above (Benner & Sismour (2005)). The 'top-down' approach prominently lead by Craig Venter tries to reduce the number of genes in a living organism to find the minimal set of genes

necessary for life (Hutchison *et al.* (1999)). The 'bottom-up' approach on the other hand tries to build a cell from molecular parts.

As shown in Figure 1.1 and in the table in Figure 1.2 in the top-down approach syn-

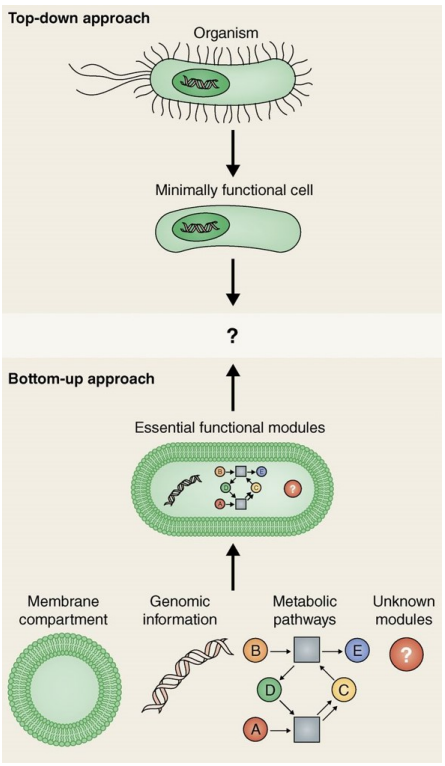


**Figure 1.1:** Comparison between top-down and bottom-up systems from (Schwille (2015)).

thetic cells are created by changing the genome and subsequently the proteins inside existing cells. The produced cell is alive and still very similar to the original cell.
One well known goal of this approach is the minimal genome project (Supramaniam *et al.* (2019)). These cells are less complex than even simple cells that occur in nature but also in these organisms the biological function of many of the genes that have been experimentally found to be essential for proliferation remain unknown.
As mentioned above the top-down approach is based on genetic engineering and uses engineering concepts such as modularity, standardization and structures based on logical operators similar to the ones used in information processing (Schwille (2011)) (Endy (2005)).

In bottom-up synthetic biology, building blocks consisting of biological or chemical parts are used to create biomimetic systems and ultimately an artificial cell (Mutschler *et al.* (2019)). The bottom-up approach is less established and advanced than the top-down approach but it has the potential to not only create new bioengineered systems

that have features which can not be created by genetic engineering, it might also give us a better understanding of the mechanisms and the origin of life.

The idea of the bottom-up approach is elegantly summarized in a quote by Richard

**Table 1.** A comparison between the use of a cell-free protein system and a more traditional in vivo cell system.

| Feature | Cell-Based System | Cell-Free System |
|---|---|---|
| DNA Template | Plasmids or genome | PCR or Plasmid |
| Production of toxic proteins | No | Yes |
| Incorporation of modified amino acid | Not possible | Possible |
| Complexity of system | High | Low |
| Manipulation of translational and transcription cycle | No | Yes |
| Self-Replication | Yes | No |
| Generation of functional and folded proteins | Yes | Yes, soluble proteins more straightforward. Membrane proteins more challenging, methods needed to stabilise aggregation of nascent polypeptides e.g., detergents or artificial membranes |
| Ability to produce specific desired protein | Restricted due to complex cellular metabolism | Yes, no interaction with various other metabolic pathways |
| Biomanufacturing | Modest production rate and yield. Product purification requires complex steps and cell lysis | High production rate and production yield Simple product purification with no cell lysis |
| Production time | Days: transformation of the host with the template DNA, growth of colonies, clonal amplification, and finally induction, to produce a desired protein | Hours: mix reagents |
| Cost | Low to moderate | Moderate to high |

**Figure 1.2:** Comparison between top-down and bottom-up systems from (Supramaniam *et al.* (2019)).

Feynman "What I cannot build I do not understand".
Bottom-up synthetic biology is not limited to rebuilding biological systems step by step, but utilises the possibility of using other materials - such as various polymers or nanoparticles - to perform a certain task more efficiently and robustly in a specific environment.
For example polymersomes have been shown to form very robust membranes with adjustable features while providing a suitable environment for membrane proteins (Choi & Montemagno (2005)) (Rideau *et al.* (2018)). Another example is the creation of 3D structures using DNA bricks (Delebecque *et al.* (2011)).
The research presented in this thesis is, as a part of the MaxSynBio project, a contribution towards an artificial cell built from scratch.

**Bottom-up assembly of minimal synthetic cells.** It is not fully understood how cellular self-assembly and self-organization works. Therefore a strategy is needed for creating standardized parts and their combination Jia & Schwille (2019). Figure 1.3 shows

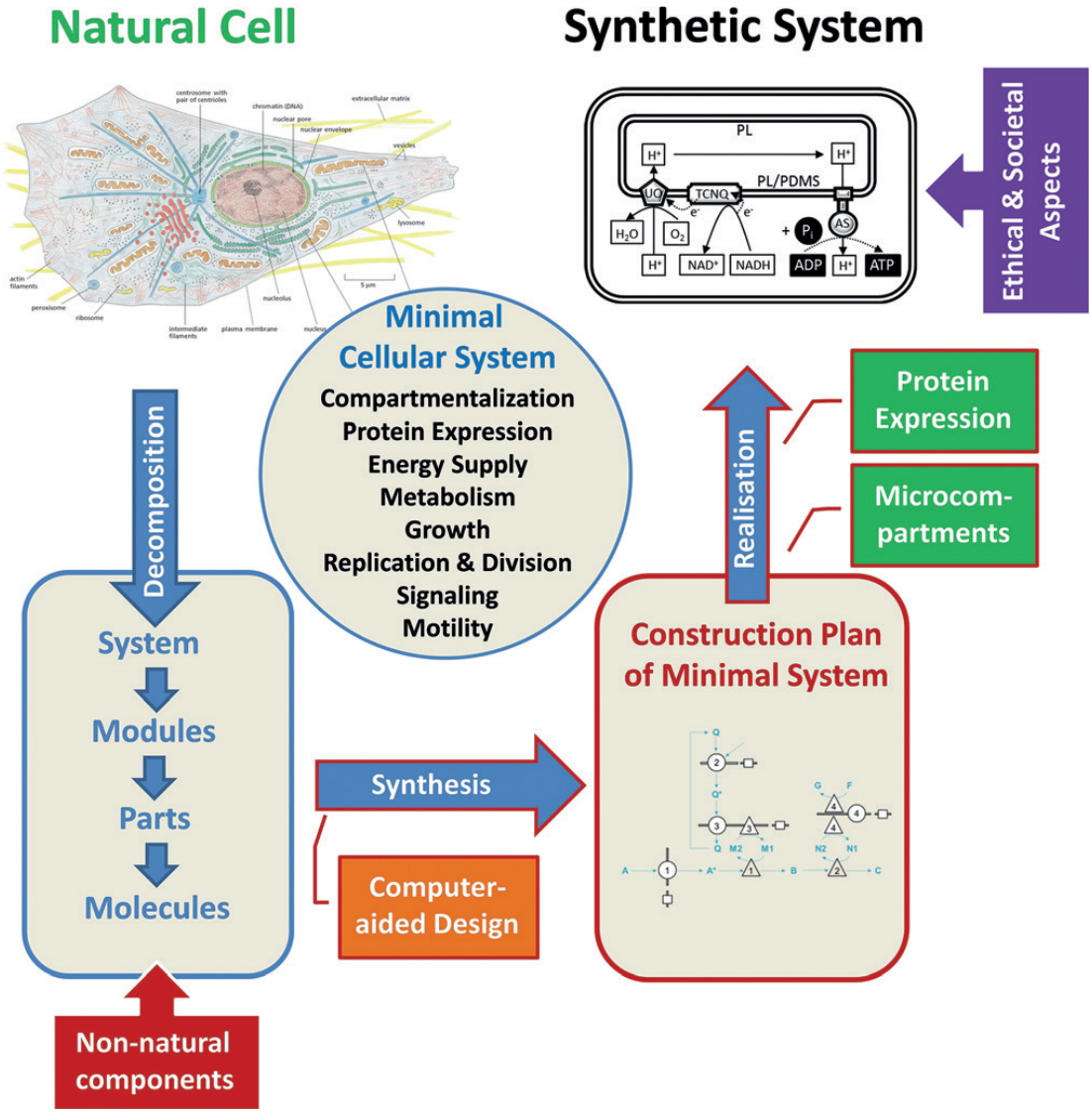


**Figure 1.3:** MaxSynBio workflow and essential features to create a minimal cell (Schwille *et al.* (2018)).

the MaxSynBio workflow for a bottom-up assembly strategy. Initially natural cells are analysed and their essential components are isolated, recreated and characterized. The parts and modules do not have to be exact copies of the natural counterparts but can be artificial components like synthetic molecules and nanoparticles mimicking the functionality of the natural counterparts and adding additional traits like an increased

stability in certain environments or a responsiveness to external signals such as light. With the help of technologies such as computer simulations and microfluidics, the minimal systems are planned, built and optimized (Jia *et al.* (2017)) (Schwille *et al.* (2018)).

## 1.2 Membranes and lipids

Lipids are the main component of biological membranes and responsible for their basic features. They are amphiphilic molecules with a polar head group and an non-polar tail which in most cases is a fatty acid. Lipids in general have a range of functions inside living organisms, such as triglycerides as energy storage.
The arrangement of these molecules depends on the surrounding solution. They are able to self-assemble into complex structures like monolayers at interfaces, micelles and bilayers. In biological membranes they are assembled as bilayers. Phospholipids can also self-assemble into lipid bilayers in solution (Monnard & Deamer (2002)).
Depending on the temperature and the lipid properties, membranes can be present in two different phases. The phase transition temperature marks the temperature between the ordered gel phase and the disordered liquid phase (Weiss (2018)) (Eze (1991)) (Koynova & Caffrey (1995)). In temperatures below the phase transition temperature lipids show a slow lateral diffusion resulting in a higher rigidity of the lipid bilayer. In higher temperatures the hydrophobic chains are less ordered leading to higher mobility (Weiss (2018)). If a bilayer contains a mixture of different lipids, phase separation can occur with one kind of lipid concentrating in a certain region of the membrane resulting in a different phase than other regions of the membrane (Heberle & Feigenson (2011)).

**Biological membranes.** There are different types of lipids in biological cell membranes. Three examples of different membrane lipids are shown in Figure 1.4 but there is a much bigger variety than shown here. For example both phospholipids and glycolipids can contain a sphingosine group instead of the glycerol group.
Figure 1.4a shows a schematic representation of phosphatidylcholine an example from the group of glycerophospholipids and a very common lipid in biological membranes. Glycolipids contain a sugar, for example glucose, instead of the phosphate group. The fatty acids can be either saturated with straight chains or contain double bonds resulting in bended chains. Sterols (Figure 1.4c) have a very different structure from other membrane lipids. They do not have fatty acid chains but four hydrophobic hydrocarbon rings. A common membrane lipid from the sterol group is cholesterol. Steroids are not present in bacterial membranes but are important components of eukaryotic membranes (Watson (2015)).

In 1972 the fluid mosaic model of the structure of cell membranes was proposed (Singer & Nicolson (1972)). It states that membranes have a dynamic fluidity with the ability of lipids and proteins to diffuse laterally through the membrane (Watson (2015)).

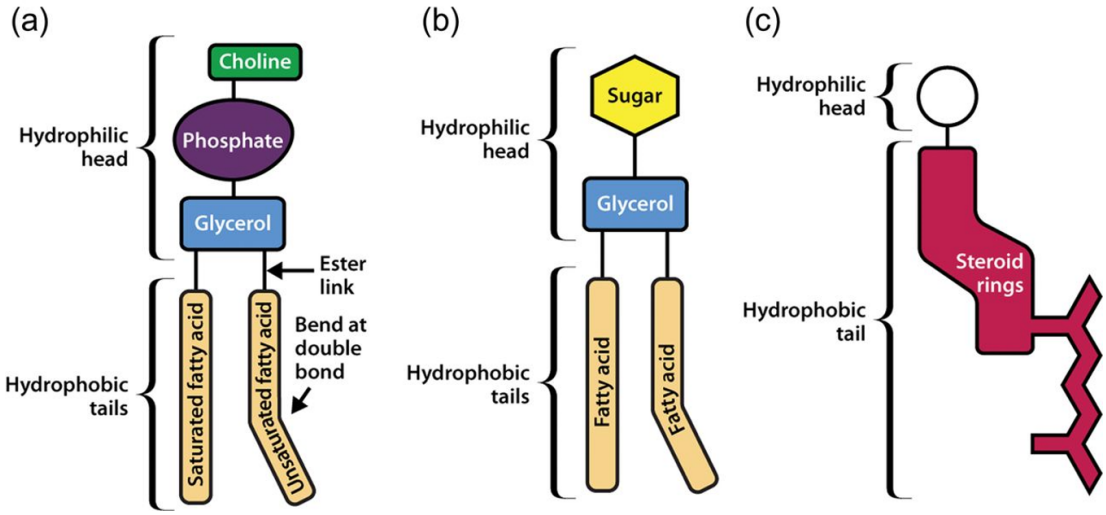


**Figure 1.4:** Schematic drawings of three types of membrane lipids. (a) Phosphatidylcholine (b) Glycolipid and (c) Sterol. Image from (Watson (2015)).

One method to observe the movement of membrane components is to measure the fluorescence recovery after photobleaching (FRAP) with either fluorescent labelled lipids or proteins (Reits & Neefjes (2001)). This method is also a useful tool in membrane characterization of artificially produced membranes like giant unilamellar vesicles (GUV) (Rayan *et al.* (2010)).
In addition to lipids, proteins and sugars are important components of biological membranes. They are attached to lipids, or proteins and can act as cell markers because of their structural diversity. For example the sugar chain composition on our red blood cells determines our blood group (Watson (2015)).

**Membrane proteins.** Just as compartmentalization is a feature of life so is the ability of cells to exchange matter, information and energy across their membranes. Membrane proteins enable active or passive transport and receptors can pass on signals (Mulkidjanian *et al.* (2009)) (Apellániz *et al.* (2010)).
These proteins can span the membrane or just be attached to it. Transmembrane proteins often have an alpha-helix or beta-barrel structure with lipophilic amino acids on the outside. Membrane transport proteins can enable diffusion of molecules or ions across the membrane, a process driven by a concentration gradient between the two sides of the membrane and not requiring energy. In addition they can also facilitate active transport against a concentration gradient. Active transporters are usually much more specific for one or a very small group of molecules or ions (Ragunath (2006)). Figure 1.5 gives an overview of the various membrane transport mechanisms.
Using membrane proteins for synthetic biology applications is more challenging than

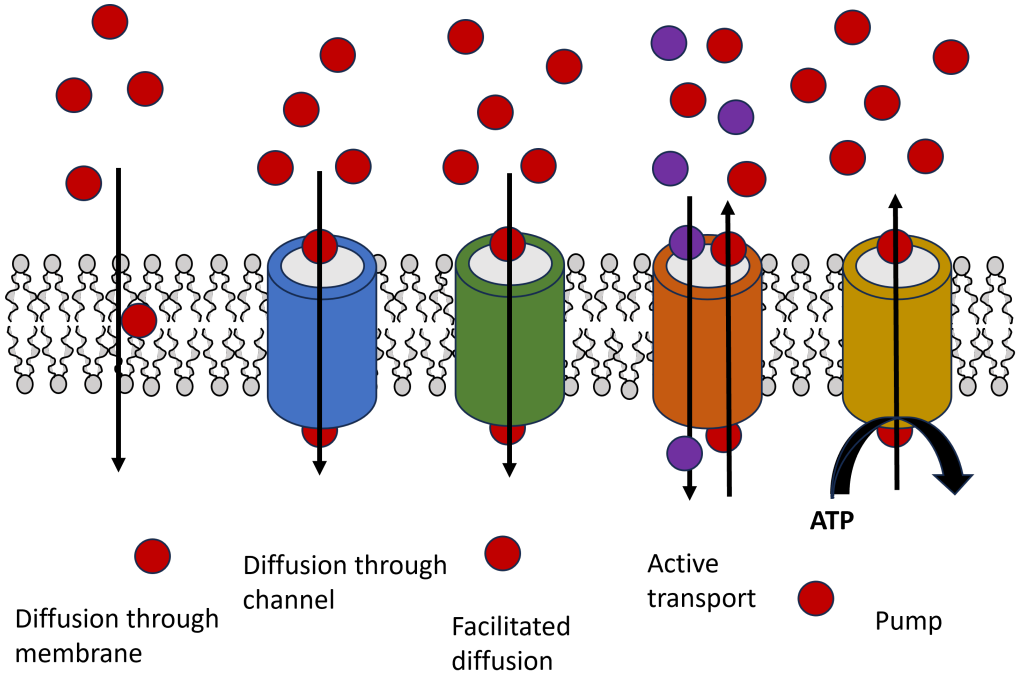


**Figure 1.5:** An overview of membrane transport mechanisms in cells.

using soluble enzymes because they have to be removed from their natural environment, the cell membrane, during the purification and require reconstitution into the artificial membrane without destroying the protein and other encapsulated substances. There are already a couple of examples for encapsulated, cell-free protein biosynthesis inside GUVs producing membrane proteins which incorporate themself into the membrane (Gessesse *et al.* (2018)).

### 1.2.1 Model membranes

As briefly outlined above, cell membranes are very complex. To study the biophysical properties of lipid bilayers isolated models were developed (Chan & Boxer (2007)). The first model lipid systems were developed in 1962 by Mueller and his colleagues (Mueller *et al.* (1962)), leading to the development of black lipid membranes (Montal & Mueller (1972)) (Cama (2016)). These are lipid membranes across a tiny hole in a Teflon wall and the only separation between the solutions inside the two chambers (Schmitt *et al.* (2006)). Using electrophysiology the movement of molecules through membrane transporters can be measured.
In addition to the planar lipid models mentioned above lipid vesicles or liposomes are used as membrane models. A subgroup, used in this thesis, are GUVs with sizes in the micrometer range similar to the size of biological cells. They are often made of one or a few lipids (Chan & Boxer (2007)) and are used to study the behaviour of lipids and lipid

mixtures. In molecular biology and biotechnological research they serve as simplified cell models and in the pharmaceutical industry they serve as delivery systems for drugs and vaccines (Schwendener (2014)).

## 1.3 Compartmentalization

Compartmentalization is a fundamental feature of life. Examples for compartmentalization in biology are of course cell membranes and cell walls but also subcellular organelles like the nucleus, chloroplasts or the Golgi apparatus. Complex multicellular organisms also have higher forms of compartmentalization like the blood brain barrier to control which substances are able to enter the central nervous system.
Compartments have several functions inside the cell. They allow for a separation of reactions which require different conditions, like pH values, within one cell. Another feature is to influence which substances that can enter and leave the compartment. Because of their size, enzymes and DNA stay inside, while small, uncharged molecules can move more freely and selective ion channels allow a controlled crossing of charged particles for fast information transfer inside the body due to the resulting membrane potential in nervous or muscle cells.

## 1.4 Microfluidics

Microfluidics is the manipulation of fluids in dimensions in the micrometer range (Baldacchini (2015)). Environments with microfluidic flow exist also in nature e.g. in the microvascular system in humans. The capillary blood vessels in humans are 5 to 70 $\mu$m diameter, a similar size to the channels in the microfluidic chips used in this thesis.
Early applications and motivations for microfluidic systems were the development of small replication of known analytical methods for example gas chromatography (Terry *et al.* (1979)). Later the further development was pushed by military funding hoping to develop portable sensors for biological and chemical weapons. The third motivation was from molecular biology with the goal of high throughput DNA sequencing (Redman *et al.* (2015)) and the fourth element of the foundation of the field of microfluidics was the inspiration and transfer of methods from microelectronics (Whitesides (2006)).
Scientific questions that can be investigated with this technology are in fluid physics and single cell or even single molecule analysis due to the possibility to use very small amounts of sample. Recently microfluidics moved back to its roots with applications not in biology and chemistry but in electronics for example as a cooling system (van Erp *et al.* (2020)).
PDMS (poly(dimethylsiloxane)) is the most common material for microfluidic systems nowadays (McDonald & Whitesides (2002)). The first systems were inspired by microelectronics and used silicon and glass (Saluz *et al.* (2012)). PDMS allows for rapid and inexpensive device preparation without a clean room (McDonald *et al.* (2000)). A clean

room is only needed for micropatterning of the wafers which can be used multiple times to make microfluidic devices using soft lithography.
Microfluidics introduces automation on a small scale to biological research which can improve reproducibility (Jessop-Fabre & Sonnenschein (2019)), new insights through high throughput experiments and the discovery of phenomena that would go unnoticed with smaller sample numbers. Automation in biology nowadays is done predominantly by using liquid handling robots essentially automating pipetting of liquids in volumes that are also used while pipetting by hand.

### 1.4.1 Segmented and continuous flow

Microfluidics differs from microelectronics because the fluid physics changes more rapidly with decreased size (Squires & Quake (2005)). The fluid flow is laminar and not turbulent because the flow in microfluidic channels is dominated by viscous shear forces caused by the higher surface to volume ratio. The smaller dimension leads to faster mass and heat transfer (Kenis & Stroock (2006)).
The bigger surface to volume ratio allows electro-osmotic flow (flow driven by an electric field) in contrast to pressure driven flow used in larger scale systems (Kenis & Stroock (2006)). An issue of larger surface to volume ratio is higher non-specific adsorption especially of proteins, which is a potential problem in many synthetic biology applications but can be also useful for example by using BSA (bovine serum albumin) adsorption to make the surface less hydrophobic. The mixing behaviour of different fluids can be slow and solely driven by diffusion in a continuous flow system or rapidly by chaotic advection inside a segmented flow system for example in moving droplets (Gonidec & Puigmartí-Luis (2019)).

### 1.4.2 Applications in synthetic biology

Microfluidics is a key technology to enable various processes in synthetic biology such as creation, manipulation and analysis of microcompartments (Fallah-Araghi *et al.* (2012)) (Tayar *et al.* (2017)). Compartments such as droplets or vesicles can be created and manipulated enabling replication of processes in cell sized volumes (Teh *et al.* (2008)) (Utada *et al.* (2005)).
Microfluidics offers the possibility to miniaturize batch experiments and creates new possibilities for experiments that would not be possible in batch scale. Additionally it allows for high-throughput production and screening of samples on a single cell or single vesicle level (Agresti *et al.* (2010)). Microfluidics is also used in top-down synthetic biology for analysis of single cells on a genetic and metabolic level (Lan *et al.* (2017)) (Klein *et al.* (2015)) (Eyer *et al.* (2017)) or high-throughput cell culture (Hung *et al.* (2005)).

### 1.4.3 Aim of this thesis

The aim of this thesis is to show that microfluidic systems are necessary tools for bottom-up synthetic biology. There are two focus areas:
(I) Compartment production and encapsulation of other modules
(II) Observation of processes inside the compartments

Focus (I) addresses the following questions:
1. Can microfluidic systems be used to create homogenous compartments with controllable membrane properties?
2. Is this production system suitable for the encapsulation of other functional modules?
3. What are minimal requirements when combining two modules?

Focus (II) addresses these questions:
1. Is a microfluidic system that physically immobilizes compartments a useful tool for their observation and manipulation?
2. Can this system be used for the measurement of membrane transport on a single vesicle level?

This thesis was started at the beginning of the MaxSynBio research collaboration (Section 1.1.2). As part of this project working groups would develop parts and functional modules as building blocks for the bottom-up creation of biological systems (Figure 1.3). In context of the MaxSynBio project two microfluidic focus areas were chosen that would be necessary for the project from the very beginning and that would provide necessary tools for the progress of the whole project.
The first focus area for the thesis was chosen because compartments are fundamental features of life. The encapsulation of a large variety of parts and modules was a mandatory property of a compartment production method. In addition features of the compartment like size, membrane composition and inner fluid composition had to be controllable and adjustable to allow the proper function of the encapsulated parts and modules.
The second focus area was chosen to characterize the membranes produced in the first part and to confirm the functionality of encapsulated modules. This is another fundamental tool needed from the beginning of the project. This part helps with the characterization of a variety of parts and modules either isolated or combined. This tool is part of the engineering principle to build systems out of parts with known properties and to confirm the functionality of the system during every step in the building process.

Chapter 2 shows the development of a microfluidic compartment production system. The microfluidic design used here allows high-throughput production of double emulsions with a high encapsulation efficiency. In this chapter the operation of the chip and the optimization steps that were taken to achieve a stable double emulsion production

are explained. One focus was to vary the compositions of the outer, middle and inner fluids for the optimization of the production process. In addition the composition of the fluids can influence other parts and modules that will be later combined with the compartment module, such as membrane proteins or encapsulated enzymes. To avoid possible interactions the system was optimized towards the minimal number of components in the fluids to maximize compatibility with other modules.
One challenge of vesicle production with double emulsion is the removal of residual oil from the membrane. This is the second focus of Chapter 2 which resulted in a novel method for oil removal using an osmotic gradient.

Chapter 3 builds on Chapter 2 and shows several examples of the encapsulation of complex modules in compartments produced with microfluidic systems. The main challenge behind the results shown in this chapter was the adjustment of buffer solutions that would allow a stable compartment production as well as creating a suitable environment for the encapsulated modules. In the first part of the chapter an energy module containing the E. coli respiration chain is encapsulated in water-in-oil droplets using microfluidics. In the second part of the chapter the double emulsion method shown in Chapter 2 is used to encapsulate enzymes. The first step was to encapsulate a single enzyme and all the substances it needed to function. Lastly a more complex metabolic pathway was encapsulated in double emulsion vesicles.

One of the challenges in the work presented in Chapter 2 and 3 was testing membranes and confirmation that an encapsulated module is still functional inside the compartment. This is the focus of Chapter 4, which focuses on a microfluidic system for vesicle immobilisation. The first part of the chapter shows the optimization of the chip design and the implementation of an membrane permeation assay. This assay allows time resolved measurement of membrane permeation on an individual vesicle level. In this chapter the possibilities and limitations of this assay to determine membrane permeability are tested under a broad spectrum of conditions. In the last part of this chapter the assay on the immobilization chip is applied to a vesicle modified with a transmembrane protein that allows the permeation of certain molecules.

Finally, the thesis is summarized and concluded in Chapter 5. Furthermore, an outlook is given and future perspectives are discussed.

# Chapter 2

# Microfluidic GUV production

## 2.1 Literature review of GUV production methods

### 2.1.1 Non-microfluidic GUV production methods

The first liposome production methods emerged in the 1960s (Reeves & Dowben (1969)) and since then plenty of methods were developed before the first microfluidic devices were ever assembled. This section focuses on the non-microfluidic production of GUVs with special emphasis on electroformation because it is a very commonly used method and the vesicles in Chapter 4 of this thesis, used for membrane permeability and transport experiments, were produced with electroformation.
For many applications microfluidic GUV production is not necessary because GUVs produced by batch methods can be simply added later to a microfluidic system as it was done for the experiments presented in Chapter 4. Therefore also the most common non-microfluidic preparation methods are presented here. For reviews with more production methods, see the following publications (Walde *et al.* (2010)) (Kamiya & Takeuchi (2017)) (Patil & Jadhav (2014)).

**Gentle hydration.** One of the first methods for the preparation of giant vesicles, described by Reeves and Dowben, is the hydration of a dried lipid film (Reeves & Dowben (1969)). During the gentle hydration method a dried lipid film is slowly hydrated. This method is commonly used due to its simplicity and mild conditions. However, it takes a long time which might lead to lipid oxidation or degradation of substances to be encapsulated and uncharged lipids and salt in the buffer can lead to low-efficiency (Osaki *et al.* (2011)).

**Electroformation.** Electroformation is now the most widely used method for the preparation of GUVs and was described first by Angelova and Dimitrov in 1986 (Angelova & Dimitrov (1986)). It is part of a group of preparation methods starting from a dried lipid film. As shown in Figure 2.1 lipids are dried on an electrically conductive glass surface (usually coated with indium tin oxide (ITO)) and then hydrated while an

electric field is applied. Depending on the conditions a relatively homogenous solution of unilamellar GUVs can be produced (Walde *et al.* (2010)). The lipids are usually stored in organic solvents which are fully evaporated before the hydration. Therefore the removal of solvent after the GUV formation is not a problem. The application of an electric field speeds up the production process compared to other hydration methods.

Electroformation is a widely used method for several research applications for example

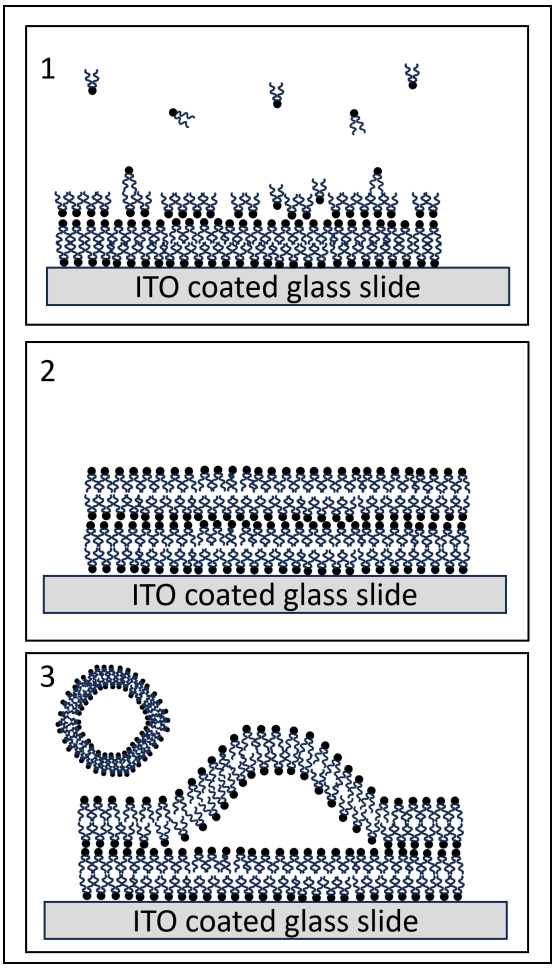


**Figure 2.1:** Schematic image showing the electroformation process. A lipid solution is spread on an ITO glass slide (1) and the organic solvent is evaporated resulting in a dried lipid film (2). The lipids are then hydrated with a buffer and an alternating electric field is applied which leads to the formation of GUVs (3).

to study membrane biophysics or protein reconstitution in the membrane (Schmid *et al.* (2015)).

However, there are a couple of drawbacks of this method. Lipid oxidation can be caused by charge transfer from the electrode (Zhou *et al.* (2007)) and preparations using lipid mixtures do not necessarily result in equal distribution of lipids (Morales-Penningston

*et al.* (2010)) (Steinkühler *et al.* (2018)). Also ageing of the ITO slides can affect the quality of the GUV and encapsulation of molecules during the formation is inhomogeneous and especially for large molecules inefficient (Walde *et al.* (2010)). Electroformation has also been used to produce polymersomes (compartments with polymer walls instead of lipid membranes) (Kunzler *et al.* (2020)).
There are also examples of liposome production via electroformation on a microfluidic chip (Estes & Mayer (2005)) (Kuribayashi *et al.* (2006)). The flow chamber was used to introduce a buffer with high ionic strength at the end of the electroformation process and for fusion assays (Estes *et al.* (2006)). The advantage of the preparation inside a microfluidic channel was the high concentration of vesicles and the possibility to easily add various fusiogenic agents (Robinson (2019b)). Figure 2.2 shows vesicles prepared

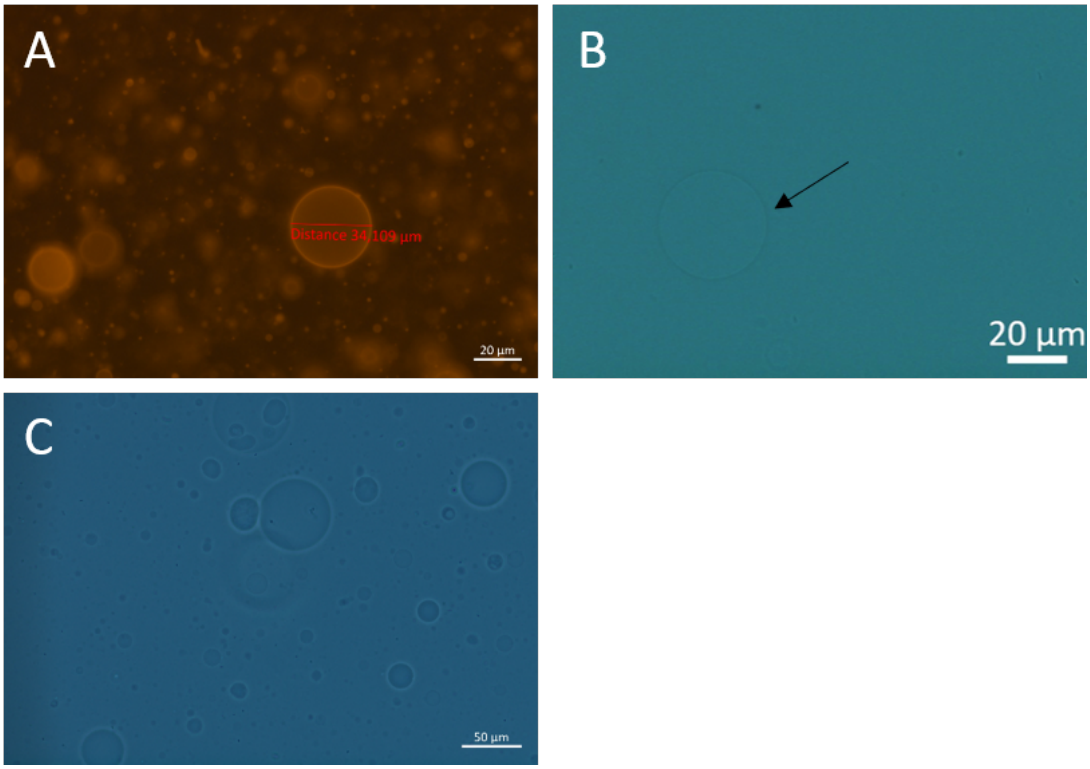


**Figure 2.2:** Microscopic images of vesicles prepared with electroformation (A) fluorescence with rhodamin in membrane (B) brightfield (C) phase contrast mode.

by electroformation. As visible in Figure 2.2A, this method produces a huge range of vesicle sizes and also some lipid structures that are not vesicles but look like threads of one or several lipid layers. The majority of GUVs produced with this methods are unilamellar, however a certain number of GUVs contain either other GUVs or SUVs, which are encapsulated during the production process. For the experiment shown in Chapter 4 of the thesis electroformation vesicles were used.

**Droplet transfer method.** It is also possible to form liposomes from a lipid-stabilized water-in-oil (w/o) emulsion, the inverted emulsion or droplet transfer method (Pautot *et al.* (2003b)) (Moga *et al.* (2019)) (Walde *et al.* (2010)). The latter method does not use dried lipid films but lipids dissolved in an organic phase.

Figure 2.3 shows the key steps of the droplet transfer method. First a lipid monolayer

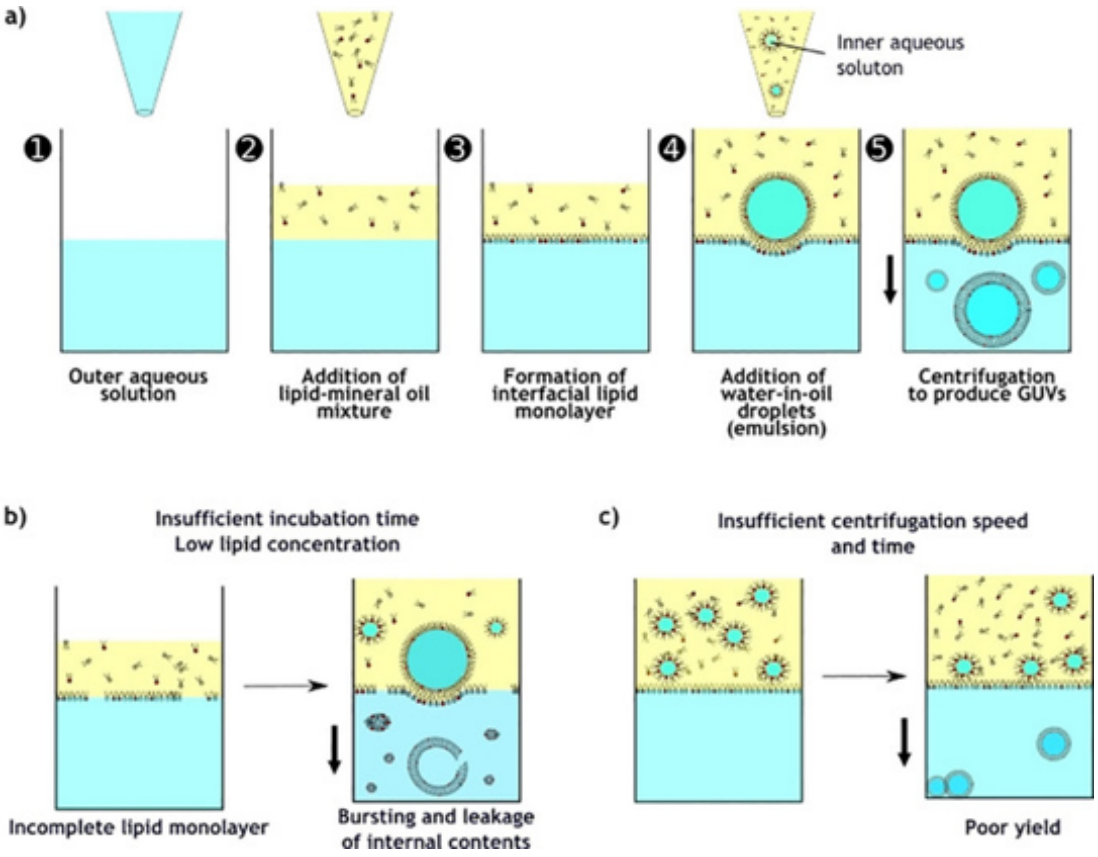


**Figure 2.3:** Schematic image showing the steps of the droplet transfer method. Image from (Moga *et al.* (2019)).

forms on a water-oil interface. Then an already prepared w/o emulsion is added to the top oil phase followed by a gentle centrifugation step to support the GUV formation. Compared to electroformation the encapsulation of a wide range of molecules is easier and, due to the separate formation of the inner and outer lipid monolayer, the creation of asymmetric lipid bilayers is possible (Pautot *et al.* (2003a)).

This method is the batch version of the microfluidic double emulsion method presented in this chapter.

### 2.1.2 Microfluidic GUV production

Additionally there are several microfluidic production methods. While most microfluidic liposome production methods focus on GUVs, there are also microfluidic designs for SUV production (Kastner *et al.* (2014)).
Some of the classic non-microfluidic methods have been transferred to microfluidics for specific applications.
In the microfluidic jetting method an aqueous solution is shot by a pulsed microfluidic jet at a phospholipid bilayer (Stachowiak *et al.* (2008)).
Continuous droplet interface crossing (cDICE) is a variation of the double emulsion method. A capillary is fixed in the middle of a rotating disk and droplets of an aqueous solution are pushed though an organic layer driven by centrifugal forces (Abkarian *et al.* (2011)). The main advantage compared to other microfluidic methods is the relatively simple setup.
Droplet stabilized GUVs were developed by the Spatz group by picoinjection of SUVs into a water droplet inside a microfluidic system (Weiss *et al.* (2018)). The smaller vesicles are fused and form a mechanically stabilized GUV inside the droplet.
The earlier mentioned droplet transfer method is the most common method used with microfluidic setups. Disadvantages are that they are often based on PDMS which requires some channels to be hydrophilic and others to be hydrophobic, adding another step to the setup. Furthermore not all chemicals are compatible with PDMS (Robinson (2019b)). Because of the importance of this method for the work presented in this thesis, the already published approaches, materials and designs will be reviewed in detail in the next subsections.

In conclusion microfluidics can be used to create a high number of vesicles under controlled conditions leading to uniform size and concentration of encapsulated material. General advantages of the microfluidic methods are monodisperse liposomes, high encapsulation efficiency and continuous production. The main disadvantage that all the microfluidic methods have in common is the often complex setup. Therefore, a lot of equipment and experience is necessary just to get started with the production. Most of the non-microfluidic methods require very little to no specialized equipment and the methods can be learned in one or two days.

#### 2.1.2.1 Chip materials

While there is a plethora of materials available for microfluidics (Li *et al.* (2008)) (Zhang & Haswell (2006)) for double emulsion production either PDMS (Polydimethylsiloxane) or glass is used.
Certain application may require a high speed of fluid flow which can lead to very high pressure inside the chip and this can make certain materials unfit for this specific experiments (Kenis & Stroock (2006)). However, this was not a problem with the applications

presented in this thesis. The material of which the device is made is important for the double emulsion process, as it influences the organic phases that can be used.
The Weitz Group was the first to publish a double emulsion method using glass capillaries (Shum *et al.* (2008)). Each capillary can be treated before the assembly. The disadvantage is the difficult assembly and no possibility to integrate several functionalities on one chip. The Huck group published promising results of vesicles prepared with a glass capillary device and chloroform/hexane as the organic phase (Deng *et al.* (2017)).
The other main material is the polymer PDMS, which is one of the most commonly used materials for microfluidics in general (Mata *et al.* (2005)) (Quake & Scherer (2000)) and has been used to produce chips for double emulsion production (Petit *et al.* (2016)) (Deshpande *et al.* (2018)) (Karamdad *et al.* (2015)).
PDMS is thermally stable, chemically inert and permeable to gases (Mata *et al.* (2005)) and can be chemically modified. Its surface is hydrophobic and requires a hydrophilic coating for the double emulsion production which is discussed in Section 2.2.2. A disadvantage is that it is also permeable to certain solvents.
As the PDMS is usually attached to glass coverslips many groups use actually a combination of glass and PDMS which has to be considered for example when choosing a coating method. The Dekker group described that they also coat the glass with a thin layer of PDMS to have PDMS on all sides of the channel (Deshpande & Dekker (2018)). During the experiments shown in this Chapter it was never tested if it makes a difference to coat the glass surface with PDMS.

#### 2.1.2.2 Microfluidic chip designs

Figure 2.4 shows the most common design strategies for double emulsions. Figure 2.4a and b are PDMS channels and Figure 2.4c is a glass capillary design. The PDMS designs all have three fluid inputs for inner, organic middle and outer fluid. There are two ways how the double emulsion is created. As visible in Figure 2.4a there are two junctions, at the first junction a water-in-oil emulsion is created and at the second junction the double emulsion. The other design (Figure 2.4b) creates the double emulsion in one spot where all three fluids meet at once.
There are a couple of other variations in different designs mostly changing the length of the channels between the inlet and the junction or between the two junctions. Additionally there are differences in the designs after the double emulsion production is done. This will be explained in Section 2.3.

### 2.1.3 Encapsulation efficiency

The encapsulation efficiency and the general possibility to encapsulate a wide range of substances are crucial for bottom-up synthetic biology. Therefore GUV production

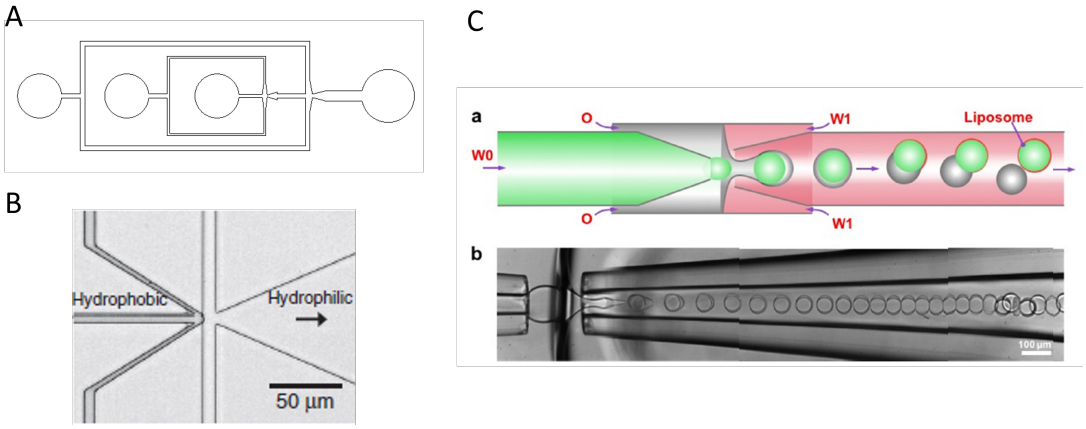


**Figure 2.4:** Design by (A) Julien Petit (from (Petit *et al.* (2016))), (B) design from the Dekker group (from (Deshpande & Dekker (2018))) and (C) design from the Huck group using glass capillaries (from (Deng *et al.* (2017))).

methods have to be chosen in regard to their encapsulation potential and possibly optimized to allow efficient encapsulation of a wide range of buffers, large biomolecules, nanoparticles and also other vesicles from SUVs to smaller GUVs without destroying their functionality in the process.

In general encapsulation of large molecules or charged compounds is not efficient via electroformation (Walde *et al.* (2010)). Substances can be added afterwards via microinjection (Wick *et al.* (1996)). However, the volume that can be injected without rupturing the vesicle is relatively small. There are a few methods how encapsulation efficiency can be enhanced. Dominak and Keating show a positive effect of macromolecular crowding on the encapsulation efficiency of fluorescent polymers (Dominak & Keating (2008)).

The aforementioned transfer of the electroformation method into a microfluidic flow chamber opened the possibility to add a solution with high ionic strength at the end of the electroformation procedure and successfully exchange the encapsulated buffer (Estes & Mayer (2005)). The microfluidic cDICE method was optimized in regard to its encapsulation efficiency specifically to allow future synthetic biology applications (Van de Cauter *et al.* (2021)).

In Section 2.5.1 results of a fluorescent dye encapsulation with electroformation and the microfluidic double emulsion method are presented and further encapsulation experiments are shown in Chapter 3.

## 2.2 Microfluidic double emulsion production

### 2.2.1 Microfluidic designs

Figure 2.6 shows an image of the double emulsion production. The second junction is visible with water-in-oil droplets coming from top and the outer fluid arriving from the sides.

Figure 2.7 shows two of the designs that were developed within this work. The general

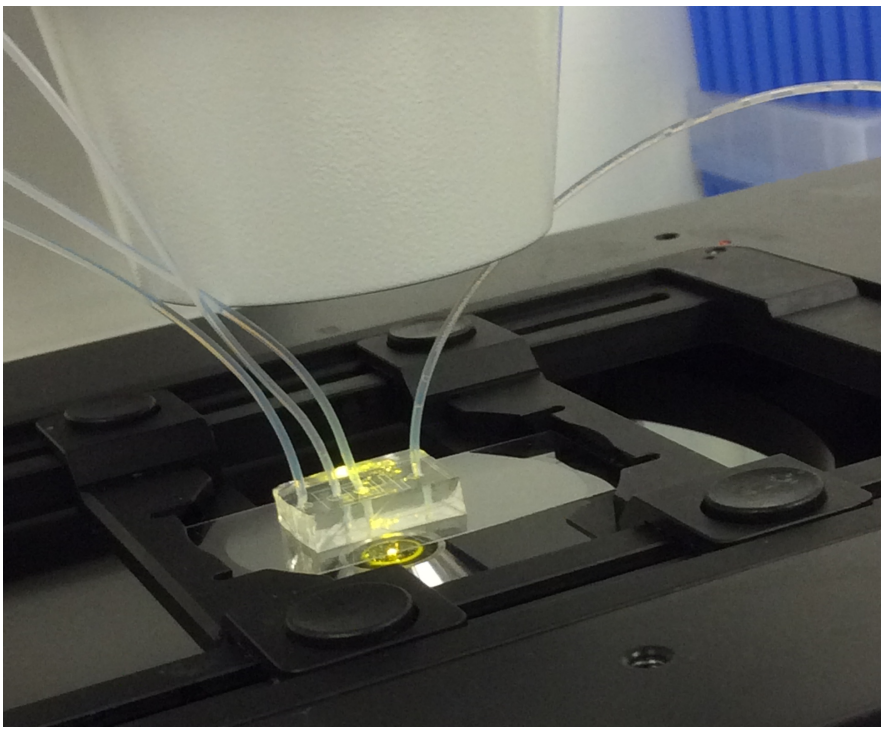

**Figure 2.5:** Double emulsion chip during operation.

principle is the same as in the Petit design (Petit *et al.* (2016)) with three inlets and a double junction. One change in the design compared to the original one by Petit et al was to extend the length of the channel between the second junction and the outlet hoping the oil could be removed. Additionally several designs with varying channel sizes were made to test if they would produce vesicles of different sizes. During tests of the chips it became clear that the flow speed of the liquids had a stronger influence on the vesicle size than the channel widths.

In later designs the channel widens shortly before the outlet (visible in Figure 2.7A) because it happened frequently that there were particles in the outlet part that broke the double emulsions.

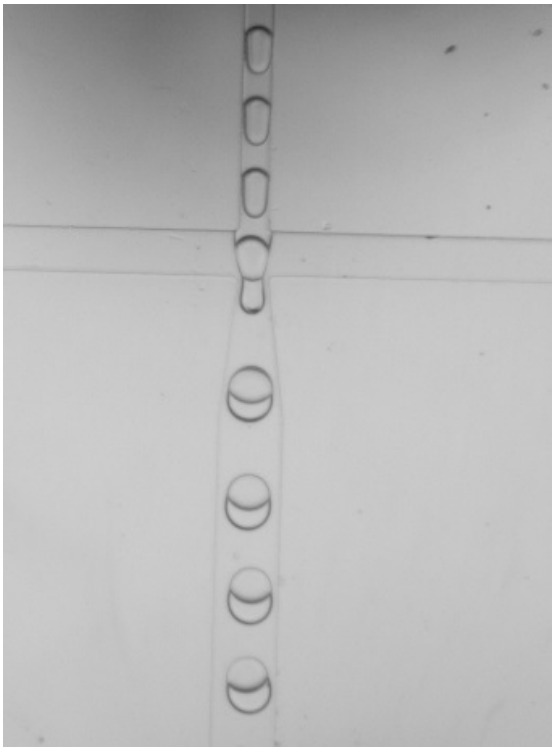

**Figure 2.6:** Microfluidic double emulsion production.

### 2.2.2 Channel coating

PDMS is a hydrophobic material. When using two different liquids inside the chip, one hydrophilic (water) and the other one hydrophobic (organic phase), to form an emulsion the presence or absence of an hydrophilic wall coating controls which of the liquids becomes the outer liquid of the emulsion and which one the inner one.
When the goal is to produce a simple water-in-oil emulsion no coating is necessary because the oil will naturally be the outer phase. This is what happens in the chips used for this work after the first junction. However, an oil-in-water emulsion with oil drops dispersed in water as the outer phase would not be possible if the chip was not coated. This is the desired effect at the second junction.
Figure 2.8 shows the chip without coating. At the first junction the w/o emulsion is formed but at the second junction, instead of a double emulsion, more w/o emulsions with the outer fluid are formed.

A number of methods for channel coating has been published and a couple of them have been tested. The channel coating method described by Petit (Petit *et al.* (2016)) includes three different solutions which are run though the OF channel. In Figure 2.9 it is visible which of the channels inside the chip were coated and which had to be kept free from the coating agent. First the channel was oxidised using a 1:1 mixture of hydrogen peroxide and hydrochloric acid. Then, after washing the channel with water,

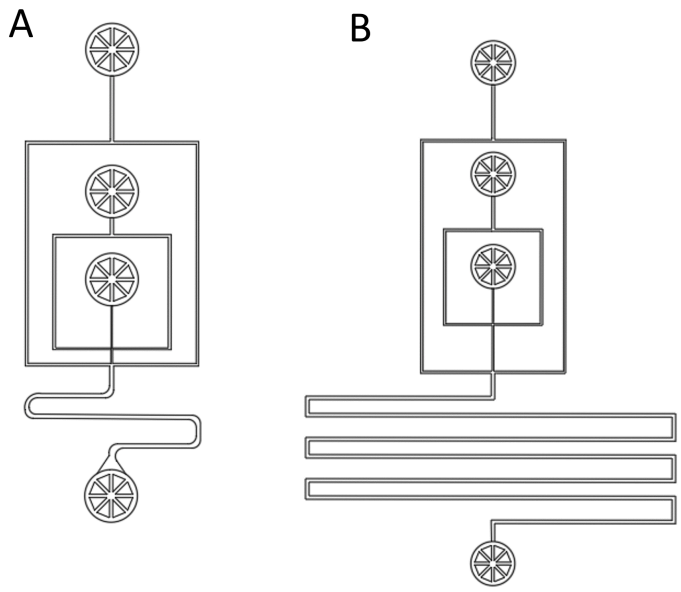


**Figure 2.7:** Two new designs with different outlet lengths.

first the positively charged polymer poly(diallylammonium chloride) (PDADMAC) and afterwards the negatively charged polymer poly(sodium 4-styrenesulfonate) are flushed through the channel.

The Dekker group published a detailed protocol of their chip production and operation, including the coating procedure. After the plasma bonding there is a 4 hour resting time before the coating is done. The channels are coated with a 2,5% (wt/vol) PVA (Poly vinyl alcohol) solution inserted through the outer channel, the channels for the inner and middle fluid are filled with air. Once the correct channel is filled with PVA it is incubated for 3-5 minutes, the PVA is removed and the chip is baked at 120 °C for 15 minutes (Deshpande & Dekker (2018)).
Earlier Teh et al. published a coating procedure very similar to the Dekker protocol whereby the main difference was that the coating was performed directly after the plasma bonding without the 4 hour incubation time (Teh *et al.* (2011)).

All three methods mentioned above were tested with the presented setup. The method described by Petit was used in the beginning and worked with a few adjustments. Mainly the polymer solutions were more diluted to make them less viscous. However, this method has some disadvantages. The procedure requires substantial preparation time as the hydrogen peroxide and the HCl have to be mixed directly before the pro-

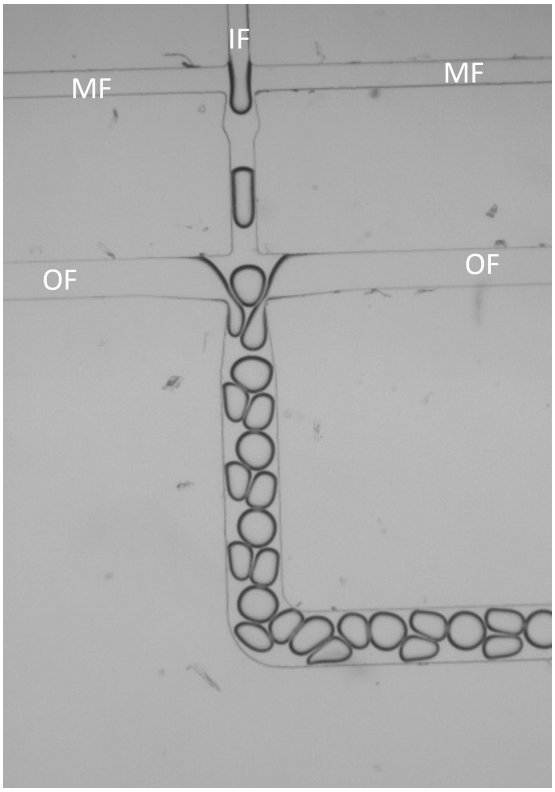


**Figure 2.8:** No coating - no double emulsion, oil phase remains outer phase. The droplets at the first and second junction are formed from IF and OF while the MF remains as the outer phase after the second junction. IF=aqueous inner fluid; MF: organic middle fluid; OF: aqueous outer fluid.

cedure. Moreover, the mixture is more hazardous and therefore requires caution when handling. Another problem is that the chips have to be used on the same day as the coating usually lasts only for around 12 hours.
Channel coating using PVA is a much simpler and less dangerous alternative. PVA has been shown to irreversibly absorb to surfaces of various materials such as silicon and hydrophobic polymers (Kozlov *et al.* (2003)) and, using cycles of incubation and heat immobilization, a hydrophilic coating, that can last for several months, is formed (Wu *et al.* (2005)).
The coating solution was usually inserted through the outlet hole and removed via the OF inlet hole. Figure 2.6 shows a double emulsion production with a PVA coated chip. Some protocols mention that the channels for the inner and middle fluid are blocked during the coating procedure. The current experiments showed that a complete blocking of the channels often results in a backflow of the coating solution into the middle channels which makes the chip unusable because the water in oil droplets are not formed properly.

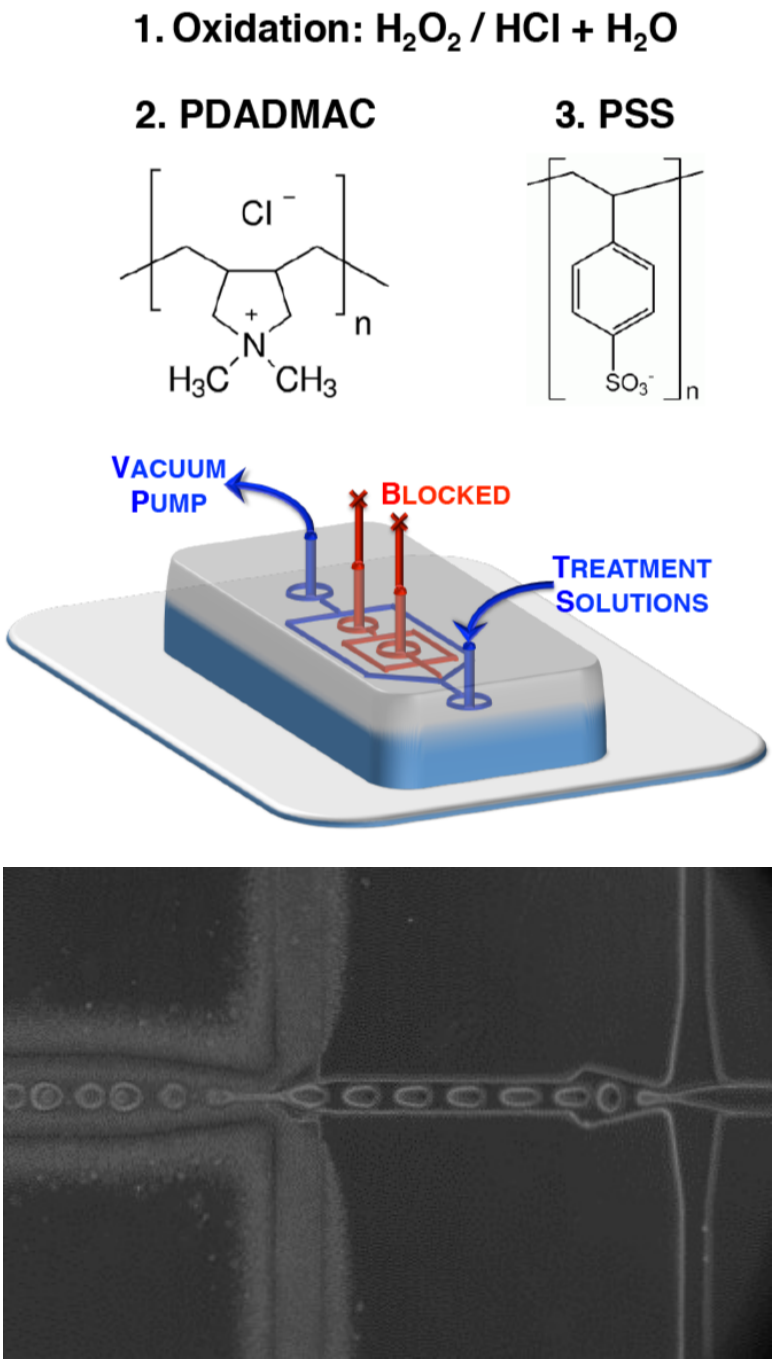


**Figure 2.9:** Microfluidic channel coating procedure from (Petit *et al.* (2016)) and an image of the coated channel with the Petit method.

The dewetting chip did not need hydrophilic coating, however, to improve vesicle sta-

bility it was coated with BSA.

### 2.2.3 Fluid compositions

Figure 2.10 shows an image of the double emulsion chip with the different fluids. In this section the composition of the three fluids and the functionality of the components are described.

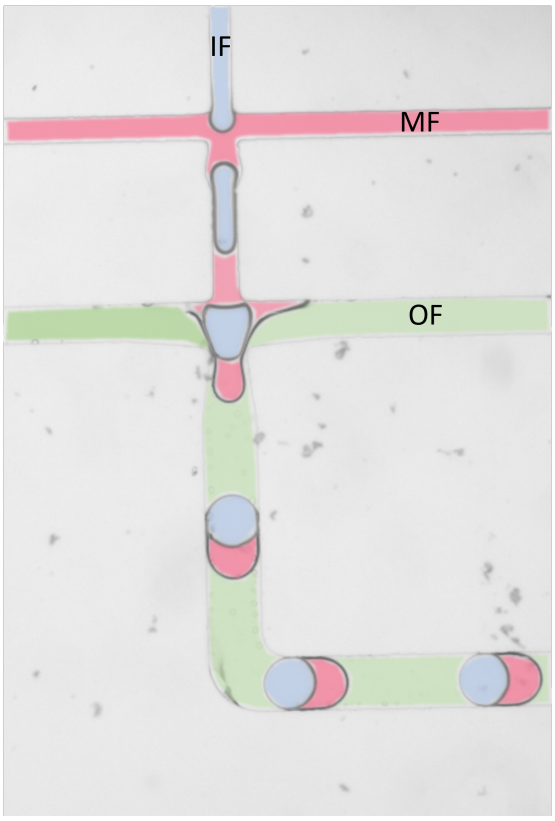


**Figure 2.10:** Double emulsion production with highlighted fluids. Inner fluid (blue), middle fluid (red) and outer fluid (green).

Inner fluid:
The inner fluid is based on water and usually contains also sucrose. The sucrose concentration was usually between 50 and 200 $\mu$M l$^{-1}$ and was added to balance the osmotic pressure with the outer fluid. A surfactant, usually either Pluronic F108 or P188, was added in concentrations between 1 and 5 % to stabilize the water/oil interface during the production process. The surfactants and their properties are described in more detail later in this thesis. Because the surfactant denatured the enzyme horseradish peroxidase (results shown in section 3.3.1) it was tested if it is necessary to add it to the inner solution. As a result it was found to be optional as long as it is added to

the outer fluid. Finally, a buffer and various substrates were added depending on the application. The buffer was usually adjusted to provide a suitable environment for the substrate. Sometimes fluorescein dextran was added as a fluorescent dye.

Middle fluid:
The middle fluid is composed of an organic phase with the phospholipids or polymers dissolved inside and on the surface. The organic phase serves as a carrier for the lipids and should be removed to the best possible extent after the double emulsion formation. The lipids described in the literature are usually the standard lipids used for vesicle generation like DOPC while in this thesis for most experiments alpha-PC lipids were used.
Additionally nile red, a hydrophobic dye, or lipids modified with rhodamine were added to the organic phase. It both made the double emulsions visible in fluorescent microscopy and served, in case of nile red, as a quality control for the removal of the oil from the membrane.There is a number of organic phases described in the literature and some were tested here for their suitability. Their properties and the experimental results will be described in detail in the following section.

Outer fluid:
The outer fluid contains a surfactant to stabilize the double emulsion, glycerol (for example 14%) to increase shear forces and sucrose in a similar concentration as in the inner fluid to balance the osmotic pressure. Various publications mention the addition of ethanol in concentrations up to 15% but it was found to be optional and did not improve results.

Different organic phases, described in literature, were tested for the double emulsion generation. Due to their importance in the production and their varying properties they will be described in more detail in the following three subsections. Dewetting of the double emulsions and possible explanations are mentioned briefly throughout the chapter and will be explained in detail in Section 2.3.

#### 2.2.3.1 Oleic acid as organic phase

Initially oleic acid was used as an organic phase and 28 v% ethanol was added to the outer solution as described in (Petit *et al.* (2016)). This method produced stable double emulsion at first but no dewetting was observed and the inner volume decreased during the course of several days.
Subsequently the ethanol concentration was decreased to 15 % as described by Teh et al (Teh *et al.* (2011)). The double emulsions stopped shrinking but there was still no dewetting.

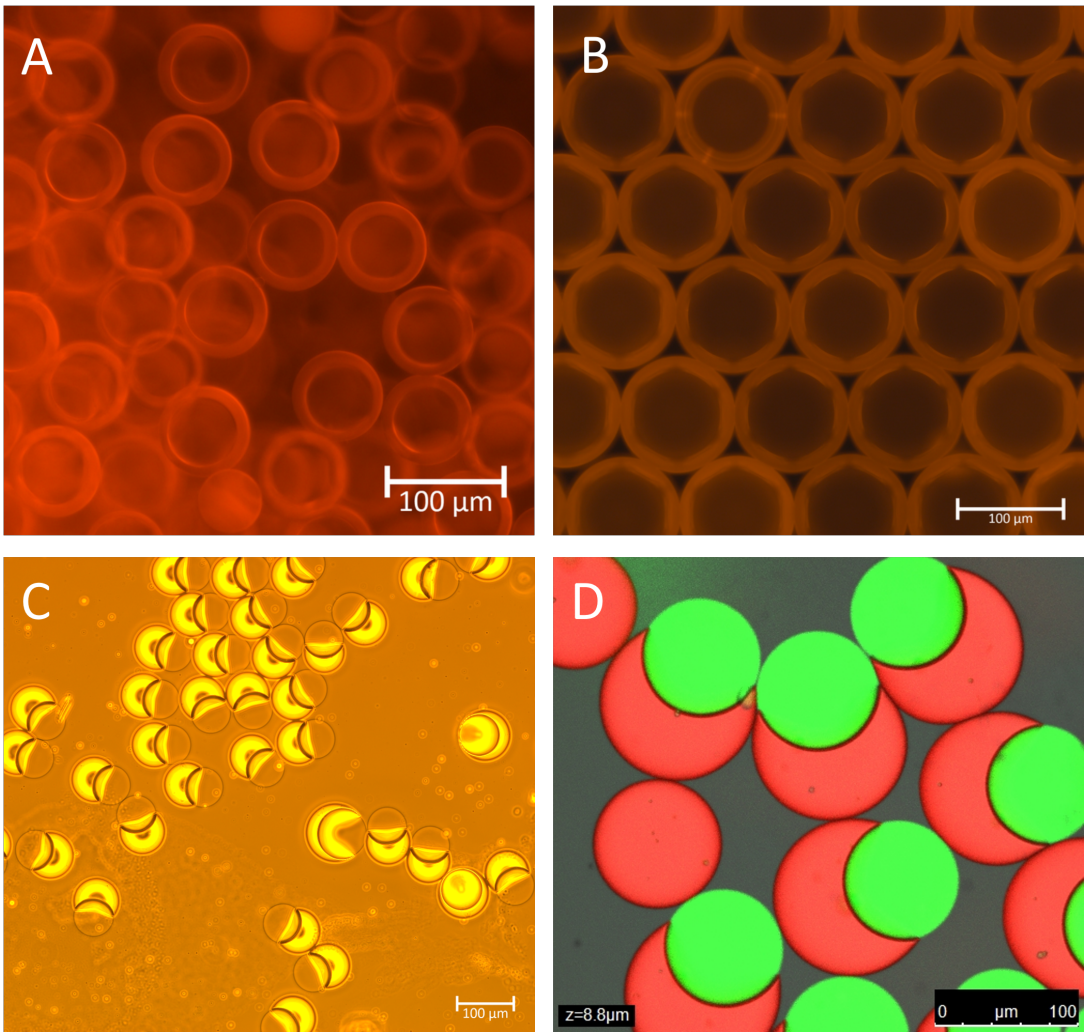


**Figure 2.11:** Images of oleic acid double emulsions recorded with fluorescence (A and B), brightfield (C) and confocal (D) microscopy.

After the initial repetition of published results did not work and in order to understand the system and the role of the individual components better, the fluid compositions were simplified and individual components were added step by step. The table below shows the combinations that were tested to determine a minimal fluid composition.

| | Inner Fluid | Middle fluid | Outer fluid |
|---|---|---|---|
| 1 | $H_2O$ | oleic acid | $H_2O$ |
| 2 | $H_2O$ | oleic acid + 1% PC | $H_2O$ |
| 3 | $H_2O$ | oleic acid | $H_2O$ + 1 % F108 |
| 4 | $H_2O$ | oleic acid + 1% PC | $H_2O$ + 1 % F108 |

The first combination was not sufficient to produce double emulsions inside the chip at all. The second and third combination did lead to double emulsion formation at the second junction but they were so unstable that they broke before leaving the chip. The lipids in combination 2 worked as a surfactant but it took some time for them to form a monolayer at the oil water interface. The bulk double emulsion method works without surfactants in the water phases but is much slower than the microfluidic method and some protocols also include an incubation time for a monolayer to form at the interface. The fourth combination appears to be a minimal system to form stable double emulsions. However, no dewetting could be observed after the production.

**How long does it take to stabilize the water oil interface with a surfactant?**
To form stable droplets that do not coalesce when they touch each other and to form stable double emulsions a surfactant has to stabilize the water oil interface. In the present case at least one surfactant should be phospholipids to form the desired bilayer. Thutupalli and colleagues have investigated the influence of added flow on the time a detergent needs to assemble at the interface (Thutupalli *et al.* (2013)). With respect to the droplet transfer method mentioned in the introduction, the majority of the protocols for this method usually require long incubation times for a lipid monolayer to assemble at the interface. As the double emulsion method is based on the same mechanism why does the surfactant stabilize the interface so much faster?
In both methods the lipids are initially dissolved in the oil phase. If the lipid concentration inside the oil exceeds the critical micelle concentration (CMC) the lipids self assemble as micelles. CMC of eggPC in water is between 5 and 50$\mu$M/l (Haberland & Reynolds (1975)).
In the present case the CMC of eggPC inside oleic acid is relevant, however, no data has been published about it so far. If the concentration is above the CMC and there is an interface, the lipids form a monolayer. In the batch method the speed of the monolayer formation depends on the concentration of lipids in the solution and diffusion of the lipids.
Moga and colleagues optimized the batch method and showed that higher lipid concentrations and longer incubation times lead to an increased GUV yield. They tested incubation times between 5 and 60 minutes (Moga *et al.* (2019)).
Figure 2.12 shows an experiment by Thutupalli et al with lipid dissolved both in the organic and the aqueous phase taking around 17 minutes to decrease the interfacial tension that the formation of a monolayer can be assumed (Thutupalli *et al.* (2013)). In the microfluidic double emulsion method the monolayer has to establish within milliseconds to create a stable double emulsion. Usually additional surfactants are added to the inner and outer solution to prevent the double emulsion from collapsing. The experiments described above to determine a minimal system show that without lipids or other surfactants there is no double emulsion formation. The addition of 1% PC to the organic phase leads to double emulsions which are quite unstable.

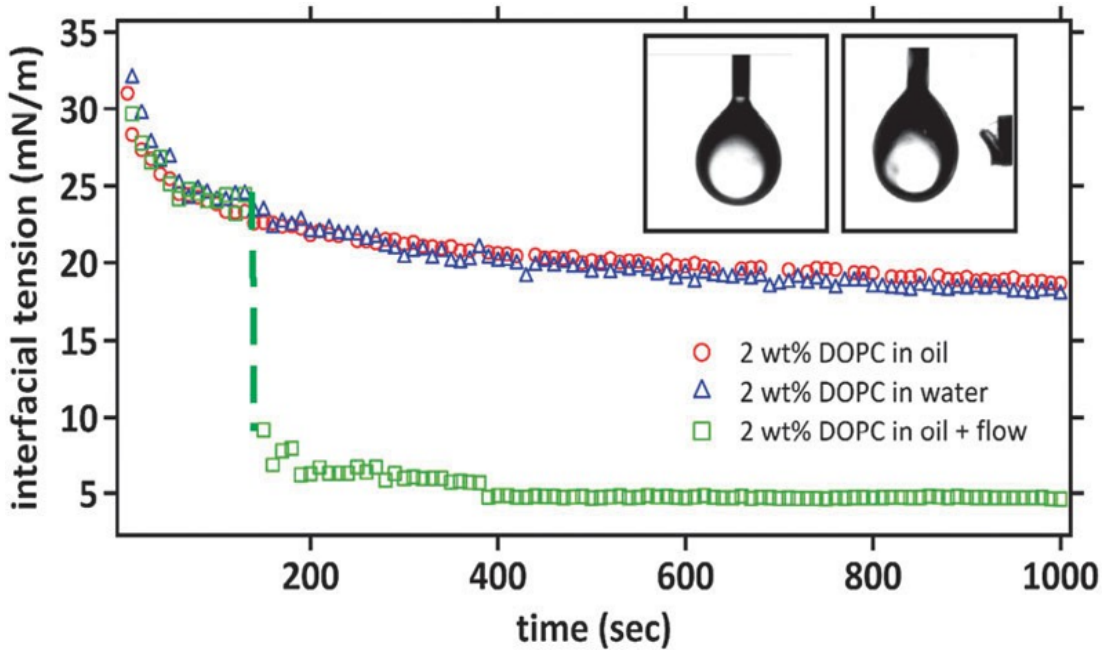


**Figure 2.12:** Water droplets in hexadecane and their interfacial tensions over time. In the curve with the green squares flow in the hexane phase was induced with a needle. From (Thutupalli *et al.* (2013)).

The minimal stable system that could be determined has lipids in the organic phase and an additional surfactant in the outer solution. The experiments of Thutupalli (green graph in Figure 2.12) show that the addition of flow in the organic phase leads to a sudden, sharp drop in the interfacial tension. Further experiments in microfluidic systems showed that additional flow of an oil phase with lipids prevented two water phases from coalescing and lead to the formation of a lipid bilayer between the water phases within milliseconds (Thutupalli *et al.* (2013)).
In the main microfluidic design used in this thesis the time intervals are probably still too short for the interfaces to stabilize completely without additional surfactant. However, these experiments suggest that if the time between the first and the second junction and between the second junction and the outlet could be extended, the double emulsion production could be done completely without surfactant and the problems induced by the surfactant could be avoided. The time intervals could be mainly extended by changing the design and increasing the distances between the first and second junction and the outlet.
An additional but smaller impact could be achieved by reducing the flow rates. The distance between the second junction and the outlet is important because it was observed that unstable double emulsions often flow inside the channel without bursting but break at the outlet where the flow can become turbulent and there are often sharp PDMS edges from punching the hole.

Another option would be to prepare the first emulsion on a separate chip or in batch and the double emulsion on a separate chip. However doing the whole process on one chip is in most cases more convenient and there might be a substantial loss of single emulsions in the process and the sizes might be not as uniform.

Oleic acid from Acros organics with a purity of 99% was used for the shown experiments. Later on oleic acid from Sigma Aldrich was used instead with a higher purity of 99.9%. A lot of experiments especially the dewetting could not be reproduced with the new oleic acid.
When a new bottle of the Acros organics oleic acid was bought the original results could be reproduced. This could mean that the interfacical tensions are an important driving force for the initial dewetting and the oleic acid from the two different companies might result in slightly different interfacial tensions with the inner fluid.

#### 2.2.3.2 Octanol as organic phase

Parallel to the above described experiments the replication of other published methods was attempted.
Deshpande et all describe a microfluidic method for double emulsion production with a PDMS chip. They use octanol as the organic phase with a different surfactant from the poloxamer/synperonic group in the inner and outer fluid. They show spontaneous dewetting and splitoff of the organic phase inside the chip after the production.
Figure 2.13 shows the a schematic drawing and fluorescent images of the chip and the

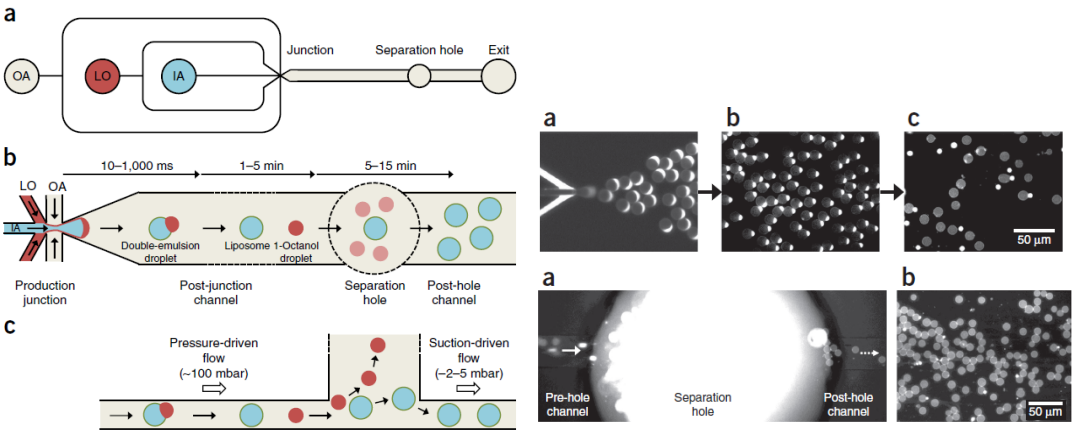


**Figure 2.13:** Schematic drawing of the chip design and fluorescent images from the oil split off and the oil phase separation (from (Deshpande & Dekker (2018))).

oil removal process (Deshpande & Dekker (2018)). A likely explanation why we could not reproduce the spontaneous oil splitoff might be the separation hole and the strongly

varying flow velocities created by this hole. The oil removal shown in this image will be discussed in more detail in Section 2.3.

In the experiments presented here alpha-PC lipids were used by us instead of DOPC and the lipid concentration was increased to 1% inside the octanol solution.
To test if a change of oleic acid to octanol and of the surfactant F108 to F68 would lead to a more simple production method of oil-free vesicles, similar compositions of the oil phase and inner and outer fluids were used while the chip design was not modified.

Variations on the original composition:
Glycerol was replaced with sucrose, because further encapsulation experiments with glycerol as a substrate and membrane diffusion test with glycerol were planned. Sucrose has been also shown to stabilize the membrane (Surewicz (1984)).
An important observation of the experiments shown in Chapter 3 was that the addition of F108 inactivated the enzyme horseradish peroxidase. This led to the worry that it could generally interact with different encapsulated substances.
Therefore it was tested if the surfactant in the inner fluid could be replaced. Inner fluid with only sucrose and no further additions did not lead to stable double emulsions. The addition of PVA to the inner fluid as also described by Deshpande et al (Deshpande *et al.* (2016)) led to stable vesicles without having to add glycerol and surfactant. Glycerol and F108 surfactant were, however, added to the outer fluid to stabilize the double emulsion.
While the double emulsions were stable, no dewetting could be observed with this combination. Adding weakly alkaline and salty buffers to the inner fluid together with oleic acid in the middle fluid often caused clogging of the channels. Because this kind of buffers are a commonly used environment for biological reactions, this is a problem if one aims to create a compartment module for synthetic biology applications. Octanol as an organic phase showed to be more compatible with commonly used buffers in molecular biology such as MOPS (3-(N-morpholino)propanesulfonic acid) buffer.

The first important step in the microfluidic vesicle production is the creation of stable double emulsions. The second step is to remove the oil from the membrane. Several compositions of inner, middle and outer fluid were found that produced stable double emulsions.
However, no combination would lead to complete or even partial dewetting. It was only possible to decrease the thickness of the oil layer by swelling the vesicles (Figure 2.14), which is no active removal of oil and to produce vesicles with a very small amount of oil that would not spread equally on the surface but concentrate in one spot (Figure 2.14).
Since the the flow rates of the different fluids can be adjusted individually, it is often necessary to test different flow speeds every time an experiment is started. The outcome can be influenced by small variations in the channel width and smoothness occurring during the production process and the repeated use of one wafer to produce chips.

Likewise another factor are small dirt particles or not completely dissolved components. Altogether it seems possible to adjust the flow inside a chip so that every double emulsion has very little oil due to the varying flow regimes depending on the capillary number (this effect is explained in detail in Section 2.2.5) resulting in vesicles that appear unilamellar under the microscope. But this method is not always reliably reproducible and the amount of oil left in the membrane usually varies between batches of vesicles and even inside one batch.
Except for microscopy it was not further checked if the majority of membrane is in fact unilamellar. Assuming that the membrane is unilamellar it is additionally unclear what effect an octanol pocket in the membrane would have. It could for example lead to the accumulation of lipophilic substrates inside this pocket. While this effect could have a negative impact on a number of applications it could also be an advantage. One could imagine such a small oil pocket as a reservoir for lipophilic substrates that would be slowly released.
For such an application the reproducible production, long term stability and exchange rates of target molecules would have to be investigated.

Ultimately, after the dewetting described by Deshpande (Deshpande & Dekker (2018)) could not be easily reproduced and while stable double emulsions could be produced but no reliable dewetting occurred, the focus was shifted on oleic acid as the organic phase.
However, the octanol method described here was used to encapsulate an enzymatic pathway because of its compatibility with MOPS buffer in the inner fluid. That experiment is described in Chapter 3.

#### 2.2.3.3 Chloroform hexane as organic phase

Intrigued by the experiments by the Huck group (Deng *et al.* (2017)) especially being interested in the oil removal by interfacial tension mentioned in Section 2.3, a mixture of chloroform and hexane as an organic phase was tested. One challenge was that the used chemicals are volatile and toxic therefore the setup was operated under a fume hood. The standard chips described above were used and not the glass capillaries from the original publications (Deng *et al.* (2017)).
The results are shown in Figure 2.15. There was partial dewetting but not a spontaneous full removal of the oil phase. It is likely that because the organic phase was kept in plastic syringes, went through a plastic pipe and finally was used in a PDMS chip that is permeable for chloroform, the composition of the organic phase changed before the droplets were produced and the surface tension necessary for the split off of the organic phase was not maintained.
Additionally, the surface to volume ratio inside the channels is very high which could increase the evaporation through the PDMS. Due to the difficult handling because of the toxicity of the chemicals this direction was not further investigated and optimized.

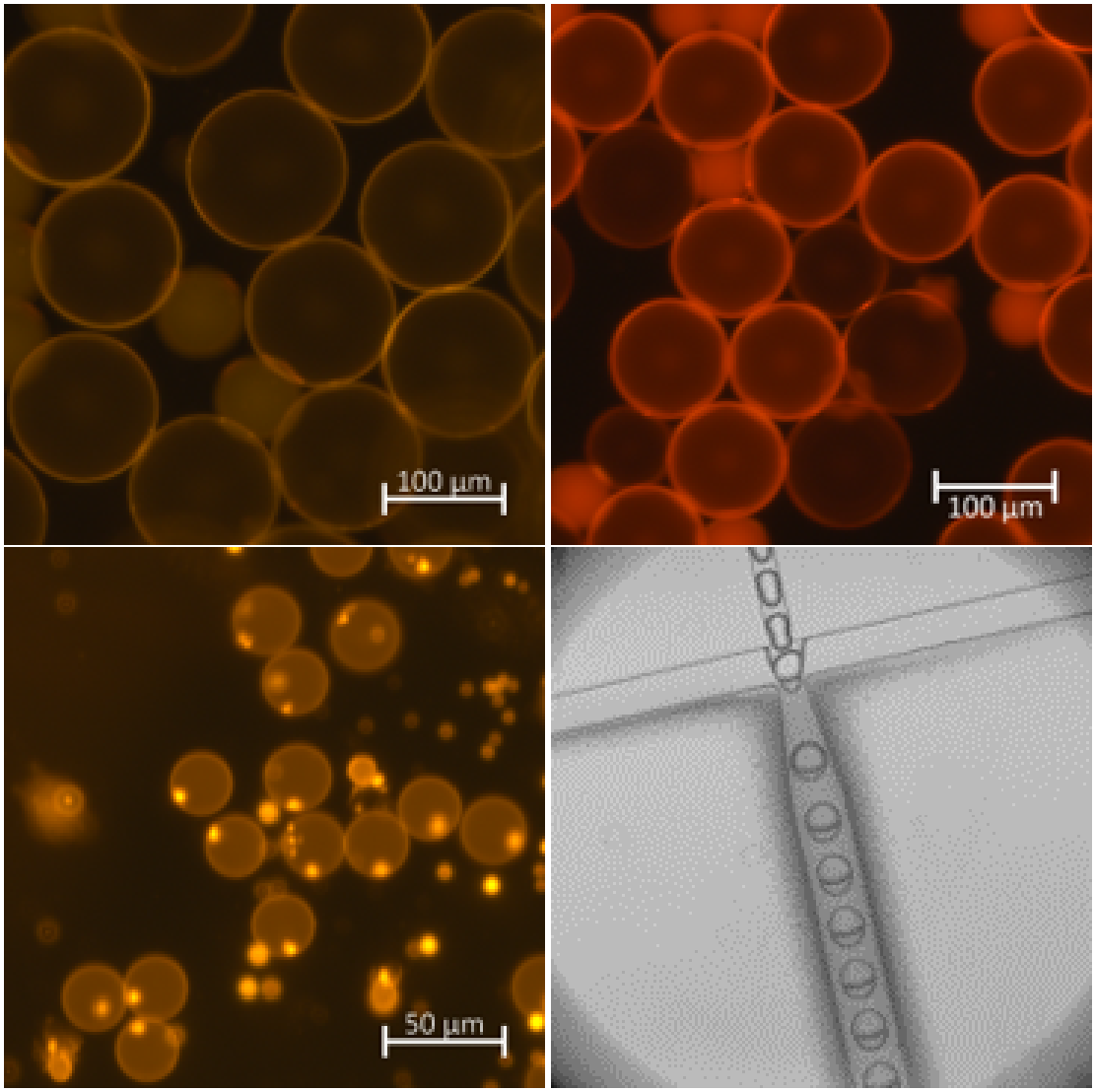


**Figure 2.14:** Octanol double emulsions.

This experiment shows how crucial the material that the microfluidic chip is made of can be for the success of the method.

### 2.2.4 Composition of the aqueous phases

#### 2.2.4.1 Influence of buffers

The influence on ions in buffers on the electroformation process was, next to the encapsulation efficiency, one of the main reasons to look for alternative vesicle production methods. For synthetic biology applications a maximal freedom of buffer choice is desired.

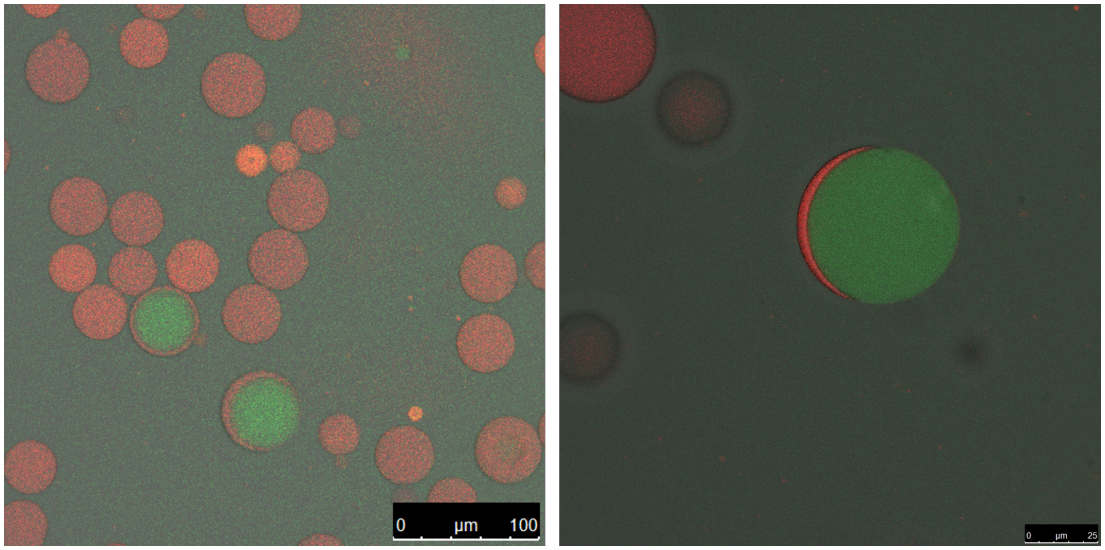


**Figure 2.15:** Confocal microscopy images of chloroform hexane double emulsions. Images are overlay of red fluorescence, green fluorescence and brightfield scans.

In theory the double emulsion method should work with all buffers. However, some buffers especially ones with higher concentrations of ions seem to produce small agglomerates of lipid and buffer which were clogging the microfluidic channels. This happened especially when the chip was used several times.
During the double emulsion production usually there was no problem but before the outer, middle and inner fluid are in a balanced ratio and reach a stable flow they mix and fluids may shortly flow back into the channels of the other fluids.
As the inner fluid contents were concentrated during the osmotic shrinking process described later, using a more diluted buffer was a workaround for this problem.

#### 2.2.4.2 Influence of detergents

To stabilize the water-oil interfaces in a very short period of time surfactants were added to the aqueous solutions. In the literature two surfactants from the synperonic group are described to support the double emulsion formation, F108 (synonym P338) and P188. The structure, nomenclature and membrane interactions of these group of surfactants are described in detail in Chapter 4. The surfactants did help to form stable double emulsions but caused many secondary problems.

Membrane fluctuation is a method to characterise membrane properties and compare various membranes (described in more detail in Section 2.4). Because no membrane fluctuation could be observed in the vesicles produced with the double emulsion method a

few control experiments were done with vesicles produced with electroformation. Normal vesicles showed membrane fluctuation in a solution with a slight osmotic disbalance as expected. Once F108 detergent was added to the solution also the electroformation vesicles did not show any membrane fluctuation.
Based on this observations more experiments were done to investigate the influence of the detergents, used during the production, on the membrane, especially their impact on membrane permeability (results shown in Chapter 4).

Additionally the presence of the surfactants seemed to interfere with enzymatic reactions that were supposed to be encapsulated and the addition of F108 made the measurement of the interfacial tension impossible.
The surfactants were therefore removed from the inner solution but kept in the outer fluid for stability. This made the method accessible for enzyme encapsulation experiments but still prevented several membrane characterization experiments.
Testing how much the surfactant concentration can be decreased and if this particular surfactant can be replaced would be important future tasks to make the method more useful for synthetic biology applications.

### 2.2.5 Parameters influencing double emulsion formation

To optimize the formation conditions it is important to look at the processes during the double emulsion formation in the channel from a theoretical perspective and identify the influencing parameters.
While a lot of theoretical work and models have been published on droplet formation (Seemann *et al.* (2011)), there only few publications on double emulsion formation in microfluidic channels.
A recent publication, however, extended an existing lattice Boltzmann model of double emulsion formation (Wang *et al.* (2020)). This subsection will summarize the most relevant results from this publication.

The two most important parameters in this theoretical work simulating the behaviour of three different liquids in a microfluidic system with two junctions are the capillary number and the interfacial tensions between the liquids.
The capillary number in droplet microfluidics describes the ratio of viscosity to interfacial tension.

$$Ca = \frac{U\mu}{\gamma} \tag{2.1}$$

Ca is the dimensionless capillary number, U is the velocity of the flow, $\mu$ is the viscosity of the fluid and $\gamma$ is the interface tension. An increase in the capillary number means a decrease in the droplet diameter and therefore it influences if small spherical droplets or large plugs are formed (Tice *et al.* (2004)).

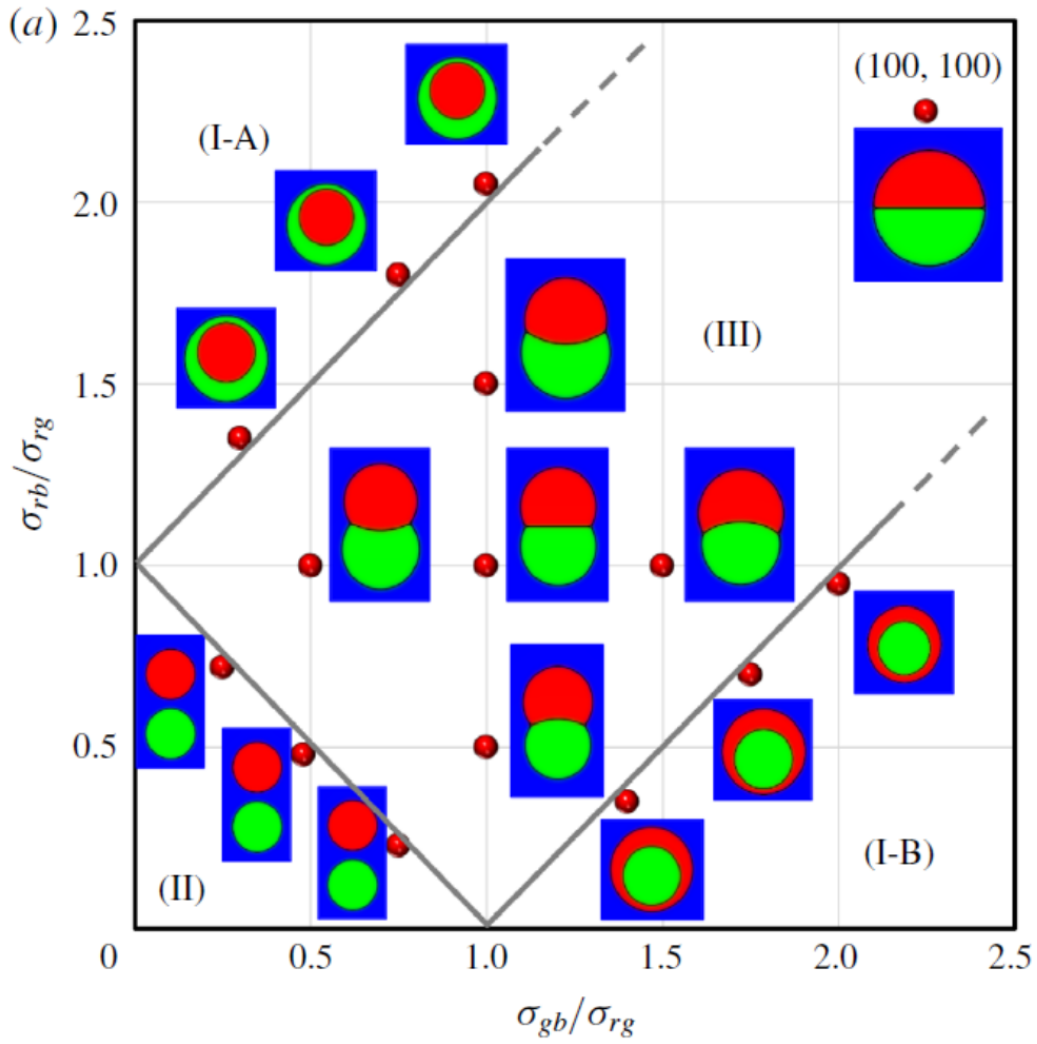


**Figure 2.16:** Morphology diagram for two equal sized droplets (red and green) inside an outer solution with varying interfacial tensions ($\sigma$)from (Wang *et al.* (2020)).

As explained later in this chapter, the interfacial tensions between the inner, middle and outer solutions important factors for the behaviour and interaction of the three solutions. They are crucial for the stability of the double emulsion as well as for the subsequent oil removal.

Wang et al. used their model to show the various morphologies of two droplets of liquids with varying interfacial tensions placed in an outer liquid (Wang *et al.* (2020)).

Figure 2.16 shows the diagram from the publication with the various possible morphologies. Section I-A and I-B show the initial state of the double emulsions after the production. Depending on the composition, the double emulsions would either remain

in this state or the inner solution would partly detach from the middle fluid as shown in Section III.
Section II shows the ideal result, i.e. detached inner and middle fluids.

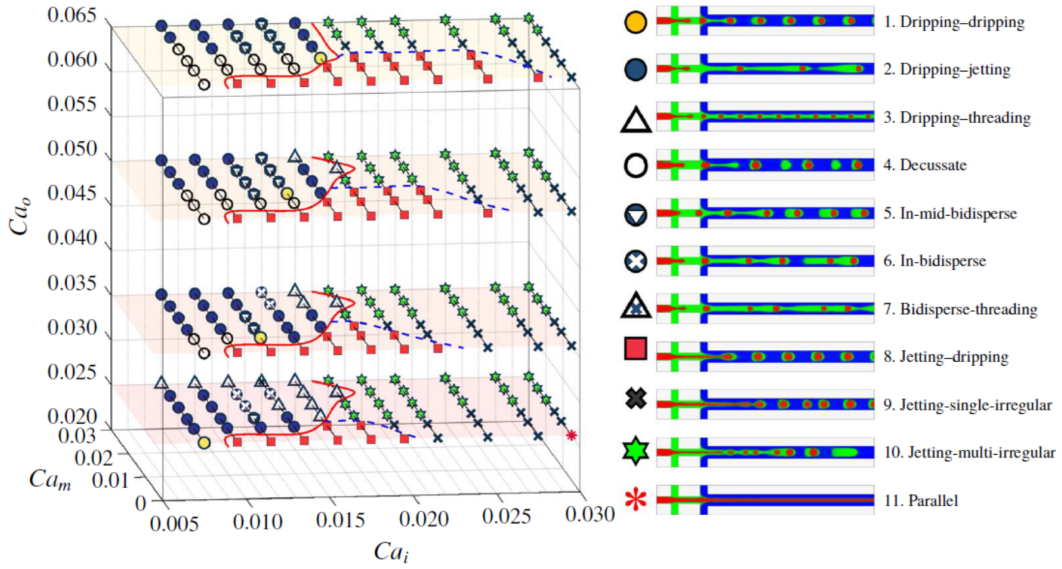


**Figure 2.17:** Flow regimes for varying capillary numbers, from (Wang *et al.* (2020)).

The model is applied to a two junction microfluidic system with three varying liquids, very similar to the design used in this chapter.
Figure 2.17 shows different flow regimes based on variations in the capillary number. The capillary number in this simulation is changed by varying the flow rates of the three different fluids.
Different flow regimes depending on the capillary number have been analyzed and described before for droplet formation (Liu & Zhang (2011)).

The double emulsion formation adds obviously complexity and results in a higher variety of flow regimes. In the experimental setup presented here the preferred flow regime was No. 1 dripping-dripping.
The box on the left in Figure 2.17 shows that this flow regime exist only under narrow circumstances. This results are in accordance with the experimental observations from this thesis. It took quite a bit of practice, experience and daily adjustment to find the right flow rates for the double emulsion production.
These simulation results also show why it is not possible to have fixed flow rates for all experiments. As the flow regimes depends on the capillary number, which is influenced by the flow rates as well as the interfacial tensions, small changes in the interfacial tensions have to be addressed with an adjustment of the flow rates.

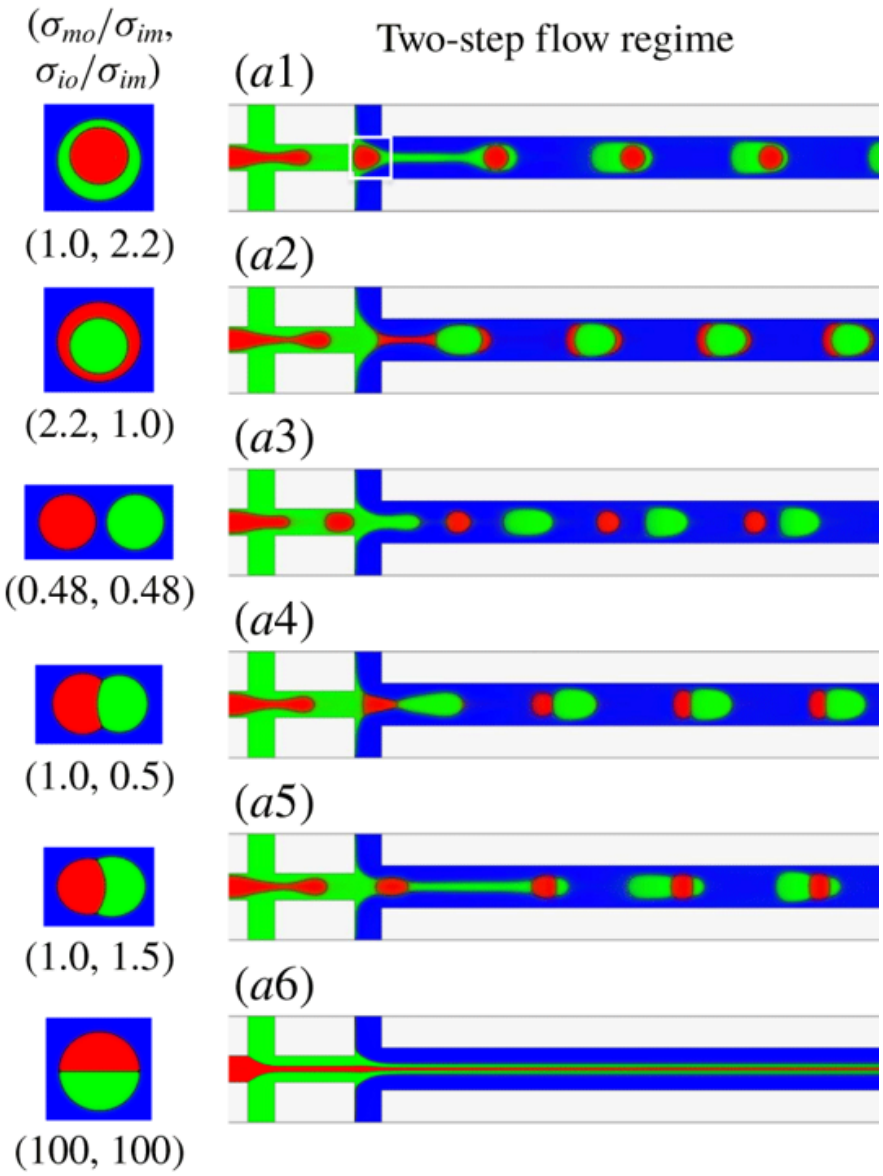


**Figure 2.18:** Emulsion formation behaviours with varying interfacial tensions in a two-step flow regime, from (Wang *et al.* (2020)).

While Figure 2.17 showed the formation behaviour with different capillary numbers, changed by varying the flow rates, Figure 2.18 shows the behaviour of the three solutions inside the channel with varying interfacial tensions.
The experimental conditions shown later in this chapter that resulted in stable double emulsions were likely created under conditions similar to Figure 2.18 a1 and a2.
Interfacial tensions that lead to an immediate separation of the inner and middle fluid

may seem advantageous from an oil removal perspective but from experimental experience do not produce stable liposomes as the lipids inside the middle fluid need some time to form a monolayer at the interface.

Another factor tested with the double emulsion model was the influence of the channel geometry on the double emulsion formation (Figure 13 in (Wang *et al.* (2020)), not shown here).
A variation in the distance between the two junctions did not show any impact on the double emulsion formation.
The width of the channel after the second junction did not have an influence on the size of the inner droplet in a two-step flow regime, which is expected because the droplet is already formed before the second junction. A very wide channel did lead eventually to two droplets with inner fluid encapsulated in one large middle fluid droplet.

The modelling results are in accordance with the experimental observations that were made with varying chip designs. Overall the ratio between the velocities of the three fluids during the production seemed to have a much higher influence on the double emulsion formation than minor changes in channel length or width. Some of the results form the simulation show inner fluid droplets that are completely separated from the middle fluid. As described later in this chapter this is the desired final state for the vesicle production.
Experimental experience, however, shows that this conditions during the formation do not lead to stable vesicles and it is more advisable to create stable double emulsions inside the microfluidic device and later influence the interfacial tensions to achieve a separation of the middle fluid.

## 2.3 Oil removal from double emulsions

Once the double emulsion is formed a crucial and surprisingly challenging step is the removal of the oil ideally creating a phospholipid bilayer. The removal of oil is especially important for synthetic biology applications because the compartment membrane should provide the possibility for the incorporation of membrane proteins and to some extent also diffusion through the membrane like for example carbon dioxide as needed in the example described in Chapter 3 (CETCH cycle).
In the literature several approaches for oil removal are described. While trying to replicate some of those methods, a new method for oil removal was developed using osmotic gradients.
This section will give a short overview of methods described in the literature and observations from the experiments in Magdeburg.

### 2.3.1 Ethanol extraction

The first oil removal approach that was tested was the addition of ethanol to the outer solution described in previous publications (Petit *et al.* (2016)).
However, no oil removal either in form of a dewetting process or some kind of dissolving of the oil could be observed.
Figure 2.19 shows a few examples of double emulsion behaviour with ethanol. Various ethanol concentrations between 5 and 30 vol.% were tested and double emulsions were incubated over several days. But no ethanol concentration showed improvement compared to the control experiment without ethanol.
Figure 2.19a shows double emulsions after the production with 28 vol.% ethanol in the

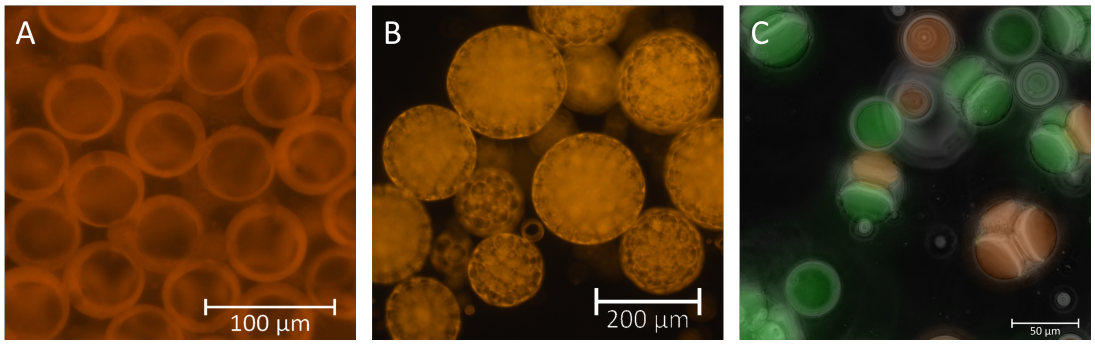


**Figure 2.19:** Images of double emulsions with ethanol in the outer solution. (A) with 28 vol.% ethanol directly after the production, (B) and (C) aggregates formed after several days with 25 vol.% ethanol in the outer solution.

outer solution. They did not show immediate dewetting. After incubation for several days the inner fluid shrank and thick oil droplets with small water bubbles inside remained (picture not shown).
In a different experiment double emulsions with 25 to 30 vol.% of ethanol started to merge and formed large aggregates (Figure 2.19b).
To show that the double emulsions start merging only a certain time after the production two sets of double emulsions were produced with red and green dye inside and mixed. Figure 2.19c shows an image of an aggregate containing water droplets with different content.
The aggregates were not further investigated but should not be left unmentioned as an interesting artefact that might be useful for certain applications in the future.

### 2.3.2 Mechanical forces

Another possible influence are the mechanical forces on the double emulsion while flowing in a microfluidic channel.
This phenomenon is not investigated in detail in any publication but the oil removal in

the design used by the Dekker group might be influenced by different pressures before and after the split off.
In the design with the long channel between the double emulsion formation and the outlet (Figure 2.10) the oil phase seemed to separate continuously while flowing inside the channel but did not detach completely. It is possible that if the channel would be longer or the flow rate could be increased by an additional fluid input or by gradually decreasing the size of the channel, the oil phase could be detached.

### 2.3.3 Interfacial tension

It has been reported that the adjustment of the interfacial tensions between the fluids can lead to complete dewetting of the oil phase (Vallejo *et al.* (2017)) (Deng *et al.* (2016)). The dewetting is defined by the spreading coefficient S which depends on the interfacial tension y between fluids (Deng *et al.* (2016)).

$$S_i = y_{ab} - (y_{ac} + y_{bc}) \tag{2.2}$$

Figure 2.20 shows a schematic drawing of the dewetting based on interfacial tensions. It means that y(IM) has to be larger than either y(OI) or y(MO), resulting in the interface between the inner fluid and the oil phase being energetically unfavourable (Vallejo *et al.* (2017)).

In the experiments presented here, depending on the addition of surfactant, buffer

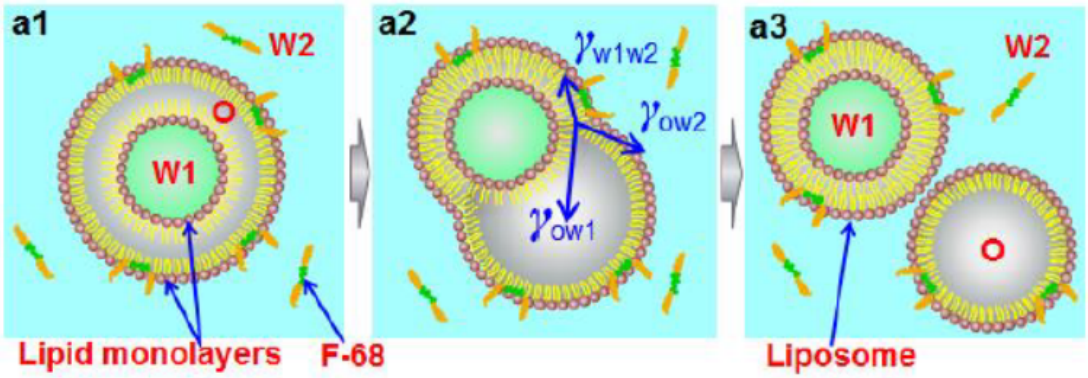


**Figure 2.20:** Image from (Deng *et al.* (2016)).

and sucrose spontaneous partial dewetting could be observed occasionally. The initial partial dewetting is likely caused by a favourable combination of interfacial tensions, however no spontaneous complete dewetting could be observed.

To test to what extent the initial dewetting in the presented experiments was induced by interfacial tensions and to further optimize the compositions the interfacial tensions of the solutions can be measured using a drop tensiometer.
This method uses a capillary filled with water which is dipped into a solution of the

organic phase with a lower density. Due to the higher density the aqueous solution forms a drop at the bottom of the capillary which eventually rips off and falls down (Berry *et al.* (2015)). Firstly the interfacial tension between distilled water and oleic acid with 0,5 wt.% PC was measured and the value was 7,5 mN/m.
Then F108 was added to the aqueous solution to mimic the outer solution. This resulted in a very irregular formation of droplets and a quick rip off. Due to this effect it was not possible to make any measurement with this method.

### 2.3.4 Osmotic gradient

As mentioned before the double emulsions showed spontaneous partial dewetting after their production. Additionally, while observing the double emulsions on a coverslip the ones on the edge seemed to be more dewetted than the ones in the middle. It was hypothesized that this effect could be caused by an osmotic gradient due to the outer solution drying at the edges. A solution with higher osmolarity was added to investigate this effect.
Figure 2.21 shows the effect of an osmotic gradient after the addition of a solution with higher osmolarity in the lower right corner. The arrow shows an increasing degree of dewetting towards the higher concentrated solution and a decrease in size of the vesicle is also visible.

The complete split off of the oil drops from the vesicles often needed an additional stirring of the solution. The detaching of vesicles in a water drop on a coverslip produced only a small number of vesicles and pipetting and further use of the vesicles was difficult.
Therefore another microfluidic chip was used specifically for the dewetting process. The chip design (Figure 2.22a) is very simple and basically represents a wide channel. Figure 2.22b-f shows pictures from inside the chip of different dewetting stages.

The dewetting chip is not necessary for the production of a high number of vesicles. This could be achieved by increasing the outer osmolarity in an eppendorf tube followed by mild centrifugation.
However, with the latter method the detaching process could not be observed and the optimization of the detachment conditions would be therefore more difficult. Moreover the dewetting chip could be attached directly to the production chip with a few adjustments like an additional inlet to change the osmolarity of the outer solution and to dilute the double emulsion solution.
The mechanism of the detachment is not entirely clear. One possible explanation is that the shrinking leads to an excess of already dewetted membrane which makes it easier for the oil to bud off supported by the shear forces present.
The osmotic driven shrinking also does change the concentration of the content in the inner fluid which subsequently changes the interfacial tensions. Vallejo et al. describe a similar experiment and attribute the oil removal to the change in the interfacial tensions

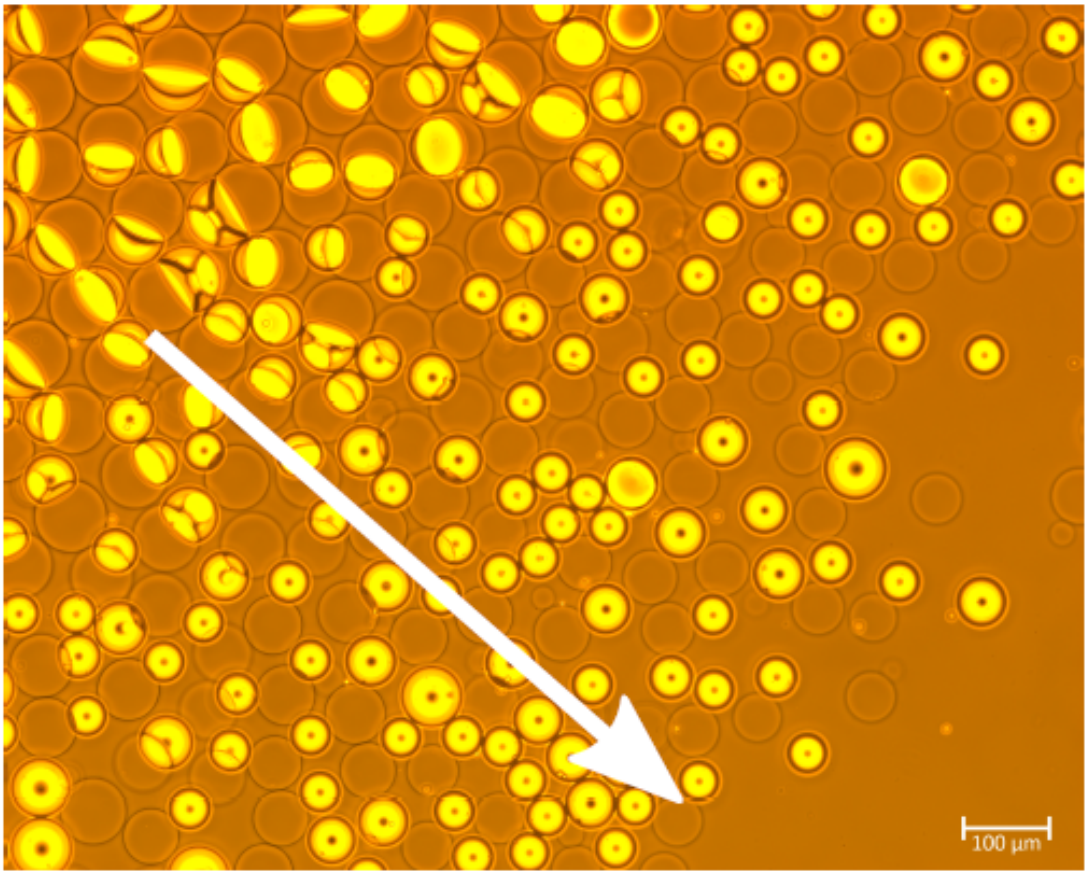


**Figure 2.21:** Micoscopic image of partial and full dewetting. After production with equal osmolarity in the inner and outer fluid of 50 mM a 100 mM NaCl solution was added on one side of the slide and created an osmotic gradient(arrow points towards higher osmotic gradient).

(Vallejo *et al.* (2017)).
It could not be determined if the main effect is the shrinking, the mechanical effect or the changing interfacial tension. It might be interesting to investigate the cause to be able to further control the budding off.

## 2.4 Membrane characterization

For further applications of the produced vesicles the characterization of the produced membrane is important. It it crucial to know to what extent the organic phase is removed from the membrane and how the preparation process and the interaction with various substances from the different fluids influences the membrane characteristics.

Visible residual oil either forms an equal layer around the inner fluid or is already

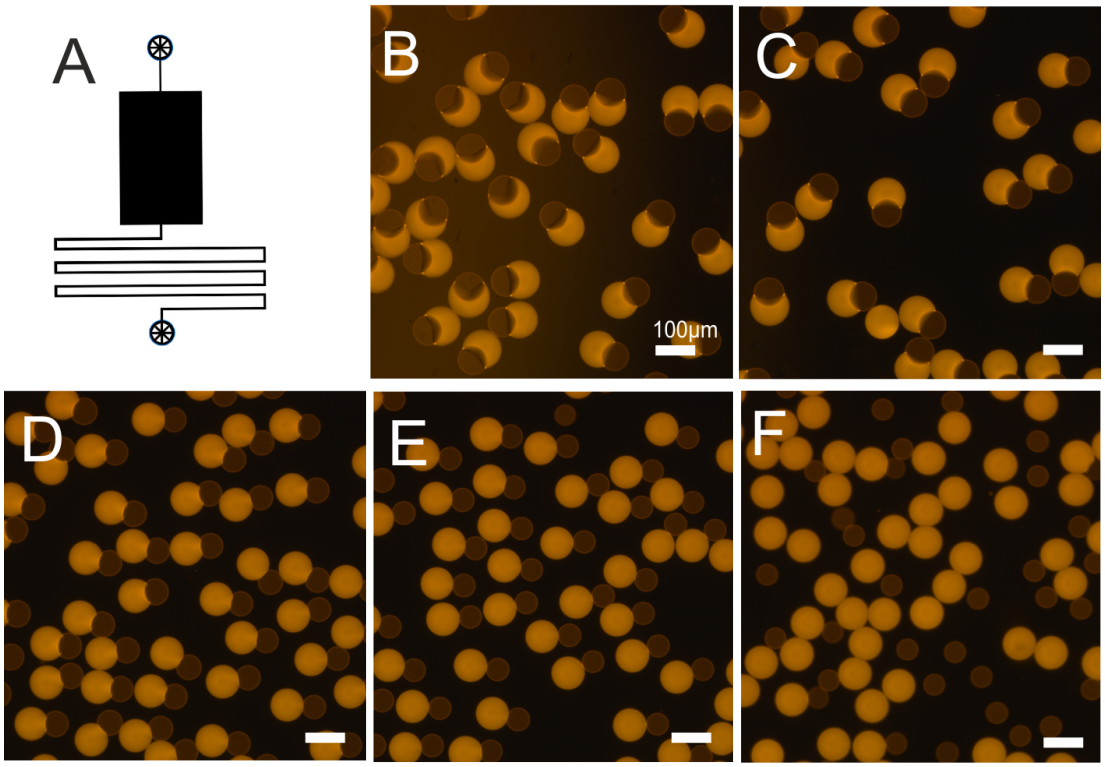


**Figure 2.22:** (A) Design of the reservoir chip used to remove oil drops. The black area is a wide, empty channel. (B-F) Images from different stages of dewetting while flowing through the chip.

partially dewetted and a lipid bilayer forms to a certain degree as shown in Figure 2.23. Figure 2.24 shows fluorescent images of vesicles after the oil removal. No oil residues are visible in the membrane any more.
The double emulsions and vesicles in the Figures 2.23 and 2.24 do not contain nile red in the oil phase but rhodamine labelled lipids. That is why the dewetted vesicles have still fluorescent membranes while nile red usually stays inside the oil phase.
In addition to an oil layer between the phospholipid monolayers oleic acid molecules are also able to incorporate themself into phospholipid membranes (Lonchin *et al.* (1999)). Oleic acid causes the membranes to be more permeable especially for charged molecules (Jin *et al.* (2018)).

An important question for the incorporation of various membrane proteins or other functionalization of the membrane is if a true bilayer was created or if there is still a thin film of organic phase between the phospholipid monolayers.
When observing electroformation vesicle membranes with non-phase-contrasting bright-field microscopy they are barely visible.
Various methods of oil removal led to microscopic images where the membrane is only

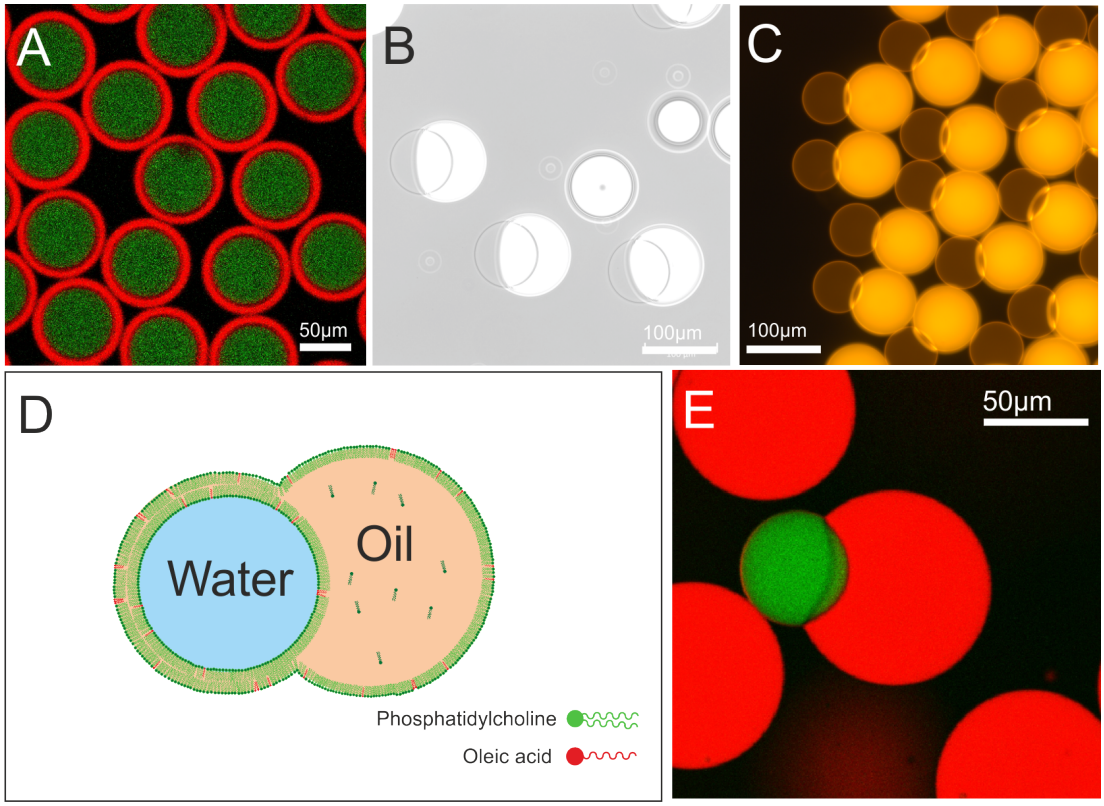


**Figure 2.23:** Partial dewetted vesicles images and schematic drawing.

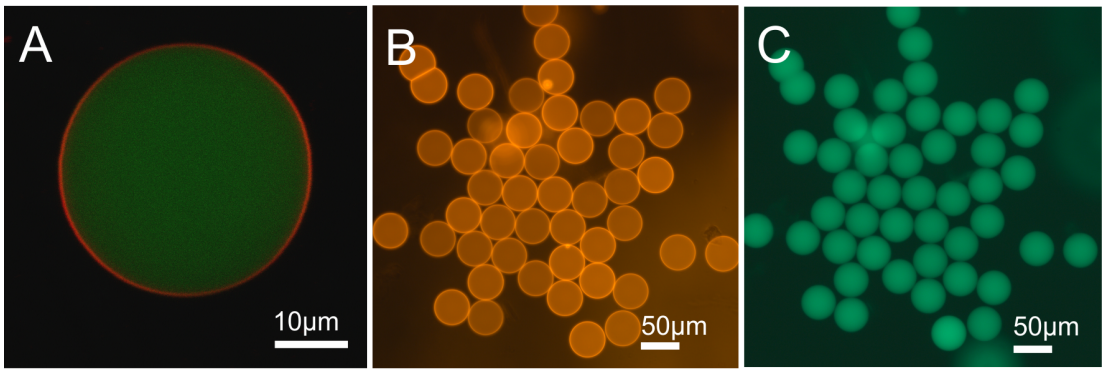


**Figure 2.24:** Fluorescent images of the resulting vesicles with rhodamine labelled lipids in the membrane (red) and encapsulated fluo-dex (green).

visible as one line in contrast to a thick oil layer where two lines of the oil phase of the double emulsion are visible. But the line visible in brightfield microscopy appears often much more prominent and well visible compared to the electroformation vesicles. This might be an indicator for leftover oil in the membrane.
One method for quality control of the resulting membrane is to use a dye that partitions

in the oil-phase.
This effect is shown in images taken with a confocal microscope (Figure 2.25). During the production of the vesicles two fluorescent dyes were used. Fluorescein coupled to a lipid (fluoresceine PE), typically used to dye membranes, and nile red, a hydrophobic dye.
While watching partly dewetted vesicles, it was observed that the fluoresceine PE is visible both in the oil drop and in the dewetted membrane while nile red is only visible inside the oil. This is a strong indicator that a phospholipid bilayer was created and there is no layer of oleic acid in between.
However, the visibility of residual oil and dissolved dye is limited to the resolution of the camera and the dye intensity this test should be used in combination with other tests (Robinson (2019b)).
Another simple method to characterize membrane properties is membrane fluctuation. A solution containing vesicles is diluted with a solution with a higher osmolarity to create a small osmotic gradient between the inside of the vesicle and the outside resulting in a bit of water leaving the vesicle. As a result the membrane becomes wobbly and starts fluctuating. This fluctuation state is recorded with a high speed camera and the membrane behaviour can be analysed (Gracia *et al.* (2010)).
Unexpectedly the dewetted vesicles did not show reproducible membrane fluctuation while vesicles produced with electroformation were fluctuating readily. A few times membrane fluctuation could be observed after exchanging most of the outer solution but this results could not be reproduced reliably.
To test if this lack of fluctuation was caused by residual oil inside the membrane or by the surfactant in the outer solution F108 was added to vesicles formed by electroformation and they also stopped fluctuating.
One explanation is that the surfactant increases the membrane permeability so that there is no osmotic gradient. Another explanation could be a strong mechanical stabilization of the membrane by the polymer surfactant that prevents the fluctuation.

Other tests for leftover oil may include composition measurements with methods like RAMAN and NMR Spectroscopy, reconstitution of membrane proteins and measurement of forces needed to pull a nanotube with optical tweezers (Robinson (2019b)).
While unfortunately not being able to further prove the unilamellarity and to test the membrane properties, the tests showed the huge impact particular detergents used in the experiments have on membrane properties and inspired further investigation presented in Chapter 4.

## 2.5 Applications for synthetic biology

As mentioned in the introduction, compartments are one of the fundamental features of life. The field of molecular biology worked for many decades with isolated cellular components to study their function. In synthetic biology the next step is to take this

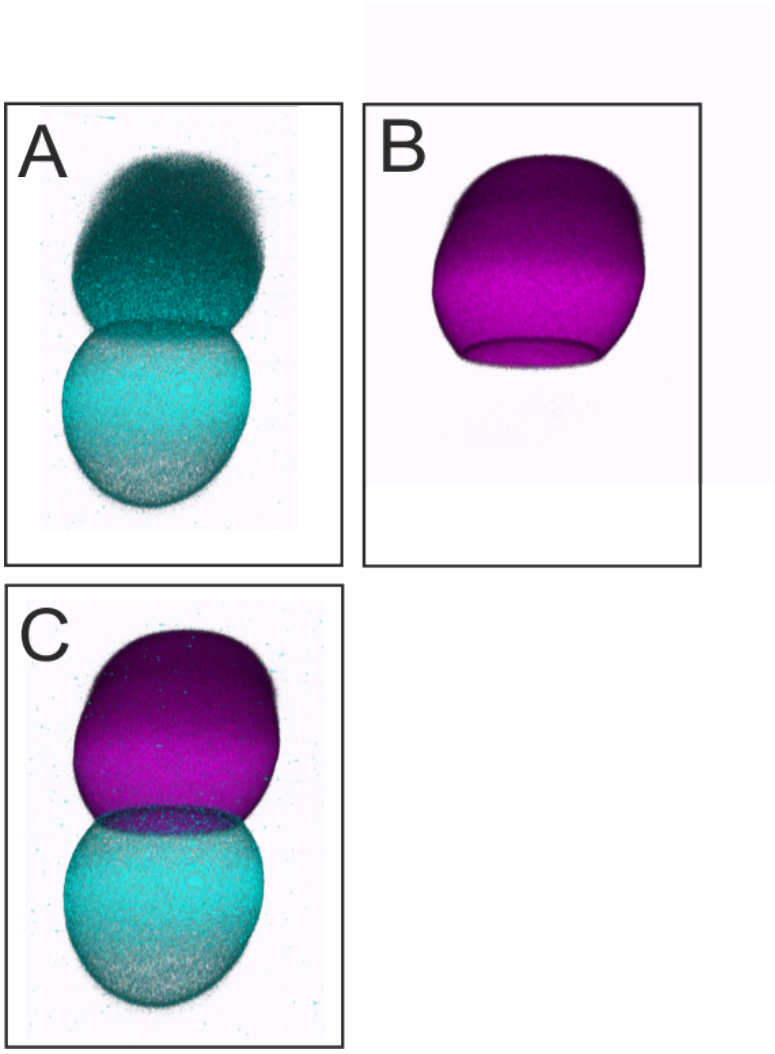


**Figure 2.25:** Confocal scan of a partly dewetted vesicle with nile red (violet) and fluorescein PE (cyan) in the middle fluid. (A) Only fluorescein PE, (B) only nile red and (C) overlay of both scans.

knowledge and assemble functional modules with increasing complexity.
One of the options for such a model is to transfer isolated molecules like proteins or DNA into compartments and observe their behaviour. The first challenge is to put these delicate molecules into compartments without destroying them. An encapsulation method is needed that allows the encapsulation of increasingly complex solutions. One possible method to deal with the first challenge was presented in this chapter. The next challenge on the way to a functional module that can be expanded in the future, is to observe, measure and potentially influence the encapsulated molecules and ongoing reactions.

Multiple methods have been developed in molecular biology to observe for example enzymatic reactions. However once the analyte is encapsulated many of the established measurement techniques can not be applied any more. The next two chapters show applications of encapsulating smaller vesicles and enzymes as well as experiments how we can observe phenomena and properties inside a vesicle.
There are several examples of encapsulation of complex biological systems like mitochondria, GUVs and E. coli cells (Göpfrich *et al.* (2019)) (Bashirzadeh & Liu (2019)) (Trantidou *et al.* (2018)).

### 2.5.1 Encapsulation of fluorescent dyes

One of the most simple encapsulation experiments is the addition of fluorescent dyes because they are often very robust and easy to visualize.
One such example is the green dye inside the vesicles (fluorescein Dextran, a polysaccharide with a fluorescent label). These relatively large molecules were chosen because some of the conditions that were tested in the beginning, especially the ethanol oil extraction, caused leakage problems with normal fluorescein.
In addition to the encapsulation efficiency the homogeneity of the encapsulated solu-

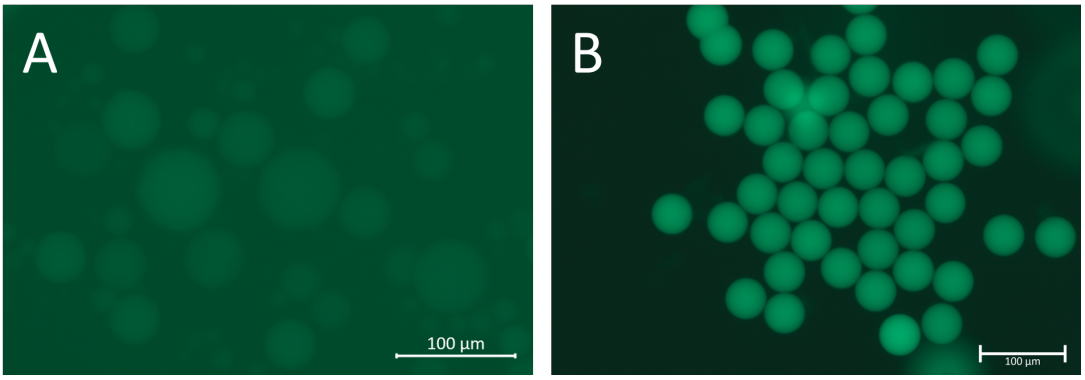


**Figure 2.26:** Encapsulation of fluorescent dye with vesicles produced by (A) electroformation and (B) double emulsion.

tion is an important advantage of the microfluidic liposome production.
To compare the homogeneity the fluorescence intensity of vesicles produced with electroformation and with microfluidics was compared. The results are shown in Figure 2.27.
This method however has its limitations and can only serve as a rough estimation. One problem is that after the electroformation the dye is in the inner and in the outer solution. The dye in the outer solution can be diluted but it is difficult to completely remove. It could be removed by trapping the vesicles inside a microfluidic chip and then washing away the outer solution but this produces other problems like the selection of a certain group of vesicles resulting in biased data.

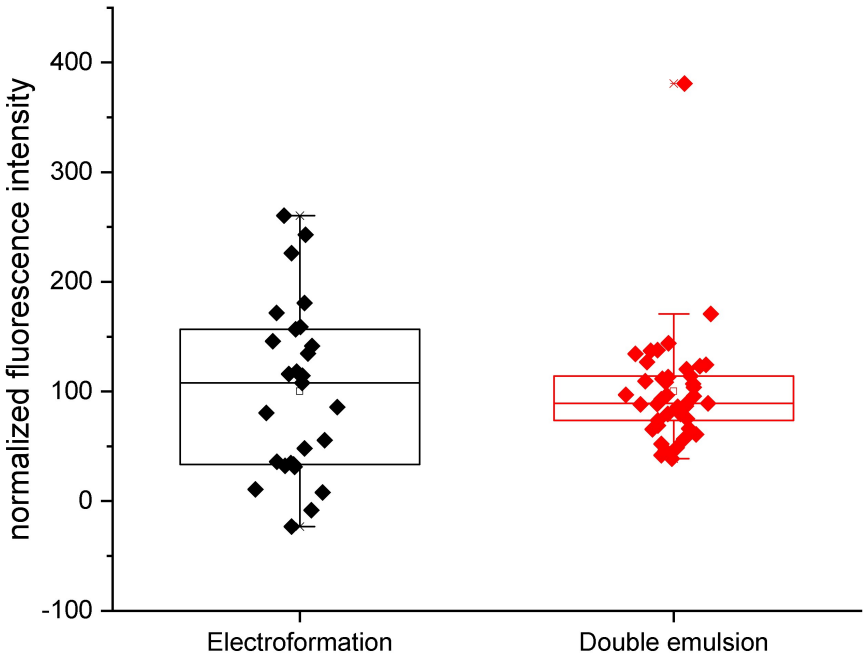


**Figure 2.27:** Normalized fluorescence intensity of encapsulated fluorescein-Dextran in vesicles produced with electroformation and double emulsion method. The average fluorescence of the respective samples was set to 100 to compare the homogeneity of the encapsulated dye.

However, the resulting background fluorescence should be equal across the image and increase the brightness of all electroformation vesicles to a similar extent. This could be a problem when comparing the absolute brightness to compare the encapsulation efficiency. Here the brightness values are normalized and only the homogeneity is compared.

### 2.5.2 Encapsulation of SUV and GUV

Figure 2.28 shows the encapsulation of smaller GUV and also of SUV. For this experiment the smaller vesicles were produced separately and then added to the inner fluid.

There are a few examples of similar experiments in the literature. SUVs were encapsulated into droplets to be fused later and form GUVs (Weiss *et al.* (2018)) and LUVs or smaller GUVs were encapsulated to mimic cell organelles (Romanov *et al.* (2019)).

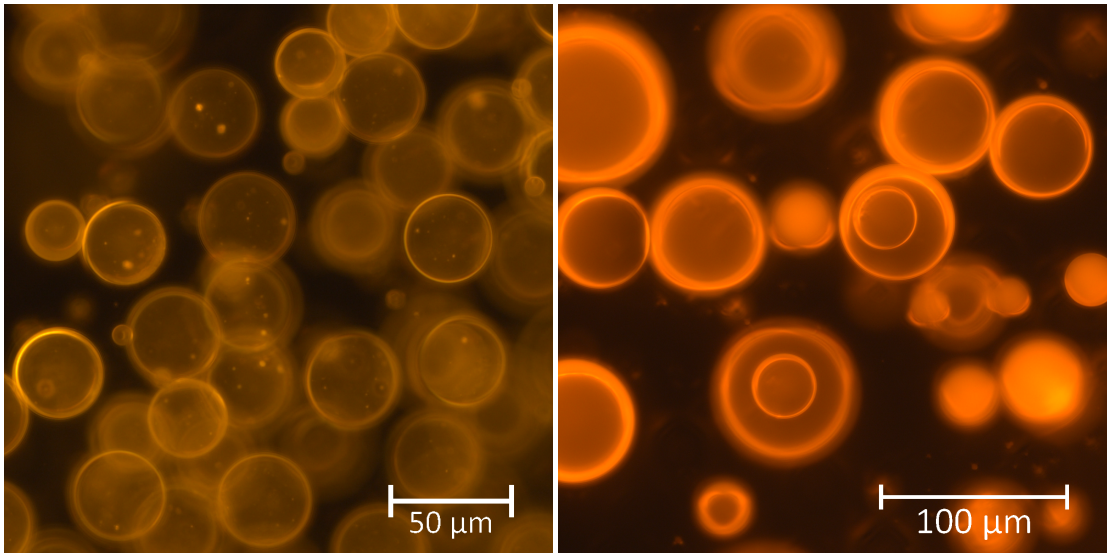


**Figure 2.28:** Encapsulation of (A) SUVs and (B) GUVs inside GUVs with the double emulsion method.

These encapsulation experiments paving the way to a synthetic cell are enabled by microfluidic technologies (Kamiya (2020)).

The next chapter investigates microfluidic encapsulation further and shows two examples of encapsulation of complex systems.
First small vesicles that work as energy modules are combined with enzymatic reactions and encapsulated into water-in-oil droplets in cooperation with the Baret group in Bordeaux and second a complex enzymatic cascade is encapsulated into vesicles using the method shown in this chapter.

# Chapter 3

# Characterization and encapsulation of energy and metabolic modules

## 3.1 Functional modules

In this chapter a few combinations of modules are presented, namely the combination of an energy supply and a metabolic module and the combination of a metabolic module and a compartment. These experiments were relatively simple combinations and not in all cases were the used modules fully synthetic.
The goal was to gain experience and learn about challenges of combining separately prepared modules. These experiments gave some first insights to fundamental features functional modules should have to be combined with other modules.
Here the focus is on compartmentalization, cofactor regeneration and metabolism. Other functional modules being developed in the MaxSynBio network are growth, replication and division, signalling and motility (Booth *et al.* (2019)) and protein expression (Jia *et al.* (2019)) (Schwille *et al.* (2018)).

### 3.1.1 Energy supply modules

All living organisms need a constant supply of energy, either from outside or from other parts of the organism. For example energy consumption during the production of chemical substances or energy generation while metabolizing nutrients (Schwille *et al.* (2018)).
Energy supply is fundamental for most other functional modules. In molecular biology or during the development of isolated modules molecules with high energy or gradients providing necessary energy can be added or created.
However, once the modules are encapsulated in compartments continuous supply of energy becomes more difficult. Therefore easily integratable energy modules are a fundamental requirement for the creation of a synthetic cell.

Organisms transform chemical energy in the form of nutrients or radiant energy in the form of light via an electron-transfer chain into a proton gradient which is subsequently used to generate ATP. ATP production can be coupled with the regeneration of the cofactors NAD(H) or NADP(H) or with the light-driven bacteriorhodopsin (Schwille *et al.* (2018)).
Synthetic ATP production systems are, so far, mostly coupled bacteriorhodopsin with ATPsynthase in small liposomes (Steinberg-Yfrach *et al.* (1998)) (Kleineberg *et al.* (2020)).
Within the MaxSynBio project ATPsynthase was integrated into the membrane of droplet-stabilized GUVs which were produced inside a microfluidic system (Weiss *et al.* (2018)). In addition an ATP generating module driven by chemical energy has been created but not yet integrated with other modules (Otrin *et al.* (2017)).

Nicotinamide cofactors are involved in many enzymatic reactions. They support the transport of electrons between molecules catalysed by oxidoreductases, for example the oxidoreductases in the respiration chain. In addition to their importance in redox reactions they are known to be involved in ADP-ribosylation and an extracellular function as a neurotransmitter was proposed (Mutafova-Yambolieva *et al.* (2007)).
Their regeneration is therefore important both in context of energy supply as well as in respect to sustaining metabolic pathways.
Inside MaxSynBio the cofactor regeneration is a great example for the potential of synthetic biology to go beyond copying biological systems and add new synthetic components. As an example a membrane was functionalized with a synthetic small molecule to allow NAD regeneration (Wang *et al.* (2018)).
In this section inverted membrane vesicles were used as energy modules, coupled with an enzymatic reaction and encapsulated in droplets inside a microfluidic system in cooperation with the Baret group in Bordeaux.

### 3.1.2 Metabolic modules

Metabolism is another fundamental feature of life. Metabolic pathways in cells form a very complex network (Jeong *et al.* (2000)). Modifications of those pathways in living cells might affect behaviour of the cells in unpredictable ways (Yadav *et al.* (2012)). Cell-free metabolic engineering (Dudley *et al.* (2015)) is a promising alternative.
In addition to the fundamental importance for living organisms, the enzymatic production of specific molecules is also relevant for industrial applications. One advantage of enzymatic production of complex molecules is the stereoselective formation of the product, which is often very difficult in chemical synthesis. The goal would be a tailored construction of a minimal cellular factory to produce compounds as an alternative to traditional top-down biotechnology approaches (Schwille *et al.* (2018)).
In addition to the replacement of traditional chemical synthesis, synthetic cell inspired

production facilities potentially have several advantages compared to the production of substances in genetically modified organisms (GMO) most important an easier purification, the possibility to produce substances that would be too toxic for biological organisms and possibly a higher efficiency.
An important advantage to cell-free enzymatic reactions in batch is the possibility to have reactions with contrary conditions next to each other in separate compartments similar to the biological cell strategy.

Most publications show reconstructed existing pathways and simple ones were already encapsulated. However, the full potential of synthetic biology in exemplified in the CETCH cycle, a synthetic pathway to capture carbon dioxide. It is comprised of enzymes from various organisms including three engineered enzymes (Schwander *et al.* (2016)).
In the second part of this chapter the results of encapsulation tests with the double emulsion method of this pathway are shown. This experiments were done in cooperation with the Erb group in Marburg.

## 3.2 Inverted membrane vesicles as energy modules

This section shows the combination of a energy module with a metabolic module.
The energy regeneration module in this experiment was not a fully synthetic one. It is a proof of concept experiment of an enzymatic reaction using a cofactor which is being regenerated by the energy module.This combination is being encapsulated and measured with microfluidic tools. The goal was the examination of the experimental conditions and tools with a model system and to determine criteria for the design process of the synthetic energy modules.

Isolated membrane vesicles are used to study features of the bacterial membrane such as energy production and active membrane transport without the cytoplasmic content of the intact cell (Berrisford *et al.* (2016)) (Heikal *et al.* (2014)) (Kaback (1974)) (Konings & Kaback (1973)) (Futai (1974)).
Here inverted vesicles of the inner membrane of E. coli cells were used. E. coli is a gram-negative bacterium and as such has a cell wall composed of an outer and inner cell membrane with the periplasmatic space in between. The transmembrane proteins of the respiration chain are located on the inner membrane. The proton gradient necessary for the ATP-Synthase to produce ATP is generated across this membrane with proteins like the NADH hydrogenase pumping protons into the periplasmatic space. This gradient allows the ATP-Synthase to produce ATP in the cytosol. In eucaryotic cells this process takes place on the inner membrane of the mitochondria.
Inverted inner membrane vesicles are produced by separating the inner E. coli membrane from the outer membrane and the cell content. Then inverted vesicles are produced with the respiration chain pumping protons into the vesicle and the ATPsynthase generating

ATP on the outside (Figure 3.2) (Jewett *et al.* (2008)). The outward orientation of the ATPsynthase in SUVs occurs spontaneously due to its size (Futai (1974)).

### 3.2.1 IMV production

E. coli (MG1655) were cultured in LB medium containing 20mM Glucose.
The cells were harvested in three centrifugation steps. First they were centrifuged for 20 minutes at 10.000 x g at 4°C, the cells were resuspended in washing buffer (50 mM Tris-HCl pH 8.0, 1mM EGTA) and centrifuged again for 20 min at 10.000 x g at 4°C. The pellet was resuspended in washing buffer and centrifuged a third time for 30 minutes at 5.000 x g at 4 °C (Heitkamp *et al.* (2013)). Afterwards the pellet was frozen in liquid nitrogen and stored at −80 °C.

The cell pellet was covered with washing buffer, thawed in a waterbath at 30 °C and then resuspended. The suspension was centrifuged for 10 minutes at 15.000 x g at 4 °C and the resulting pellet was resuspended in 300 mL washing buffer. The cells were centrifuged again for 10 minutes at 15.000 x g at 4 °C and the pellet was resuspended in lysis buffer (50 mM MOPS, 175 mM KCl, 10 mM MgCl2, 0.2 mM EGTA, 0.2 mM DTT, 0.1 mM PMSF, pH 7.0), homogenized with a glass tissue homogenizer and stirred on ice for 1 hour.
1 unit per gram cell mass of DNAse was added and the cells were pressed through a cooled french press three times at 1000 bar. The solution was checked under the microscope to determine of the french press treatment was successful. The homogenized cells were frozen in liquid nitrogen and stored overnight at −80 °C.
The frozen suspension was thawed in a waterbath at room temperature and centrifuged for 20 minutes at 25.000 x g at 4 °C and the pellet was discarded. The supernatant was ultracentrifuged (Ultrazentrifuge Optima XPN 100, Beckman Coulter) for 120 minutes at 54.000 rpm at 4 °C.
The pellet contained now the inner and outer membrane and was resuspended in membrane buffer (50 mM Tris-HCl, 0.2 mM EGTA, 5 mM $MgCl_2$, 6 mM PAB, 10% (v/v) Glycerol, 2 mM DTT, 0.1 mM PMSF, pH 8.0) using a brush. The resuspended pellet was again ultacentrifuged for 90 min at 54.000 rpm at 4 °C and resuspended in membrane buffer. The last ultracentrifugation took 90 minutes at 54.000 rpm at 4 °C and the pellet was resuspended in membrane buffer.
The solution was frozen in liquid nitrogen and stored overnight at −80 °C and quickly thawed again the next day in at waterbath at 30°C. Next a density gradient centrifugation was performed. The ultracentrifugation tubes were filled with 6 mL 50 wt.% Sucrose, 8 mL 40 wt.% Sucrose, 10 mL 30 wt.% Sucrose, 10 mL 20 wt.% Sucrose and 1-2 mL sample on top. This was centrifuged for 24 hours at 30.000 rpm(swinging bucket rotor SW 32 Ti) with the acceleration and deceleration at the lowest possible level (Miura & Mizushima (1968)) (Jewett *et al.* (2008)).

The membrane is between 35 wt.% and 45 wt.% sucrose and the darker fraction is carefully collected. The protein content of the fractions was measured with a nanodrop and they were resuspended 1:4 in membrane buffer. The resulting solution was ultracentrifuged for 2 hours at 54.000 rpm (fixed angle rotor type 70 Ti) (Osborn *et al.* (1972)) and the pellet was dried and weighted. The pellet was resuspended in membrane buffer and the solution was pressed through a sterile filter (0.22 $\mu$m).
This solution containing the IMVs was frozen in 500 $\mu$L aliquots in liquid nitrogen and stored at −80 °C (Wuu & Swartz (2008)).

### 3.2.2 IMV characterization

Concentration and size distribution of the IMVs were determined using tunable resistive pulse sensing (TRPS) on a qNano device (Izon Science, Christchurch, New Zealand) and results are shown in Figure 3.1. TRPS is a high throughput method for quantitative size measurement of nanoparticles (Vogel *et al.* (2011)).

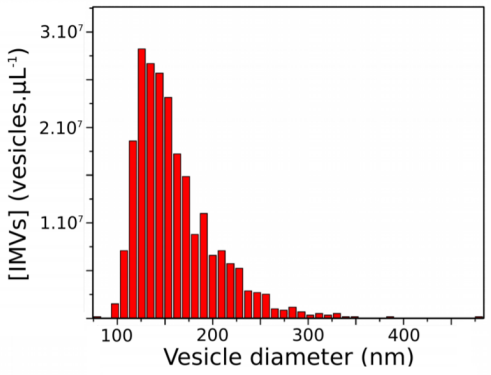


**Figure 3.1:** Inverted Membrane Vesicles size distribution. IMVs size versus IMVs concentration. Concentration and size of the vesicles were determined using tunable resistive pulse sensing (TRPS).

For the measurement a NP200 stretchable nanopore was used, which was calibrated with carboxylated polystyrene beads (mean size 350 nm). The lower fluid cell was filled with 80 ul membrane buffer and 30 ul of the vesicles diluted with membrane buffer were added to the upper fluid cell.
Size distribution and concentration was calculated from the measurement data with the instrument software (Izon Control Suite 2, Christchurch, New Zealand). The average concentration was 2.2 x $10^{11}$ particles/ml (SD 0.376 x $10^{11}$) and the average size was 167 nm (SD 38.75).
The concentration was important during the encapsulation experiments in Bordeaux because the average number of vesicles in one droplet could be determined this way.

### 3.2.3 ATP production

The ATP production was measured to test the energy production functionality of the IMVs.

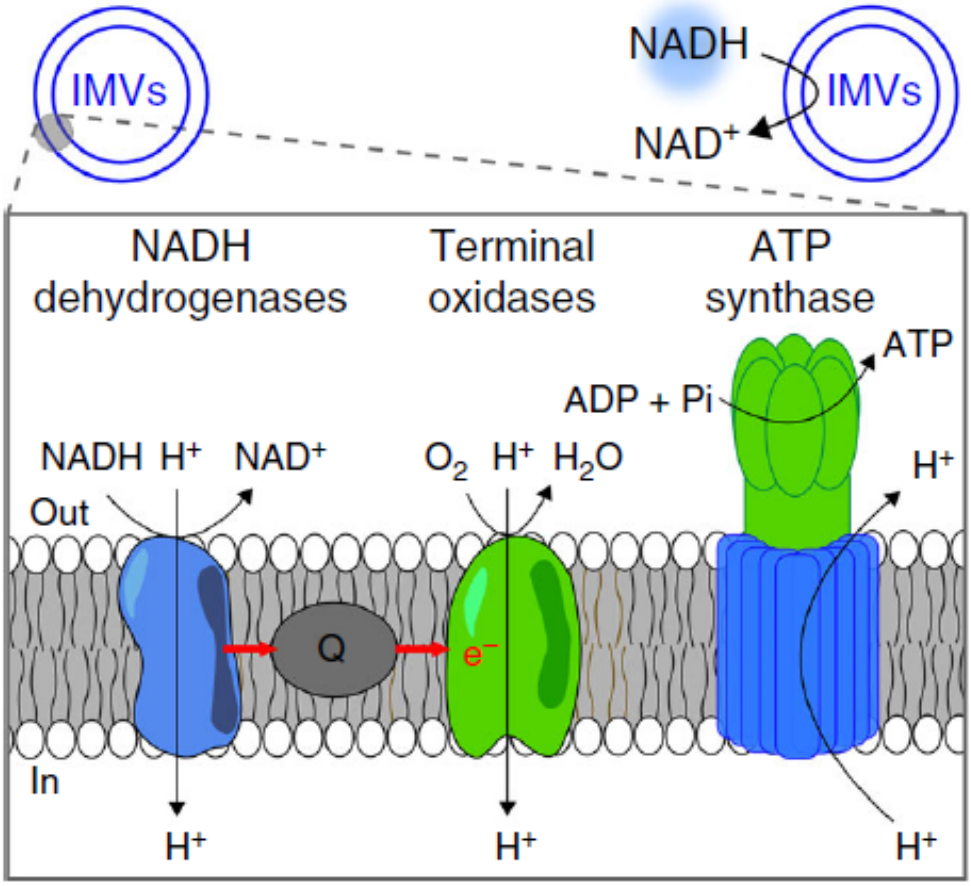


**Figure 3.2:** Schematic visualization of the respiratory chain proteins on the IMV membrane. From (Beneyton *et al.* (2018)).

The IMVs contain the proteins of the respiratory chain and the ATPsynthase (Jewett *et al.* (2008)). Those allow the regeneration of NAD and the production of ATP. The ATP production depends on the NAD regeneration.
The generation of ATP from ADP is a process that consumes energy. The chemical energy stored inside the ATP molecule can later be used by other enzymes to catalyse other reactions.
The ATPsynthase is a membrane protein that converts energy from a proton gradient

across the membrane to produce ATP. In case of the IMVs the proton gradient is produced during the NAD regeneration as shown in Figure 3.2. That means without the NAD production as a first step there can not be any ATP production.

The ATP concentration in the experiment shown in Figure 3.4 was measured with the Luciferin/Luciferase assay. The priciple is shown in Figure 3.3.
Firefly luciferase is an enzyme that catalyses the reaction from Luciferin to Oxyluciferin using ATP and releasing light. This bioluminescence can be measured.
This assay is often used in cells with excess ATP and Luciferin to measure the expression of the luciferase gene but with excess enzyme and substrate it can also be used to quantify ATP (Manfredi *et al.* (2002)).

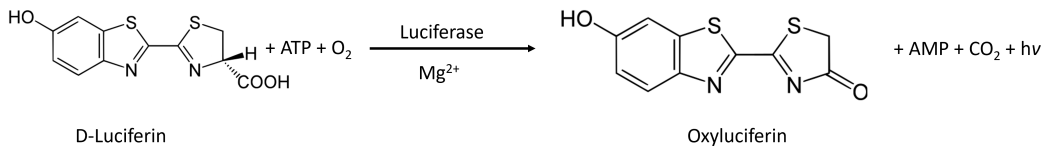


**Figure 3.3:** Mechanism of the Luciferase assay.

The experimental confirmation of the ATP production involved several steps as shown in Figure 3.4. After adding the main buffer containing the luciferase and Luciferin, a second buffer containing ADP was added to the solution. Commercially available ADP is usually contaminated to a certain extent with ATP, that is why the luminescence is increasing until all the ATP is used up by the luciferase.

As a side note, this is also a control step to confirm that the luciferase assay is working properly during each experiment. Because there is no proton gradient build up yet inside the IMVs there is no immediate ATP production. The ATP concentration inside the solution increases only after the addition of NADH, which is converted to NAD on the IMV membrane and creates the high proton concentration inside needed to fuel the ATPsynthase.
This experiment was performed in a batch setup inside a 96 well plate with a luminometer which measures the Relative Light Units (RLU) per second, a unit that is proportional to the emitted photons per second.
It was done as a part of several preparatory steps before the IMVs were measured inside the microfluidic system.

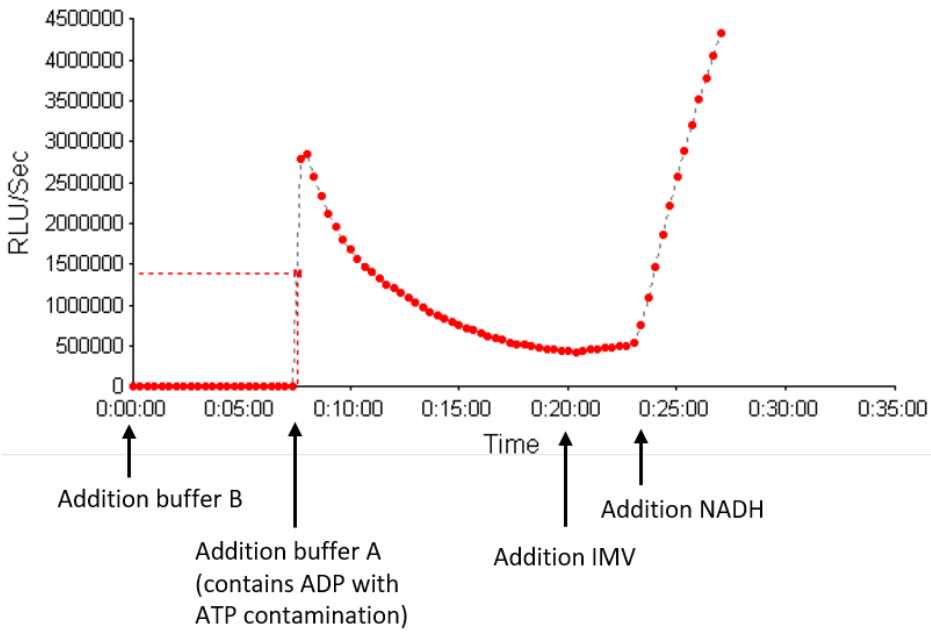


**Figure 3.4:** IMV respiration chain ATP production. RLU=Relative Light Unit, in presence of the luciferase assay an increase in light is directly proportional to an increase in ATP concentration.

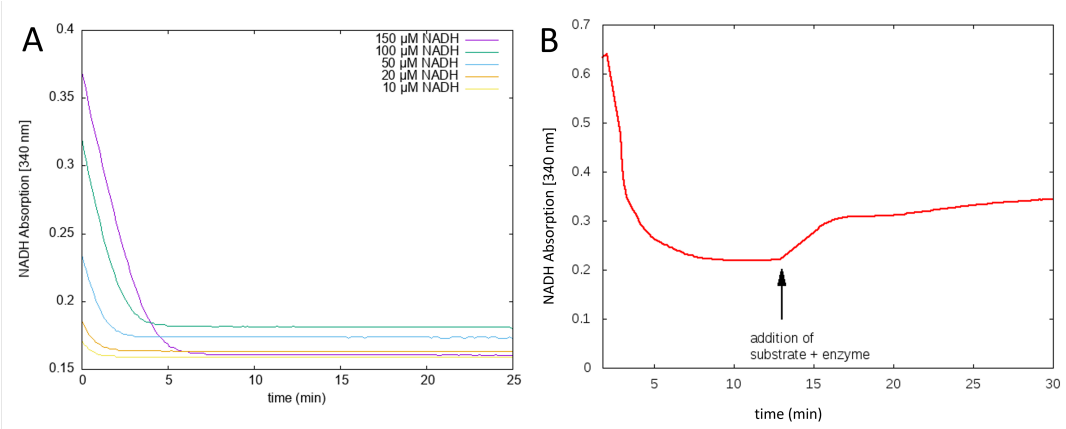


**Figure 3.5:** Measurement of NADH fluorescence at (A) different NADH concentrations decreasing after IMV addition and (B) NADH first decreasing after addition of IMV, then increasing after addition of substrate and enzyme

### 3.2.4 NAD regeneration

Although the ATP production measurements already showed the dependence on the presence of NADH a few more tests were done to confirm the functionality of the whole

protein chain inside the isolated membrane.
Figure 3.5a shows the initial high absorption of NADH in solutions with different NADH concentrations and an immediate drop due to the addition of IMV to the solution.
Figure 3.5b shows the combination of IMVs and an enzyme in batch. Again the initial solution contains buffer with NADH which is decreasing because of the addition of IMVs just before the measurement started. Once the absorption reached a plateau the enzyme and substrate were added and the NADH concentration increased for a short time and then stabilized on a higher level than before.

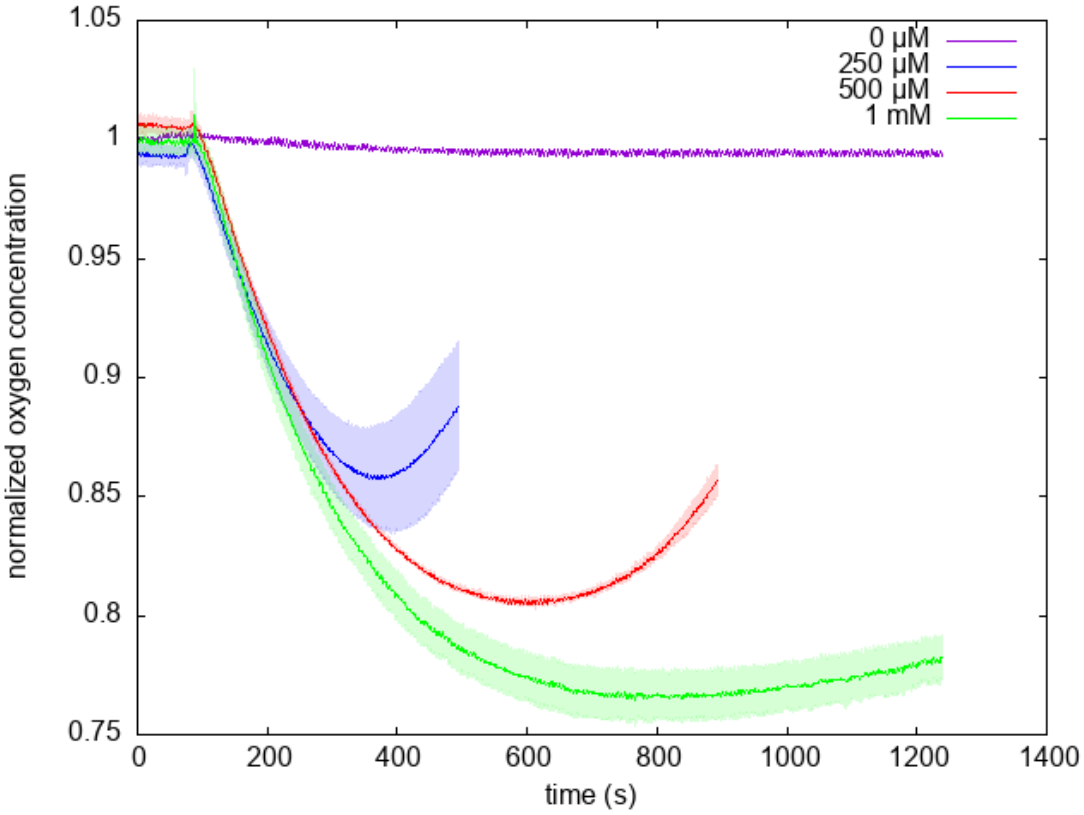


**Figure 3.6:** IMV NADH oxygen measurement. IMV solution diluted 1:50 and the same in all experiments. Different colours represent varying NADH concentrations.

As shown in Figure 3.6 and Figure 3.2 the NAD regeneration and subsequent proton pumping is consuming oxygen.
As a test to confirm this functionality of the proteins inside the IMV membrane the oxygen depletion in a solution with IMVs after the addition of varying concentrations of NADH was measured.
Figure 3.6 shows that the IMV solution has a constant oxygen level if no NAD is added (violet curve). Adding increasing concentrations of NADH is temporarily decreasing

the oxygen concentration.
Measuring oxygen consumption is a common method to confirm the functionality or inhibition of the respiration chain (El-Mir *et al.* (2000)).
The presence of the respiration chain proteins and the ATPsynthase and their functionality were therefore confirmed with the experiments shown above.

### 3.2.5 Coupling of IMV with an enzymatic reaction

First the enzymes to be coupled with the IMVs had to be selected and tested.
The setup could only measure the NADH fluorescence and the NAD regeneration is necessary to produce the proton gradient for the ATP generation. Ideally we would use two reactions one using NAD and the second one ATP to use both elements of the IMV energy production functionality.
Initially the Glycerokinase and Glycerol-3-phosphate dehydrogenase powered by the IMVs were tested. The problem with this combination was that the first reaction needs ATP which can only be produced after the NADH to NAD conversion by the IMVs. Therefore the whole cycle will not start or the observed reactions will be fuelled by ATP contamination in the added ADP and not by ATP produced by the IMVs.
On the other hand when the second reaction uses ATP it would only confirm that the first reaction is running due to the experimental constrains. For this reason we decided to simplify the experiment and use only one enzyme which is using NAD.

Therefore the following reaction with the enzyme Glucose-6-phosphate dehydrogenase (G6PDH) was chosen to be coupled with the IMVs:

$$\text{Glucose-6-phosphate} + \text{NAD}^+ \xrightarrow{\text{G6PDH}} \text{6-Phosphogluconolactone} + \text{NADH}$$

Figure 3.7 shows results of the encapsulation experiment. The reaction catalysed by G6PDH uses NAD regenerated by the IMVs while the NADH concentration is monitored.
The measurements done in a batch solution in Magdeburg were repeated inside the droplets in Bordeaux with matching results (Beneyton *et al.* (2018)).
Figure 3.7 shows the final experiments with encapsulated IMVs and enzymatic reaction (Schematic drawing in Figure 3.7a). Figure 3.7b shows the dependence of the system on the presence of the substrate Glucose-6-phosphate (G6P). The more G6P is added the longer the NADH concentrations remains stable.
If the NADH would be not used by the IMVs to regenerate NAD the NADH concentration would initially increase. Once the substrate is depleted the NADH concentration slowly decreases because it is still used by the IMVs until the whole module stops.
Figure 3.7d shows that an increase in the number of added IMVs decreases the time until the NADH is consumed.

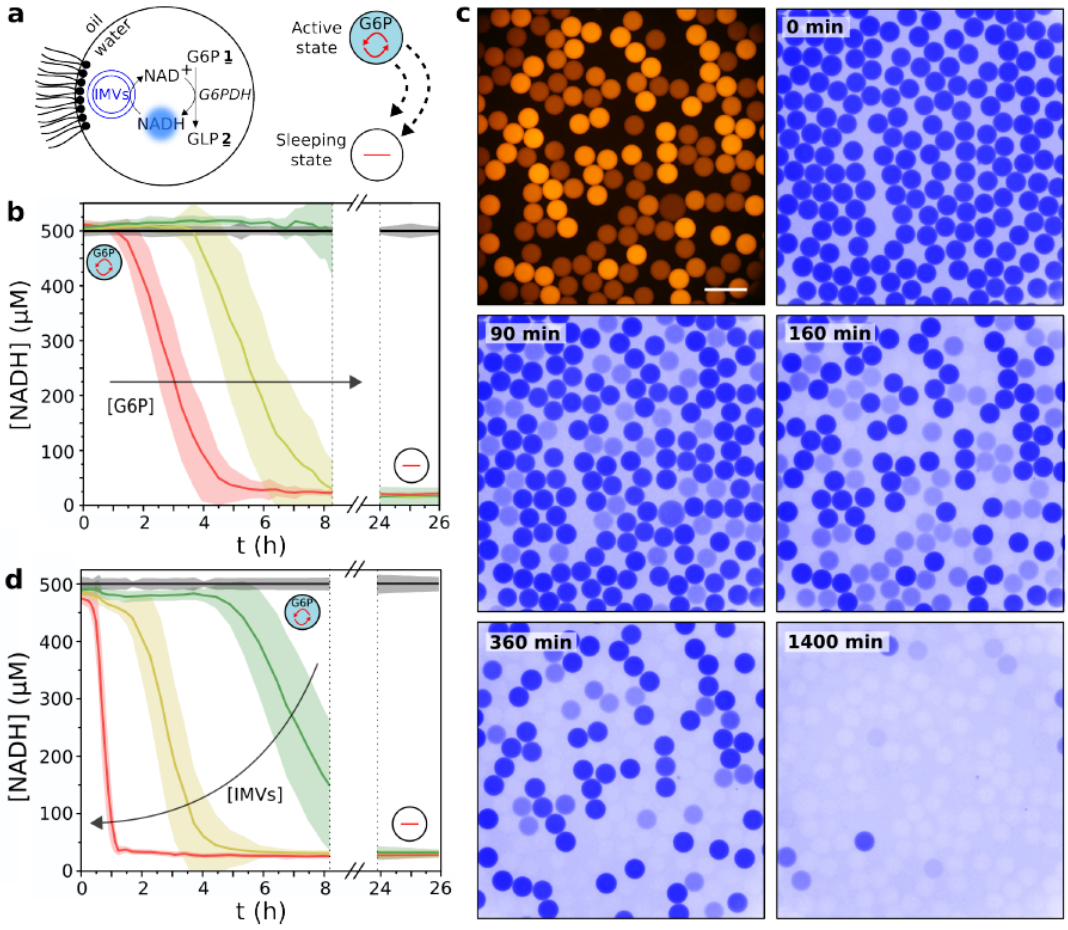


**Figure 3.7:** Self-sustained compartmentalized metabolism. Image from (Beneyton *et al.* (2018)).

As a side note, these experiments also show the potential microfluidic tools have to enable high throughput experiments. Each experimental condition in Figure 3.7 was measured in 10,000 droplets.

## 3.3 Encapsulation of enzymes

In the first part of this chapter the integration of an enzymatic cascade with an energy regeneration module was shown. Compartmentalization was necessary in this example for the energy regeneration module to function and additionally the IMVs together with an enzyme and substrate were encapsulated inside water-in-oil droplets.
Advantages of encapsulation are the stability of the droplet and in this case the possibility for a sensitive fluorescence measurement of the reaction inside the compartment.

This measurement would not have been possible in a double emulsion vesicle because the oil without any florescence allows to automatically distinguish the individual droplets.

Measuring components inside vesicles is addressed in the next chapter. In this part two examples of encapsulation of enzymes inside vesicles using the microfluidic double emulsion method are shown.
The main reason to establish vesicle production methods like these for synthetic biology, compared to easier methods like electroformation, is the possibility to encapsulate complex solutions with delicate and large biomolecules such as proteins or DNA.

### 3.3.1 Horseradish Peroxidase

To test the encapsulation and the functionality of an enzyme, a simple and relatively robust enzymatic reaction with a fluorescent product was selected.
Horseradish peroxidase (HRP) is an enzyme that reacts in presence of hydrogen peroxide with a number of substrates and forms colourful and fluorescent products.
The reaction with AmplexRed is often used as a method to detect hydrogen peroxide. Recently a publication showed a microfluidic detection system for hydrogen peroxide in blood using the HRP assay (Gaikwad *et al.* (2021)).

$$\text{AmplexRed} + H_2O_2 \xrightarrow{\text{HRP}} \text{resofurin} + H_2O$$

The reactants were encapsulated with the double emulsion method described in Chapter 2.
Initially no resofurin production inside the vesicles could be observed. The reaction was then repeated in batch and measured with a UV/Vis spectrometer. During some of the control batch experiments the surfactant poloxamer F108 was added to the solution and as a result the batch experiments showed no resofurin production. Therefore it seems as if this surfactant interacts with the enzyme or another component of the reaction.
The encapsulation was repeated without surfactant in the inner solution and the reaction could be observed under the microscope.
Another problem was that resofurin shows strong photobleaching making it impossible to document the experiment with a standard fluorescent microscope.
However, a confocal microscope can take images with much lower light exposure to the sample and images recorded with a confocal microscope are shown in the next section.

### 3.3.2 CETCH cycle

The following subchapter describes the encapsulation of a short enzymatic pathway in a complex buffer including cofactors. This is the most complex integration of various modules shown in this thesis and serves as a preliminary proof of concept of the suitability of the microfluidic double emulsion method for encapsulation of synthetic biology

modules.
The encapsulated enzymatic cascade is part of the CETCH cycle developed by the Erb group at the MPI for Terrestrial Microbiology (Marburg). It is a synthetic enzymatic pathway that fixates carbon dioxide and binds it in organic products (Schwander *et al.* (2016)).

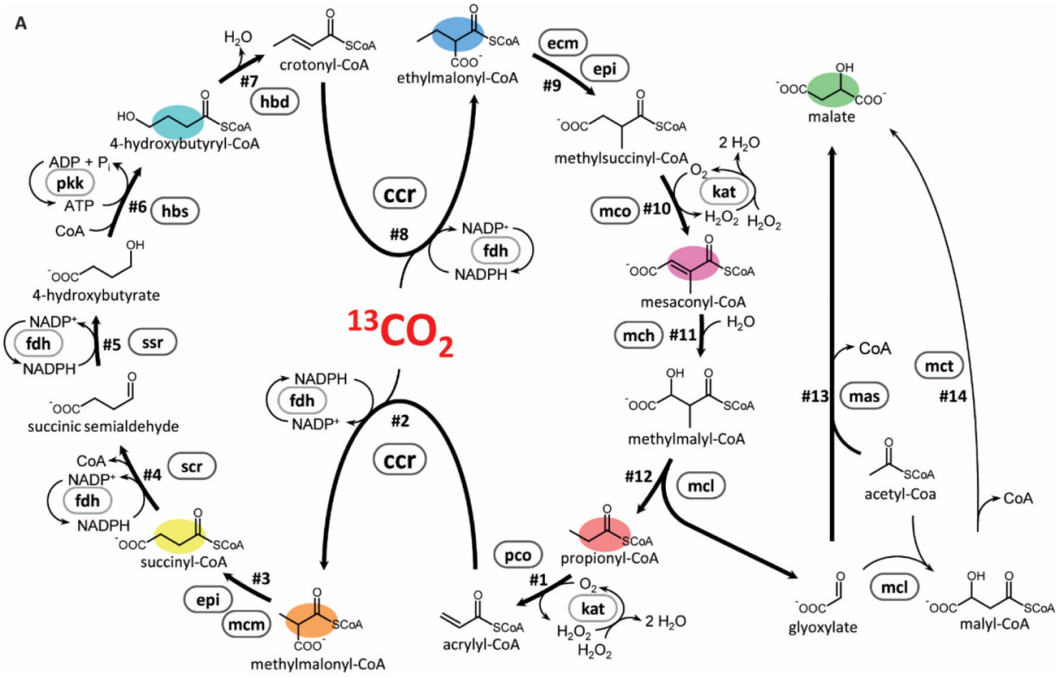


**Figure 3.8:** CETCH cycle from (Schwander *et al.* (2016)).

In the experiment presented in this chapter the first part of the cycle was encapsulated in GUVs using the double emulsion method presented in Chapter 2 of this thesis. Carbon dioxide was produced in excess outside of the vesicles, diffused across the membrane and was used as a substrate by the enzymes to produce mesaconyl-CoA. During the last step of the cascade hydrogen peroxide was produced as a byproduct (Figure 3.8). For the encapsulation experiment the hydrogen peroxide was then coupled to the reaction with horseradish peroxidase (HRP), described in the previous section, to visualize the working cascade inside the vesicles.

One possible problem with the presented experimental design was that some of the red fluorescence could be produced by the fluo-dex, as the red fluorescence was very weak and a high laser intensity had to be used to record the image.
Fluorescein has its peak emission at 517 nm but shows a lower but possibly still visible emission at a broader range of wavelengths. The fluo-dex was added to the inner fluid

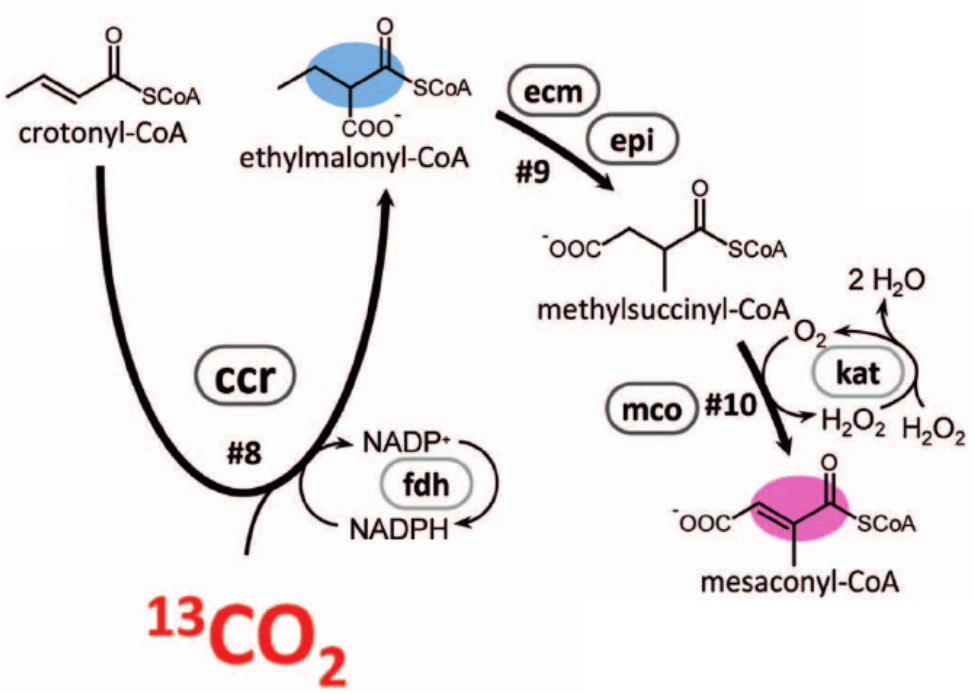


**Figure 3.9:** The part of the CETCH cycle that was used for encapsulation experiments (graphic from (Schwander *et al.* (2016))).

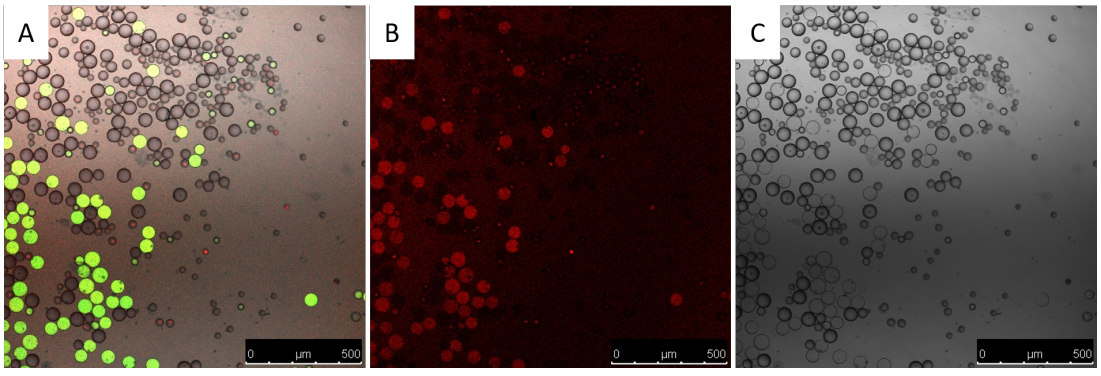


**Figure 3.10:** Images recorded with a confocal microscope showing vesicles with the encapsulated CETCH cycle. (A) Overlay image of the vesicles with fluo-dex (green) as encapsulation control and non fluorescent oil drops visible. (B) Red fluorescence inside the vesicles and (C) brightfield image of the mixture of vesicles and oil droplets.

during the vesicle production as a control for encapsulation in case no red fluorescence from the reaction would be visible and also to be able to locate the vesicles quickly

under the microscope without bleaching the resofurin.
However, because of the concern that the red fluorescence is just a fluorescein artefact as a further control we encapsulated the cascade without the fluo-dex to have only resofurin as a fluorescence producing agent.
During the vesicle production a certain number of vesicles break, therefore the inner fluid is also present in the outer solution, but much more diluted than inside the vesicle. For the presented images the outer solution was additionally diluted to show the reaction is happening inside the vesicles. The biggest problem as mentioned in an earlier section was the quick photobleaching of resofurin which also made it impossible to observe the reaction over time.

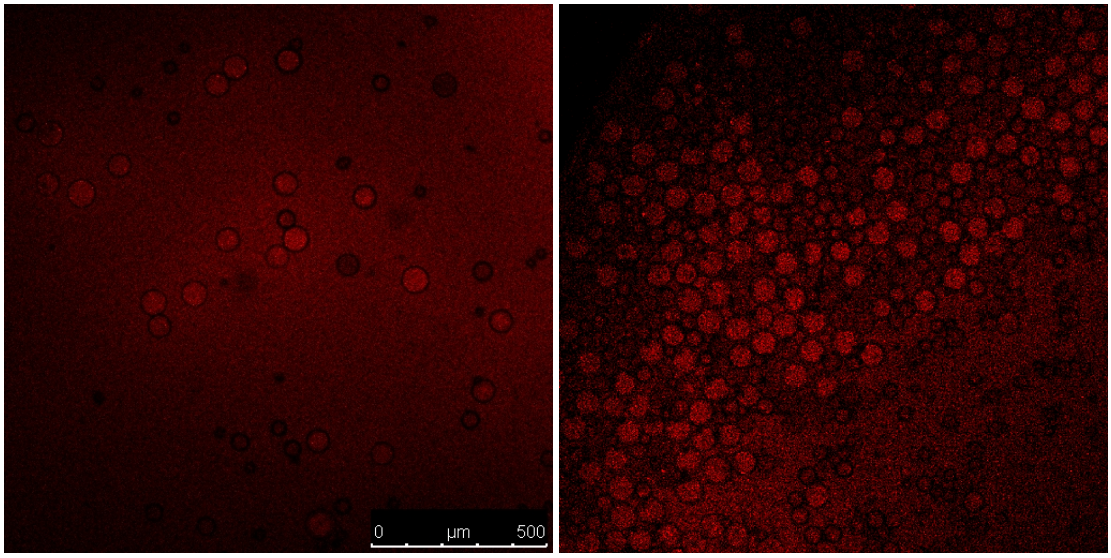


**Figure 3.11:** Images recorded with a confocal microscope showing encapsulated CETCH cycle without fluoDex as a control.

# Chapter 4

# Microfluidic GUV trapping

## 4.1 Introduction

In Chapters 2 and 3 it was shown how vesicles can be produced using microfluidics and how complex solutions can be encapsulated.
Once there is a compartment either empty or with already encapsulated modules, like metabolic modules or gene expression modules, the next step is to test the properties of the compartment itself, observe the compartment and possibly a reaction inside and interact with the compartment and the encapsulated components for example by exchanging the outer solution.
The outer solution may contain substrates that permeate or are transported across the membrane to start a reaction inside the vesicle or other vesicles could be introduced to fuse with the first one.
In molecular biology enzymatic reactions are measured in batch solutions, using for example UV/Vis spectroscopy. However, those methods are not differentiating between reactions that happen inside compartments vs the outside solution and are not designed to follow processes that involve an interaction with a membrane. Additionally, the vesicle volume is very small compared to the volume of the outer solution so the average changes of absorption or fluorescence in the whole solution might be very small and difficult to measure.
Also those methods measure a reaction in a whole batch of vesicles and not on an individual level.
For the broad range of synthetic biology applications new methods for observation and interaction with vesicles are necessary.

This part of the thesis gives an overview of microfluidic and non-microfluidic methods to handle and immobilize GUVs and a microfluidic chip for physical immobilization that allows exchange of the outer solution and microscopic observation is presented. The suitability of this system for synthetic biology applications is tested by measuring membrane permeability and membrane transport of a fluorescent dye and advantages,

disadvantages and possible improvements are discussed.
Other synthetic biology applications such as induction and observation of vesicle fusion are also possible with a trap design as shown by Dittrich et al. (Robinson *et al.* (2013)).

### 4.1.1 Handling of GUVs

Compared to biological cells liposomes are more delicate and are more difficult to immobilize, observe and manipulate. Therefore the handling of GUVs for synthetic biology applications requires new methods, a selection of which is shown in this section.
For more detailed information there are a few reviews on handling of GUVs (Robinson (2019a)) (Robinson (2019b)).
First some of the traditional, non-microfluidic methods of GUV handling are described and afterwards various microfluidic approaches are shown.

#### 4.1.1.1 Non-microfluidic handling of GUVs

GUVs can be observed with light and fluorescent microscopy. Depending on the production method the vesicle solution can be very concentrated and it is advisable to dilute it in order to see individual vesicles. Always when an additional fluid is added it should have the same osmolarity as the inside of the vesicles otherwise they might burst or deflate.

Observation in a water drop on a standard glass slide can be done only for a short amount of time because the liquid dries quickly changing the osmolarity of the outer solution. Adding a coverslip significantly slows the drying of the water but depending on the properties and stability of the vesicles they do burst after touching the glass surface. Therefore this method is sufficient for a quick look at the GUVs for example as a control if the production method worked well but can not be used for longer observations or experiments.

Observation chambers create a more stable environment for the GUVs and additionally the vesicles can sediment by adding a solution of equal osmolarity with a solvent that has a lower density than the one inside the vesicle (Robinson (2019b)). It is common practice to grow the vesicles in a sucrose solution and later add a glucose solution. In addition to the resulting sedimentation this method has the advantage the vesicles are visible in phase contrast mode and a fluorescent dye inside the membrane is not necessary.
However long-term observation of individual vesicles is difficult because they are not completely immobilized and a before/after control of individual vesicles after adding an additional solution is basically impossible due to the movement that the addition of the solution creates.
These problems can be partially solved by the biochemical immobilization of the GUVs

on the surface (Kuhn *et al.* (2012)).
There are also several methods for physical immobilization including micropipettes (Sorre *et al.* (2012)), electrical fields (Steinkühler *et al.* (2016)) and optical tweezers (Delabre *et al.* (2015)). Several of these methods have also been applied inside microfluidic systems but outside of these they remain low throughput and might not allow investigations on a single vesicle level (Robinson (2019b)).

#### 4.1.1.2 Microfluidic handling and analysis of GUV

Observing a vesicle while changing the outer environment is an important experimental tool. To observe individual vesicles for a certain time period and to fully exchange the surrounding solution the vesicles have to be immobilized.
Additionally there are other experiments like sorting of vesicles that do not require immobilization. There are also several microfluidic systems designed for handling biological cells, but many of them rely on the self attachment of cells onto the surface (Khademhosseini *et al.* (2005)).

Some immobilization methods developed for bulk experiments were adapted for microfluidics. The glass bottom of the channel can be for example functionalized with a biotinylated molecule and then used to immobilize vesicles containing biotinylated lipids. This method was used to observe membrane transport similar to the results presented in this part (Li *et al.* (2011)) (Runas & Malmstadt (2015)). Another group used cholesterol to functionalize the surface. This eliminates the necessity to modify the membrane lipids (Kuhn *et al.* (2012)). However, the bonds might not last during high flow rates necessary to quickly exchange the outer solution and surface adhesion can additionally alter membrane properties (Robinson (2019a)).

Other immobilization methods include hydrodynamic flow (Cama *et al.* (2014)) where vesicles are not trapped but can be observed. This method allows for high throughput applications.
Optical traps both external (Shiomi *et al.* (2014)) and integrated (Delabre *et al.* (2015)), can be used for immobilization and also for manipulation for example mechanical testing. Current setups, however, are low throughput.
An example for a contact free immobilization method is dielectrophoretic trapping (Johann (2006)) (Voldman *et al.* (2002)) (Robinson *et al.* (2014)).

The most common immobilization technique in microfluidics is the physical trapping using microstructured features inside the chip.
Reported structures include side channels (Vrhovec *et al.* (2011)) which have been used for trapping bacteria and observing their growth (Probst *et al.* (2013)), rapid liquid exchange is probably difficult, but for experiments that need a low flow around the sample and to study long term exposure to certain substances it is a suitable design.
Other microstructures include wells for trapping GUV (Yamada *et al.* (2014)), trap and

release systems (Nuss *et al.* (2012)) and, the method used in this thesis, pillars inside the channel more narrow than the diameter of the object that has to be trapped (Robinson (2019a)). A more detailed comparison of various pillar trap designs is presented in Section 4.2.
Applications of microfluidic handling other than immobilization include electrofusion (Tresset & Takeuchi (2004)) and vesicle division (Deshpande *et al.* (2018)). For a detailed review on microfluidic handling of GUVs for synthetic biology applications see (Robinson (2019a)).

### 4.1.2 Importance of single vesicle analysis

One new feature of the presented assay is the time resolved analysis on a single vesicle level. This is a huge advantage compared to bulk methods that measure for example fluorescence in a photometer.
Single cell analysis for specific applications for example counting, sorting and fluorescence detection is well established with flow cytometry (Di Carlo *et al.* (2006)).
Enzymatic reactions and most other molecular biology experiments are currently performed in bulk. This experimental setup often smooths out differences because they do not happen exactly at the same time. With single cell/single vesicle analysis it can be determined how rapid a process actually happens.
Reactions of encapsulated molecules inside vesicles can be seen as bulk experiments in a very small container as we still do not see the single molecule or single enzyme level. However, reaction rates inside vesicles with the additional surface interaction and confinement effects are probably closer to the reaction environment inside a biological cell.

When membrane permeability is measured in bulk experiments, it is difficult to differentiate if a part of the vesicles release all their content or all of them release a certain amount. Analysis of processes in single GUVs as model systems have lead to more accurate knowledge of the mechanism of certain proteins, for example permeability inducing proteins (Apellániz *et al.* (2010)).
It also can reveal subpopulations due to heterogeneities in structure and function. This is important as, depending on the vesicle production method, only a certain percentage of the created vesicles will be unilamellar or there might be other differences in the membrane. The unilamellarity is an issue with vesicles formed by electroformation as used in this part of the thesis. Freeze-thaw cycles can be used after the electroformation to obtain unilamellar vesicles. The microfluidic double emulsion from part one produces unilamellar vesicles with a homogenic size but the amount of leftover residual oil might differ and change the membrane properties.

During the experiments shown in this part, individual vesicles would show no permeation of the dye while other vesicles were significantly brighter then the outside solution. Most single cell or vesicle analysis methods have been described for eukaryotic cells and

GUVs which are visible with light microscopy. In addition also a nanofluidic chip for the analysis of vesicles or biological samples like viruses in the 100 nm range was developed (Friedrich *et al.* (2017)).
If it becomes visible that there is a subgroup not showing the expected behaviour it gives a chance for further optimization of the liposome preparation process or the protein reconstitution process and therefore can be used to improve the overall stability and efficiency of the system. It allows also to have a more realistic estimation of the actual process under observation.

### 4.1.3 Membrane permeability and transport

When reactions are not just measured in solution but are transferred into compartments, it is necessary to supply the substrate across a membrane and in some cases to remove a product or to transfer it to another compartment. For the optimization of processes inside the compartment it is not only important to know if a substance is able to permeate the membrane, but also to be able to measure the kinetics to optimize for example supply of the substance for a reaction.

Membrane permeability is an important factor in drug development. No matter how high the affinity of a drug to the target receptor or enzyme is, if it can not reach it because it is not able to cross membranes inside the body it is abandoned very early in the development process.
A simple model estimating the permeability of biological membranes to a range of molecules is the Overton's rule (by Charles Ernest Overton 1899) 'the higher the lipid solubility of a molecule, the higher the permeability' (Al-Awqati (1999)) (Missner & Pohl (2009)). The problem for most biological applications is that molecules that have a high lipid solubility often have a low water solubility and are not able to reach the membrane. Additionally hydrophobic molecules can accumulate inside the membrane which is later shown in Section 4.5.3.2.
A common and very simple way to predict the membrane permeability, for example during a drug development process, is the partition coefficient of a substance between water and octanol (Leo *et al.* (1971)) (Stein (2012)). But the partition coefficient does not reflect the various compositions of membranes. Additionally the membrane permeability depends on the size of the molecule. The partition coefficient merely measures the lipophilicity of a molecule but for large molecules that easily dissolve in octanol crossing a membrane can still be difficult (Levin (1980)).
Other well established tests in the pharmaceutical industry are Caco-2 cell cultures. These are human epithelial colorectal adenocarcinoma cells which can provide a realistic measurement of the absorption of a molecule inside the human gut (Sambuy *et al.* (2005)). This cell model has also been integrated into microfluidic chips (Tan *et al.* (2018)). They do not necessarily provide an accurate prediction of the permeability into other mammal cell types and even less about the permeability across the

membranes of other organisms such as fungi and bacteria or artificial liposomes. Cell culture experiments also require a lot of equipment, specialized rooms that allow work under sterile conditions and a significant effort growing the cell culture and performing the experiments.
In synthetic biology there is also the possibility to modify membranes with nanoparticles or replace phospholipids with polymers tailoring the membrane features for a specific application. Therefore a simple, direct measurement of permeability through the membrane used would be advantageous especially for synthetically modified membranes.
A widely accepted theory for the transport of small molecules across membranes is the solution-diffusion model (Mathai *et al.* (2008)) (Cama (2016)).

$$P = \frac{KD_c}{d_c} \tag{4.1}$$

It states that the permeability coefficient P is proportional to K, the partition coefficient and $D_c$, the diffusion coefficient inside the membrane and it is inversely proportional to the thickness of the membrane $d_c$ (Mathai *et al.* (2008)). This model, however, seems not be able to predict the membrane permeability for passive transport accurately in many cases (Xiang & Anderson (1998)).
In addition to the influence of the properties the molecule that crosses the membrane, the permeability is influenced by the lipid composition of the membrane. It has been shown that the presence of cholesterol and sphingolipids decreased the water permeability of the membrane and the structure of different phospholipids also influences the permeability (Mathai *et al.* (2008)). This will be relevant to explain experimental results shown in section 4.5.
Additionally other substances in the solution especially surfactants can strongly influence the membrane permeability. For many surfactants the effect on membranes is concentration dependent. At very low concentrations they often have no influence on the permeability until a critical amount is reached and the permeability increases but the cell or liposome stays intact. At concentrations usually above the CMC the surfactant leads to a solubilization of the membrane (Ueno (1989)) (Koley & Bard (2010)).

#### 4.1.3.1 Methods for membrane transport measurement

One method for measuring membrane permeability and transport is based on change in osmotic pressure. Unilamellar liposomes filled with caboxyfluorescein are exposed to a sudden increase in outside osmotic pressure. This leads to a deflation of the vesicles by outflow of water and subsequently to an increased concentration of the fluorescein and self-quenching of the dye. The rate of the fluorescence decrease is measured (Lande *et al.* (1995)).
There is another assay that also uses the self quenching effect but the other way around. Liposomes are filled with concentrated, self-quenching dye and if this dye is released to the outer solution it is diluted enough to be fluorescent again (Braun (2016)).

Black lipid bilayers with electrophysiology measurements can be used to measure movement through membrane proteins by detecting a blockage of ionic current while the molecule is moving trough. This method has been used to characterize OmpF facilitated transport (Delcour (1997)). For this measurement the bilayer is usually placed between two chambers with volumes in the order of a millilitre. It can measure very precisely the movement of individual molecules through the channel, but it does not detect the transport kinetics present across a liposome membrane with a very small inner volume compared to the much bigger outer volume.
More recently there are also microfluidic systems for membrane transport measurements as shown in Figure 4.1 (Cama *et al.* (2014)).

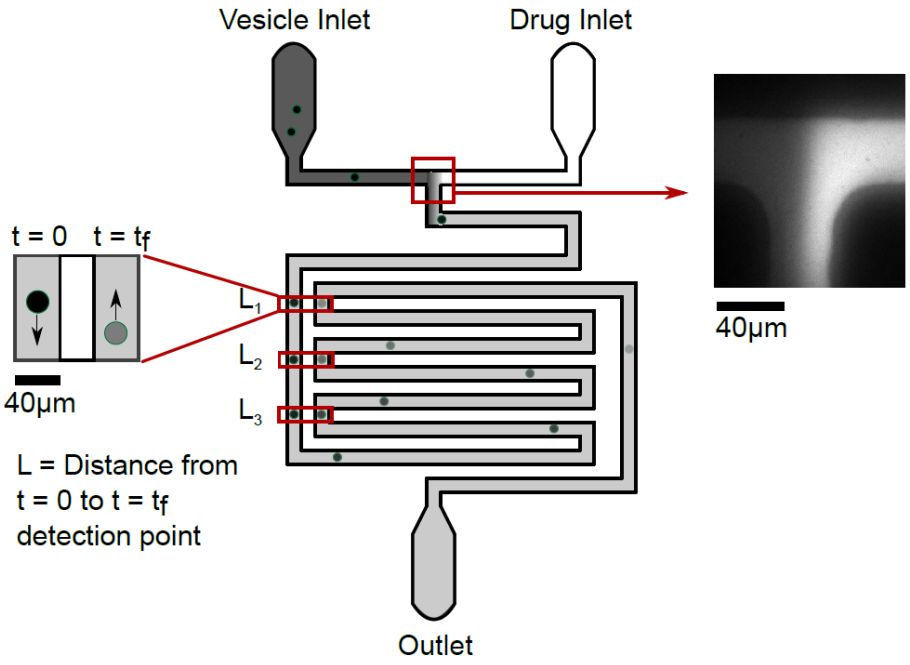


**Figure 4.1:** Image from (Cama (2016)). Schematic drawing of the chip used by Cama.

In the transport assay by Cama the vesicle solution is mixed 1:1 with the dye solution. This mixture then flows through a long channel where three different points an early part of the channel and a later part are designed to be very close to each other so these parts of the channel can be observed under the microscope at the same time. The membrane permeability is calculated from the difference between the vesicles at time points $t_0$ and $t_1$. The advantage of this system is that the chip and the setup is simple and the vesicles can be observed in a continuous manner. To be able to track the vesicles individually and to ensure a sufficient time passed between $t_0$ and $t_1$ the flow rate was set very low, resulting in a throughput of ca. 100 vesicles per hour. The disadvantage is that there is no continuous measurement of the dye permeating or being transported

into the vesicle but only one time point.
The Dittrich group developed several methods for GUV immobilization including chemical and physical immobilization. Notably they developed physical traps and showed time resolved dye outflow as a result of on-chip Hemolysin incorporation (Robinson *et al.* (2013)).

#### 4.1.3.2 Transport kinetics

Experiments by Cama and colleagues showed with confocal measurements that the time limiting step when suspending vesicles inside a solution of norfloxacin, an antibiotic that shows autofluorescence, is the permeation across the membrane while the diffusion of the substrate inside the vesicle happens almost instantaneously (Cama *et al.* (2014)) (Cama (2016)).

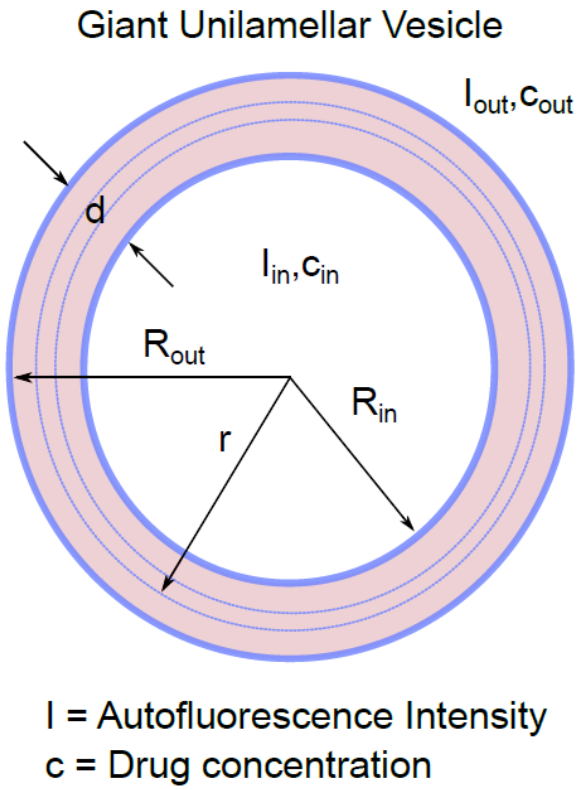


**Figure 4.2:** Image from (Cama (2016)). Schematic drawing of a vesicle.

Compared to transport measurements with electrophysiology across a black lipid membrane the inflow into a vesicle gives useful informations for synthetic biology applications and metabolic engineering because it does not only monitor the actual mem-

branes crossing process, but takes into account the decreasing concentration gradient between the inside and the outside solutions. Black lipid membrane setups usually have huge liquid volumes on both sides of the bilayer especially compared to the size of the bilayer.
An interesting and novel aspect of the presented method in this thesis is the time resolved measurement of the transport kinetics. The number of measurements is mainly limited by the exposure time of the camera.
Cama et al. calculated the permeation inside the vesicle based on the following equations (Cama *et al.* (2014)).
The permeation rate of molecules *J(t)* through the membrane at a given time $t$ is given by equation 4.2.

$$\frac{J(t)}{4\pi r^2} = -KD\frac{dc}{dr} \tag{4.2}$$

Which after integration results in:

$$J(t) = 4\pi R_{in}R_{out}\frac{KD}{d}(c_{out} - c_{in}(t)) \tag{4.3}$$

with $D$ as the diffusion coefficient and $K$ as the partition coefficient. This equation works for a constant $c_{out}$, for an increasing outside concentration like in the later presented system at the beginning or in general changing outside concentrations this equation gives incorrect results. The thickness of the bilayer is $d$ and is depending on the lipid 5-7 nm (Roberts *et al.* (2002)). Compared to the radius of the GUV, $R$, it is negligible. Therefore $R_{in}$ and $R_{out}$ can be considered as nearly equal (Cama *et al.* (2014)).
Additionally, as the concentration inside the vesicle is homogenous the following equation can be written (Cama *et al.* (2014)):

$$J(t) = \frac{dc_{in}(t)}{dt}\frac{4\pi R^3}{3} \tag{4.4}$$

Equating the two equations gives:

$$\frac{dc_{in}(t)}{dt} = \frac{3KD}{Rd}(c_{out} - c_{in}(t)) \tag{4.5}$$

Solving this equation with the permeability coefficient $P$ defined as $P=KD/d$, we get the following solution (Cama *et al.* (2014)):

$$P = -(\frac{R}{3t})ln(\frac{c_{out} - c_{in}(t)}{c_{out}}) \tag{4.6}$$

Cama and colleagues performed experiments without continuous measurement and only had two data points t0 and t1 after a fixed amount of time. They used the equation to determine the permeability coefficient for various conditions (Cama (2016)).

The experimental setup in this thesis is different and a continuous measurement is

possible. The equation can be used to draw an idealized curve of the permeation kinetics and to understand which factors influence the membrane permeability.
Figure 4.3 shows a graph of a theoretical transport kinetics curve based on Equation 4.6. The radius was set to 50 $\mu$m, the outside concentration was set to an idealized

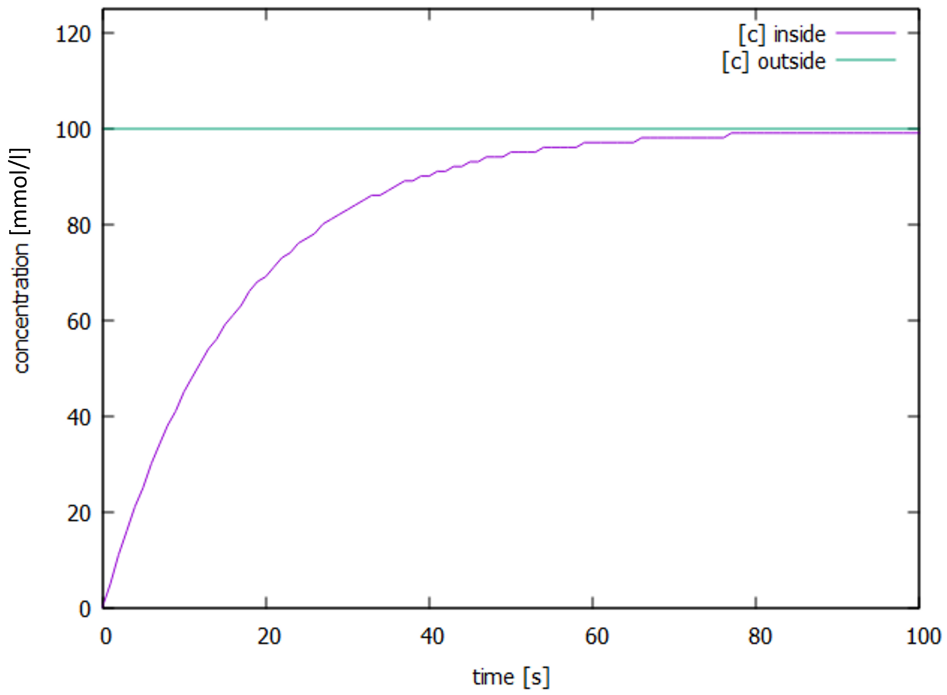


**Figure 4.3:** Calculated concentration profile over time for P=1.

constant 100 mmol/l. This of course does not reflect that the exchange of the outer solution does not happen immediately but takes several seconds.
This model takes into account the changing concentration inside the vesicle. The outside concentration, once the solution is completely exchanged, can be assumed to be constant due to the flow and continuous supply of fresh dye solution.
This is an advantage compared to the non-microfluidic handling methods. While to some extent an exchange of the outer solution is possible, the concentration directly around the vesicles will decrease adding diffusion processes to the kinetics.

When there are reactions inside proceeding (like the CETCH cycle) it is important to know the transport kinetics to guarantee input of substrate to keep the reaction running and in some cases it is also important to remove the product with a transporter to prevent product inhibition. At the same time all the intermediate products should stay inside the liposome otherwise the reaction will stop.
So membrane permeability and accessibility for existing membrane transporters have

to be tested for substrates, intermediate products and final product.
It might be not possible to enable movement across the membrane via permeability or a transporter just for the substrate and the product but not for the products of the intermediate steps. In this case it could make sense to modify the membrane to be highly permeable for all small molecules but not for proteins. Creating an equal concentration of the substrate and the intermediate products inside and outside of the vesicle and freely move back and forth while the proteins stay confined inside, close to each other.

## 4.2 Device design

### 4.2.1 Reported designs

For a review on microfluidic trapping with further examples see (Robinson (2019b)).
As mentioned before the Dittrich group published several microfluidic trapping designs. One of them used for trapping single GUVs and exchanging the external liquid is shown in Figure 4.4. It has separate chambers each of them with one trap.
Once the traps are filled with GUVs there is another PDMS layer on top which can be pressed down. This results in a ring structure to be lowered around the traps while the liquid can still flow freely in the remaining chip. The solution outside of the ring can now be exchanged. This allows a rapid exchange of external solution around the GUV once the ring is lifted again. In addition it also diverts the flow around the traps and avoids high pressures on the GUV which can lead to deformation or breaking of the vesicle.

The traps used inside this design were the fundament for the designs shown in this thesis. The trap designs with single traps in chamber, without the additional ring layer, were provided to me by T. Robinson (MPI for Colloids and Interfaces, Potsdam/Golm) and the first trapping experiments were done with this design.
An extension of the "Donut-Design" is a trap with four pillars supposed to trap two vesicles. Additionally a layer with two electrodes next to the traps was added to enable the observation of electrofusion of two trapped vesicles (Robinson *et al.* (2014)).
Similar trapping designs have also been published for the immobilization of individual mammalian cells (Di Carlo *et al.* (2006)). Most methods for single cell analysis are high throughput flow cytometry systems, which are widely used. They are, however, not suitable for continuous observations of individual cells for example for measuring a change in enzyme concentration inside a cell.

### 4.2.2 Novel designs

The first experiments shown here were done with designs from (Robinson *et al.* (2013)) and (Robinson *et al.* (2014)) without the pressure layer as shown in Figure 4.6. The

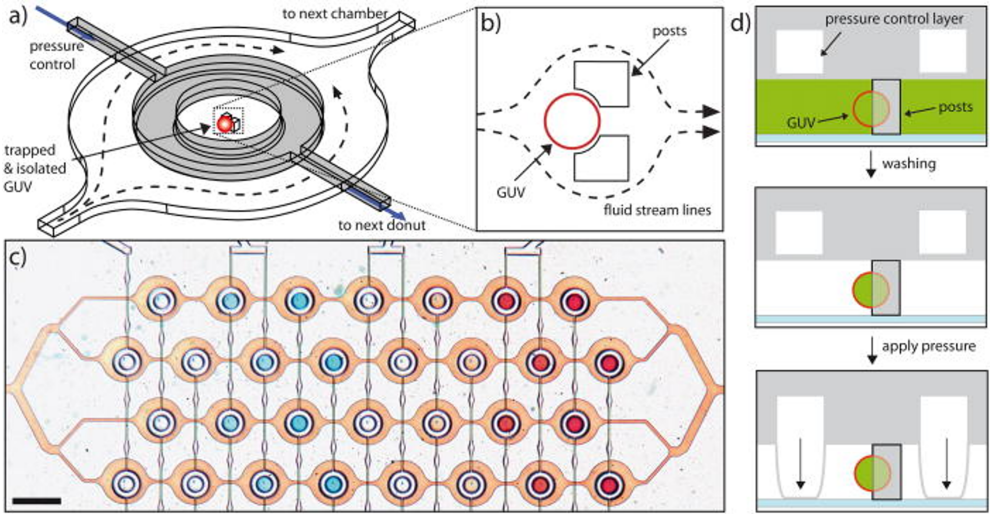


**Figure 4.4:** Image from (Robinson *et al.* (2013)). Vesicle is trapped and doughnut is lowered around the vesicle. Then the outside fluid is exchanged. When the donut is lifted the fluid around the vesicle is rapidly exchanged.

problem was that it only allowed observation of one trapped GUV in one run and often trapped more than one vesicle. If the GUV broke or was flushed out during the measurement the experiment had to be repeated. Novel designs were created to trap as many vesicles as possible in one compartment to be able to observe multiple vesicles at the same time. Various chips with different arrangement and number of traps were designed to test for differences in tapping behaviour.

Figure 4.7 shows the general chip design. The wheel like inlet and outlet and the filter structure after the inlet were copied from the initial design shown in Figure 4.6. The size of the chambers is designed so one whole chamber is visible in the microscope camera (the camera has a smaller field of vision that a person looking directly through the microscope) at a 400-fold magnification.
The chip has eight channels and in total 56 chambers. The number and arrangement of the traps varies between chip designs. The different designs are shown in Figure 4.8. All the corners are rounded to make the flow smoother. The channels were designed that each of them would have the same length of the way from inlet to the outlet and the water would flow equally in the whole chip. This attempt was not fully successful as the way through the four middle channels seemed to be slightly shorter than though the four outer channels. A side effect was that in the inner channels there were usually also more vesicles trapped.

Figure 4.8 shows the different trap arrangements inside the chamber. During the operation of the chip no huge difference could be observed between the different designs. The chips with the alternating traps seemed to fill up a bit better with vesicles than the traps that were arranged in one line. A high number of traps in the chip turned

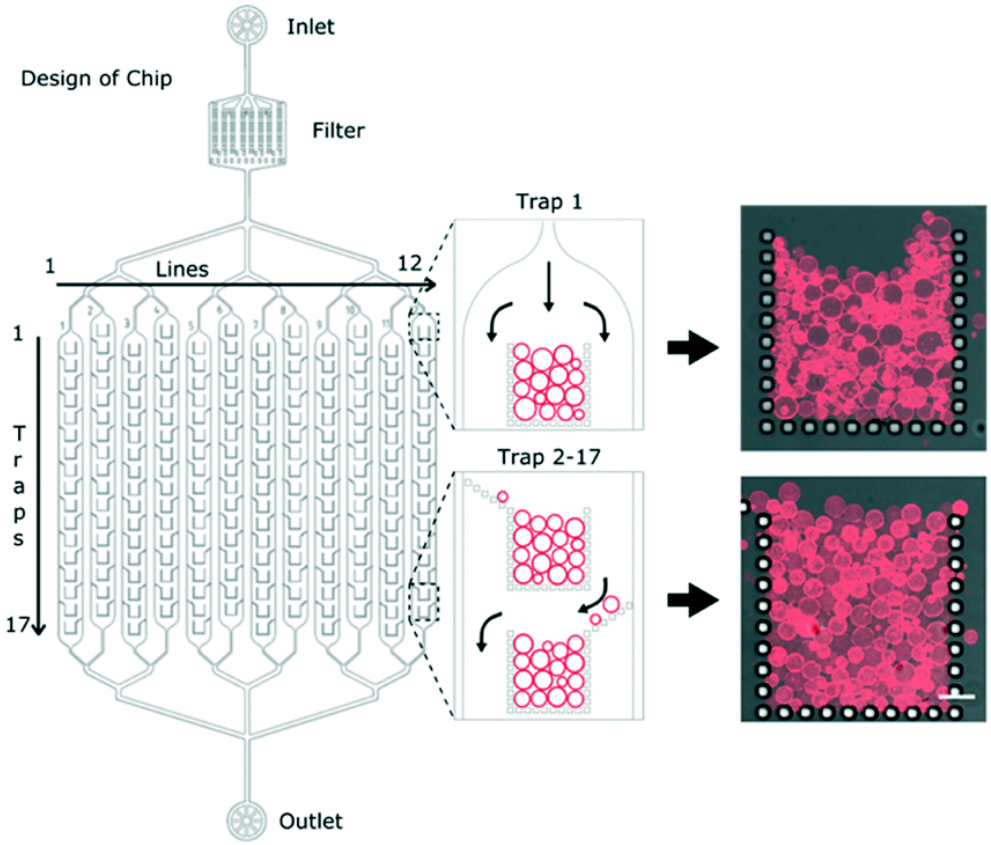


**Figure 4.5:** Image from (Yandrapalli & Robinson (2019)). Traps to capture more than 100 GUVs and observe them at the same time.

out to have no negative effect on the trapping. As a conclusion the best design for the experiments was design number 5 as it trapped the most vesicles and could be used longer even if a certain amount of traps were already broken.

Figure 4.9 shows another design that is called 'Pyramid design'. It has the same inlet and a similar outlet to the other chip but the middle part is just one triangle and the whole area is evenly filled with traps. It was a test how the vesicles would fill up such a big field of traps. Unfortunately the trapping posts were too small to hold up the PDMS ceiling during the chip production. The ceiling usually collapsed and the chip was not usable. The design was later updated with a few pillars with a wider diameter as structural support (design not shown) and it worked better. However, due to the already established experiments with the channel chips the updated chip was not used for any experiments.

Figure 4.10 shows the sizes of the trap posts in the original CAD drawing and inside the chip.

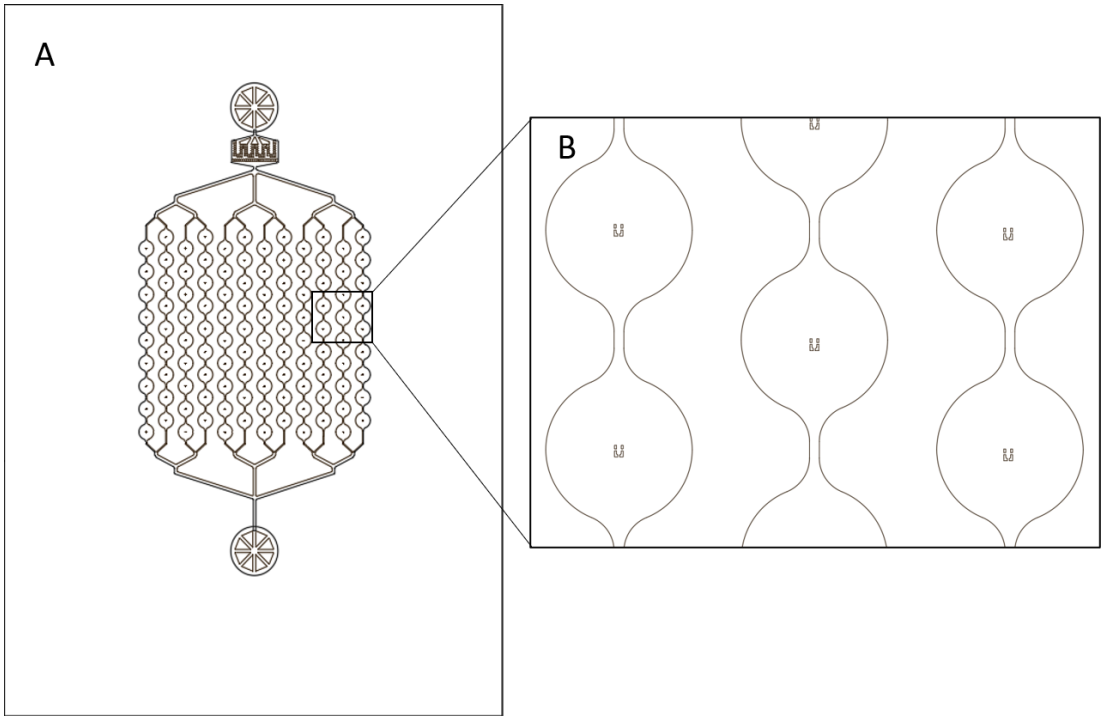


**Figure 4.6:** An overview of the whole chip with a zoom in on the chamber with the individual traps. This chip was initially designed by Tom Robinson supported by the Dittrich group for electrofusion experiments.

On top of the chip around the inlet channel is a reservoir for easy exchange of the inflowing solutions. The reservoir changes the light conditions under the microscope and therefore the design should leave enough space between the inlet and the rest of the chip. The rectangular structure with a lot of small poles inside works as a filter to keep bigger particles from blocking the channels and was adopted from an existing design. However, no dirt or any particles trapped in this filter were observed. Due to the limited size between the pillars large GUVs were sometimes trapped there, but due to the higher flow rates they either busted or were squeezed through the narrow channels.
One useful but originally unintended feature of the filter was that the structure is large enough to be visible without a microscope and helped to distinguish between inlet and outlet during the chip preparation and the placement of the reservoir.

A general issue to consider during the chip design is the variation of flow rates in the different channels and parts of the chip. The flow rate depends on the width of the channel. If there are several parallel channels their widths add up and the flow rate decreases.
As a result the flow rate is especially high in the inlet and the filter segment and prob-

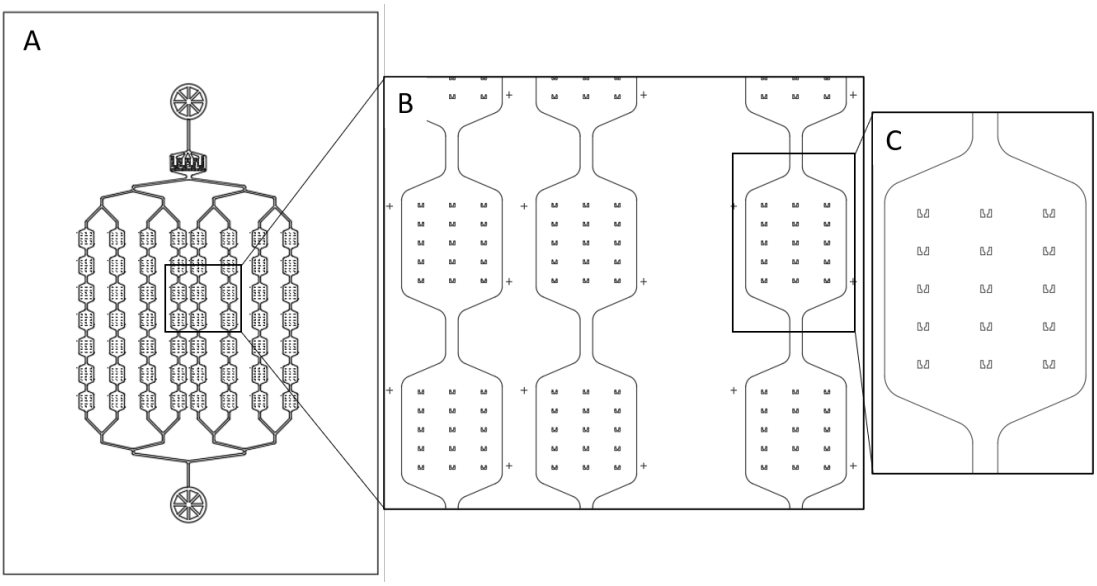


**Figure 4.7:** General chip design as drawn in the CAD program. (A) overview of the whole chip (B) enlarged view on several channels and chambers and (C) one chamber with traps.

ably a lot of vesicles break in this part. This could be problematic for the experimental results as a certain selection of the vesicles is taking place in this part of the chip. It might be interesting to repeat the experiments with a wider chip design and compare the results.

Figure 4.11 shows how broken and intact traps look like. In the brightfield images the broken traps are not always easily recognizable. To demonstrate the difference two chambers one with broken and one with good traps filled with fluorescent dye are shown. The shape of the traps Figure 4.11d is nicely visible and they appear completely black as the trap posts are touching the glass surface and no dye can flow below. The broken traps are still visible as there is a bit of PDMS hanging from the chip ceiling, but their outline is blurred and there is clearly dye flowing underneath them.

Figure 4.12 shows a design for larger traps than in the original designs to be used for example for the larger double emulsion vesicles. The silicon wafer for these traps was not made with masks out of chrome on glass but plastic masks were used that were also used to create the double emulsion wafers. The size of the structures that can be prepared with these masks during the UV exposure is not as small as with the chrome masks.

For this bigger traps the plastic masks were used to test if they can be used to prepare

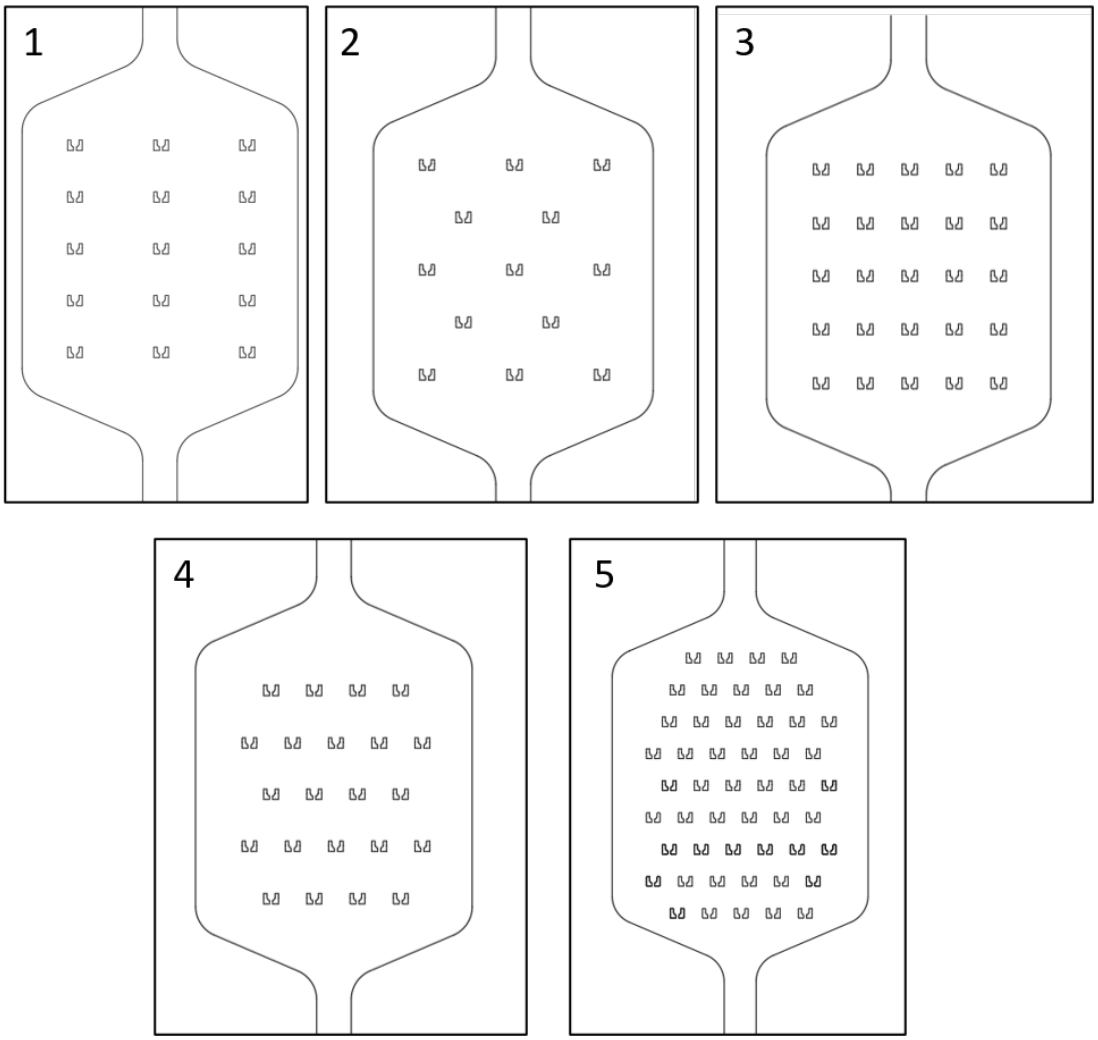


**Figure 4.8:** Designs 1 to 5 of different number and arrangements of the traps inside the chambers.

larger traps but as visible in Figure 4.12 they are still too inaccurate for such small structures and the resulting wafers were not usable.

## 4.3 Device operation

### 4.3.1 GUV preparation

Giant unilamellar vesicles (GUVs) were prepared by use of electroformation. The mechanism of this production method is explained in Chapter 2.
The general procedure is very similar for different samples, but depending on the lipid

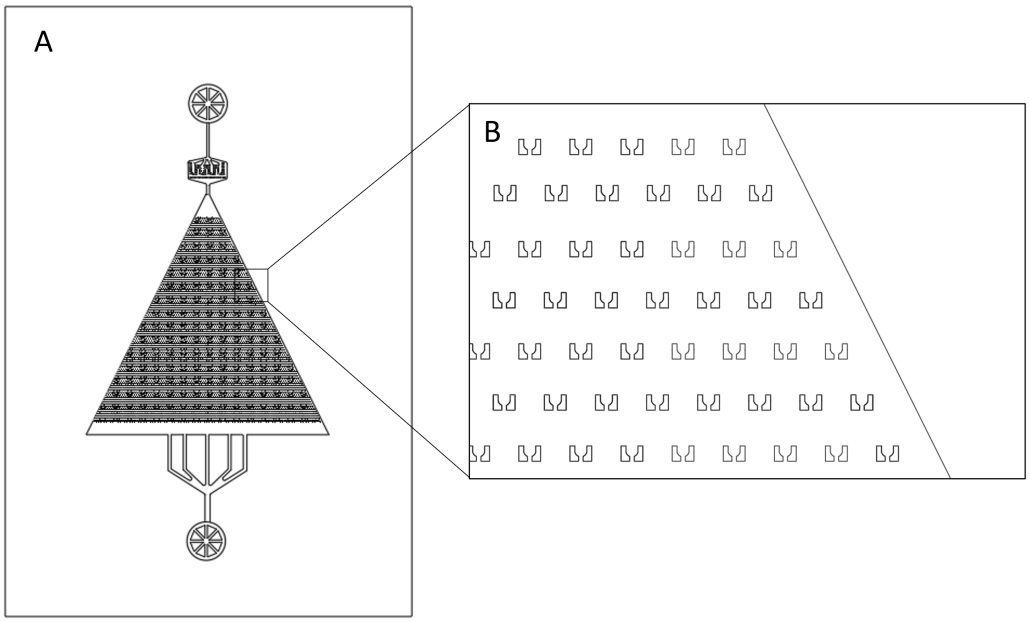


**Figure 4.9:** The pyramid design is a triangle with the whole area covered with traps. In total there are roughly 5000 traps on this chip.

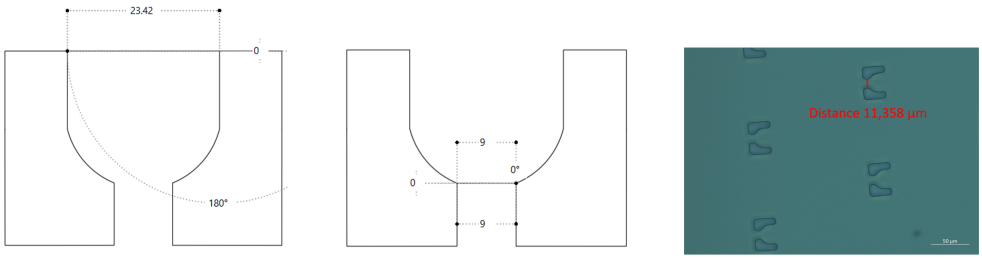


**Figure 4.10:** The first two images show the drawing inside the CAD program with a distance between the pillars at the upper side of ca. 23.5 $\mu$m and on the lower end where the vesicles get trapped of 9 $\mu$m. The smallest distance between the trapping posts of an actual chip under the microscope was ca. 11.4 $\mu$m.

composition the amount of lipid initially spread on the glass and the exact voltage, frequency and duration of the applied electric field varies. This conditions were optimized for various lipid compositions. Also the sucrose solution may contain additional substances. Below is one example protocol used to prepare DPhPC liposomes.
15 ul DPhPC (10 mg/ml) were spread on ITO glass slides and dried under nitrogen for 20 minutes. The lipid was rehydrated with 200 mM sucrose and GUVs were formed

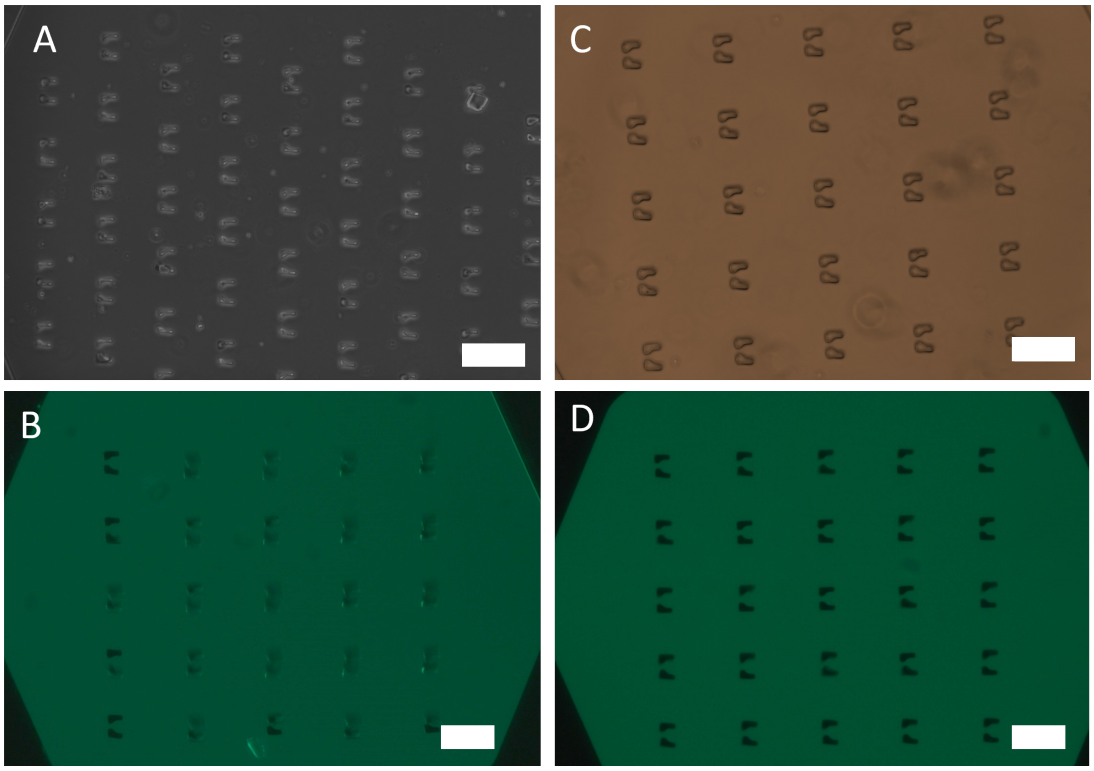


**Figure 4.11:** (A) and (B) show broken traps in bright-field and under fluorescent light with calcein inside the chip. Images (C) and (D) show intact traps in bright-field and fluorescent mode. Scale bar = 100 $\mu$m.

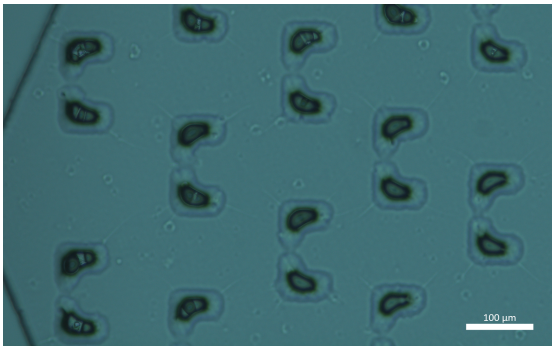


**Figure 4.12:** Large broken traps (designed for double emulsions). Scale bar = 100 $\mu$m.

by applying 2 V at 10 Hz for 4 hours followed by 3 V at 5 Hz for 1 hour. They were harvested by pipetting and stored at room temperature.

### 4.3.2 Filling of the device

Unlike the double emulsion chip described earlier, the bubble-free filling of this chip is more difficult. Due to the fact that there are several parallel channels simply plugging in the tubing and start pumping will result in equal filling of the chip until the first channel is completely filled. Once there is a water connection between the inlet and the outlet the flow will more likely proceed with a high speed through this one channel and not push out the air bubbles in the other channels. Additionally, even if a channel is filled with liquid, air bubbles tent to remain around the traps and are very difficult to wash out.

An alternative method to fill the chips is to fill the reservoir with water and to centrifuge the chips slowly. The success of this method depends very much on the available centrifuge.
There are two major problems. First, the chips break very easily even during very slow centrifugation due to the thin glass bottom. In general the bigger the diameter of the centrifuge rotor the easier it is to tape the chip to the bottom or to build a supporting structure. The second problem is that if the rotor is fixed and not swinging bucket, usually only half of the chip is filled after the centrifugation.
It is possible to work with a partially filled chip, but depending how many channels are filled the flow speed inside the individual channels changes which makes it more difficult to compare measurements recorded with different chips.

A method to fully fill the chips quickly and reliably is based on air removal by reduced pressure. The chip is taped to the bottom of a small bowl which is then filled with enough water to cover the chip. It is then placed in a desiccator connected to a vacuum pump.
PDMS is permeable for gasses and after a few seconds gas bubbles are visible on the surface of the chip. After 2-3 minutes in the desiccator the chip is completely filled with water and ready to use.

### 4.3.3 BSA coating

As mentioned in Chapter 2 the surface of PDMS is hydrophobic. The surface of PDMS can absorb and adsorb various substances.
Notably PDMS can absorb water which can lead to concentration changes (Robinson (2019b)), but is likely not a problem in the setup presented here as it is an continuous flow system and the channels had enough time to absorb the water before the experiment is started.
However, vesicles will easily adsorb to the surface and burst and lipids probably form a monolayer on the PDMS or glass surface. This can be also confirmed when observing vesicles under the microscope between a glass slide and a coverslip.
One option to decrease the number of vesicles bursting but not completely preventing

it is to coat the surface. There are different substances that can be used to coat PDMS surfaces the most common being BSA and beta-casein (Woo *et al.* (2013)) (Yandrapalli & Robinson (2019)). BSA seems to work on a wider pH spectrum (Robinson (2019b)) (Zittle (1966)). Here BSA was used for surface coating of the microfluidic devices.

For the coating, the chip was filled with a 2% BSA solution and incubated at room temperature for 15 minutes.
Without coating it was basically impossible to observe the vesicles for more than a few seconds as they immediately busted. With the coating an acceptable number of vesicles would remain stable. However if the vesicles contained a lipid membrane dye it was clearly visible that after the experiment was over especially around the traps a lot of vesicles had burst.
When the chip was reused the lipid layer on the glass and the PDMS made it easier for other vesicles to stick to that spot. This led to a situation that after a few uses of the chip a lot of vesicles, also very small ones and some "lipid threads" stuck to the surface at random places inside the chip not necessary in a trap (Figure 4.13). Additionally a lot of traps got blocked by blobs of small vesicles and could not be used for the experiment.

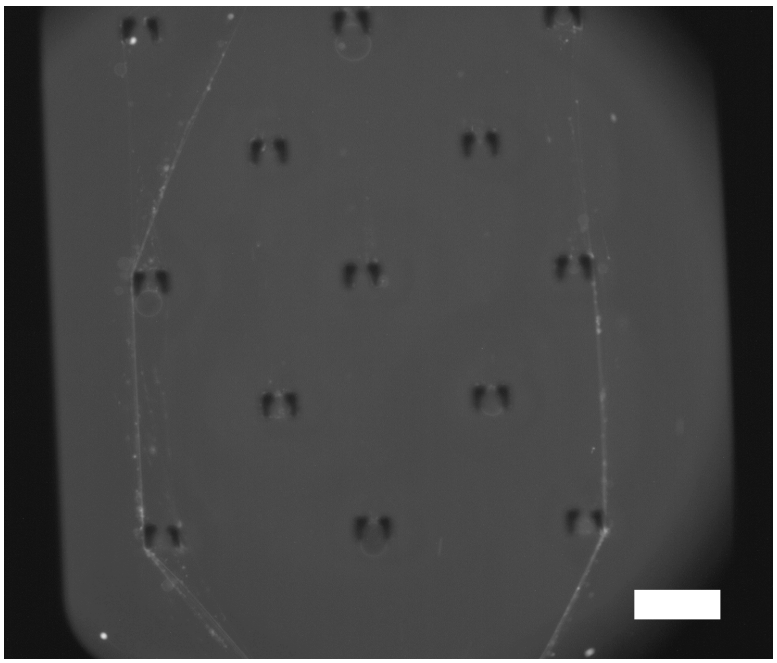

**Figure 4.13:** Strings of lipids and small vesicles on the traps after reusing the chip several times. Scale bar = 100 $\mu$m.

It is possible to wash the chip with ethanol and remove most of the lipids on the surfaces. However, the influence on the BSA coating is unclear and it would have to be

repeated. Therefore the chips were used for not more than three experiments and discarded afterwards.

### 4.3.4 Loading traps with GUVs

The experiments described in this chapter were made with GUVs preformed with electroformation. This vesicles were then introduced into the device.
A possible problem with this procedure is that it could cause unknown rupturing of the vesicles and may result in a biased population (Robinson (2019b)). Rupture of the vesicles was observed but no control experiments were done to determine if a certain group of vesicles would be more likely to break. As described later in this chapter incubation with certain surfactants caused the vesicles to break more easily to an extent that no data could be recorded with these samples.

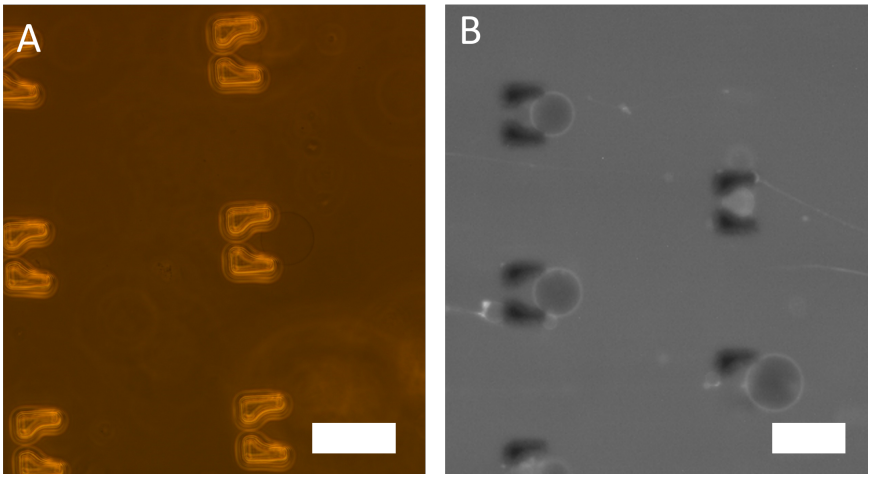


**Figure 4.14:** Vesicles in the traps pictures taken in (A) brightfield mode and (B) fluorescent mode. Scale bar = 50 $\mu$m.

Figure 4.14 shows vesicles inside the traps under the microscope in bright-field and fluorescence mode. The vesicles visible in Figure 4.14b were labelled with a fluorescent dye in the membrane.
For the membrane permeability experiments no fluorescent dye was used inside the membrane because it could change its properties. Without fluorescent marker in the membrane and fluorescent dye in the solution the vesicles and other chip features are not visible in fluorescent mode.
The various chip designs were described in Section 4.2.2. As mentioned there, the flow inside the chip was not completely uniform and as a result the inner channels were filled up more quickly than the outer channels.

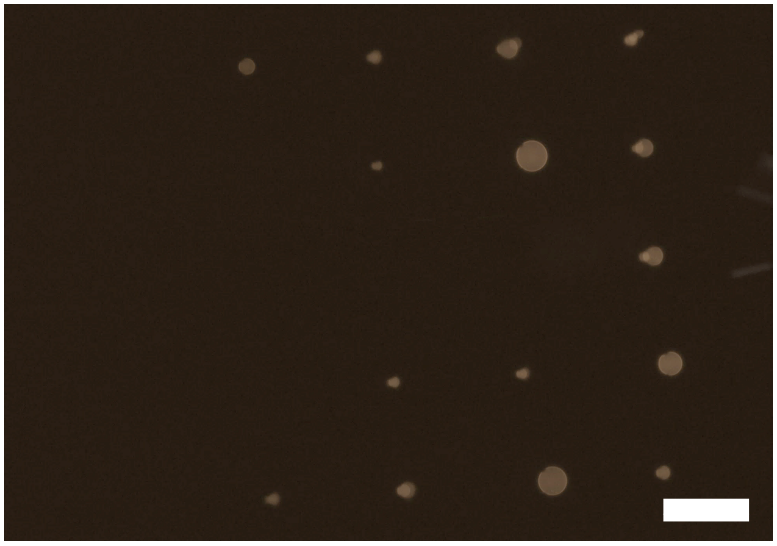

**Figure 4.15:** Chamber partly filled with vesicles. Scale bar = 100 $\mu$m. (Brightness of image increased for better visibility)

Another observation was that usually just the traps in the chambers close to the inlet were filled partly or completely and the chambers close to the outlet were mostly empty. This also did not change with longer waiting time.
Possibly a large portion of the vesicles burst before they could be trapped. The filling inside the chamber did not follow any distinctive pattern although the traps on the edges of the chamber were filled slightly more often than the traps in the middle (Figure 4.15). As mentioned before, the alternating traps seemed to fill up better than the traps that were arranged in a straight line.
Finally, something that would be useful to achieve in future would be a possibility to not only observe one chamber during one run but the whole chip. In the presented setup with the given camera resolution and technical equipment and the speed of the process that was recorded, it was only possible to record one chamber during one run. The design used in the reported experiments had 56 chambers.
Even considering that usually the chamber with the most trapped vesicles was chosen for recording, the number of data sets during one run could be more than ten times higher if there was a possibility to record all of the chambers. There are a few possibilities how this could be done. If the process that one would want to observe would be much more slow it would be possible to use an automated microscope table to record pictures one chamber after the other. Depending on the number of chambers, the exposure time and the speed of the table movement each chamber could probably be recorded every 1 to 5 minutes. If the process to be observed lasts several hours this would be an acceptable acquisition rate.
Another possibility would be the use of a camera with a higher resolution and a different

chip design that would either have no chambers, as was attempted with the triangular shaped chip or significantly bigger chambers. Here the challenge would be to find a design that would result in an even distribution of vesicles among the traps.

## 4.4 Experimental design

### 4.4.1 Selection of fluorescent molecules

A fundamental question for the following experiments in this chapter is how to observe permeation or transport of a molecule across the membrane. Depending on the method different groups of molecules can be observed.
Fluorescence microscopy was used which requires fluorescent molecules. Molecules that are not fluorescent can be labelled with a fluorescent tag but that changes the properties of said molecule. The easiest way for a proof of concept measurement of the setup is to choose a molecule that shows autofluorescence. Another problem is that quite many molecules that are fluorescent also show strong photobleaching (Demchenko (2020)).
The molecules used in the described experiments were selected with the OmpF membrane transport in mind. The perfect substance for this experiment should show no photobleaching, low membrane permeability, but at the same time be a substrate for the OmpF porin.
A substance used by Cama et al. (Cama *et al.* (2014)) for GUV membrane permeability measurements is the antibiotic norfloxacin. It was tested with the presented setup but the photobleaching was too strong.
A couple of other molecules were tested but most of them were not suitable because of their photobleaching. Using a confocal microscope that decreases the photobleaching because much less light is needed to excite the sample would drastically increase the number of suitable molecules.
Another option would be to observe a colourful (not fluorescent) molecule. Experiments showed that the colour was not visible enough under the microscope for reliable data collection and detecting small changes.
In the end most of the experiments were done with the substance cresyl violet a laser dye also used in histological experiments. It shows no photobleaching under the conditions necessary for the experiments and was expected to pass though OmpF.

### 4.4.2 Data acquisition and analysis

Images were recorded with an inverted Axio Observer 5 light microscope from Zeiss and two different cameras.
The first camera, used mostly for the OmpF transport assays, was the Phantom v611 high-speed camera from Vision Research controlled with the software PCC 2.6 (Phantom Camera Control Application, Vision Research) which was also used to record the videos. The Phantom camera has a 1 Mega Pixel resolution and a pixel size of 28 x 28

microns and produces greyscale images.
The other camera used was an Axiocam 506 colour (D) from Zeiss with 6 Mega Pixel resolution and a Pixel size of 4.54 x 4.54 microns.

An issue that makes comparability of individual experiments shown in this thesis difficult is the use of two different cameras for recording the data. For the initial experiments the phantom high speed camera was used. It was required for the droplet and double emulsion microfluidic experiments that require a high speed camera.
The number of images per second is limited by the exposure time, which has to be higher in fluorescence mode than in brightfield imaging. Videos were recorded with 24 frames/second with the Phantom camera and 10 frames/second with the Zeiss camera. The resulting videos were exported in the .avi format. Afterwards the videos were broken down into single frames using a script. This frames were then analysed with a software called vesicle scout written specifically for the analysis of this data. In this software points on the image could be marked, for example the inner part of a vesicle or the surrounding solution as control data.
One difference between the two cameras was that the Zeiss camera recorded blue, green and red light and generated a colourful image with three values for each pixel while the phantom camera recorded a greyscale image with one value for each pixel.
For the data analysis the images recorded by the Zeiss camera were later transformed into greyscale images generating one value comprised of the three existing ones. The greyscale values were used because that is also how the Phantom camera generated its pixel values. The results would not be expected to change if only the red colour would be analysed because the videos were recorded with fluorescence mode and the light filter has only a narrow range of wavelengths that it lets through.

The vesicle scout software showed one of the frames of the video and allowed the user to mark a number of round spots in the image. This spots were placed in the trapped vesicles unless marked differently. The diameter of the spot could be adjusted according to the vesicle diameter. The software then takes the pixel values covered by the spot and generates as average value for each spot and each frame. This list of values for the frames are then exported as a list of values and a graph.

Sometimes a vesicle burst or moved slightly. Also sometimes after a vesicle burst a second vesicle would enter the trap.
This is visible by a sudden change of brightness in the graph (Figure 4.16). It was decided in every individual case if data from this vesicles would be either discarded or part of the generated data was used. Data from different vesicles from the same run as well as from repetitions under the same conditions were used to generate an average value for a vesicle under a certain condition. This is how the data in the graphs shown in this part of the thesis was generated.
In addition, the outside brightness curve in Figure 4.16 occasionally showed a sudden

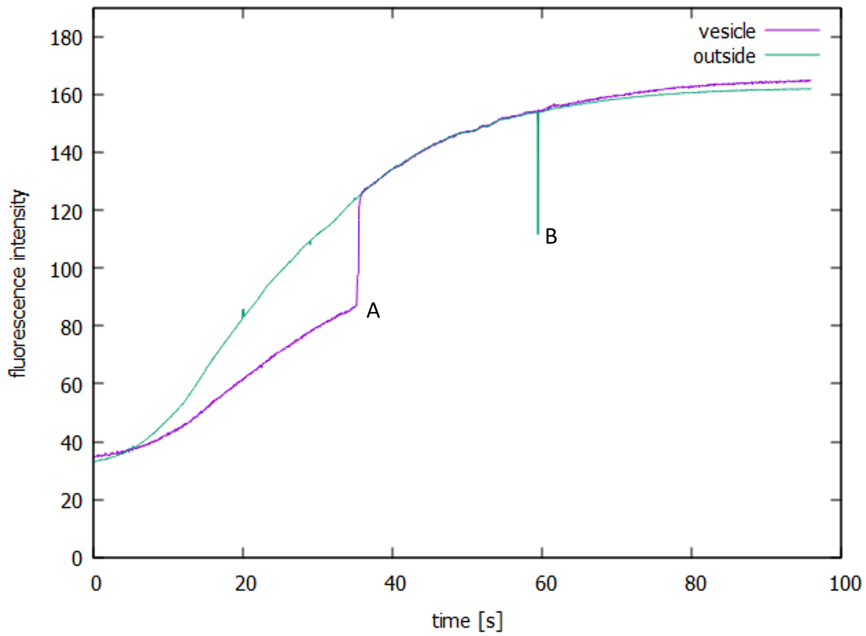


**Figure 4.16:** The violet curve shows the full dataset of a run with a vesicle leaving the trap resulting in the sudden increase in brightness (A) and a vesicle flowing through the channel causing a very short drop in brightness in the outside measurement (B).

drop at one point and then was restored to the previous level. This happens when a vesicle with lower brightness appears in some of the frames. If this happened either a different spot for the outside data was selected or the low value datapoint was removed.

### 4.4.3 Challenges and problems

Figure 4.17 indicates a fundamental problem during measurements with a fluorescent microscope. The excitation light goes through the glass slide, and the full height of the channel. The measured fluorescence does not only arise from the inside of the vesicle but also from the outside fluid above or below the vesicle inside the channel.

Additionally due to small variations in channel heights between chips and a certain variation in vesicle diameters the space inside the channel filled by the vesicle varies for each individual vesicle.

Furthermore the centre of the vesicle has the smallest amount of fluorescent liquid above or below resulting in the most realistic values there. The more the focus moves away from the centre to the side of the vesicle, the more fluorescence comes from the outer fluid. When observing the vesicle under the microscope a dark spot which gradually brightens is visible.

Better data could be acquired using a confocal microscope. Through a confocal mi-

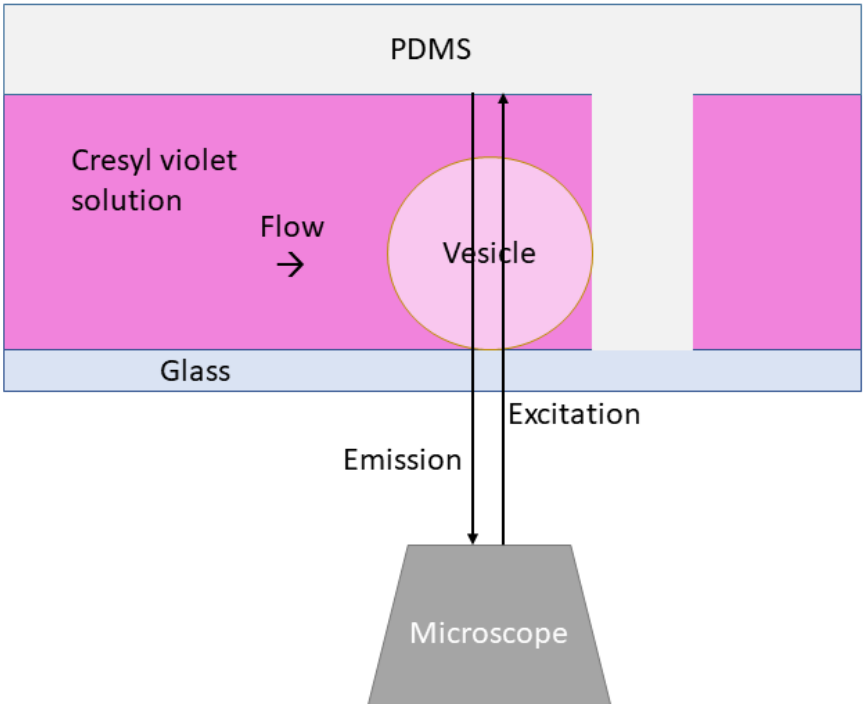


**Figure 4.17:** Schematic drawing of the fluorescence measurement inside the channel in a normal fluorescent microscope.

croscope an optical slice of the sample can be visualized. The probe is scanned with a point source of light from a laser. The light then has to pass through a pinhole that reflects out-of-focus light (Nwaneshiudu *et al.* (2012)).

Due to these various issues a quantitative measurement would be extremely difficult to achieve with a non-confocal fluorescent microscope. Even with a fluorescence microscope it would require extensive method validation and regular calibration and measurement of control samples.

However, conclusions can still be drawn from measuring different samples and comparing how the brightness of the inside of the vesicle changes compared to the background brightness of the chip. The data with the background brightness can be extracted from each experiment individually without additional experimental effort.

Unfortunately, a calculation of the absolute dye concentration inside the vesicle over time was not possible.

### 4.4.4 Determination of permeation coefficients from experiments

In Section 4.1.3.2 a formula for calculating the permeation coefficient, used by Cama et al. (Cama (2016)), is presented. It used two measurement points, one at the beginning and one after a fixed amount of time, controlled by the device design and the flow speed and the outside concentration was assumed to be always stable at 100 %.
This formula does not work for calculating the permeation coefficient in the here discussed experiment because of the changing outside dye concentration. Two additional factors that make the determination of the permeability coefficient from experimental data difficult are the possible absorption of light by the membrane components and the additional light that is emitted by the dye in the channel above and below the vesicle. In this section a simple model is shown that takes into account the problems mentioned before.
The following variables are used:

| | |
|---|---|
| $\alpha$ | absorption of light from inside the vesicle by the membrane |
| $\beta$ | normalized diameter of the vesicle as a percentage of the whole channel (example: beta=0.7 means that the vesicle diameter is 70 % of the channel height) |
| $\gamma$ | membrane permeability coefficient |
| $I_{in}$ | fluorescence from inside the vesicle |
| $I_{out}$ | fluorescence of the surrounding liquid |
| $\phi_{in}(t)$ | concentration of dye inside the vesicle as a function of time |
| $\phi_{out}(t)$ | concentration of dye outside the vesicle as a function of time |

In the presented experimental setup the observed light is emitted both from inside the vesicle and from the surrounding liquid.

$$I(t) = I_{in} + I_{out} \tag{4.7}$$

The light emitted by the surrounding fluid depends on the outside dye concentration and on the space inside the channel that is not occupied by the vesicle.

$$I_{out}(t) = \phi_{out}(t)(1 - \beta) \tag{4.8}$$

The light emitted by the vesicle is proportional to the dye concentration inside the vesicle, the diameter of the vesicle and the light absorption of the membrane.

$$I_{in}(t) = \phi_{in}(t)\beta(1 - \alpha) \tag{4.9}$$

Therefore I(t) can be described with the following equation:

$$I(t) = \phi_{in}(t)\beta(1 - \alpha) + \phi_{out}(t)(1 - \beta) \tag{4.10}$$

For $\phi_{out}(t)$ real measurement data from a spot in the channel outside a vesicle was used to show the influence of the changing outside concentration in the beginning of the measurement. The dye concentration inside the vesicle $\phi_{in}(t)$ can be calculated using equation 4.5., which was used by Cama et al. with a constant outside concentration, while here the outside concentration is changing with time.

$$\frac{d\phi_{in}(t)}{dt} = \frac{3DK}{Rd}(\phi_{out}(t) - \phi_{in}(t)) \tag{4.11}$$

Cama et al. used the permeability coefficient P defined as $P=KD/d$, not including the vesicle radius. As in the following calculations the vesicle radius is assumed to be constant, the coefficient $\gamma$ is introduced. Changes in $\gamma$ in the following graphs reflect changes in the permeability.

$$\gamma = \frac{3DK}{Rd} \tag{4.12}$$

Resulting in the following equation.

$$\frac{d\phi_{in}(t)}{dt} = \gamma(\phi_{out}(t) - \phi_{in}(t)) \tag{4.13}$$

The equation is solved numerically using the Euler method with the time step $\Delta$(t).

$$\phi_{in}(t) - \phi_{in}(t - \Delta(t)) = \gamma\Delta(t)(\phi_{out}(t) - \phi_{in}(t)) \tag{4.14}$$

With t equal to one divided by the number of data points in the outside measurement. This formulas were incorporated into a python script and the following graphs show the results of the simulation with varying inputs for $\alpha$, $\beta$ and $\gamma$ to visualize their respective influences on the measurement data.

Figure 4.18 shows how the inflow of dye into the vesicles would look like if there was no surrounding fluid and no membrane absorption of light. This condition is shown for two different values for the permeation coefficient D.

Figure 4.19 shows the influence of light absorption by the membrane. Again it is assumed here that the vesicle fills the whole channel and there is no fluorescence of the surrounding liquid. The green graph simulates measurements with no membrane absorption and in contrast the blue graph shows how measurements with 20 % light absorption would look like. The result of the membrane absorption is a ceiling effect. The measured fluorescence from inside the vesicle never reaches the same brightness as the outside fluorescence. This is an effect observed very often in the actual measurements presented later in this chapter.

Figure 4.20 visualizes the influence of background fluorescence on the measurement data. The green graph is presented for comparison and has no background fluorescence.

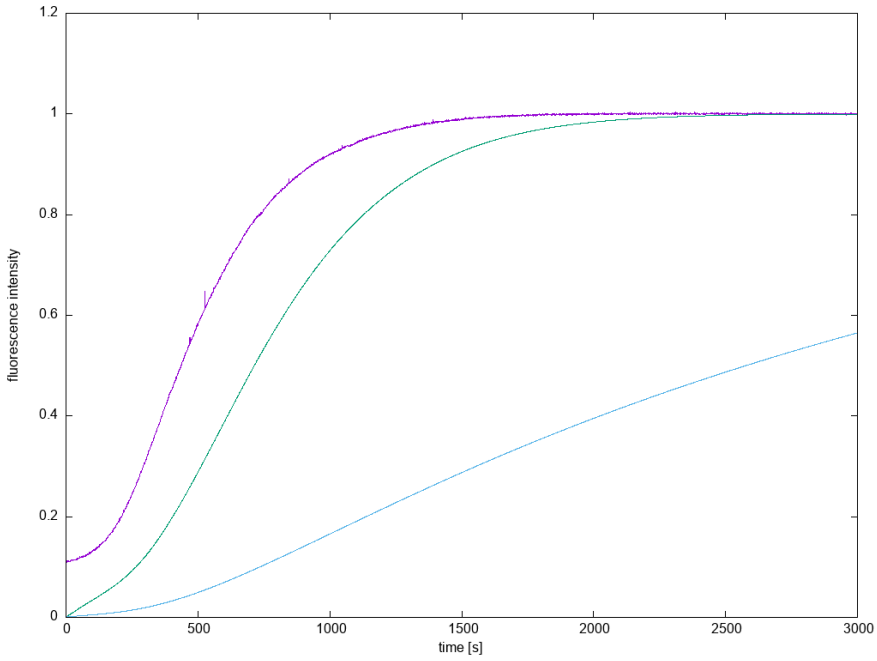


**Figure 4.18:** Fluorescence intensity outside the vesicle (violet) and two calculated curves with $\gamma$=10 (green) and $\gamma$=1 (blue).

The red graph shows fluorescence intensity of a vesicle with the same permeability coefficient but it is assumed the vesicle height is only 70 % of the channel height and there is some background fluorescence influencing the steepness of the curve. The yellow graph shows a theoretical curve of a completely impermeable vesicle that occupies 70 % of the channel height.

Figure 4.21 shows a simulation with all three factors influencing the measured fluorescence. The graph from this figure is very close to many of the graphs with experimental data.

These simulated factors are most likely not the only ones influencing the measured fluorescence. However, they show the influence on the fluorescence intensity curve and the difficulty to extract the permeability coefficient from the measurements. The influence of the membrane absorption is relatively easy to determine from the graphs because it just lowers the total measured fluorescence intensity.
It is much more difficult to separate the background fluorescence from the fluorescence inside the vesicle because the background fluorescence just makes the curve a bit steeper similar to the effect of a slightly higher permeation coefficient.
One possibility for the determination of the factor the background fluorescence played would be to measure the vesicle diameter in the recorded videos. One problem with that is that the vesicle could have a not perfectly spherical, slightly flattened shape due

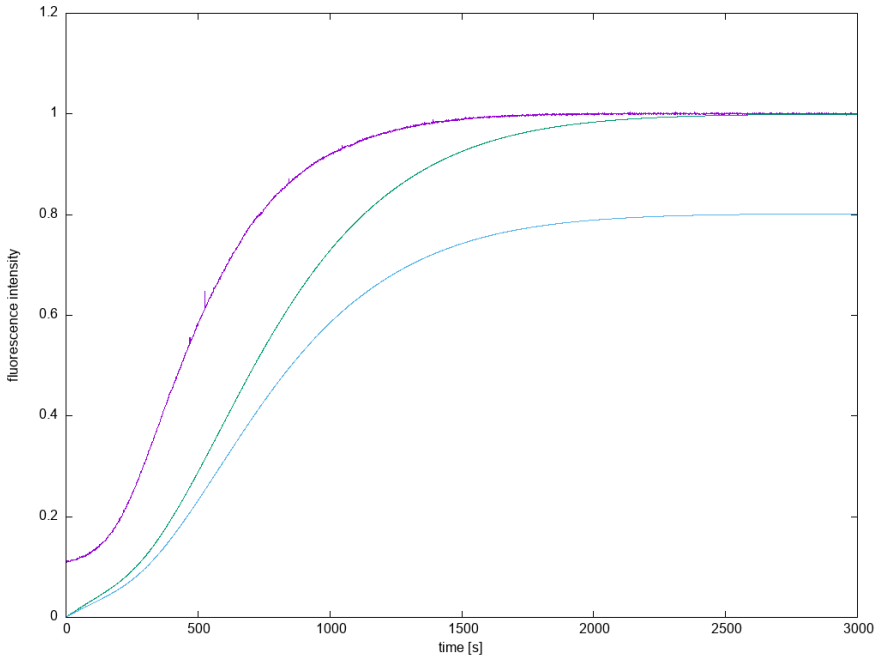


**Figure 4.19:** Fluorescence intensity outside the vesicle (violet), $\gamma$=10, no $\alpha$ (green) and $\gamma$=10, $\alpha$=20 (blue).

to the flow of the outside fluid. Additionally, the height of the patterns on the silicon wafers are very similar but not exactly the same and it is not known if the height of the channel in the PDMS chip is the same as the height of the pattern on the wafer.
Due to this reasons it was not possible to calculate an permeability coefficient from the measurement data. It is, however, possible to compare the recorded graphs to see trends in measurements with different conditions. These observations are presented in the following section.

## 4.5 Results

Figure 4.22 shows the general experimental procedure. First traps are loaded with GUVs and the surrounding solution is the same as the inner solution of the GUVs. Once the traps are loaded the suction pumps are stopped and the solution inside the reservoir is exchanged. Then the pumps are started again at a rate of 300 $\mu$l per hour and after a few seconds the sample solution slowly fills the observed chamber until the external solution inside the chamber is fully exchanged and the fluorescence change inside the trapped vesicle can be observed. The recording was started at the same moment as the pumps were restarted to also record the solution exchange.

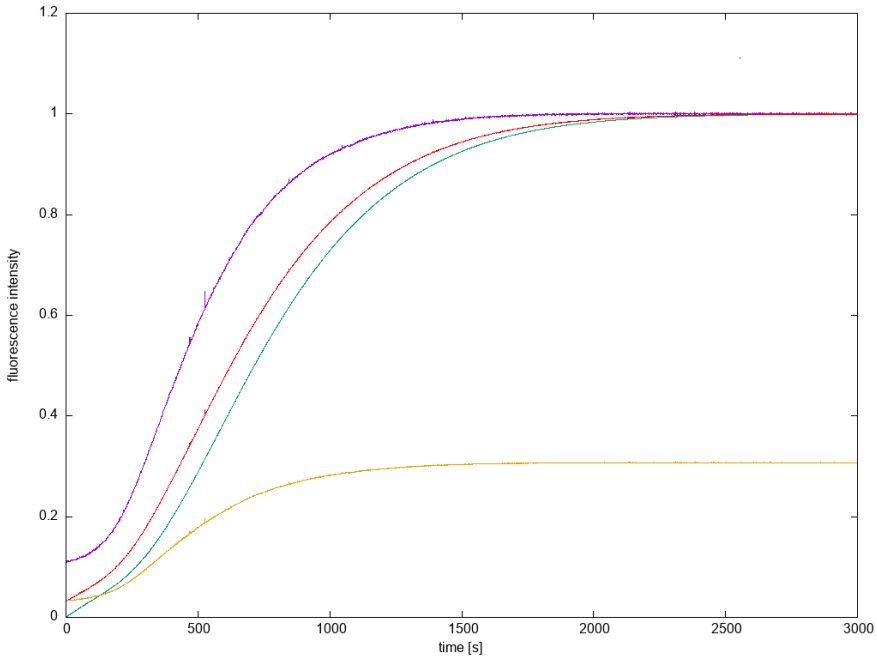


**Figure 4.20:** Fluorescence intensity outside the vesicle (violet) and (A) $\gamma$=10 (green), (B) $\gamma$=10 and vesicle is 70 % of measured volume ($\beta$=0.7) (red) and (C) vesicle is 70 % of measured volume but there is no fluorescence inside ($\beta$=0.7 and $\gamma$=0.1) (yellow).

### 4.5.1 General method validation

The consistency and reproducibility of the results is fundamental to compare and draw conclusions from different measurements.
Figure 4.23 shows a combination of outside control data sets all from different measurements. Apart from a couple of clear outliers, the final brightness when the chamber is fully filled with dye seems to form two groups.
The data was acquired on different days with different chips. The upper values are all from measurements with the detergents OG or OPOE in the solution.
As this graphs all show the background brightness inside the chamber and are not from inside vesicles it seems that certain substances can adhere to the PDMS or glass surface or even penetrate the PDMS and change the surface adhesion or permeability of the chip for the dye. The measurements from the lower group were control measurements as well as experiments including the surfactants F108 and P188.

The data presented in this chapter was collected over several years with a change of microscope and camera for the recording. The background brightness data sets presented in Figure 4.23 are all from the final setup with the same microscope, camera and lightning settings. Data from other settings was not included here because the absolute pixel values inside the images can differ quite substantially.

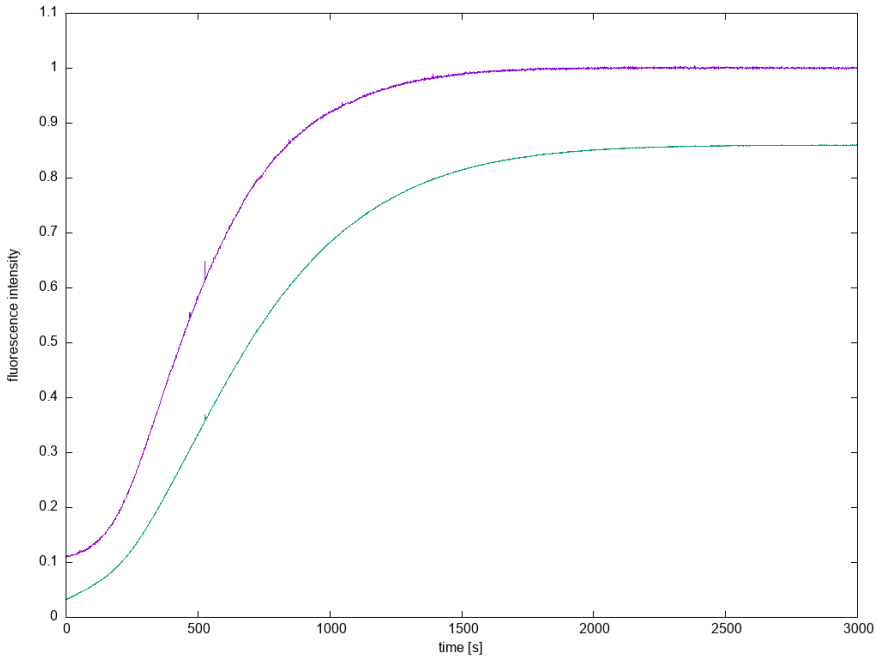


**Figure 4.21:** Fluorescence intensity outside the vesicle (violet) and inside with $\alpha$=20, $\beta$=0.7 and $\gamma$=10 (green).

Therefore it is also not possible to compare the absolute values recorded with different settings like for example the F108 and the OmpF transport measurements. Measurements shown in this chapter in the same figure were recorded with the same equipment and light settings.

As mentioned earlier, the transport kinetics also depend on the radius of the vesicle. In the literature the radius is sometimes factored in when calculating values such as an permeability coefficient (Cama (2016)) which was not done in this thesis. Due the chip design only vesicles of a narrow size range get trapped and therefore this factor was not considered during the data processing.
However it might be an important factor in future experiments depending on the scientific question. The microfluidic trapping method potentially offers an opportunity to selectively trap vesicles of various diameters by changing the trap sizes in the design. Different trap sizes could be even combined on one chip.

### 4.5.2 Photobleaching

One of the biggest challenges during the development of the measurement method is photobleaching of the fluorescent dyes. This can happen to normal dyes as well as fluorescent dyes.
Photobleaching can be also useful to detect diffusion inside the membrane and inside

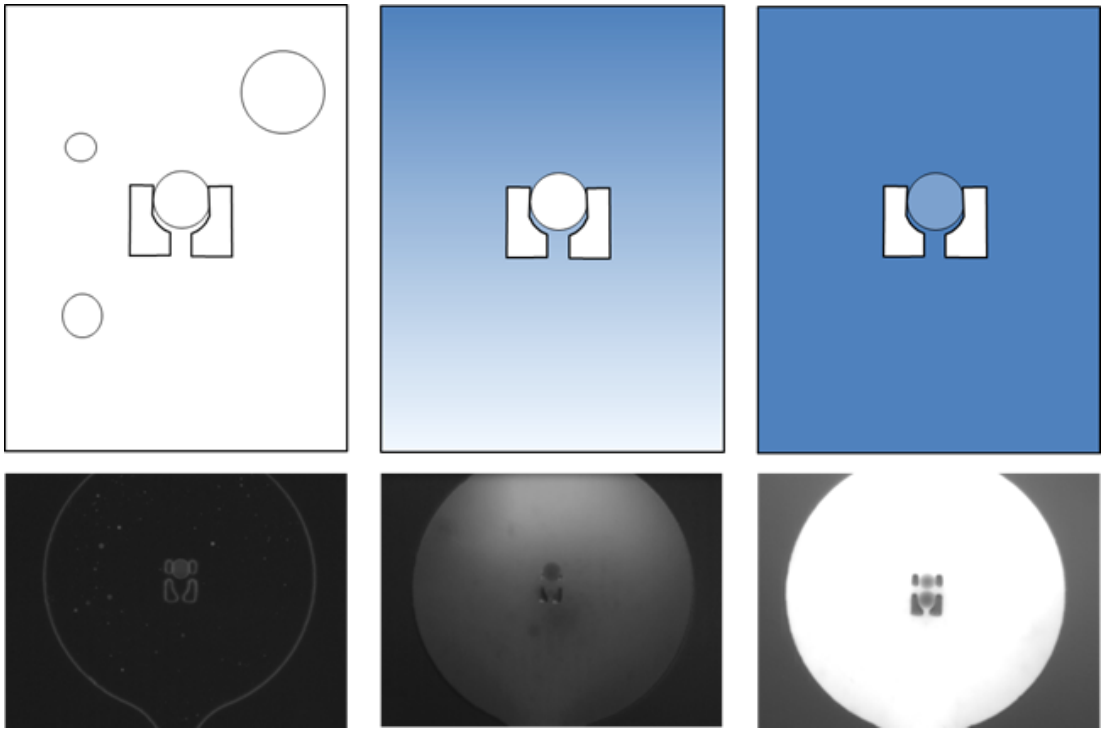

**Figure 4.22:** Schematic drawing and example images of the transport assay.

the vesicle by bleaching a specific spot with a short time interval of very high light intensity. Then the time until the same spot has the same colour as the surrounding area is measured. This is for example used in the FRAP (fluorescence recovery after photobleaching) analysis (Blumenthal *et al.* (2015)).
It is quite challenging to test the impact of photobleaching on the dye inside the vesicle. The outside solution is in a continuous flow and is therefore constantly exchanged. Hence, photobleaching mostly impacts the dye molecules inside the vesicle.
Additionally there is an exchange of molecules across the vesicle membrane. So bleached molecules are constantly leaving the vesicle and unbleached molecules are entering. The extent of this exchange depends on the membrane permeability. In addition, the photobleaching mechanism often involves permanently changing the structure of the fluorescent dye, making it not fluorescent any more but possibly changing the molecules membrane permeability properties.

There are different possibilities to test for photobleaching. A very simple test is to completely fill the chambers with the desired fluorescent dye or just put the dye on a coverslip under the microscope and expose it to the desired amount and wavelength of light for the time that the experiment takes without flow or other exchange of the dye and see if the fluorescence significantly drops.
It can be recorded and the decrease in brightness can be analysed from the images or

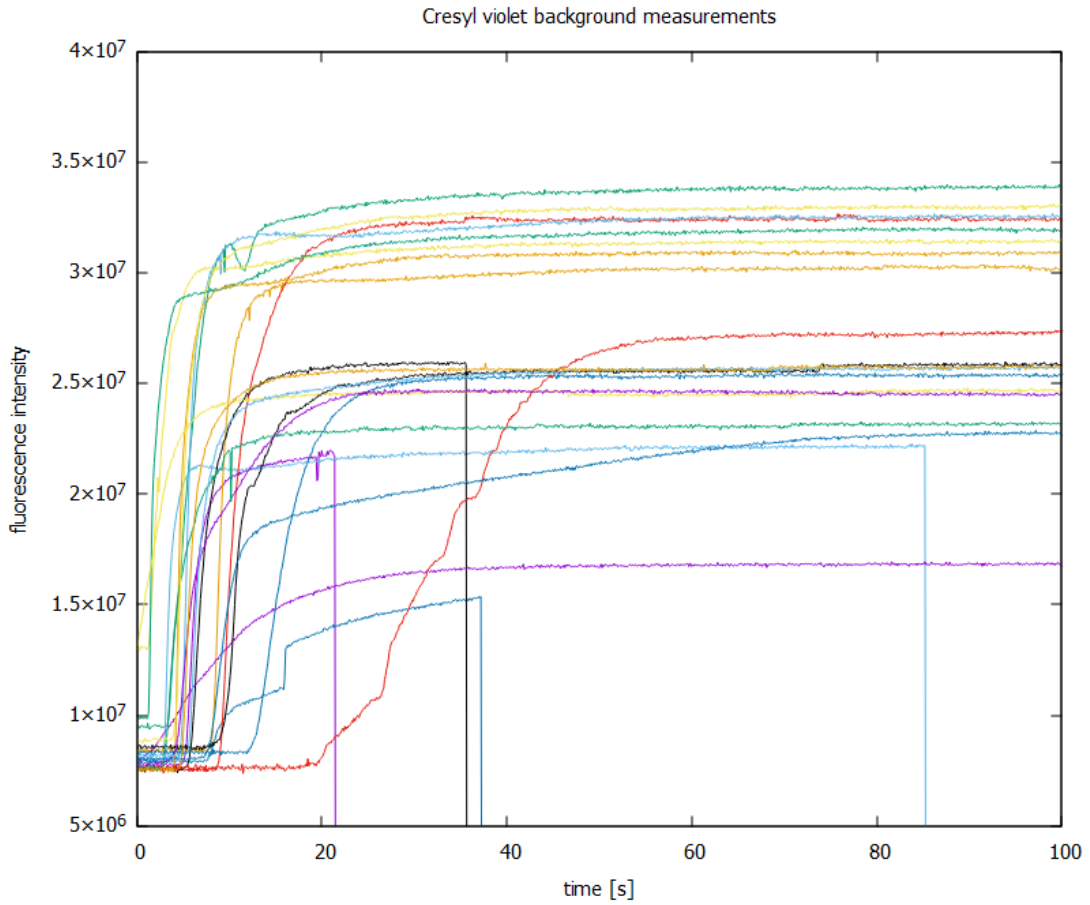


**Figure 4.23:** Combined cresyl violet background measurements (varying colours for better visibility).

for a very simple test the exposed region can be compared to a part of the chip that was not exposed.
This way a lot of fluorescent molecules were ruled out that would have been very interesting to test, including the antibiotic norfloxacine, used by J. Cama (Cama *et al.* (2014)), and, especially interesting for the MaxSynBio project, NADH.
Besides molecules that are completely bleached in a couple of seconds and molecules like cresyl violet that show no bleaching there are also a couple of molecules that show moderate bleaching and might be still stable enough for measurements. In this cases it is important to know how much of the decrease in fluorescence is due to bleaching and how much is due to membrane permeability. The following experimental design was established to measure this.

Calcein is a substance that is used as a fluorescence marker in cellular and molecular

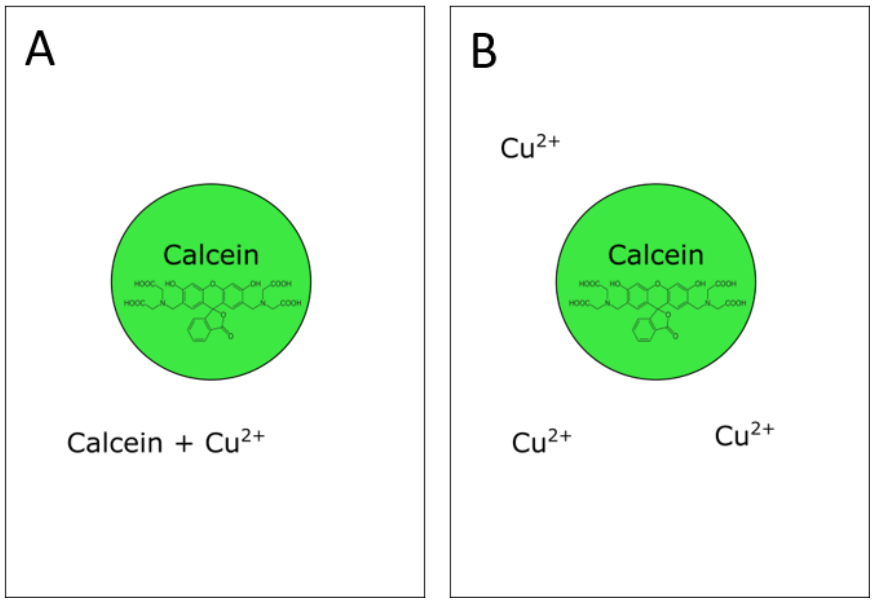


**Figure 4.24:** Photobleachig control experiment with (A) calcein inside and outside to test for photobleaching inside and (B) calcein only inside the vesicle to measure photobleaching and membrane permeability.

biology experiments. It shows moderate photobleaching which is sometimes used for experiments. Additionally calcein forms non fluorescent complexes with certain ions such as copper. This specific feature was used to test calcein photobleaching versus membrane permeability. In the control experiment calcein was encapsulated inside the vesicles during electroformation in its fluorescent form and stored in a solution with the same calcein concentration inside and outside of the vesicle.
After trapping the vesicles, the outer solution was exchanged with a calcein solution with the same concentration as the inner solution but with the addition of copper ions. As a result the calcein concentration inside and outside the vesicle was equal but the calcein solution outside was not visible to not disturb the measurement.
Under these conditions the decrease in fluorescence should be only due to photobleaching. It is, however, not a perfect setup because there could be still an exchange between bleached calcein from the inside and unbleached calcein from outside. As there is a constant flow of the outer solution the quenched calcein outside is likely not bleached yet. But calcein has a very low membrane permeability and is also used to test for membrane leakage (Katsu *et al.* (2007)) so this effect should be not very significant.
In the second setup the added effects of the photobleaching and the membrane permeability were to be tested. Again vesicles, filled with calcein during electroformation and kept in a calcein solution of the same concentration, were trapped. This time the outer solution was exchanged with a pure copper ion solution without calcein.

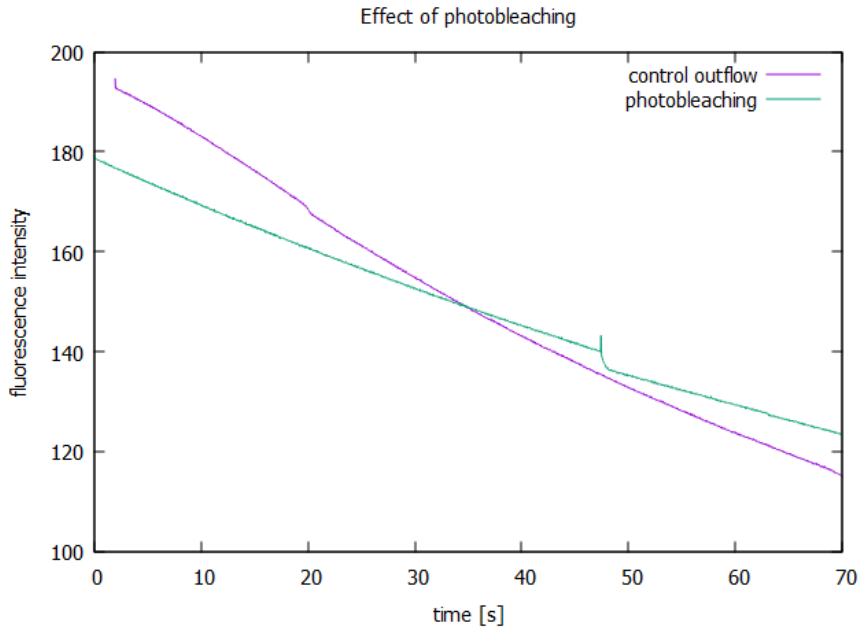


**Figure 4.25:** Vesicles with quenched calcein outside and control with no calcein outside.

Figure 4.25 shows the results of this experiment. The control sample shows a slightly steeper decline than the photobleaching experiment. It shows that for calcein the photobleaching influences the fluorescence intensity so much that it is not suitable for membrane transport measurements.
If the membrane permeability experiment would have been conducted without this control experiment, the decline in fluorescence would have been attributed to calcein leaving the vesicles while in fact it is mostly caused by photobleaching.
It could be interesting to add another experiment with an addition that causes a huge increase in membrane permeability, such as hemolysine, and to see if it would result in a visible difference.
This particular photobleaching control was not performed with cresyl violet because there is no known quenching agent and because never any photobleaching was observed for cresyl violet in preliminary experiments.

### 4.5.3 Membrane permeability

Encapsulated metabolic modules often need external supply of substrate and it can be desirable to release a product into the outer solution. Therefore in context of synthetic biology, but also for drug delivery applications, it is important to move molecules across the membrane.
The easiest situation is that the molecule has a membrane permeability that is high

enough to supply the reaction inside the vesicle. The membrane permeability depends on the molecule, on the membrane composition and can be further influenced by other components in the solution like surfactants used during the vesicle production or a membrane protein reconstitution. The influence of these factors are shown in experiments in the following subsections.
For the characterization and optimization of a compartment and the supply rate of a substrate for a reaction knowing the membrane permeability kinetics of a certain molecule into this compartment is important. There might be also situations where a low membrane permeability of a molecule is desired and it is necessary to have a simple test for that.
For the experiments in this section with the exception of the first subsection only one molecule, cresyl violet was used and various other factors like pH, lipid composition of the membrane and presence of surfactants were varied to test their influence on membrane permeability.

#### 4.5.3.1 Carbostyril vs cresyl violet

In this section the membrane permeability of two molecules across a membrane with DPhPC lipids is compared.

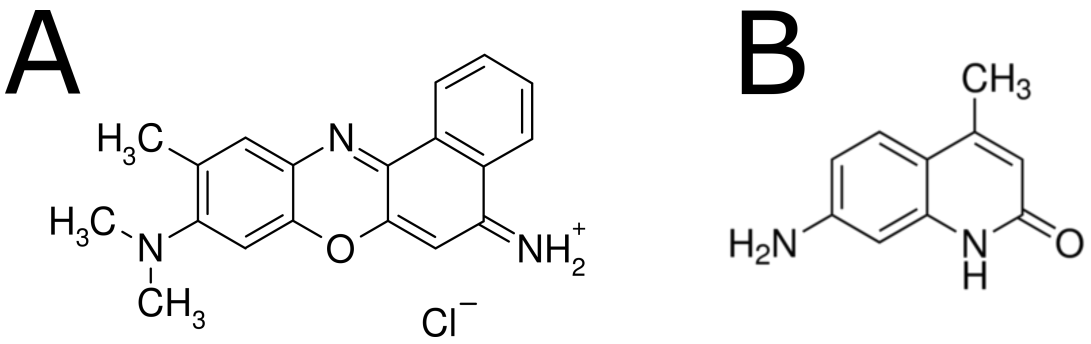


**Figure 4.26:** (A) Structure of cresyl violet and (B) structure of carbostyril 124.

Based on their properties and structure (Figure 4.26) carbostyril 124 is expected to have a higher membrane permeability than cresyl violet. First carbostyril has a molecular weight of 174 g/mol while cresyl violet has a molecular weight twice as high (340 g/mol) . Smaller molecules usually permeate the membrane easier and faster than larger molecules. In drug development usually the molecular weight should be lower than 500 Da unless a transporter is used.
More important than the weight is the charge of the molecule. If a molecule has a permanent charge it can usually not permeate an intact membrane even if it is just a small ion. In this case both molecules are weak bases and are present at physiological pH in the charged and uncharged form. This is an important feature for a molecule with good membrane permeability, because if it would be too hydrophobic its water

solubility would be too low.

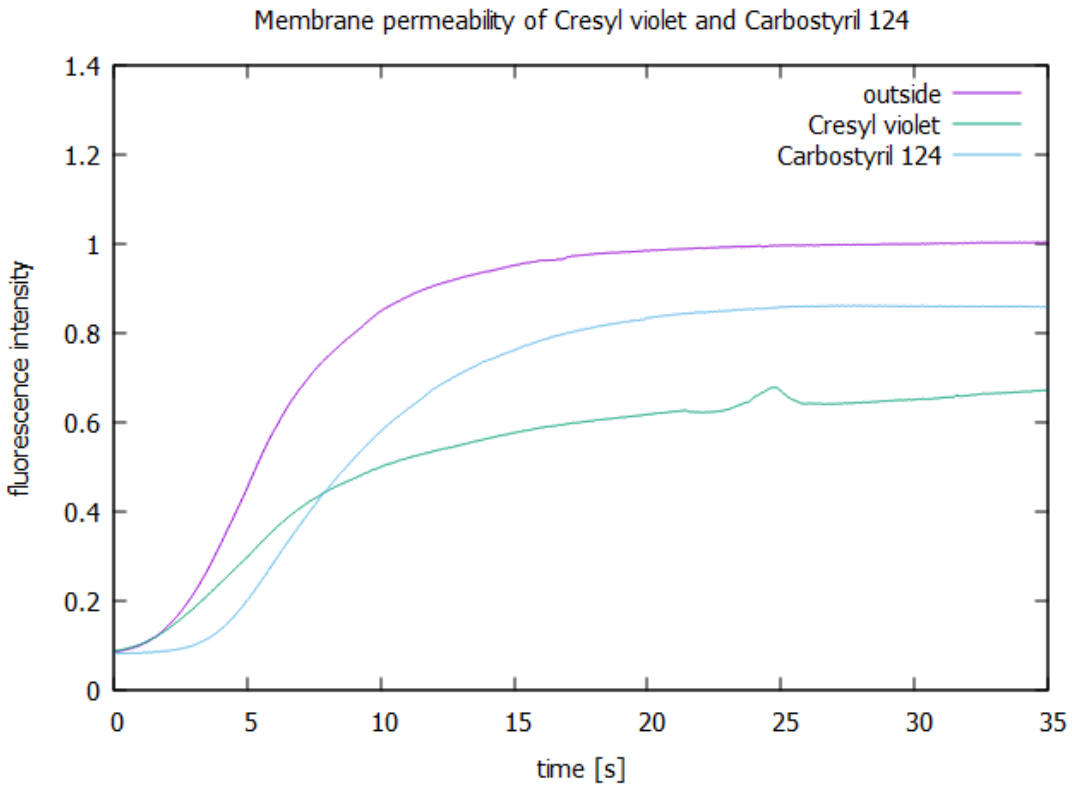


**Figure 4.27:** Comparison of the permeability of carbostyril 124 (n=8) and cresyl violet (n=4) in DPhPC vesicles.

This experiment was included to show the difference between a molecule with a very high membrane permeability versus a moderate permeability and to test how well the assay would show these differences. An example of a molecule with a low membrane permeability would be calcein but as mentioned before its photobleaching was too high to include the data.

#### 4.5.3.2 Influence of pH level

Cresyl violet is a weak alkaline molecule. That means that in neutral and acidic solutions the molecule is partly charged, the more acidic the solution is a higher percentage of the molecules have a positive charge.
In alkaline solutions the molecule is mostly uncharged. Most drugs have similar properties because they are sufficiently water soluble while still being able to permeate membranes at a physiological pH.

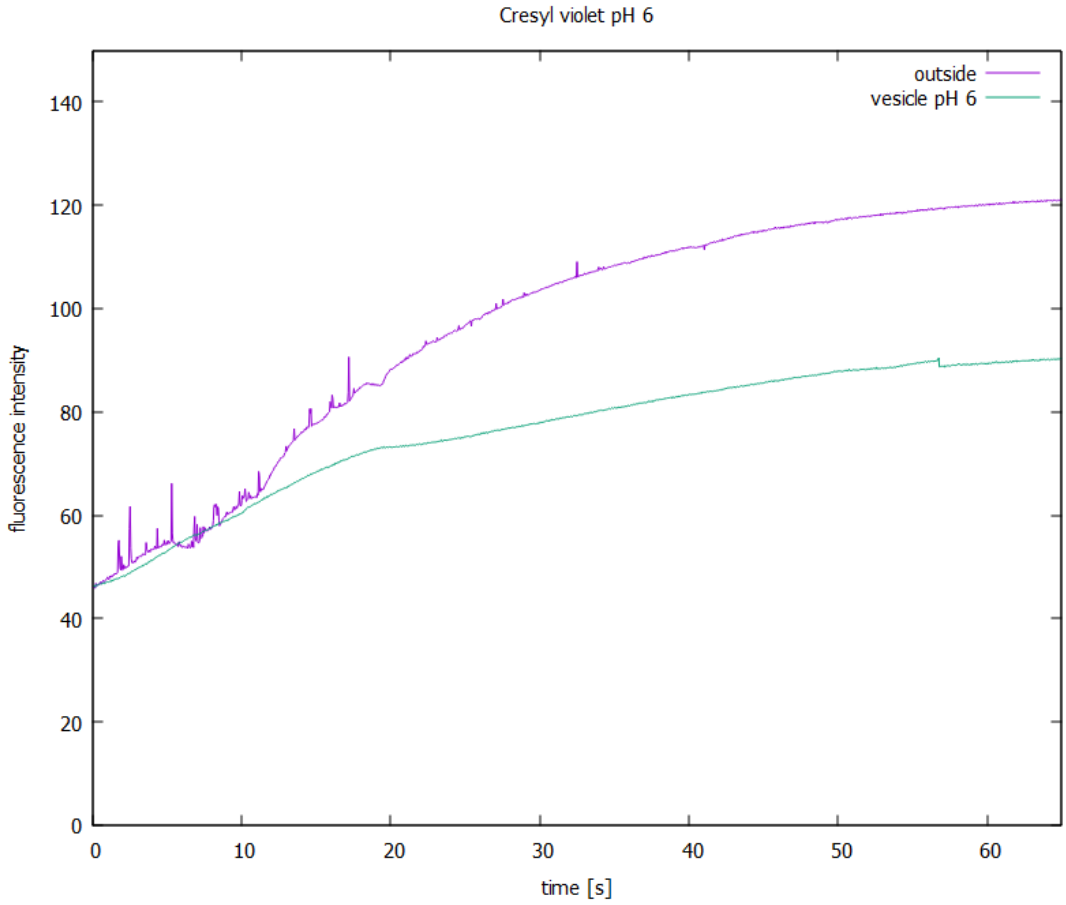


**Figure 4.28:** The pH dependence of cresyl violet permeability. Fluorescence intensity data of background and vesicles at pH 6 (one example data set out of several measurements).

To test the dependence of the pH on the membrane permeability, cresyl violet solutions of pH 6 and pH 9 were flushed around the vesicles. The pH 6 sample behaved as expected and in accordance with earlier experiments.
The results of the pH 9 samples were quite surprising. The membrane permeability did not only increase but the vesicles were much brighter than the outside solution. The solubility of cresyl violet at pH 9 in water is significantly lower than at pH 6. This explains the difference between the outside background measurements in Figure 4.298 and 4.29.

The hydrophilic cresyl violet at pH 9 did in fact not only permeate the membrane but also accumulated inside the membrane as visible in Figure 4.30. This lead to the extremely high brightness of the vesicles that even exceeded the outer background solution.

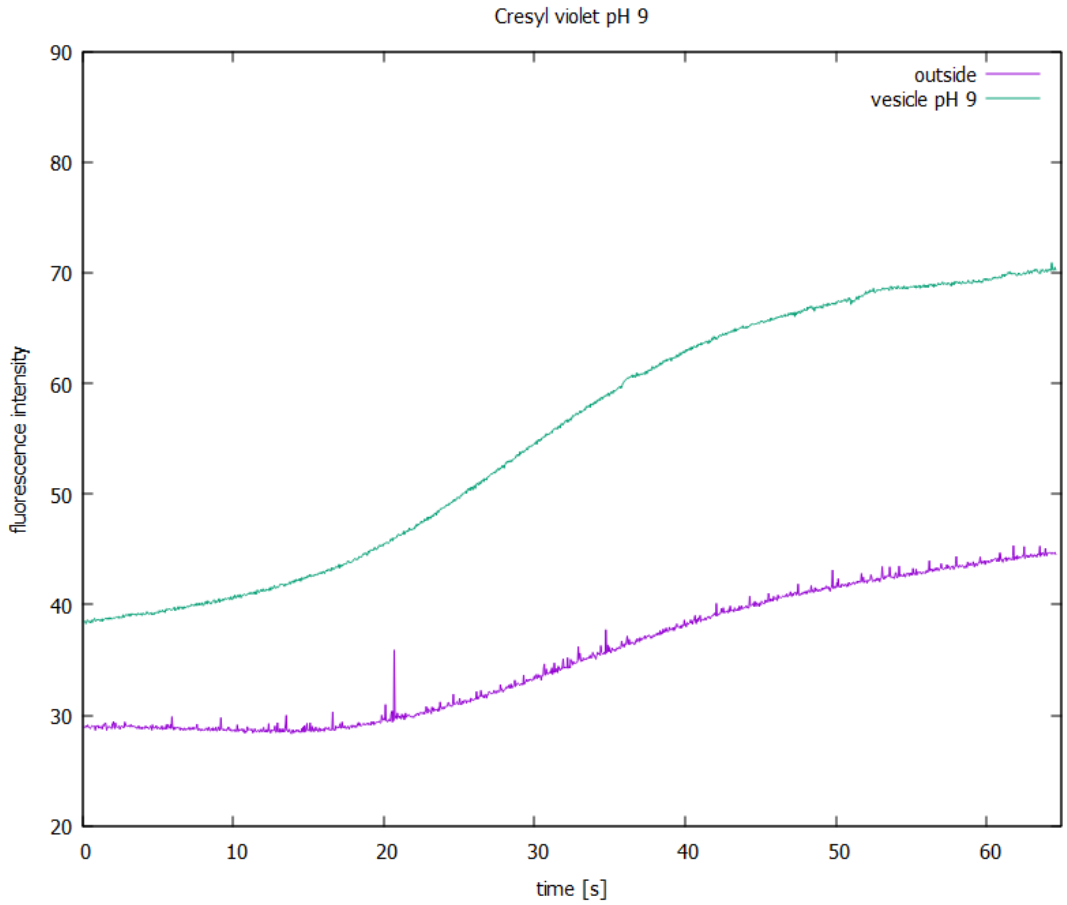


**Figure 4.29:** The pH dependence of cresyl violet permeability. Fluorescence intensity data of background and vesicles at pH 9 (one example data set out of several measurements).

#### 4.5.3.3 Inflow vs outflow

In synthetic biology applications especially when a compartment is combined with a metabolic module it might not only be important that a substrate can move inside the compartment but also that a product can leave the compartment or that an intermediate product does not leave the compartment.
If a product can leave the compartment and can be then removed from the outer solution an enzymatic reaction can run much longer and with higher output than in a batch setup where purified enzymes are mixed with the substrate because of lower product inhibition.
For this application it was tested if also the outflow of a substrate can be observed. The outflow of a substance has different kinetics than the inflow. The dye concentration

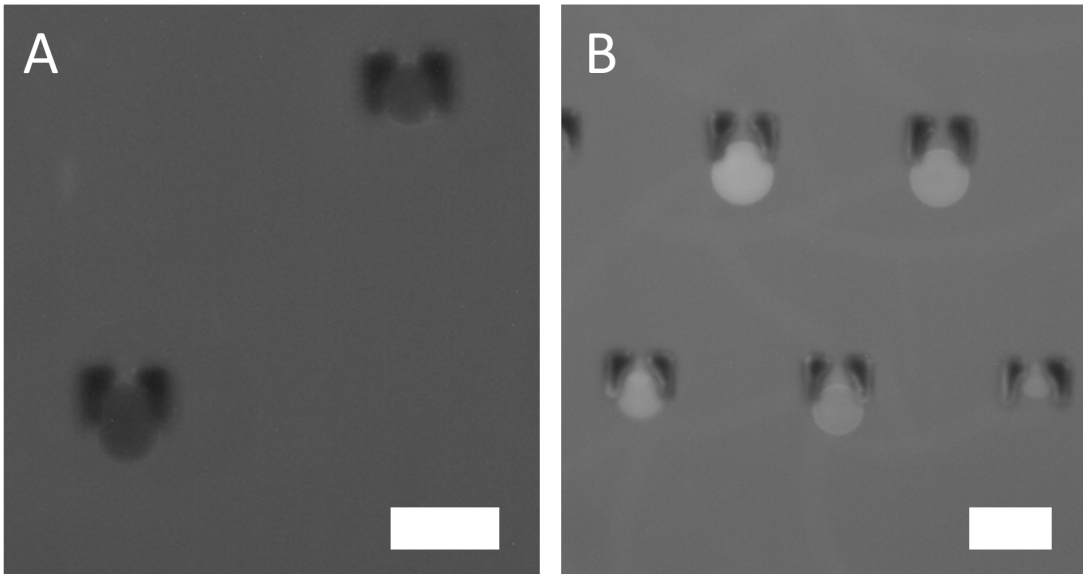


**Figure 4.30:** The pH dependency of cresyl violet permeability. Image of trapped vesicle at (A) pH 6 and (B) pH 9. Scale bar = 50 $\mu$m.

inside is 100 % at the beginning of the measurement and the outside concentration is 0 %. The difference to the inflow experiment is that the outside concentration stays at 0 % for the duration of the measurement because the dye that left the vesicle is immediately flushed away. Therefore the permeation kinetics depends only on the inner concentration.

In Figure 4.31 it is shown that the outflow of cresyl violet from pre filled vesicles can be measured just like the inflow. The vesicles were filled during electroformation with a 100 $\mu$M cresyl violet solution and kept in a solution with the same dye concentration. Once the vesicles were trapped inside the chip the outer fluid containing the dye was flushed out. The same limitation as during the inflow experiments, like photobleaching, apply.

#### 4.5.3.4 Influence of lipid composition

There is a huge structural variety of lipids membranes can be composed of. In this thesis the used lipids were glycerophospholipids.
The lipids in this group differ in the length of the fatty acid chains and if the chains are saturated or unsaturated. Figure 4.32 shows the structures of the two phospholipids compared in this section POPC (1-palmitoyl-2-oleoyl-glycero-3-phosphocholine) and DPhPC (1,2-diphytanoyl-sn-glycero-3-phosphocholine).

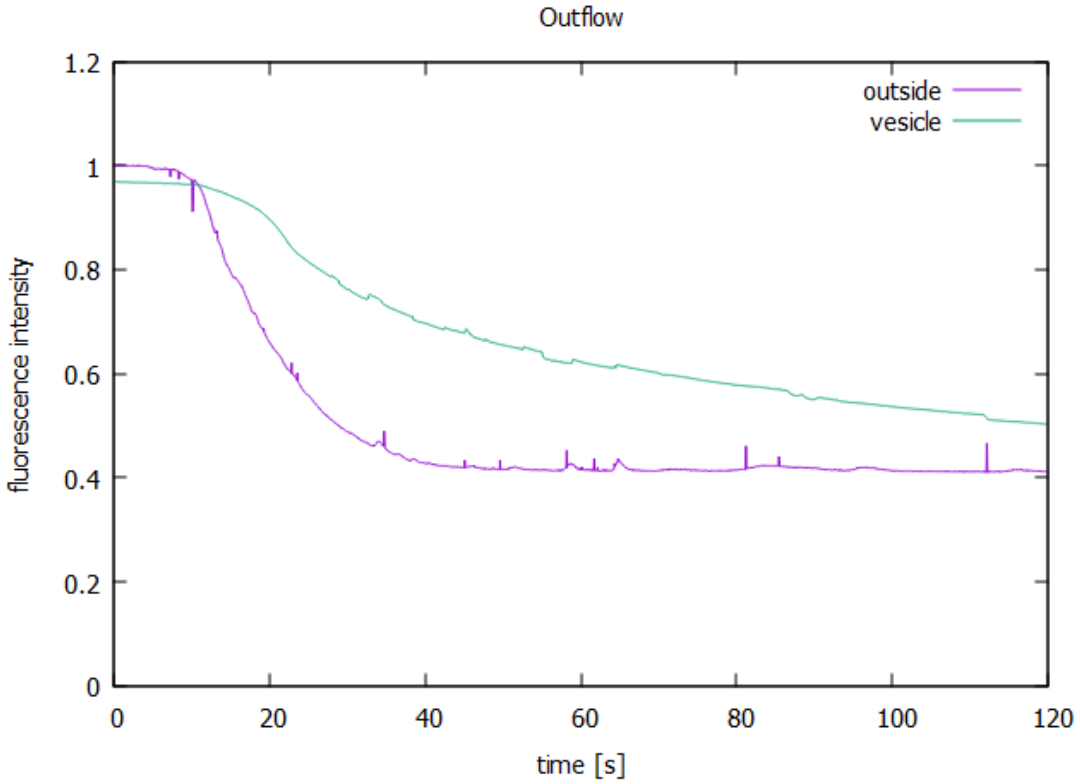


**Figure 4.31:** Outflow of cresyl violet from vesicle (n=3).

POPC is a phosphatidylcholine lipid with one unsaturated fatty acid chain. It naturally occurs in eukaryotic membranes and is widely used for the preparation of artificial membranes.
DPhPC is a lipid found in Archaea microorganisms and is known to form membranes with low permeability to ions and water that are highly resistant to oxidation. Interestingly, it does not show a gel-to-liquid phase transition (Salvador-Castell *et al.* (2020)). In contrast to phospholipids usually found in prokaryotic or eukaryotic membranes DPhPC has straight phytanyl chains.
Figure 4.33 shows the cresyl violet membrane permeability across POPC and DPhPC membranes. Both samples had no other lipids in the membrane.

As published by other groups (Cama (2016)) DPhPC is known to form tighter membranes than other phospholipids. As visible in this experiment the POPC sample shows a higher membrane permeability than the DPhPC sample. This effect was first noticed during the optimization of the OmpF measurement.
The measurement results raise the question what causes the permeability difference between POPC and DPhPC.

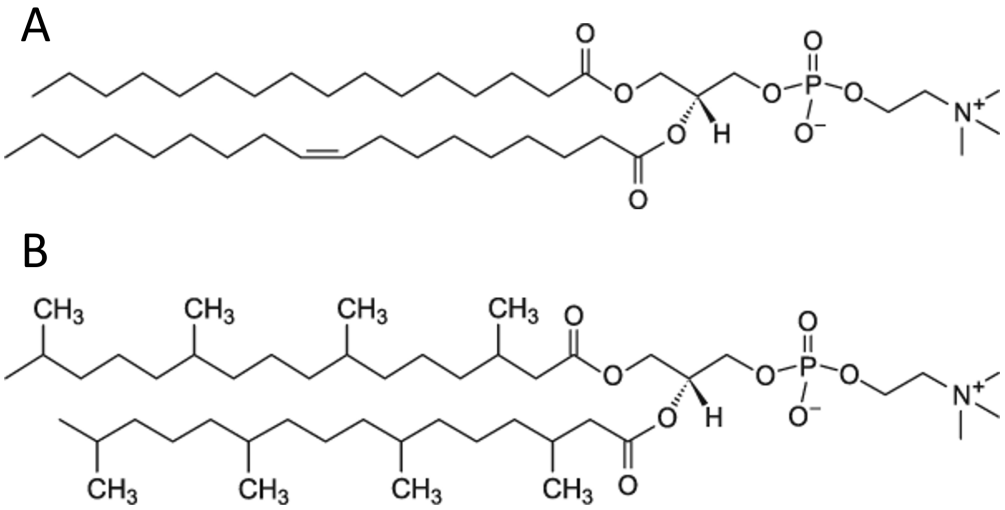


**Figure 4.32:** Structures of (A) POPC and (B) DPhPC (Images from Avanti Polar Lipids).

The effects of side branching on membrane permeability have been studied with molecular dynamics. The membrane permeability was significantly lower because the branched chains of DPhPC had a decreased free volume or cavity formation inside the hydrophobic part of the membrane and made it therefore more difficult for molecules to move through the membrane (Shinoda *et al.* (2004)) (Shinoda (2016)).
This explanation is consistent with experimental results from other groups (Tristram-Nagle *et al.* (2010)) (Cama (2016)).

#### 4.5.3.5 Influence of surfactants

Artificial membranes are very often exposed to various surfactants either because they are used during the production, like in the double emulsion method in Chapter 2, or afterwards because they are used for a membrane protein reconstitution like in the experiments shown later in this chapter.
Measuring the impact of the surfactants P 188 and F108 (P338) was inspired by the results presented in Chapter 2 and 3.
During the microfluidic double emulsion production both surfactants were tested because both were described in different publications for similar procedures. As mentioned in Chapter 2, several methods to characterize the membranes of the produced vesicles were tested and it was observed that the addition of F108 strongly influenced the membrane characteristics and interfacial tension resulting the samples to be unsuitable for several standard membrane characterization tests.

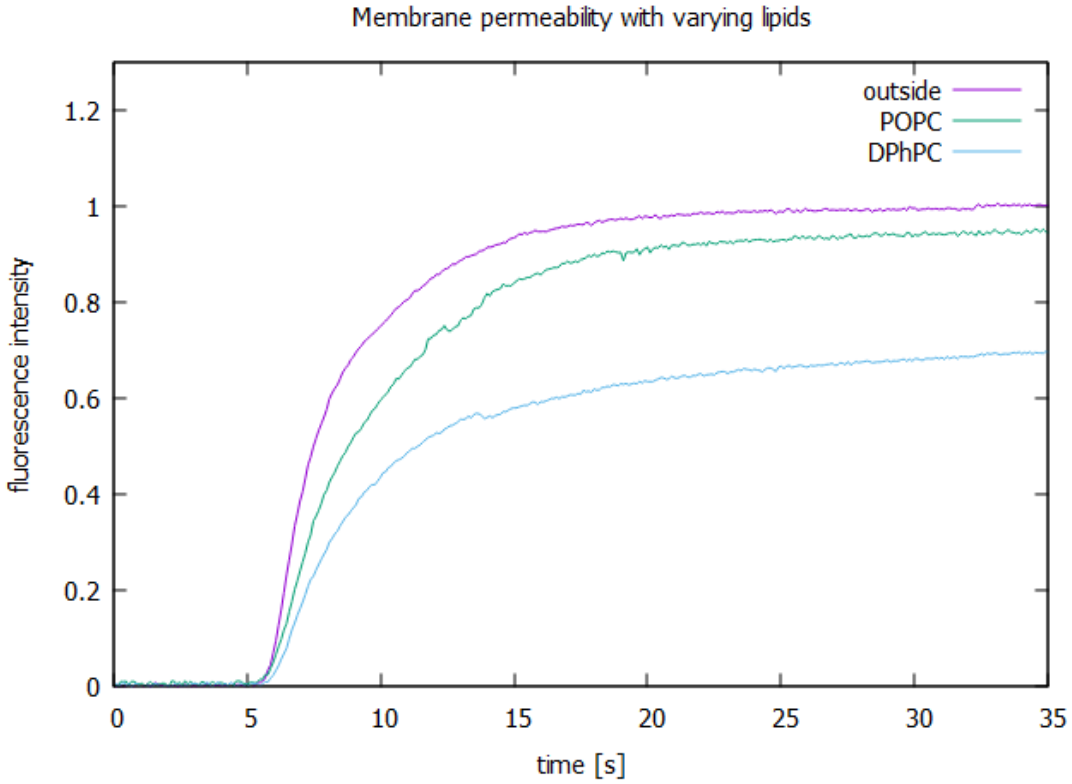


**Figure 4.33:** Comparison between cresyl violet membrane permeability between POPC (n=7) and DPhPC (n=4) vesicles. For better comparability the data shown here was normalized with the respective outside start data as 0% and the end value of the outside measurements as 100 %.

It also seemed as if the osmotic driven oil removal did not work well after longer incubation with the outer fluid containing surfactant. That is why the double emulsions were directly eluded into an solution of equal osmolarity but without detergent.

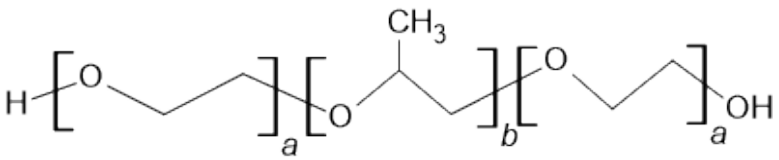


**Figure 4.34:** Basic structure of poloxamer polymers.

Poloxameres are a group of surface active amphiphilic copolymers. They are sold under the trade names Synperonic and Pluronic.
Figure 4.34 shows the basic structure of poloxamers, a combination of hydrophilic PEO

(poly(ethylene oxide)) and hydrophobic PPO (poly(propylene oxide)) blocks, resulting in a large number of compounds with varying molar mass and hydrophilicity. The names are composed of a P for poloxamer and a three digit number. The first two digits multiplied by 100 stand for the approximate molecular mass. The third digit multiplied by 10 indicates the percentage of the PEO content.
P188, used by several groups for double emulsion production (Deshpande & Dekker (2018)), is a very hydrophilic poloxamer and is known to stabilize cell membranes damaged by mechanical trauma and is investigated for its therapeutic potential in heart failure treatment (Mina *et al.* (2009)) (Cheng *et al.* (2012)) (Yasuda *et al.* (2005)) (G Moloughney & Weisleder (2012)).
The most hydrophobic poloxamer P181 (not tested in this thesis) is known to increase membrane permeability and facilitate the uptake of drugs into cells (Cheng *et al.* (2012)) (Krylova *et al.* (2003)) (Venne *et al.* (1996)) (Maskarinec *et al.* (2002)).
Cheng and colleagues measured the membrane interaction with poloxamers of different hydrophilicity. As shown in Figure 4.37 both types of polymer initially adsorb to the surface but only the hydrophobic one inserts itself into the bilayer (Cheng *et al.* (2012)) (Wang *et al.* (2012)).
The experiments presented here were performed to measure the influence of the two poloxamers P188 and P338 on the membrane permeability. The experiments were performed with POPC liposomes.
Figure 4.35 and 4.36 show measurements of the membrane permeability with the trapping assay. Because the membrane-polymer interactions have been shown to develop over several hours, vesicles have been incubated for various time intervals with both P188 and F108 to see how the poloxamers affect the membrane permeability.

The two poloxameres used in this experiment, P188 and P338, were selected because of their use in the double emulsion production. The percentage of PEO and therefore the hydrophilicity are very similar and they differ mainly in their molar mass.
Cheng and colleagues investigated the difference in membrane interaction of polymers of different hydrophilicity but not of molar mass and did not primarily measure membrane permeability (Cheng *et al.* (2012)).
As visible in Figure 4.35 and 4.36 both polymers do not show a change in membrane permeability depending on the incubation time. As both are not expected to insert themselves into the membrane but just adhere to the surface a significant drop in membrane permeability would not be expected.

Poloxamers are surfactants used during the double emulsion vesicle production to stabilize the oil and water phases. Other surfactants are also used for different applications for example the reconstitution of membrane proteins.
The OmpF reconstitution for the transport measurements presented in Section 4.5.4 was initially done with the surfactant octyl glucoside (OG), because it was also used

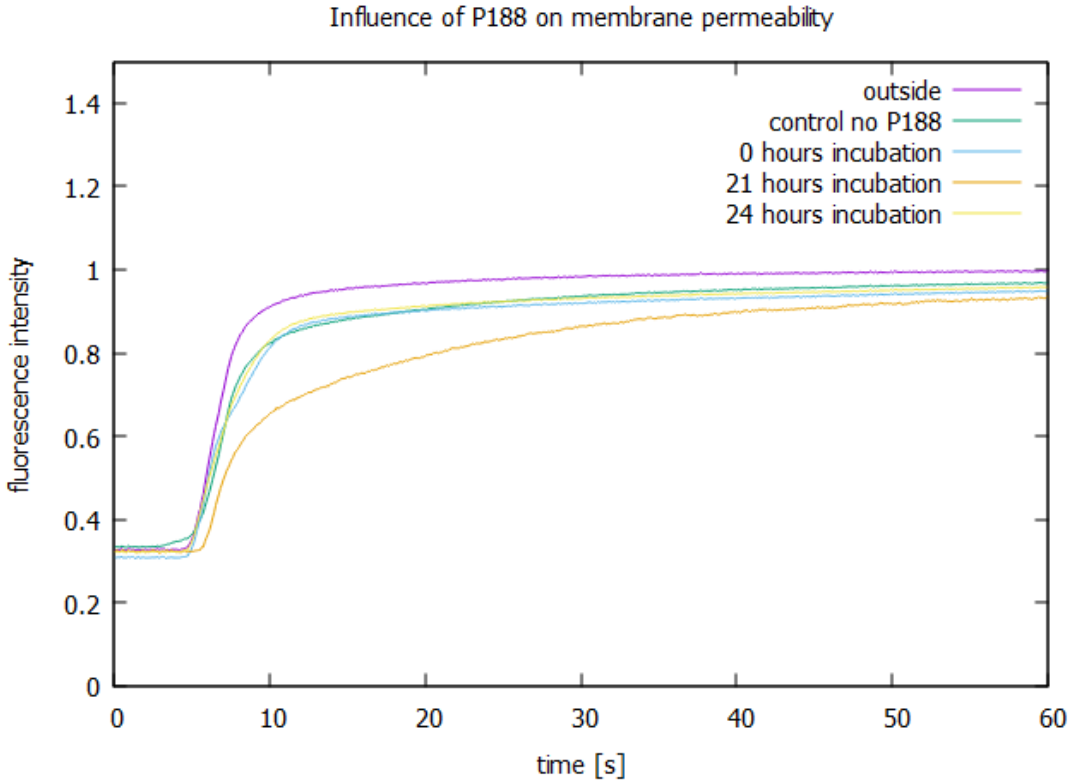


**Figure 4.35:** Membrane permeability of POPC vesicles at different exposure times to P188 (0h n=3, 21h n=7, 24h n=5).

during the OmpF purification from the E. coli membrane.
For the control measurements liposomes were incubated for the same amount of time with OG and exactly as for the OmpF samples after the incubation time biobeads were added to the solution to remove the detergent.
With this setup there was no difference between the OmpF containing liposomes and the control liposomes. This could have different reasons as the reconstitution might not have worked or the OmpF porin might have been not functional. However, both control and OmpF samples had a higher permeability than the DPhPC liposomes that were not exposed to any further treatment, pointing towards an influence of the detergent.
As Cama used a different detergent for his OmpF measurements (Cama (2016)), n-Octylpolyoxyethylene (O-POE), the influence of the two detergents on the membrane permeability was tested.

OG is known to enhance permeability in cells (Tirumalasetty & Eley (2006)) and was used in the procedure to purify OmpF from E. coli membranes.
Initially the purified OmpF was stored in a solution containing OG and it was also

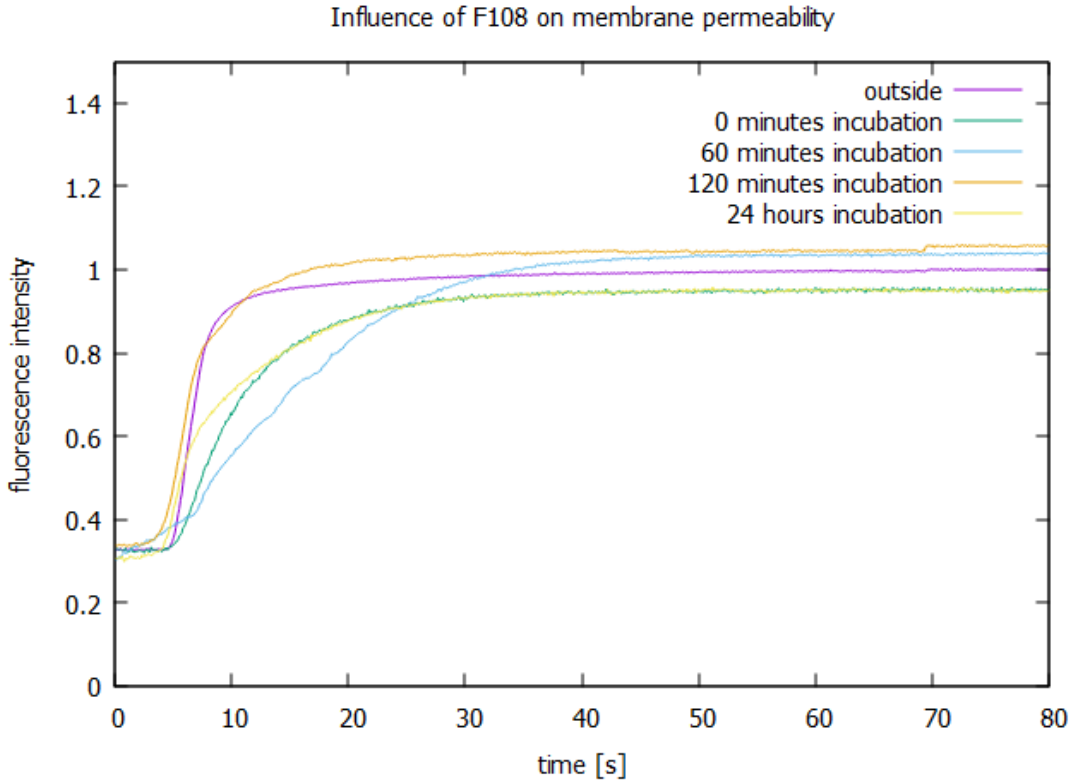


**Figure 4.36:** Membrane permeability of POPC vesicles at different exposure times to F108 (0h n=3, 1h n=4, 2h n=4, 24h n=3).

present during the membrane reconstitution and later removed with biobeads. During the early OmpF transport experiments it was observed that the control vesicles who were treated with an OG solution without OmpF had a higher membrane permeability than the pure DPhPC control vesicles. Because of this observation the influence of common reconstitution surfactants on membrane permeability was further investigated.

O-POE is a detergent which is frequently used in the reconstitution of membrane proteins (Winterhalter *et al.* (2001)). O-POE was the detergent used to reconstitute OmpF in the experiments in Section 4.5.4. The reconstitution protocol was adapted from (Cama (2016)) and involved incubation with a O-POE solution at room temperature for one hour and then adding biobeads and incubation overnight to remove the detergent from the solution. The experiment in Figure 4.39 was done to test the influence of O-POE on the liposome membrane permeability with and without the addition of biobeads.
Figure 4.39 shows that the sample with O-POE and subsequent removal with biobeads has a very similar membrane permeability to the control DPhPC liposomes without any

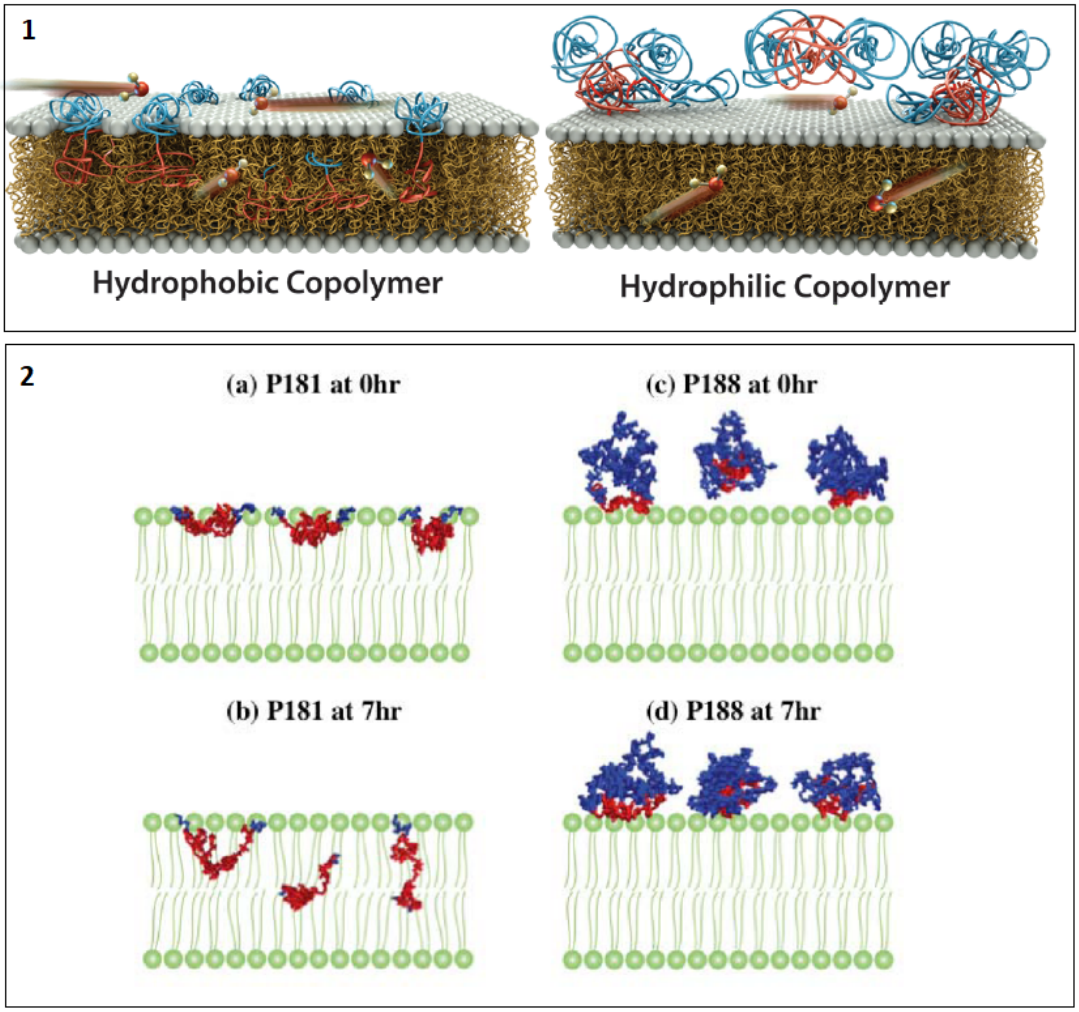


**Figure 4.37:** (1) Simulation of the membrane-copolymer interactions with two different polymers from the poloxamer group. (2) Schematic image of two poloxamers incorporating or adhering to the membrane over time. Images from (Cheng *et al.* (2012)).

surfactant. The sample incubated with O-POE but without addition of biobeads shows a higher permeability.

Figure 4.39 shows the effects of O-POE and Figure 4.40 shows the additional measurement of liposomes incubated with OG and addition of biobeads.
OG was also tested without biobeads but the vesicles in the sample incubated without biobeads were so unstable that it was not possible to record any useful data because they would burst too easily inside the chip.
The measurements show that the liposomes with OG and biobeads are as permeable as the samples with O-POE without the biobeads.

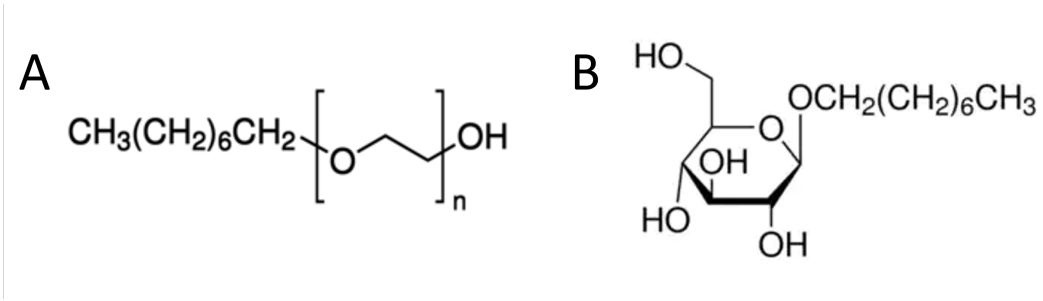


**Figure 4.38:** Chemical structures of (A) Octyl-POE and (B) OG.

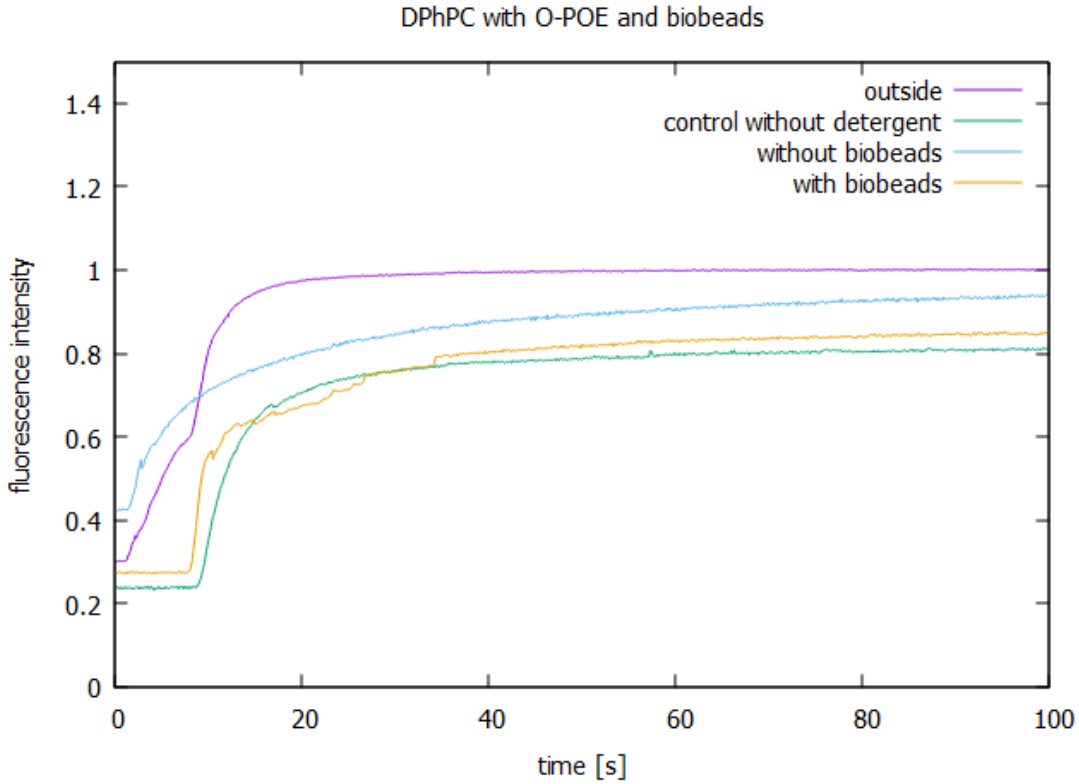


**Figure 4.39:** Membrane permeability of DPhPC vesicles incubated with O-POE with (n=7) and without (n=3) biobeads to test influence of biobeads.

Past studies on the effect of OG on membrane permeability show that the OG molecules are incorporated into the membrane. The influence of this detergent depends on its concentration inside the membrane. The authors hypothesize that as soon as the concentration inside the membrane is so high that the individual molecules come into contact with each other the membrane barrier efficiency drops (Ueno (1989)).
This is an example how a molecule used in a different procedure can change mem-

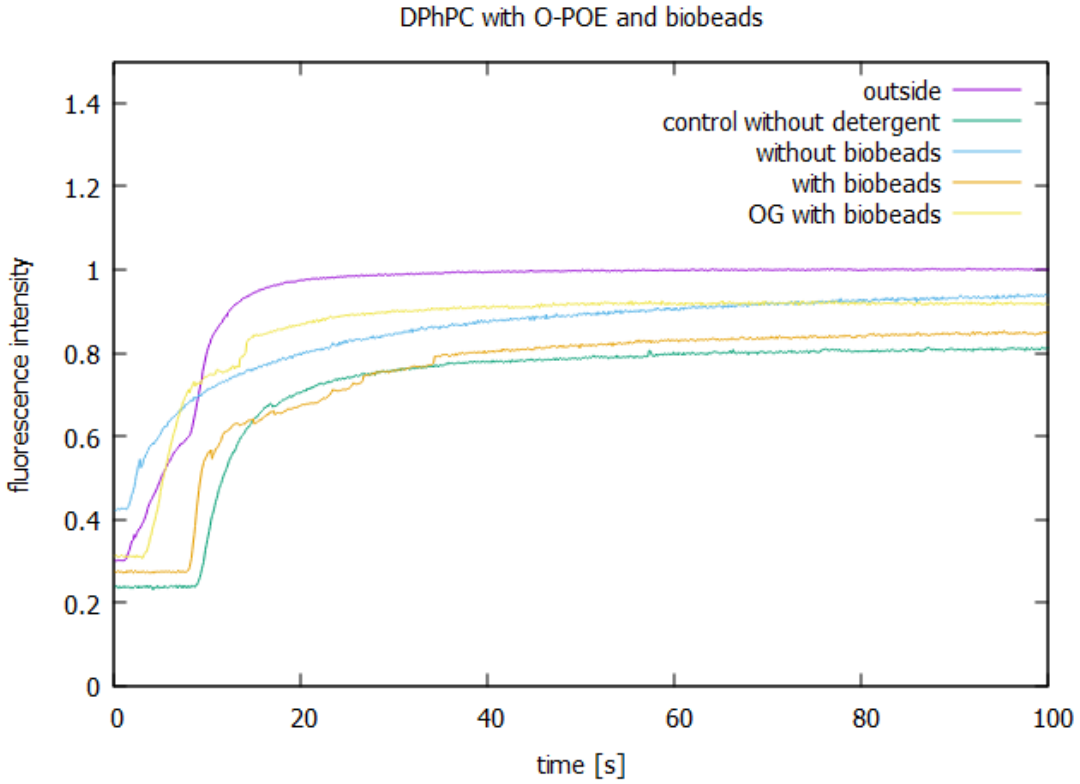


**Figure 4.40:** Membrane permeability of DPhPC vesicles incubated with O-POE with and without biobeads in comparison with OG incubation (n=4).

brane properties. These experiments show the importance of testing all the possible influencing factors in a given system.

### 4.5.4 Membrane transport assay

As shown in the section before, some molecules can enter a compartment by permeating the membrane and there are various factors influencing the membrane permeability.
If a high membrane permeability is needed for an application it can be adjusted by the choice of lipids or the addition of surfactants. However, those additions result in a non selective increase in membrane permeability and it has also been shown that certain surfactants, while strongly increasing the membrane permeability, can also decrease the stability of the vesicle.
Additionally charged molecules will still have difficulties permeating the membrane. Moreover the supply of a molecule via membrane permeability might be too slow to run a reaction at the desired speed. Therefore in many cases membrane transporters are necessary.

This section shows the incorporation of OmpF, a porin that allows passive transport, into the vesicle membrane and the measurement of transport through this porin.
Transmembrane proteins allow hydrophilic molecules and ions to cross the membrane. For synthetic biology the ability to functionalize the membrane with active or passive transporters allows faster and more specific membrane transport and is an essential step for creating life.
One class of passive transporters or nanopores are porins.

#### 4.5.4.1 OmpF

The porin used for membrane transport experiments in the following section is the Outer membrane porin F (OmpF) from E. coli. OmpF is the most abundant protein in the E. coli outer membrane (Delcour (2009)).
In the membrane three OmpF proteins are located together (Figure 4.41) and each of them is a water filled channel with a weak preference for cations and size below 600 Da (Cowan *et al.* (1992)) (Nikaido (2003)). Its structure consists mainly of slightly tilted beta-sheets forming a barrel like structure which is responsible for its stability (Cama (2016)).

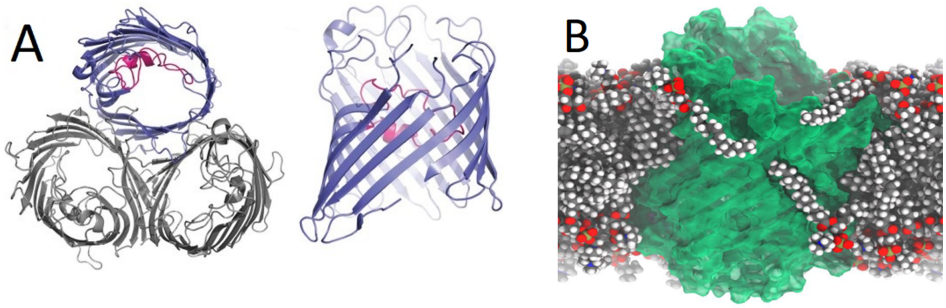


**Figure 4.41:** The OmpF porin (A) Top and side view of the protein (Image from (Mathavan & Beis (2012))) (B) Protein inside membrane (Image from molecular model by Eric Schulze from MPI DCTS).

As mentioned in Chapter 3, gram-negative bacteria such as E. coli have a double membrane cell wall with peptidoglycan in between. For the IMV experiments the inner membrane with its respiration chain proteins was used. Here a porin from the outer membrane was purified and inserted into liposomes.
Stability is a problem when inserting proteins into liposomes. Firstly, most proteins require a labour intensive and delicate purification procedure. Additionally membrane proteins are usually more difficult to purify than water soluble enzymes.
While there are some methods to quantify the amount of purified protein in a solution, it is very difficult to determine the percentage of proteins that were damaged during

the purification or after a certain storage time and are not active any more. Often a genetic modification of the protein like the addition of a His-tag is necessary to be able to separate the target protein from all other cellular proteins during the purification.
OmpF has the advantage that in addition to its stability, which makes the purification procedure easier, it is the most abundant protein in the outer membrane of E. coli. Therefore a genetic modification can be avoided and it can be purified by first separating the outer membrane and then dissolving the protein with a surfactant.
It has been shown to be insertable in polymer membranes (Meyer *et al.* (2021)) which is a problem for many proteins because of the thickness of the polymersome membranes. Furthermore it facilitates passive transport, so no source of energy or other molecules are necessary necessary which would make the process to be observed more complicated. The orientation in the membrane is not important as transport proceeds bidirectionally.
OmpF was chosen as a membrane protein to test if the microfluidic traps and the observation via microscope is suitable for measuring membrane transport for various reasons. The two most important reasons were that due to its beta-Barrel structure it is very stable and therefore easy to handle and secondly a wide range of molecules can pass through but it is not as unselective as for example Hemolysin.
It was used previously as a frame for redesign to be more selective, which might be interesting for synthetic biology applications (Chowdhury *et al.* (2018)).
As shown in section 4.5.3.2 the membrane permeability of cresyl violet is pH dependent. Due to the cation selectivity of the porin also the movement of cresyl violet through OmpF is pH dependent although in the other direction. Here a low pH will improve the movement through the pore. Cresyl violet is expected the behave similar to the antibiotic norfloxacin which has been shown to have a pH dependent transport through OmpF (Cama (2016)). The buffers used for the transport experiments were therefore adjusted to pH 5.

#### 4.5.4.2 Transport measurement

**OmpF purification.** E. coli Omp8 cells were grown on a LB-Amp plate overnight at 37 °C, a colony was picked and grown in 2YT-Amp medium. OmpF overexpression was induced by addition of IPTG (final conc. 0.4 mM) and cells were shaken for 16 hours at RT. The cells were harvested by centrifugation. They were resuspended in lysis buffer and pressed 3x through French press. The protein was extracted using three ultracentrifugation steps and the purity of the protein was verified with SDS-PAGE. OmpF was kept in 1 % OG and stored at 4 °C.

**OmpF reconstitution.** Purified OmpF (6.5 mg/ml) was stored in 1% OG. The stock solution was dialysed against PBS and Biobeads for 6 hours and 1% o-POE was added to the OmpF solution. OmpF stock (1 $\mu$l) was added to 50 $\mu$l vesicle solution and incubated for 60 minutes at RT. Afterwards biobeads were added to remove detergent

and the mixture was incubated for 60 minutes at room temperature and then stored at 4 °C overnight and used within 48 hours.
The control vesicles came from the same electroformation batch and underwent the same procedure. The only difference was that they were incubated in a control buffer without OmpF but otherwise with the exact same composition including surfactants.

The transport measurement results shown here are a result of an optimization process. After OmpF was selected as a transporter various fluorescent molecules were tested. After cresyl violet was selected as a suitable substrate control experiments were carried out with POPC and DOPC liposomes.
These test showed no significant difference between control and OmpF sample. At this point it was unclear if the transport through the porin did not work or the rest of the membrane was not tight enough to show a significant difference between the movement of cresyl violet across the membrane and through the porin.
As shown in section 4.5 the lipid DPhPC forms tighter membranes and was therefore used as the membrane lipid to continue the experiments. However, the difference between control and sample was not enough to investigate the porin transport properties. In E. coli cells the outer membrane is covered with lipopolysaccarides that make the membrane tighter. Liposomes have usually a much higher permeability than biological cell membranes. Unfortunately, to my knowledge there is no literature with direct comparative measurements comparing membrane tightness of E. coli cells and GUVs.

As mentioned before purification and reconstitution of OmpF was done with the surfactant OG but even after removal with biobeads it visibly increased the membrane permeability of the vesicles. Other groups working with OmpF used O-POE for the reconstitution (Cama (2016)).
The purified OmpF solution was dialysed to remove the OG and O-POE was added. The measurement results after this optimization are shown in Figure 4.42. This experiment was done before the membrane permeability tests in the section before. The optimization process for the transport measurement showed that there are multiple factors influencing membrane permeability and was the motivation to take a step back and test the influence of different lipids and surfactants on membrane permeability.

The initial increase of the vesicles containing OmpF and the control vesicles up to second 25 is very similar and afterwards the OmpF curve becomes more steep than the control. This initial effects are probably due to the outer solution containing fluorescent dye that flows above or below the vesicles.
Like in the membrane permeability measurements the upper graph shows the background brightness in the chamber. The green line shows the increase in brightness in the sample with OmpF porins in the membrane and the red line is the control sample. Additionally like in the earlier samples differences between the individual vesicles were visible. Some vesicles stayed completely dark while others were much brighter than the

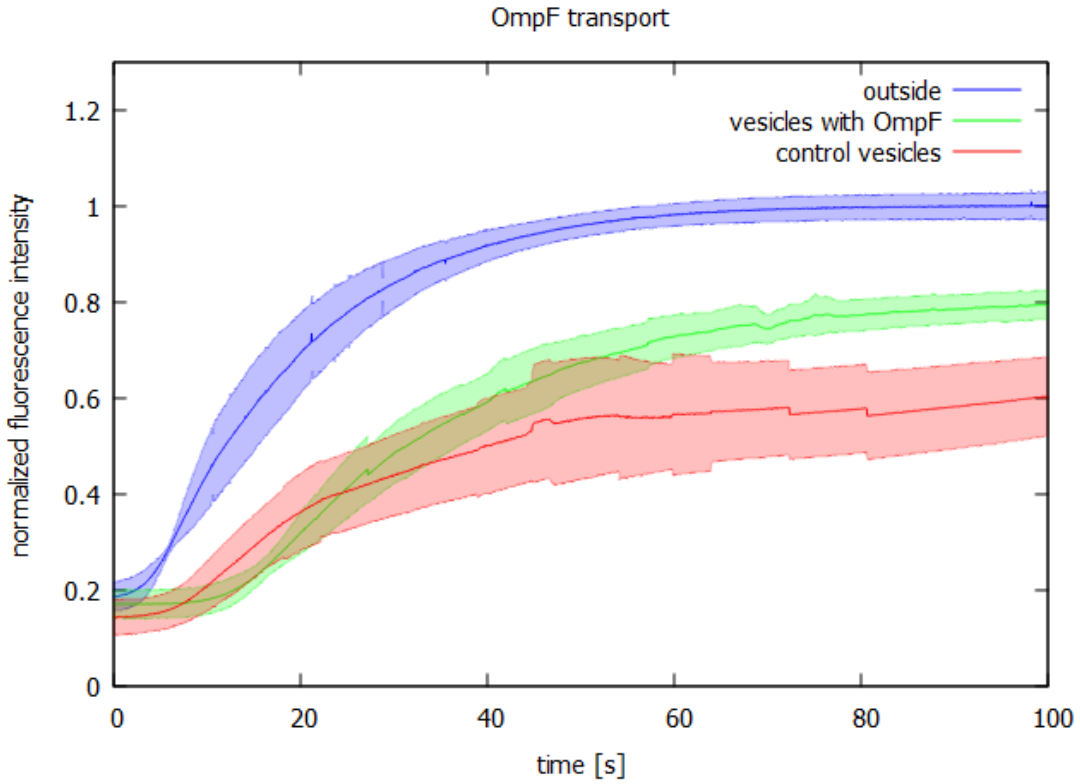


**Figure 4.42:** Ompf cresyl violet transport measurement in DPhPC GUVs with outside brightness (blue) control vesicles (red)(n=6) and vesicles containing OmpF (green)(n=10).

surrounding solution. The much brighter vesicles were typically very small ones.

A further experiment could be to measure the amount of incorporated membrane protein, for example by attaching a fluorescent dye followed by a membrane transport measurement of those individual vesicles and a quantification of the protein inside the membrane.
As a result a transport rate related to the present porins could be calculated. This would be a study that would make the individual measurement of vesicles necessary and would be not possible with bulk methods.

# Chapter 5

# Concluding Remarks

## 5.1 Summary

This thesis is an interdisciplinary work at the interface of microfluidics, membrane biophysics, molecular biology, biotechnology and synthetic biology in the broader context of the MaxSynBio project.
The aim of this thesis was to develop microfluidic tools for bottom-up synthetic biology applications. The focus was on two microfluidic systems that are necessary for the bottom-up assembly of artificial cells.

The first tool (Chapter 2) is a microfluidic chip for the production of vesicles using the double emulsion method. The preparation and operation of the chip were shown. Including the optimization of the chip coating, design and operation conditions for a stable high-throughput vesicle production.
On the microfluidic chip three fluids are used, the aqueous outer and inner fluids and the middle fluid with an organic phase and phospholipids. The composition of the fluids is important for a stable double emulsion production and influences the subsequent removal of the organic phase. In addition the composition of the inner fluid interacts with encapsulated modules.
Varying fluid composition have been tested. Oleic acid was the best organic phase for the specific microfluidic setup regarding subsequent oil removal. The inner fluid was optimized to contain only sucrose and no other substances to minimize interactions with encapsulated modules.
The surfactants in the outer fluid influenced several tests for membrane characterization but was necessary for the interface stabilization during the production and could not be easily removed or replaced.
The second focus in this chapter was the removal of the organic phase after the microfluidic production.
Based on a review of experimental and theoretical results published in the scientific

literature as well as the observations during the performed experiments, the most important factor in the spontaneous dewetting and subsequent detachment of the organic phase are the interfacial tensions between the inner, middle and outer fluids.
A new method for the removal of the organic phase using osmotic gradients was developed and first tested in small batches on a coverslip and then transferred into a microfluidic dewetting chip.

In Chapter 3 functional modules were combined. The first combination was an enzymatic reaction with an energy regeneration module, namely the isolated respiration chain of the inner E. coli membrane (IMV). The functionality of the IMVs was confirmed in batch and they were combined with an enzymatic reaction that relies on a cofactor regenerated by the IMVs. The buffer solution had to be adjusted as both the enzymatic reaction and the IMVs were first optimized separately and had slightly different requirements for their environment.
This combination was encapsulated into water in oil droplets using microfluidics.
The second part showed the encapsulation of enzymatic reactions in double emulsion compartments. A challenge was the inactivation of the enzyme by a surfactant used during the compartment production. The fluid composition used during the microfluidic production was successfully changed and a part of the complex, partly synthetic CETCH cycle was encapsulated in double emulsions.

To use the vesicles as compartments their membrane properties have to be characterized. A major limiting factor for the choice of reactions and processes used in Chapter 3 was an available method the measure the reaction.
Chapter 4 focused on a microfluidic tool for vesicle trapping and observation.
The trapping tool is very flexible because it allows membrane characterization, observation of reactions inside the vesicle and is fundamental for the development of transport modules.
The focus here was on the development of an assay for membrane permeability and transport. Several chip designs were tested in regard to maximizing the number of trapped vesicles that are observable at the same time.
The advantage of the microfluidic assay is the time-resolved measurement of membrane permeability kinetics on a single vesicle level.
The assay was tested with a variety of factors that influence membrane permeability such as pH, membrane composition and surfactants. The motivation for the surfactant experiments came from the experience with the surfactants used during the vesicle production and the influence of surfactants from membrane protein purification.
The results helped with the exchange of a surfactant used for the reconstitution of the porin OmpF and allowed the measurement of passive transport through OmpF into the vesicle using the assay.

## 5.2 Conclusions and Outlook

The aim of this thesis, as stated in the introduction, was to show that microfluidic systems are essential tools for bottom-up synthetic biology exemplified by the production of compartments and the observation of processes inside compartments.

The first part focused on the fundamental task of compartment production (Chapter 2).
It was shown that microfluidic systems are suitable to produce compartments and are superior to batch methods in terms of homogeneity of the compartments. In addition, it was shown that the method allowed for very efficient and homogenous encapsulation and it enables the encapsulation of very complex solutions with large and fragile components, the fundamental feature for bottom-up synthetic biology.
An important aspect of the vesicle production via water-oil-water double emulsions is the subsequent oil removal, which is a problem that is not fully solved yet.
The experiments as well as the literature show the importance of the interfacial tensions for the removal of the organic phase. A crucial step for the optimization and better understanding of the occurring processes would be the identification of a method for the measurement of the interfacial tensions that would work with the added surfactants or the replacement of the surfactants.

The most important novel contribution from Chapter 2 is the removal of residual oil from the membrane and they discovery that this can be achieved by shrinking the vesicle with an osmotic gradient.
The underlying mechanisms of the developed osmotic gradient detachment method are not fully understood. It is hypothesized that the shrinking process might lead to excess membrane which closes then around the inner fluid or the gradient might change the interfacial tensions in a way that favours the detachment. The second hypothesis could be verified by measuring the respective interfacial tensions with varying osmolarities and comparing the values with the theoretical ratios necessary for detachment.

Future improvements of the compartment production would be the adjustment of the chip design to achieve on-chip oil removal. For example by extending the channel after the double emulsion production, adjusting the channel width and adding another fluid inlet to adjust the interfacial tensions or the outer osmolarity.
Another future task would be the characterization of membrane properties to make the compartments a functional module with well known and adjustable features. The characterization includes the membrane composition and permeability but also the stability of the compartments over the course of days and weeks.
In the context of synthetic biology, it would be also interesting to use different materials for the compartment membrane or wall such as polymers.

Chapter 3 addressed the following questions asked in the introduction:
What are minimal requirements when combining two modules?
Is the compartment production system suitable for the encapsulation of other functional modules?
Regarding the first question, the combination of the enzymatic reaction with the IMVs energy module as well as the encapsulation of the enzymatic pathways showed how crucial the buffer composition as well as any other added substances are, once several modules are combined.
When modules are tailored to specific, optimized conditions, harmonizing the environments of two or more such modules for cohesive functionality can be challenging. As a result, their combined efficiency might not reach the individual potentials observed in isolated conditions. A foundational buffer could be established early in the project. The aim would then be to, if possible, optimize the modules to function within this standardized buffer.
Another strategy, inspired by biological cells, could be the development of a design where individual modules are housed in smaller compartments, each with its tailored conditions. These compartments could then be placed within a larger one, allowing for localized optimization while still ensuring inter-module collaboration.
Furthermore, the scope of experiments conducted was often limited by the available measurement techniques. This shows the need for innovative and diverse measurement methods. Relying solely on fluorescence might not capture the full picture. A broad spectrum of measurable attributes, embedded directly into microfluidic systems, can provide a more broad and accurate insight into the processes at play.

Chapter 4 shows a microfluidic chip for physically trapping vesicles. The most important contribution in this chapter is the development of the membrane permeation assay.
This allows measuring time resolved movement of molecules across the membrane and though a transmembrane protein. In addition this measurements are done on an individual vesicle level, which is a crucial tool in the optimization of the production of biological systems.
Utilizing this methodology presents distinct advantages over conventional bulk experiments. The visibility of individual vesicles facilitates single-vesicle analysis, offering a comprehensive understanding of sample homogeneity. This perspective also reveals potential outliers and unforeseen effects. Such insights could pave the way for novel research questions that are unattainable without this visual feedback. Another aspect of this approach is the capability for time-resolved kinetic measurements.
As a result, with this method the permeability under varying conditions could be compared and the results were in accordance with expected results derived from scientific literature. Additionally the results were used to gain a better understanding of the effects of two surfactants used during the vesicle production and allowed optimization of the reconstitution of the membrane protein OmpF.

However, at the presented stage of development, there are a lot of limitations. One being the very limited number of observable molecules due to, for example, photobleaching. This could be improved by using a confocal microscope. Additionally, a combination with other measurement methods like electrophysiology (Czekalska *et al.* (2015)) could widen the spectrum of observable processes even further.
Another limitation that will have to be addressed is that the direct comparison of permeability with slight variations in the conditions is possible but no measurement of the analyte concentrations inside the vesicle. This could, again, be improved by using a confocal microscope because the background fluorescence would be filtered out.
In addition, the quantification would require extensive calibration and validation with regular control measurements, because the amount of light caught in an microscopic image can vary based on a large number of factors, like room brightness and ageing of the lamp.
One big advantage and promise of automation is high-throughput measurement, which has not been achieved with the presented microfluidic design. The advancement of automation of the whole measurement procedure and the data analysis would increase the sample numbers and make the resulting data more reproducible while also increasing the different conditions that can be tested in a given amount of time.
Aspects to be automated could include the pumping cycles and a possibility to observe more than one chamber on one chip. It is also imaginable to change the design of the chip to include a trap and release mechanism for the vesicles, so several measurement loops can run on one chip.

The overall microfluidic design could be moved towards integrated chips that combine production and observation, where several groups are working on (Robinson (2019b)) (Schaich (2020)) (Matosevic & Paegel (2013)) (Paterson *et al.* (2014)).

In conclusion this thesis showed how microfluidic tools can contribute to experimental challenges arising from the creation, assembly and characterization of synthetic, biomimetic functional modules and systems and are enabling the implementation of technical solutions to these tasks.

# Chapter 6

# Materials and methods

## 6.1 Materials

Sucrose, n-octanol (hereafter only referred to as octanol), F108 surfactant, F68 surfactant (10wt% stock solution in water, sold under the commercial name Poloxamer 188), poly(vinyl alcohol) (PVA,MW9000-10000, 80% hydrolized), polyethylene glycol (PEG, MW 6000), glycerol, poly(diallyldimethylammonium chloride) (PDADMAC, 20wt% stock solution in water), poly(sodium 4-styrenesulfonat) (PSS, avg. MW 1000000), Nile Red, Bovine serum albumine (BSA) and fluorescein isothiocyanate dextran (fluoDEX, avg. MW20000) were all purchased from Sigma Aldrich.
Sodium chloride and 3-morpholino propane-1-sulfonic acid (MOPS) were both purchased from Carl Roth.
Oleic acid 98 % was purchased from AcrosOrganics.
Hydrochloric acid (32 %), hydrogenperoxide (30 % Suprapure), ethanol (99.9 %, ethanol for analysis), chloroform ( 99.8 %) were purchased from Merck KGaA.
Polydimethylsiloxane (PDMS, SYLGARD silicone elastomer) and the curing agent (SYLGARD silicone elastomer curing agent) were obtained from DOW CROWNING.
1,2-dioleoyl-sn-glycero-3-phosphocholine (DOPC),
1,2-diphytanoyl-sn-glycero-3-phosphocholine (DPhPC), soy L--phosphatidylcholine (-PC), 1-palmitoyl-2-oleoyl-glycero-3-phosphocholine (POPC), 1,2-dioleoyl-sn-glycero-3-phosphoethanolamine-N-(carboxyfluorescein) (CF PE) and 1,2-dioleoylsn-glycero-3-phosphoethanolamine-N-(lissamine rhodamine B sulfonyl) (Liss Rhod PE) were obtained from Avanti Polar Lipids.
Biobeads (Bio-Beads SM-2 Adsorbent Media, 20-50 mesh) were purchased from Bio-Rad Laboratories.
Small cover glass slides (22mm × 18mm) were purchased from Gerhard Menzel Glasbearbeitungswerk.
Large cover slides (24mm × 50mm, microscope cover slide) from VWR.
1 ml plastic syringes were purchased from B. Braun Melsungen AG and needles (0.7mm

× 25mm from Becton Dickinson. Polytetrafluoroethylene tubing (0.56mm inner diameter, 1.07mm outer diameter) was purchased from Adtech Polymer Engineering. 0.2m filters made of nylon were purchased from Carl Roth. The tape used (MAGIC tape) was purchased from SCOTCH.

## 6.2 Microfluidics

### 6.2.1 Microfluidic design

Microfluidic designs were made with Autocad and Freecad.

### 6.2.2 Wafer production with photolithography

The silicon moulds for all designs were prepared with soft lithography. Silicon wafers (4 inches, Si-Mat) were spun coated with SU-8 3050 (MicroChem, USA) for 2250 rpm for 30 seconds to achieve a height of around 70 $\mu$m for the double emulsion chips and a height of around 23 $\mu$m for the immobilization chip. The photomask was a film mask (double emulsion) and a glass with chrome coating mask (immobilization) (both from Micro Litho, UK) and alignment and UV exposure was done with a UV-KUB 3 (KLOE, France). After UV exposure for 5 seconds, the wafer was baked on a hot plate and the unexposed photoresist was dissolved by a developer.

### 6.2.3 PDMS chip production

The wafer was cleaned with isopropanol and a 10:1 mixture of poly(dimethyl siloxane) base and crosslinker (PDMS, Sylgard 184, Dow Corning, USA) was poured on the wafer. The PDMS was degassed in vacuum and baked at 80 °C for at least 4 hours. Then the cured PDMS was cut with a scalpel and holes for the inlets and outlets were made with a biopsy puncher. A 24x50 mm microscopy glass coverslip was attached to the PDMS chip after 1 min air plasma treatment (Plasma Cleaner PDC 32-G-2, Harrick Plasma, USA). After the plasma treatment the chip was incubated at 80 °C to strengthen the bonding.
While the double emulsion chips were coated afterwards, a reservoir was attached on top of the inlet of the trapping chips to enable an easy exchange of solutions.
To create the reservoir the wider end of a 200 ul pipette tip was cut of. A 10 ul pipette tip was plugged into the inlet hole to prevent clogging. Then the wider end of the Cut pipette tip was dipped into PDMS and placed around the inlet home on top of the chip. To solidify the PDMS, the chips were incubated for at least 2 hours at 80 °C.

### 6.2.4 Chip coating

The outer fluid channel of the double emulsion chip was coated with PVA.
1 wt.% PVA (MW 9000-10000, 80% hydrolyzed, Sigma Aldrich) in ultrapure water was heated to 80 °C for 5 minutes to dissolve the PVA and afterwards mixed well. After the plasma bonding the chip was incubated at 80 °C for up to 5 minutes to prevent detaching of the chip during the coating. The outer fluid channel of the double emulsion chips was coated with 1 wt% PVA for 1 minute 5 minutes after the plasma treatment and afterwards incubated at 120 °C for at least 20 min. To ensure that only the channel for the OF was coated, the other two inlets were left open to allow air flow through the other channels. The chips with the vesicle traps as well as the dewetting chip were coated with BSA by flowing a 2 wt% BSA solution through the chip for at least 15 minutes directly before use. If a chip was washed with ethanol the BSA coating was repeated afterwards.

### 6.2.5 Microfluidic device operation

The fluids were either sucked or pushed through the chip using NEmesys S syringe pumps (CETONI GmbH, Germany).
The the fluids for the double emulsion chip were pumped using three separate pumps with varying speeds.
The fluid exchange in the immobilization chip was done by exchanging the fluid in the reservoir by replacing the liquid five times.

## 6.3 Double emulsion production

The observation of the processes inside the microfluidic chips and the fluorescent and brightfield images were done with a ZEISS Axio Observer 5 Microscope with a HXP 120 V lightsource and images were recorded with a ZEISS Axiocam 506 colour microscope camera. For the observation of the double emulsion production and the recording of the videos a Phantom V611 highspeed camera was used.
The confocal images were recorded with a Leica TCS SPE confocal microscope.

### 6.3.1 Fluid compositions

The inner and outer solutions were filtered (0.2 $\mu$m) to prevent potential blocking of the microfluidic channels. The inner fluid (IF) was composed of varying concentrations of sucrose and NaCl and usually fluorescein isothiocyanate-dextran was added at a final concentration of 0.1 mg/ml. The middle fluid (MF) was prepared by drying the necessary amount of soy-PC lipids in a glass vial under nitrogen for at least 30 min. Afterwards oleic acid was added to a final lipid concentration of 1 wt%. To ensure

proper dispersion of the lipids in the oil, the mixture was incubated for at least 1 h and vortexed frequently. Depending on the application either Nile Red or Rho-PE were added as fluorescent dyes for the lipid phase. Nile Red was used at a final concentration of 1.6 $\mu$g/ml and Rho-PE at a final concentration of 0.01 mg/ml. The outer fluid was composed of varying concentrations of sucrose, glucose and NaCl with an addition of 1 wt% of F108 to stabilize the formation of the double emulsion and the membrane.

### 6.3.2 Microfluidic double emulsion generation

For the double emulsion generation the IF, MF and OF were put into syringes and placed into neMESYS syringe pumps (Cetoni, Germany). The syringes were connected to the respective chip inlets with polytetrafluoroethylene (PTFE) tubing (0.56 mm inner diameter, 1.07 mm outer diameter, Adtech Polymer Engineering) and the outlet was connected to an Eppendorf tube. Double emulsions were formed at a rate of approximately 3 kHz and the formation was monitored under a microscope using a high-speed camera (Phantom, Phantom Vision, USA). Stable double emulsions could be achieved at flow rates around 40 $\mu$l/h (IF), 40 $\mu$l/h (MF) and 400 $\mu$l/h (OF). However, variation of the flow rates allows for manipulation of the size and MF/IF ratio.

### 6.3.3 Osmotic driven oil removal

Dewetting was achieved by pumping the double emulsion solution through a dewetting chip at flow rates between 70 and 120 $\mu$l/h. Dewetting was followed through light of fluorescent microscopy and the flow rate was adjusted if necessary. Unless otherwise stated the osmotic gradient between IF and OF was 1:4.

## 6.4 Encapsulation experiments

### 6.4.1 IMV preparation

E. coli (MG1655) were cultured in LB medium containing 20mM Glucose.
The cells were harvested in three centrifugation steps. First they were centrifuged for 20 minutes at 10.000 x g at 4°C, the cells were resuspended in washing buffer (50 mM Tris-HCl pH 8.0, 1mM EGTA) and centrifuged again for 20 min at 10.000 x g at 4°C. The pellet was resuspended in washing buffer and centrifuged a third time for 30 minutes at 5.000 x g at 4 °C (Heitkamp *et al.* (2013)). Afterwards the pellet was frozen in liquid nitrogen and stored at −80 °C.

The cell pellet was covered with washing buffer, thawed in a waterbath at 30 °C and then resuspended. The suspension was centrifuged for 10 minutes at 15.000 x g at 4 °C and the resulting pellet was resuspended in 300 mL washing buffer. The cells were centrifuged again for 10 minutes at 15.000 x g at 4 °C and the pellet was resuspended

in lysis buffer (50 mM MOPS, 175 mM KCl, 10 mM $MgCl_2$, 0.2 mM EGTA, 0.2 mM DTT, 0.1 mM PMSF, pH 7.0), homogenized with a glass tissue homogenizer and stirred on ice for 1 hour.
1 unit per gram cell mass of DNAse was added and the cells were pressed through a cooled french press three times at 1000 bar. The solution was checked under the microscope to determine of the french press treatment was successful. The homogenized cells were frozen in liquid nitrogen and stored overnight at −80 °C.
The frozen suspension was thawed in a waterbath at room temperature and centrifuged for 20 minutes at 25.000 x g at 4 °C and the pellet was discarded. The supernatant was ultracentrifuged (Ultrazentrifuge Optima XPN 100, Beckman Coulter) for 120 minutes at 54.000 rpm at 4 °C.
The pellet contained now the inner and outer membrane and was resuspended in membrane buffer (50 mM Tris-HCl, 0.2 mM EGTA, 5 mM $MgCl_2$, 6 mM PAB, 10% (v/v) Glycerol, 2 mM DTT, 0.1 mM PMSF, pH 8.0) using a brush. The resuspended pellet was again ultacentrifuged for 90 min at 54.000 rpm at 4 °C and resuspended in membrane buffer. The last ultracentrifugation took 90 minutes at 54.000 rpm at 4 °C and the pellet was resuspended in membrane buffer.
The solution was frozen in liquid nitrogen and stored overnight at −80 °C and quickly thawed again the next day in at waterbath at 30°C. Next a density gradient centrifugation was performed. The ultracentrifugation tubes were filled with 6 mL 50 wt.% Sucrose, 8 mL 40 wt.% Sucrose, 10 mL 30 wt.% Sucrose, 10 mL 20 wt.% Sucrose and 1-2 mL sample on top. This was centrifuged for 24 hours at 30.000 rpm(swinging bucket rotor SW 32 Ti) with the acceleration and deceleration at the lowest possible level (Miura & Mizushima (1968)) (Jewett *et al.* (2008)).
The membrane is between 35 wt.% and 45 wt.% sucrose and the darker fraction is carefully collected. The protein content of the fractions was measured with a nanodrop and they were resuspended 1:4 in membrane buffer. The resulting solution was ultracentrifuged for 2 hours at 54.000 rpm (fixed angle rotor type 70 Ti) (Osborn *et al.* (1972)) and the pellet was dried and weighted. The pellet was resuspended in membrane buffer and the solution was pressed through a sterile filter (0.22 $\mu$m).
This solution containing the IMVs was frozen in 500 $\mu$L aliquots in liquid nitrogen and stored at −80 °C (Wuu & Swartz (2008)).

### 6.4.2 IMV characterization

#### 6.4.2.1 Measurement of ATP production by IMVs

The measurements of NADH-driven ATP production in IMVs were performed in a microplate reader (Biotech, Synergy HT) using the luciferin-luciferase assay.
To a solution containing 50 $\mu$L of measurement buffer (20 mM TRIS acetate (pH 7.8), 5 mM magnesium acetate, 1 mM DTT, 0.5 mM $KH_2PO_4$, 0.25 mM $MgCl_2$, 0.25 mM ADP, 0.1 mM EDTA) and 50 $\mu$L luciferin/luciferase assay (CLSII, prepared double

concentrated according to the manufacturer's protocol), 2.5 $\mu$L IMVs were added and the baseline was recorded.
The reaction was initiated by the addition of 10 $\mu$L NADH (2 mM, 1.5 mM, 1 mM, 0.5 mM, 0.2 mM and 0.1 mM stock solutions) as soon as a constant background was detected.

#### 6.4.2.2 TPRS measurement

Tunable resistive pulse sensing (TRPS) was performed on a qNano device (Izon Science, Christchurch, New Zealand).
For the measurement a NP200 strechable nanopore was used, which was calibrated with carboxylated polystyrene beads (mean size 350 nm). The lower fluid cell was filled with 80 $\mu$l membrane buffer and 30 $\mu$l of the vesicles, diluted with membrane buffer, were added to the upper fluid cell. Size distribution and concentration were calculated from the measurement data with the instrument software (Izon Control Suite 2, Christchurch, New Zealand).

### 6.4.3 CETCH cycle

The experiment was performed at the Max-Planck Institute for Terrestrial Microbiology in Marburg. Chemicals, Enzymes and devices, except for the microfluidic setup (microscope, pumps, chips) were provided by them.
The inner fluid was prepared in 50 mM MOPS buffer at pH 7 and 50 mM sucrose. The encapsulated metabolic module contained of 20 mM formate, 50 mM bicarbonate, 5 $\mu$M NADPH, 10 $\mu$M AmplifluRed, 1250 mU crotonyl-CoA carboxylase/reductase (Ccr), 590 mU formate dehydrogenase (Fdh), 1285 mU ethylmalonyl-CoA mutase (Ecm), 7000 mU emC/mmC epimerase (Epi), 20 mU methylsuccinyl-CoA oxidase (Mco), 0.2 mg/ml carbonic anhydrase and 100 mU horseradish peroxidase (HRP).
The inner fluid was prepared on ice and the reaction started with 1mM crotonyl-CoA. Negative controls contained no crotonyl-CoA.
As a control the same setup was tested in a 96-well-plate in a fluorescent plate reader at 30 °C. In this case the assay contained 0,1 mg/ml fluorescin.

## 6.5 GUV trapping

### 6.5.1 GUV production with electroformation

For the electroformation ITO (indium tin oxide) coated glass slides (Sigma) were used. As the glass slides were washed and reused the coating was checked by measuring the resistance with a multimeter.

If the resistance was between 40 and 60 Ohm a silicone ring was used to mark the area were later the lipids were dried. Lipids were dissolved in Chloroform:Methanol 1:9 adding up to a total volume of 25 $\mu$l per coated glass slide (usually 4 slides were used and a solution of 100 ul was prepared).
The final lipid concentration varied with the kind of lipid used. If necessary lipid dye was added to this solution.
25 $\mu$l were applied to the marked area on the coated side of the glass with a glass Hamilton syringe and dried while spreading the drying solution equally on the surface with the tip of the syringe. The spreading had to be done very careful because scratching the glass surface would affect the electroformation performance.
After the visible liquid evaporated the glass slides were dried under nitrogen for an additional 20 minutes. Two glass slides were pressed together with a silicone spacer in the middle and the sides with the lipid were facing each other. Then the solution was added to the space between the slides. The attached slides were connected to a frequency generator.
The conditions were optimized for various lipid compositions. Also the solution may contain additional substances in addition to sucrose. Below is one example protocol used to prepare DPhPC liposomes.
15 ul DPhPC (10 mg/ml) were spread on ITO glass slides and dried under nitrogen for 20 minutes. The lipid was rehydrated with 200 mM sucrose and GUVs were formed by applying 2 V at 10 Hz for 4 hours followed by 3 V at 5 Hz for 1 hour. They were harvested by pipetting and stored at room temperature.

### 6.5.2 Membrane permeability assay

#### 6.5.2.1 Data acquisition

Images were recorded with an inverted Axio Observer 5 light microscope from Zeiss and two different cameras.
The first camera was the Phantom v611 high-speed camera from Vision Research controlled with the software PCC 2.6 (Phantom Camera Control Application, Vision Research). The Phantom camera has a 1 Mega Pixel resolution and a pixel size of 28 x 28 microns and produces greyscale images.
The other camera used was an Axiocam 506 colour (D) from Zeiss with 6 Mega Pixel resolution and a Pixel size of 4.54 x 4.54 microns.

Videos were recorded with 24 frames/second with the Phantom camera and 10 frames/second with the Zeiss camera. The resulting videos were exported in the .avi format. Afterwards the videos were broken down into single frames using a script. This frames were then analyzed with a software called vesicle scout. For the data analysis the images recorded by the Zeiss camera were transformed into greyscale images.

### 6.5.3 OmpF purification

E. coli Omp8 cells were grown on a LB-Amp plate overnight at 37 °C, a colony was picked and grown in 2YT-Amp medium. OmpF overexpression was induced by addition of IPTG (final conc. 0.4 mM) and cells were shaken for 16 hours at RT. The cells were harvested by centrifugation. They were resuspended in lysis buffer and pressed 3x through French press. The protein was extracted using three ultracentrifugation steps and the purity of the protein was verified with SDS-PAGE. OmpF was kept in 1 % OG and stored at 4 °C.

### 6.5.4 OmpF reconstitution

Purified OmpF (6.5 mg/ml) was stored in 1% OG. The stock solution was dialysed against PBS and Biobeads (Bio-Beads SM-2 Resin from Bio-Rad) for 6 hours and 1% o-POE was added to the OmpF solution. OmpF stock (1 $\mu$l) was added to 50 $\mu$l vesicle solution and incubated for 60 minutes at RT. Afterwards biobeads were added to remove detergent and the mixture was incubated for 60 minutes at room temperature and then stored at 4 °C overnight and used within 48 hours.
The control vesicles came from the same electroformation batch and underwent the same procedure. The only difference was that they were incubated in a control buffer without OmpF but otherwise with the exact same composition including surfactants.

# References


Abkarian, M., Loiseau, E. & Massiera, G. (2011). Continuous droplet interface crossing encapsulation (cdice) for high throughput monodisperse vesicle design. *Soft Matter*, **7**, 4610–4614. 17

Agresti, J.J., Antipov, E., Abate, A.R., Ahn, K., Rowat, A.C., Baret, J.C., Marquez, M., Klibanov, A.M., Griffiths, A.D. & Weitz, D.A. (2010). Ultrahigh-throughput screening in drop-based microfluidics for directed evolution. *Proceedings of the National Academy of Sciences*, **107**, 4004–4009. 10

Al-Awqati, Q. (1999). One hundred years of membrane permeability: does overton still rule? *Nature cell biology*, **1**, E201–E202. 71

Angelova, M.I. & Dimitrov, D.S. (1986). Liposome electroformation. *Faraday discussions of the Chemical Society*, **81**, 303–311. 13

Apellániz, B., Nieva, J.L., Schwille, P. & García-Sáez, A.J. (2010). All-or-none versus graded: single-vesicle analysis reveals lipid composition effects on membrane permeabilization. *Biophysical journal*, **99**, 3619–3628. 7, 70

Baldacchini, T. (2015). *Three-dimensional microfabrication using two-photon polymerization: fundamentals, technology, and applications*. William Andrew. 9

Bashirzadeh, Y. & Liu, A.P. (2019). Encapsulation of the cytoskeleton: towards mimicking the mechanics of a cell. *Soft Matter*, **15**, 8425–8436. 48

Beneyton, T., Krafft, D., Bednarz, C., Kleineberg, C., Woelfer, C., Ivanov, I., Vidakovic-Koch, T., Sundmacher, K. & Baret, J.C. (2018). Out-of-equilibrium microcompartments for the bottom-up integration of metabolic functions. *Nature communications*, **9**, 1–10. 56, 60, 61, 155

Benner, S.A. & Sismour, A.M. (2005). Synthetic biology. *Nature Reviews Genetics*, **6**, 533–543. 2

Berrisford, J.M., Baradaran, R. & Sazanov, L.A. (2016). Structure of bacterial respiratory complex i. *Biochimica et Biophysica Acta (BBA)-Bioenergetics*, **1857**, 892–901. 53

Berry, J.D., Neeson, M.J., Dagastine, R.R., Chan, D.Y. & Tabor, R.F. (2015). Measurement of surface and interfacial tension using pendant drop tensiometry. *Journal of colloid and interface science*, **454**, 226–237. 42

Blumenthal, D., Goldstien, L., Edidin, M. & Gheber, L.A. (2015). Universal approach to frap analysis of arbitrary bleaching patterns. *Scientific reports*, **5**, 1–9. 99

Booth, R., Qiao, Y., Li, M. & Mann, S. (2019). Spatial positioning and chemical coupling in coacervate-in-proteinosome protocells. *Angewandte Chemie*, **131**, 9218–9222. 51

Braun, S. (2016). *Biophysikalische Untersuchungen zur Wechselwirkung von grenzflächen-aktiven Substanzen mit Liposomen*. Ph.D. thesis, Albert-Ludwigs-Universität Freiburg im Breisgau. 72

Cama, J. (2016). *Quantifying passive drug transport across lipid membranes*. Ph.D. thesis, University of Cambridge. 8, 72, 73, 74, 75, 93, 98, 108, 109, 112, 113, 117, 118, 119, 155

Cama, J., Chimerel, C., Pagliara, S., Javer, A. & Keyser, U. (2014). A label-free microfluidic assay to quantitatively study antibiotic diffusion through lipid membranes. *Lab on a Chip*, **14**, 2303–2308. 69, 73, 74, 75, 89, 100

Chan, Y.H.M. & Boxer, S.G. (2007). Model membrane systems and their applications. *Current opinion in chemical biology*, **11**, 581–587. 8

Cheng, C.Y., Wang, J.Y., Kausik, R., Lee, K.Y.C. & Han, S. (2012). Nature of interactions between peo-ppo-peo triblock copolymers and lipid membranes:(ii) role of hydration dynamics revealed by dynamic nuclear polarization. *Biomacromolecules*, **13**, 2624–2633. 111, 114, 157

Choi, H.J. & Montemagno, C.D. (2005). Artificial organelle: ATP synthesis from cellular mimetic polymersomes. *Nano letters*, **5**, 2538–2542. 4

Chowdhury, R., Ren, T., Shankla, M., Decker, K., Grisewood, M., Prabhakar, J., Baker, C., Golbeck, J.H., Aksimentiev, A., Kumar, M. *et al.* (2018). Poredesigner for tuning solute selectivity in a robust and highly permeable outer membrane pore. *Nature communications*, **9**, 1–10. 118

Cowan, S., Schirmer, T., Rummel, G., Steiert, M., Ghosh, R., Pauptit, R., Jansonius, J. & Rosenbusch, J. (1992). Crystal structures explain functional properties of two E. coli porins. *Nature*, **358**, 727–733. 117

Czekalska, M.A., Kaminski, T.S., Jakiela, S., Sapra, K.T., Bayley, H. & Garstecki, P. (2015). A droplet microfluidic system for sequential generation of lipid bilayers and transmembrane electrical recordings. *Lab on a Chip*, **15**, 541–548. 125

Delabre, U., Feld, K., Crespo, E., Whyte, G., Sykes, C., Seifert, U. & Guck, J. (2015). Deformation of phospholipid vesicles in an optical stretcher. *Soft matter*, **11**, 6075–6088. 69

Delcour, A.H. (1997). Function and modulation of bacterial porins: insights from electrophysiology. *FEMS Microbiology Letters*, **151**, 115–123. 73

Delcour, A.H. (2009). Outer membrane permeability and antibiotic resistance. *Biochimica et Biophysica Acta (BBA)-Proteins and Proteomics*, **1794**, 808–816. 117

Delebecque, C.J., Lindner, A.B., Silver, P.A. & Aldaye, F.A. (2011). Organization of intracellular reactions with rationally designed RNA assemblies. *Science*, **333**, 470–474. 4

Demchenko, A.P. (2020). Photobleaching of organic fluorophores: quantitative characterization, mechanisms, protection. *Methods and applications in fluorescence*, **8**, 022001. 89

Deng, N.N., Yelleswarapu, M. & Huck, W.T. (2016). Monodisperse uni-and multicompartment liposomes. *Journal of the American Chemical Society*, **138**, 7584–7591. 41, 154

Deng, N.N., Yelleswarapu, M., Zheng, L. & Huck, W.T. (2017). Microfluidic assembly of monodisperse vesosomes as artificial cell models. *Journal of the American Chemical Society*, **139**, 587–590. 18, 19, 32, 153

Deshpande, S. & Dekker, C. (2018). On-chip microfluidic production of cell-sized liposomes. *Nature protocols*, **13**, 856–874. 18, 19, 22, 30, 32, 111, 153, 154

Deshpande, S., Caspi, Y., Meijering, A.E. & Dekker, C. (2016). Octanol-assisted liposome assembly on chip. *Nature communications*, **7**, 1–9. 31

Deshpande, S., Spoelstra, W.K., van Doorn, M., Kerssemakers, J. & Dekker, C. (2018). Mechanical division of cell-sized liposomes. *ACS nano*, **12**, 2560–2568. 18, 70

Di Carlo, D., Aghdam, N. & Lee, L.P. (2006). Single-cell enzyme concentrations, kinetics, and inhibition analysis using high-density hydrodynamic cell isolation arrays. *Analytical chemistry*, **78**, 4925–4930. 70, 77

Dominak, L.M. & Keating, C.D. (2008). Macromolecular crowding improves polymer encapsulation within giant lipid vesicles. *Langmuir*, **24**, 13565–13571. 19

## REFERENCES


Dudley, Q.M., Karim, A.S. & Jewett, M.C. (2015). Cell-free metabolic engineering: biomanufacturing beyond the cell. *Biotechnology journal*, **10**, 69–82. 52

El-Mir, M.Y., Nogueira, V., Fontaine, E., Avéret, N., Rigoulet, M. & Leverve, X. (2000). Dimethylbiguanide inhibits cell respiration via an indirect effect targeted on the respiratory chain complex I. *Journal of Biological Chemistry*, **275**, 223–228. 60

Endy, D. (2005). Foundations for engineering biology. *Nature*, **438**, 449–453. 3

Estes, D.J. & Mayer, M. (2005). Giant liposomes in physiological buffer using electroformation in a flow chamber. *Biochimica et Biophysica Acta (BBA)-Biomembranes*, **1712**, 152–160. 15, 19

Estes, D.J., Lopez, S.R., Fuller, A.O. & Mayer, M. (2006). Triggering and visualizing the aggregation and fusion of lipid membranes in microfluidic chambers. *Biophysical journal*, **91**, 233–243. 15

Eyer, K., Doineau, R.C., Castrillon, C.E., Briseño-Roa, L., Menrath, V., Mottet, G., England, P., Godina, A., Brient-Litzler, E., Nizak, C. *et al.* (2017). Single-cell deep phenotyping of igg-secreting cells for high-resolution immune monitoring. *Nature biotechnology*, **35**, 977. 10

Eze, M.O. (1991). Phase transitions in phospholipid bilayers: Lateral phase separations play vital roles in biomembranes. *Biochemical education*, **19**, 204–208. 6

Fallah-Araghi, A., Baret, J.C., Ryckelynck, M. & Griffiths, A.D. (2012). A completely in vitro ultrahigh-throughput droplet-based microfluidic screening system for protein engineering and directed evolution. *Lab on a Chip*, **12**, 882–891. 10

Friedrich, R., Block, S., Alizadehheidari, M., Heider, S., Fritzsche, J., Esbjörner, E.K., Westerlund, F. & Bally, M. (2017). A nano flow cytometer for single lipid vesicle analysis. *Lab on a Chip*, **17**, 830–841. 71

Futai, M. (1974). Orientation of membrane vesicles fromescherichia coli prepared by different procedures. *The Journal of membrane biology*, **15**, 15–28. 53, 54

G Moloughney, J. & Weisleder, N. (2012). Poloxamer 188 (p188) as a membrane resealing reagent in biomedical applications. *Recent patents on biotechnology*, **6**, 200–211. 111

Gaikwad, R., Thangaraj, P. & Sen, A. (2021). Direct and rapid measurement of hydrogen peroxide in human blood using a microfluidic device. *Scientific reports*, **11**, 1–10. 62

Garcia, S. & Trinh, C.T. (2019). Modular design: implementing proven engineering principles in biotechnology. *Biotechnology advances*, **37**, 107403. 2

Gessesse, B., Nagaike, T., Nagata, K., Shimizu, Y. & Ueda, T. (2018). G-protein coupled receptor protein synthesis on a lipid bilayer using a reconstituted cell-free protein synthesis system. *Life*, **8**, 54. 8

Gonidec, M. & Puigmartí-Luis, J. (2019). Continuous-versus segmented-flow microfluidic synthesis in materials science. *Crystals*, **9**, 12. 10

Göpfrich, K., Haller, B., Staufer, O., Dreher, Y., Mersdorf, U., Platzman, I. & Spatz, J.P. (2019). One-pot assembly of complex giant unilamellar vesicle-based synthetic cells. *ACS synthetic biology*, **8**, 937–947. 48

Gracia, R.S., Bezlyepkina, N., Knorr, R.L., Lipowsky, R. & Dimova, R. (2010). Effect of cholesterol on the rigidity of saturated and unsaturated membranes: fluctuation and electrodeformation analysis of giant vesicles. *Soft Matter*, **6**, 1472–1482. 46

Haberland, M.E. & Reynolds, J.A. (1975). Interaction of L-alpha-palmitoyl lysophosphatidylcholine with the AI polypeptide of high density lipoprotein. *Journal of Biological Chemistry*, **250**, 6636–6639. 28

Heberle, F.A. & Feigenson, G.W. (2011). Phase separation in lipid membranes. *Cold Spring Harbor perspectives in biology*, **3**, a004630. 6

Heikal, A., Nakatani, Y., Dunn, E., Weimar, M.R., Day, C.L., Baker, E.N., Lott, J.S., Sazanov, L.A. & Cook, G.M. (2014). Structure of the bacterial type II NADH dehydrogenase: a monotopic membrane protein with an essential role in energy generation. *Molecular microbiology*, **91**, 950–964. 53

Heitkamp, T., Sielaff, H., Korn, A., Renz, M., Zarrabi, N. & Boersch, M. (2013). Monitoring subunit rotation in single FRET-labeled FoF1-ATP synthase in an anti-brownian electrokinetic trap. In *Multiphoton Microscopy in the Biomedical Sciences XIII*, vol. 8588, 85880Q, International Society for Optics and Photonics. 54, 130

Hung, P.J., Lee, P.J., Sabounchi, P., Aghdam, N., Lin, R. & Lee, L.P. (2005). A novel high aspect ratio microfluidic design to provide a stable and uniform microenvironment for cell growth in a high throughput mammalian cell culture array. *Lab on a Chip*, **5**, 44–48. 10

Hutchison, C.A., Peterson, S.N., Gill, S.R., Cline, R.T., White, O., Fraser, C.M., Smith, H.O. & Venter, J.C. (1999). Global transposon mutagenesis and a minimal mycoplasma genome. *Science*, **286**, 2165–2169. 3

Jeong, H., Tombor, B., Albert, R., Oltvai, Z.N. & Barabási, A.L. (2000). The large-scale organization of metabolic networks. *Nature*, **407**, 651–654. 52

## REFERENCES


Jessop-Fabre, M.M. & Sonnenschein, N. (2019). Improving reproducibility in synthetic biology. *Frontiers in Bioengineering and Biotechnology*, **7**, 18. 10

Jewett, M.C., Calhoun, K.A., Voloshin, A., Wuu, J.J. & Swartz, J.R. (2008). An integrated cell-free metabolic platform for protein production and synthetic biology. *Molecular systems biology*, **4**. 54, 56, 131

Jia, H. & Schwille, P. (2019). Bottom-up synthetic biology: reconstitution in space and time. *Current opinion in biotechnology*, **60**, 179–187. 5

Jia, H., Heymann, M., Bernhard, F., Schwille, P. & Kai, L. (2017). Cell-free protein synthesis in micro compartments: building a minimal cell from biobricks. *New biotechnology*, **39**, 199–205. 6

Jia, H., Heymann, M., Härtel, T., Kai, L. & Schwille, P. (2019). Temperature-sensitive protein expression in protocells. *Chemical Communications*, **55**, 6421–6424. 51

Jin, L., Kamat, N.P., Jena, S. & Szostak, J.W. (2018). Fatty acid/phospholipid blended membranes: a potential intermediate state in protocellular evolution. *Small*, **14**, 1704077. 44

Johann, R.M. (2006). Cell trapping in microfluidic chips. *Analytical and bioanalytical chemistry*, **385**, 408–412. 69

Kaback, H. (1974). Transport studies in bacterial membrane vesicles. *Science*, **186**, 882–892. 53

Kamiya, K. (2020). Development of artificial cell models using microfluidic technology and synthetic biology. *Micromachines*, **11**, 559. 50

Kamiya, K. & Takeuchi, S. (2017). Giant liposome formation toward the synthesis of well-defined artificial cells. *Journal of Materials Chemistry B*, **5**, 5911–5923. 13

Karamdad, K., Law, R., Seddon, J., Brooks, N. & Ces, O. (2015). Preparation and mechanical characterisation of giant unilamellar vesicles by a microfluidic method. *Lab on a Chip*, **15**, 557–562. 18

Kastner, E., Kaur, R., Lowry, D., Moghaddam, B., Wilkinson, A. & Perrie, Y. (2014). High-throughput manufacturing of size-tuned liposomes by a new microfluidics method using enhanced statistical tools for characterization. *International journal of pharmaceutics*, **477**, 361–368. 17

Katsu, T., Imamura, T., Komagoe, K., Masuda, K. & Mizushima, T. (2007). Simultaneous measurements of K+ and calcein release from liposomes and the determination of pore size formed in a membrane. *Analytical Sciences*, **23**, 517–522. 101

Kenis, P.J. & Stroock, A.D. (2006). Materials for micro-and nanofluidics. *MRS bulletin*, **31**, 87–94. 10, 17

Khademhosseini, A., Yeh, J., Eng, G., Karp, J., Kaji, H., Borenstein, J., Farokhzad, O.C. & Langer, R. (2005). Cell docking inside microwells within reversibly sealed microfluidic channels for fabricating multiphenotype cell arrays. *Lab on a Chip*, **5**, 1380–1386. 69

Kitney, R. & Freemont, P. (2012). Synthetic biology–the state of play. *FEBS letters*, **586**, 2029–2036. 1

Klein, A.M., Mazutis, L., Akartuna, I., Tallapragada, N., Veres, A., Li, V., Peshkin, L., Weitz, D.A. & Kirschner, M.W. (2015). Droplet barcoding for single-cell transcriptomics applied to embryonic stem cells. *Cell*, **161**, 1187–1201. 10

Kleineberg, C., Woelfer, C., Abbasnia, A., Pischel, D., Bednarz, C., Ivanov, I., Heitkamp, T., Boersch, M., Sundmacher, K. & Vidakovic-Koch, T. (2020). Light-driven ATP regeneration in diblock/grafted hybrid vesicles. *ChemBioChem*. 52

Koley, D. & Bard, A.J. (2010). Triton X-100 concentration effects on membrane permeability of a single hela cell by scanning electrochemical microscopy (SECM). *Proceedings of the National Academy of Sciences*, **107**, 16783–16787. 72

Konings, W.N. & Kaback, H.R. (1973). Anaerobic transport in Escherichia coli membrane vesicles. *Proceedings of the National Academy of Sciences*, **70**, 3376–3381. 53

Koshland, D.E. (2002). The seven pillars of life. *Science*, **295**, 2215–2216. 2

Koynova, R. & Caffrey, M. (1995). Phases and phase transitions of the sphingolipids. *Biochimica et Biophysica Acta (BBA)-Lipids and Lipid Metabolism*, **1255**, 213–236. 6

Kozlov, M., Quarmyne, M., Chen, W. & McCarthy, T.J. (2003). Adsorption of poly (vinyl alcohol) onto hydrophobic substrates. a general approach for hydrophilizing and chemically activating surfaces. *Macromolecules*, **36**, 6054–6059. 23

Krylova, O.O., Melik-Nubarov, N.S., Badun, G.A., Ksenofontov, A.L., Menger, F.M. & Yaroslavov, A.A. (2003). Pluronic l61 accelerates flip–flop and transbilayer doxorubicin permeation. *Chemistry–A European Journal*, **9**, 3930–3936. 111

Kuhn, P., Eyer, K., Robinson, T., Schmidt, F.I., Mercer, J. & Dittrich, P.S. (2012). A facile protocol for the immobilisation of vesicles, virus particles, bacteria, and yeast cells. *Integrative Biology*, **4**, 1550–1555. 69

Kunzler, C., Handschuh-Wang, S., Roesener, M. & Schönherr, H. (2020). Giant biodegradable poly (ethylene glycol)-block-poly ($\varepsilon$-caprolactone) polymersomes by electroformation. *Macromolecular bioscience*, **20**, 2000014. 15

Kuribayashi, K., Tresset, G., Coquet, P., Fujita, H. & Takeuchi, S. (2006). Electroformation of giant liposomes in microfluidic channels. *Measurement science and technology*, **17**, 3121. 15

Lan, F., Demaree, B., Ahmed, N. & Abate, A.R. (2017). Single-cell genome sequencing at ultra-high-throughput with microfluidic droplet barcoding. *Nature biotechnology*, **35**, 640. 10

Lande, M.B., Donovan, J.M. & Zeidel, M.L. (1995). The relationship between membrane fluidity and permeabilities to water, solutes, ammonia, and protons. *Journal of General Physiology*, **106**, 67–84. 72

Leo, A., Hansch, C. & Elkins, D. (1971). Partition coefficients and their uses. *Chemical reviews*, **71**, 525–616. 71

Levin, V.A. (1980). Relationship of octanol/water partition coefficient and molecular weight to rat brain capillary permeability. *Journal of medicinal chemistry*, **23**, 682–684. 71

Li, S., Xu, Z., Mazzeo, A., Burns, D.J., Fu, G., Dirckx, M., Shilpiekandula, V., Chen, X., Nayak, N.C., Wong, E. *et al.* (2008). Review of production of microfluidic devices: material, manufacturing and metrology. In *MEMS, MOEMS, and Micromachining III*, vol. 6993, 69930F, International Society for Optics and Photonics. 17

Li, S., Hu, P.C. & Malmstadt, N. (2011). Imaging molecular transport across lipid bilayers. *Biophysical journal*, **101**, 700–708. 69

Liu, H. & Zhang, Y. (2011). Droplet formation in microfluidic cross-junctions. *Physics of Fluids*, **23**, 082101. 37

Lonchin, S., Luisi, P.L., Walde, P. & Robinson, B.H. (1999). A matrix effect in mixed phospholipid/fatty acid vesicle formation. *The Journal of Physical Chemistry B*, **103**, 10910–10916. 44

Manfredi, G., Yang, L., Gajewski, C.D. & Mattiazzi, M. (2002). Measurements of ATP in mammalian cells. *Methods*, **26**, 317–326. 57

Maskarinec, S.A., Hannig, J., Lee, R.C. & Lee, K.Y.C. (2002). Direct observation of poloxamer 188 insertion into lipid monolayers. *Biophysical journal*, **82**, 1453–1459. 111

Mata, A., Fleischman, A.J. & Roy, S. (2005). Characterization of polydimethylsiloxane (PDMS) properties for biomedical micro/nanosystems. *Biomedical microdevices*, **7**, 281–293. 18

Mathai, J.C., Tristram-Nagle, S., Nagle, J.F. & Zeidel, M.L. (2008). Structural determinants of water permeability through the lipid membrane. *The Journal of general physiology*, **131**, 69–76. 72

Mathavan, I. & Beis, K. (2012). The role of bacterial membrane proteins in the internalization of microcin MccJ25 and MccB17. *Biochemical Society Transactions*, **40**, 1539–1543. 117, 157

Matosevic, S. & Paegel, B.M. (2013). Layer-by-layer cell membrane assembly. *Nature chemistry*, **5**, 958–963. 125

McDonald, J.C. & Whitesides, G.M. (2002). Poly (dimethylsiloxane) as a material for fabricating microfluidic devices. *Accounts of chemical research*, **35**, 491–499. 9

McDonald, J.C., Duffy, D.C., Anderson, J.R., Chiu, D.T., Wu, H., Schueller, O.J. & Whitesides, G.M. (2000). Fabrication of microfluidic systems in poly (dimethylsiloxane). *ELECTROPHORESIS: An International Journal*, **21**, 27–40. 9

Meyer, C.E., Craciun, I., Schoenenberger, C.A., Wehr, R. & Palivan, C.G. (2021). Catalytic polymersomes to produce strong and long-lasting bioluminescence. *Nanoscale*, **13**, 66–70. 118

Mina, E.W., Lasagna-Reeves, C., Glabe, C.G. & Kayed, R. (2009). Poloxamer 188 copolymer membrane sealant rescues toxicity of amyloid oligomers in vitro. *Journal of molecular biology*, **391**, 577–585. 111

Missner, A. & Pohl, P. (2009). 110 years of the meyer–overton rule: predicting membrane permeability of gases and other small compounds. *ChemPhysChem*, **10**, 1405–1414. 71

Miura, T. & Mizushima, S. (1968). Separation by density gradient centrifugation of two types of membranes from spheroplast membrane of Escherichia coli K12. *Biochimica et Biophysica Acta (BBA)-Biomembranes*, **150**, 159–161. 54, 131

Moga, A., Yandrapalli, N., Dimova, R. & Robinson, T. (2019). Optimization of the inverted emulsion method for high-yield production of biomimetic giant unilamellar vesicles. *ChemBioChem*, **20**, 2674. 16, 28, 153

Monnard, P.A. & Deamer, D.W. (2002). Membrane self-assembly processes: Steps toward the first cellular life. *The Anatomical Record: An Official Publication of the American Association of Anatomists*, **268**, 196–207. 6

## REFERENCES


Montal, M. & Mueller, P. (1972). Formation of bimolecular membranes from lipid monolayers and a study of their electrical properties. *Proceedings of the National Academy of Sciences*, **69**, 3561–3566. 8

Morales-Penningston, N.F., Wu, J., Farkas, E.R., Goh, S.L., Konyakhina, T.M., Zheng, J.Y., Webb, W.W. & Feigenson, G.W. (2010). GUV preparation and imaging: minimizing artifacts. *Biochimica et Biophysica Acta (BBA)-Biomembranes*, **1798**, 1324–1332. 14

Mueller, P., Rudin, D.O., Tien, H.T. & Wescott, W.C. (1962). Reconstitution of cell membrane structure in vitro and its transformation into an excitable system. *Nature*, **194**, 979–980. 8

Mulkidjanian, A.Y., Galperin, M.Y. & Koonin, E.V. (2009). Co-evolution of primordial membranes and membrane proteins. *Trends in biochemical sciences*, **34**, 206–215. 7

Mutafova-Yambolieva, V.N., Hwang, S.J., Hao, X., Chen, H., Zhu, M.X., Wood, J.D., Ward, S.M. & Sanders, K.M. (2007). $\beta$-nicotinamide adenine dinucleotide is an inhibitory neurotransmitter in visceral smooth muscle. *Proceedings of the National Academy of Sciences*, **104**, 16359–16364. 52

Mutschler, H., Robinson, T., Tang, T. & Wegner, S. (2019). Special issue on bottom-up synthetic biology. *Chembiochem: a European journal of chemical biology*, **20**, 2533–2534. 3

Nikaido, H. (2003). Molecular basis of bacterial outer membrane permeability revisited. *Microbiol. Mol. Biol. Rev.*, **67**, 593–656. 117

Nuss, H., Chevallard, C., Guenoun, P. & Malloggi, F. (2012). Microfluidic trap-and-release system for lab-on-a-chip-based studies on giant vesicles. *Lab on a Chip*, **12**, 5257–5261. 70

Nwaneshiudu, A., Kuschal, C., Sakamoto, F.H., Anderson, R.R., Schwarzenberger, K. & Young, R.C. (2012). Introduction to confocal microscopy. *Journal of Investigative Dermatology*, **132**, 1–5. 92

Osaki, T., Kuribayashi-Shigetomi, K., Kawano, R., Sasaki, H. & Takeuchi, S. (2011). Uniformly-sized giant liposome formation with gentle hydration. In *2011 IEEE 24th International Conference on Micro Electro Mechanical Systems*, 103–106. 13

Osborn, M., Gander, J., Parisi, E. & Carson, J. (1972). Mechanism of assembly of the outer membrane of Salmonella typhimurium isolation and characterization of cytoplasmic and outer membrane. *Journal of Biological Chemistry*, **247**, 3962–3972. 55, 131

Otrin, L., Marusic, N., Bednarz, C., Vidakovic-Koch, T., Lieberwirth, I., Landfester, K. & Sundmacher, K. (2017). Toward artificial mitochondrion: mimicking oxidative phosphorylation in polymer and hybrid membranes. *Nano letters*, **17**, 6816–6821. 52

Paterson, D., Reboud, J., Wilson, R., Tassieri, M. & Cooper, J. (2014). Integrating microfluidic generation, handling and analysis of biomimetic giant unilamellar vesicles. *Lab on a Chip*, **14**, 1806–1810. 125

Patil, Y.P. & Jadhav, S. (2014). Novel methods for liposome preparation. *Chemistry and physics of lipids*, **177**, 8–18. 13

Pautot, S., Frisken, B.J. & Weitz, D. (2003a). Engineering asymmetric vesicles. *Proceedings of the National Academy of Sciences*, **100**, 10718–10721. 16

Pautot, S., Frisken, B.J. & Weitz, D. (2003b). Production of unilamellar vesicles using an inverted emulsion. *Langmuir*, **19**, 2870–2879. 16

Petit, J., Polenz, I., Baret, J.C., Herminghaus, S. & Bäumchen, O. (2016). Vesicles-on-a-chip: A universal microfluidic platform for the assembly of liposomes and polymersomes. *The European Physical Journal E*, **39**, 1–6. 18, 19, 20, 21, 24, 26, 40, 153, 154

Probst, C., Grünberger, A., Wiechert, W. & Kohlheyer, D. (2013). Polydimethylsiloxane (pdms) sub-micron traps for single-cell analysis of bacteria. *Micromachines*, **4**, 357–369. 69

Quake, S.R. & Scherer, A. (2000). From micro-to nanofabrication with soft materials. *Science*, **290**, 1536–1540. 18

Ragunath, V.K. (2006). *Structural Studies of Membrane Transport Proteins*. Ph.D. thesis. 7

Rayan, G., Guet, J.E., Taulier, N., Pincet, F. & Urbach, W. (2010). Recent applications of fluorescence recovery after photobleaching (FRAP) to membrane biomacromolecules. *Sensors*, **10**, 5927–5948. 7

Redman, E.A., Batz, N.G., Mellors, J.S. & Ramsey, J.M. (2015). Integrated microfluidic capillary electrophoresis-electrospray ionization devices with online MS detection for the separation and characterization of intact monoclonal antibody variants. *Analytical chemistry*, **87**, 2264–2272. 9

Reeves, J.P. & Dowben, R.M. (1969). Formation and properties of thin-walled phospholipid vesicles. *Journal of cellular physiology*, **73**, 49–60. 13

Reits, E.A. & Neefjes, J.J. (2001). From fixed to FRAP: measuring protein mobility and activity in living cells. *Nature cell biology*, **3**, E145–E147. 7

Rideau, E., Dimova, R., Schwille, P., Wurm, F.R. & Landfester, K. (2018). Liposomes and polymersomes: a comparative review towards cell mimicking. *Chemical society reviews*, **47**, 8572–8610. 4

Roberts, K., Alberts, B., Johnson, A., Walter, P. & Hunt, T. (2002). Molecular biology of the cell. *New York: Garland Science*. 75

Robinson, T. (2019a). Microfluidic handling and analysis of giant vesicles for use as artificial cells: a review. *Advanced Biosystems*, **3**, 1800318. 68, 69, 70

Robinson, T. (2019b). Microfluidics and giant vesicles: creation, capture, and applications for biomembranes. In *Advances in Biomembranes and Lipid Self-Assembly*, vol. 30, 271–315, Elsevier. 15, 17, 46, 68, 69, 77, 85, 86, 87, 125

Robinson, T., Kuhn, P., Eyer, K. & Dittrich, P.S. (2013). Microfluidic trapping of giant unilamellar vesicles to study transport through a membrane pore. *Biomicrofluidics*, **7**, 044105. 68, 74, 77, 78, 155

Robinson, T., Verboket, P.E., Eyer, K. & Dittrich, P.S. (2014). Controllable electrofusion of lipid vesicles: initiation and analysis of reactions within biomimetic containers. *Lab on a Chip*, **14**, 2852–2859. 69, 77

Romanov, V., McCullough, J., Gale, B.K. & Frost, A. (2019). A tunable microfluidic device enables cargo encapsulation by cell-or organelle-sized lipid vesicles comprising asymmetric lipid bilayers. *Advanced biosystems*, **3**, 1900010. 49

Runas, K.A. & Malmstadt, N. (2015). Low levels of lipid oxidation radically increase the passive permeability of lipid bilayers. *Soft Matter*, **11**, 499–505. 69

Saluz, H.P., Koehler, M. & Mejevaia, T. (2012). *Microsystem technology: a powerful tool for biomolecular studies*. Birkhaeuser. 9

Salvador-Castell, M., Demé, B., Oger, P. & Peters, J. (2020). Structural characterization of an archaeal lipid bilayer as a function of hydration and temperature. *International journal of molecular sciences*, **21**, 1816. 108

Sambuy, Y., De Angelis, I., Ranaldi, G., Scarino, M., Stammati, A. & Zucco, F. (2005). The Caco-2 cell line as a model of the intestinal barrier: influence of cell and culture-related factors on Caco-2 cell functional characteristics. *Cell biology and toxicology*, **21**, 1–26. 71

Schaich, M. (2020). *Microfluidic Transport Studies on Lipid Vesicles*. Ph.D. thesis, University of Cambridge. 125

Schmid, E.M., Richmond, D.L. & Fletcher, D.A. (2015). Reconstitution of proteins on electroformed giant unilamellar vesicles. *Methods in cell biology*, **128**, 319–338. 14

Schmitt, E.K., Vrouenraets, M. & Steinem, C. (2006). Channel activity of OmpF monitored in nano-BLMs. *Biophysical journal*, **91**, 2163–2171. 8

Schrödinger, E. (1946). What is life?: the physical aspect of the living cell. 1

Schwander, T., von Borzyskowski, L.S., Burgener, S., Cortina, N.S. & Erb, T.J. (2016). A synthetic pathway for the fixation of carbon dioxide in vitro. *Science*, **354**, 900–904. 53, 63, 64, 155

Schwendener, R.A. (2014). Liposomes as vaccine delivery systems: a review of the recent advances. *Therapeutic advances in vaccines*, **2**, 159–182. 9

Schwille, P. (2011). Bottom-up synthetic biology: engineering in a tinkerer's world. *Science*, **333**, 1252–1254. 3

Schwille, P. (2015). Jump-starting life? fundamental aspects of synthetic biology. *Journal of Cell Biology*, **210**, 687–690. 3, 153

Schwille, P., Spatz, J., Landfester, K., Bodenschatz, E., Herminghaus, S., Sourjik, V., Erb, T.J., Bastiaens, P., Lipowsky, R., Hyman, A. *et al.* (2018). MaxSynBio: avenues towards creating cells from the bottom up. *Angewandte Chemie International Edition*, **57**, 13382–13392. 5, 6, 51, 52, 153

Seemann, R., Brinkmann, M., Pfohl, T. & Herminghaus, S. (2011). Droplet based microfluidics. *Reports on progress in physics*, **75**, 016601. 35

Shinoda, W. (2016). Permeability across lipid membranes. *Biochimica et Biophysica Acta (BBA)-Biomembranes*, **1858**, 2254–2265. 109

Shinoda, W., Mikami, M., Baba, T. & Hato, M. (2004). Molecular dynamics study on the effects of chain branching on the physical properties of lipid bilayers: 2. permeability. *The Journal of Physical Chemistry B*, **108**, 9346–9356. 109

Shiomi, H., Tsuda, S., Suzuki, H. & Yomo, T. (2014). Liposome-based liquid handling platform featuring addition, mixing, and aliquoting of femtoliter volumes. *PLoS One*, **9**, e101820. 69

Shum, H.C., Lee, D., Yoon, I., Kodger, T. & Weitz, D.A. (2008). Double emulsion templated monodisperse phospholipid vesicles. *Langmuir*, **24**, 7651–7653. 18

Singer, S.J. & Nicolson, G.L. (1972). The fluid mosaic model of the structure of cell membranes. *Science*, **175**, 720–731. 6

Smolke, C.D. (2009). Building outside of the box: igem and the biobricks foundation. *Nature biotechnology*, **27**, 1099–1102. 2

Sorre, B., Callan-Jones, A., Manzi, J., Goud, B., Prost, J., Bassereau, P. & Roux, A. (2012). Nature of curvature coupling of amphiphysin with membranes depends on its bound density. *Proceedings of the National Academy of Sciences*, **109**, 173–178. 69

Squires, T.M. & Quake, S.R. (2005). Microfluidics: Fluid physics at the nanoliter scale. *Reviews of modern physics*, **77**, 977. 10

Stachowiak, J.C., Richmond, D.L., Li, T.H., Liu, A.P., Parekh, S.H. & Fletcher, D.A. (2008). Unilamellar vesicle formation and encapsulation by microfluidic jetting. *Proceedings of the national academy of sciences*, **105**, 4697–4702. 17

Stein, W. (2012). *The movement of molecules across cell membranes*, vol. 6. Elsevier. 71

Steinberg-Yfrach, G., Rigaud, J.L., Durantini, E.N., Moore, A.L., Gust, D. & Moore, T.A. (1998). Light-driven production of ATP catalysed by F0F1-ATP synthase in an artificial photosynthetic membrane. *Nature*, **392**, 479–482. 52

Steinkühler, J., Agudo-Canalejo, J., Lipowsky, R. & Dimova, R. (2016). Modulating vesicle adhesion by electric fields. *Biophysical journal*, **111**, 1454–1464. 69

Steinkühler, J., De Tillieux, P., Knorr, R.L., Lipowsky, R. & Dimova, R. (2018). Charged giant unilamellar vesicles prepared by electroformation exhibit nanotubes and transbilayer lipid asymmetry. *Scientific reports*, **8**, 1–9. 15

Supramaniam, P., Ces, O. & Salehi-Reyhani, A. (2019). Microfluidics for artificial life: techniques for bottom-up synthetic biology. *Micromachines*, **10**, 299. 3, 4, 153

Surewicz, W.K. (1984). Membrane actions of water-soluble fusogens: effect of dimethyl sulfoxide, glycerol and sucrose on lipid bilayer order and fluidity. *Chemistry and physics of lipids*, **34**, 363–372. 31

Tan, H.Y., Trier, S., Rahbek, U.L., Dufva, M., Kutter, J.P. & Andresen, T.L. (2018). A multi-chamber microfluidic intestinal barrier model using Caco-2 cells for drug transport studies. *PloS one*, **13**, e0197101. 71

Tayar, A.M., Karzbrun, E., Noireaux, V. & Bar-Ziv, R.H. (2017). Synchrony and pattern formation of coupled genetic oscillators on a chip of artificial cells. *Proceedings of the National Academy of Sciences*, **114**, 11609–11614. 10

Teh, S.Y., Lin, R., Hung, L.H. & Lee, A.P. (2008). Droplet microfluidics. *Lab on a Chip*, **8**, 198–220. 10

Teh, S.Y., Khnouf, R., Fan, H. & Lee, A.P. (2011). Stable, biocompatible lipid vesicle generation by solvent extraction-based droplet microfluidics. *Biomicrofluidics*, **5**, 044113. 22, 26

Terry, S.C., Jerman, J.H. & Angell, J.B. (1979). A gas chromatographic air analyzer fabricated on a silicon wafer. *IEEE transactions on electron devices*, **26**, 1880–1886. 9

Thutupalli, S., Fleury, J.B., Steinberger, A., Herminghaus, S. & Seemann, R. (2013). Why can artificial membranes be fabricated so rapidly in microfluidics? *Chemical Communications*, **49**, 1443–1445. 28, 29, 154

Tice, J.D., Lyon, A.D. & Ismagilov, R.F. (2004). Effects of viscosity on droplet formation and mixing in microfluidic channels. *Analytica chimica acta*, **507**, 73–77. 35

Tirumalasetty, P.P. & Eley, J.G. (2006). Permeability enhancing effects of the alkylglycoside, octylglucoside, on insulin permeation across epithelial membrane in vitro. *J Pharm Pharm Sci*, **9**, 32–39. 112

Trantidou, T., Dekker, L., Polizzi, K., Ces, O. & Elani, Y. (2018). Functionalizing cell-mimetic giant vesicles with encapsulated bacterial biosensors. *Interface Focus*, **8**, 20180024. 48

Tresset, G. & Takeuchi, S. (2004). A microfluidic device for electrofusion of biological vesicles. *Biomedical Microdevices*, **6**, 213–218. 70

Tristram-Nagle, S., Kim, D.J., Akhunzada, N., Kučerka, N., Mathai, J.C., Katsaras, J., Zeidel, M. & Nagle, J.F. (2010). Structure and water permeability of fully hydrated diphytanoylpc. *Chemistry and physics of lipids*, **163**, 630–637. 109

Ueno, M. (1989). Partition behavior of a nonionic detergent, octyl glucoside, between membrane and water phases, and its effect on membrane permeability. *Biochemistry*, **28**, 5631–5634. 72, 115

Utada, A.S., Lorenceau, E., Link, D.R., Kaplan, P.D., Stone, H.A. & Weitz, D. (2005). Monodisperse double emulsions generated from a microcapillary device. *Science*, **308**, 537–541. 10

Vallejo, D., Lee, S., Lee, D., Zhang, C., Rapier, C., Chessler, S. & Lee, A. (2017). Cell-sized lipid vesicles for cell-cell synaptic therapies. *Technology*, **5**, 201–213. 41, 43

Van de Cauter, L., Fanalista, F., Van Buren, L., De Franceschi, N., Godino, E., Bouw, S., Danelon, C., Dekker, C., Koenderink, G.H. & Ganzinger, K.A. (2021). Optimized cDICE for efficient reconstitution of biological systems in giant unilamellar vesicles. *ACS Synthetic Biology*, **10**, 1690–1702. 19

van Erp, R., Soleimanzadeh, R., Nela, L., Kampitsis, G. & Matioli, E. (2020). Co-designing electronics with microfluidics for more sustainable cooling. *Nature*, **585**, 211–216. 9

Venne, A., Li, S., Mandeville, R., Kabanov, A. & Alakhov, V. (1996). Hypersensitizing effect of pluronic L61 on cytotoxic activity, transport, and subcellular distribution of doxorubicin in multiple drug-resistant cells. *Cancer research*, **56**, 3626–3629. 111

Vogel, R., Willmott, G., Kozak, D., Roberts, G.S., Anderson, W., Groenewegen, L., Glossop, B., Barnett, A., Turner, A. & Trau, M. (2011). Quantitative sizing of nano/microparticles with a tunable elastomeric pore sensor. *Analytical chemistry*, **83**, 3499–3506. 55

Voldman, J., Gray, M.L., Toner, M. & Schmidt, M.A. (2002). A microfabrication-based dynamic array cytometer. *Analytical chemistry*, **74**, 3984–3990. 69

Vrhovec, S., Mally, M., Kavčič, B. & Derganc, J. (2011). A microfluidic diffusion chamber for reversible environmental changes around flaccid lipid vesicles. *Lab on a Chip*, **11**, 4200–4206. 69

Walde, P., Cosentino, K., Engel, H. & Stano, P. (2010). Giant vesicles: preparations and applications. *ChemBioChem*, **11**, 848–865. 13, 14, 15, 16, 19

Wang, J.Y., Marks, J. & Lee, K.Y.C. (2012). Nature of interactions between peo-ppo-peo triblock copolymers and lipid membranes:(i) effect of polymer hydrophobicity on its ability to protect liposomes from peroxidation. *Biomacromolecules*, **13**, 2616–2623. 111

Wang, M., Woelfer, C., Otrin, L., Ivanov, I., Vidakovic-Koch, T. & Sundmacher, K. (2018). Transmembrane NADH Oxidation with Tetracyanoquinodimethane. *Langmuir*, **34**, 5435–5443. 52

Wang, N., Semprebon, C., Liu, H., Zhang, C. & Kusumaatmaja, H. (2020). Modelling double emulsion formation in planar flow-focusing microchannels. *Journal of Fluid Mechanics*, **895**. 35, 36, 37, 38, 39, 154

Watson, H. (2015). Biological membranes. *Essays in biochemistry*, **59**, 43–69. 6, 7, 153

Weiss, M. (2018). *Microfluidic Approaches for the Sequential Bottom-up Assembly of Droplet-based Minimal Synthetic Cells*. Ph.D. thesis. 1, 2, 6

Weiss, M., Frohnmayer, J.P., Benk, L.T., Haller, B., Janiesch, J.W., Heitkamp, T., Börsch, M., Lira, R.B., Dimova, R., Lipowsky, R. *et al.* (2018). Sequential bottom-up assembly of mechanically stabilized synthetic cells by microfluidics. *Nature materials*, **17**, 89–96. 17, 49, 52

Whitesides, G.M. (2006). The origins and the future of microfluidics. *Nature*, **442**, 368–373. 9

Wick, R., Angelova, M.I., Walde, P. & Luisi, P.L. (1996). Microinjection into giant vesicles and light microscopy investigation of enzyme-mediated vesicle transformations. *Chemistry & biology*, **3**, 105–111. 19

Winterhalter, M., Hilty, C., Bezrukov, S., Nardin, C., Meier, W. & Fournier, D. (2001). Controlling membrane permeability with bacterial porins: application to encapsulated enzymes. *Talanta*, **55**, 965–971. 113

Woo, Y., Heo, Y., Shin, K. & Yi, G.R. (2013). Hydrodynamic filtration in microfluidic channels as size-selection process for giant unilamellar vesicles. *Journal of biomedical nanotechnology*, **9**, 610–614. 86

Wu, D., Luo, Y., Zhou, X., Dai, Z. & Lin, B. (2005). Multilayer poly (vinyl alcohol)-adsorbed coating on poly (dimethylsiloxane) microfluidic chips for biopolymer separation. *Electrophoresis*, **26**, 211–218. 23

Wuu, J.J. & Swartz, J.R. (2008). High yield cell-free production of integral membrane proteins without refolding or detergents. *Biochimica et Biophysica Acta (BBA)-Biomembranes*, **1778**, 1237–1250. 55, 131

Xiang, T.X. & Anderson, B.D. (1998). Influence of chain ordering on the selectivity of dipalmitoylphosphatidylcholine bilayer membranes for permeant size and shape. *Biophysical journal*, **75**, 2658–2671. 72

Yadav, V.G., De Mey, M., Lim, C.G., Ajikumar, P.K. & Stephanopoulos, G. (2012). The future of metabolic engineering and synthetic biology: towards a systematic practice. *Metabolic engineering*, **14**, 233–241. 52

Yamada, A., Lee, S., Bassereau, P. & Baroud, C.N. (2014). Trapping and release of giant unilamellar vesicles in microfluidic wells. *Soft matter*, **10**, 5878–5885. 69

Yandrapalli, N. & Robinson, T. (2019). Ultra-high capacity microfluidic trapping of giant vesicles for high-throughput membrane studies. *Lab on a Chip*, **19**, 626–633. 79, 86, 155

Yasuda, S., Townsend, D., Michele, D.E., Favre, E.G., Day, S.M. & Metzger, J.M. (2005). Dystrophic heart failure blocked by membrane sealant poloxamer. *Nature*, **436**, 1025–1029. 111

Zhang, X. & Haswell, S.J. (2006). Materials matter in microfluidic devices. *MRS bulletin*, **31**, 95–99. 17

Zhou, Y., Berry, C.K., Storer, P.A. & Raphael, R.M. (2007). Peroxidation of polyunsaturated phosphatidyl-choline lipids during electroformation. *Biomaterials*, **28**, 1298–1306. 14

Zittle, C. (1966). Precipitation of casein from acidic solutions by divalent anions. *Journal of Dairy Science*, **49**, 361–364. 86

# List of Figures